A Smart Power System Stabilizer for Dynamic Reduction of a Power System Model

By

© Mohamed Ali Masrob

A Thesis submitted to the School of Graduate Studies
in partial fulfillment of the requirements for the award of the degree of
Doctor of Philosophy in Electrical Engineering

Electrical and Computer Engineering Department
Faculty of Engineering and Applied Science
Memorial University of Newfoundland
St. John's, NL, Canada

Abstract

This thesis focuses on studying the dynamic stability of power systems and improving them by the addition of smart power system stabilizers (PSSs). A conventional design technique of a power system stabilizer that uses a single machine connected to an infinite bus through a transmission line (SMIB) has been widely used for study of elecromechanical perturbations. This approach requires estimating the external equivalent impedance and the voltage at an external bus for each machine in a multi-machine system.

This study will use the conventional mathematical method, which represents a power system with some modifications. The dynamic model is linearized by taking the high voltage side on the generation unit as a reference instead of the infinite bus voltage. By using this modification, several improvements are accomplished, the main ones of which are: the estimation of states is eliminated, the time consumed in estimating calculations is reduced, the parameters of the model are independent of the external system, and the PSS design for each machine is independent in a multi-machine environment system. This strategy enables a PSS to be designed for a single machine and then implemented in a multi-machine system.

Power systems have advanced to the point that they now cover vast geographical areas. Consequently, they are not only quite complicated, but the system orders are also high. As the complexity of these systems increases, so does the difficulty of examining their dynamic stability and adjusting their controllers. In this research, to address these issues, the reduced model technique has been employed to mathematically define smaller system models from existing models, such that the properties of both systems are comparable properties.

The parameters of the PSS are determined based on a modified Heffron- Phillips model of the power system at certain operating conditions where it can provide reliable performance. Since

the power systems are highly nonlinear with configurations and parameters that change with time, a typical PSS design, which is based on a linearized model of the power system, cannot guarantee its performance in practical operating environments. The present study attempts to overcome this limitation by implementing smart power system stabilizers. In the context of this thesis the word smart means novel technique.

An artificial neural network power system stabilizer (ANN-PSS), a novel multi input fuzzy logic power system stabilizer (FLPSS), and a modified multi-resolution proportional-integral-derivative power system stabilizer (MMR-PID-PSS), based on the dynamic reduction of a power system model. These PSSs have been developed to refine the power system dynamic performance by adjusting the regulator's parameters in real-time simulation under various operating conditions.

In the first part of this research, the digital simulations results using the proposed ANN-PSS and FLPSS are carried out on a single machine connected to a network and are then compared with conventional Lead-Lag PSS. The results show that the power system with FLPSS has a better dynamic response over a wide range of operating conditions and parameter changes. Next, the digital simulations results using the proposed MMR-PID-PSS is carried out on a single machine connected to the network, a 4-machine 10-bus power system, and a 10-machine 39-bus power system and then compared with FLPSS. The results validate the effectiveness of the proposed MMR-PID-PSS regarding reduced overshoot, undershoot, and settling time under a different type of disturbances.

Acknowledgment

I would like to express my profound acknowledge to my supervisor Dr. M. A. Rahman for his guidance, valuable suggestions, encouragement, and his patient throughout my study at the Memorial University of Newfoundland. I also wish to thank my supervisory committee members Dr. Glyn George and Dr. Vlastimil Masek for their useful explanations and suggestions that helped to refine this work. Also, I would like to express gratitude to the Faculty of Engineering and Applied Science for supplying resources to complete this study. I am very grateful to Dr. Michael Hinchey for his valuable assistance throughout this work.

I sincerely acknowledge financial support from the Ministry of Higher Education in my country during my study at the Memorial University of Newfoundland.

I would like to express gratitude to my wife for her patience and support during my study; I would like to dedicate this work to my father, the spirit of my dear mother, my children, my brother, my sisters, and my colleagues.

Table of Contents

Table of Figures

List of Tables

List of Symbols and Abbreviations

A	System matrix
B	Control matrix
X	State vector
U	Control vector
Δ	Linearized incremental quantity
s	Complex number frequency parameter
P.U	Per unit
λ	Eigenvalues
ζ	Damping ratio
M	Matrix of eigenvectors
Λ	Diagonal matrix of eigenvalues
A^r	Reduced system matrix
B^r	Reduced control matrix
Δx^r	Reduced state vector corresponding to the retained state vector
Λ^r	Diagonal matrix of the dominant eigenvalues
i_s	Armature current
$i_d,\ i_q$	Armature current, direct and quadrature axis components
$e_d,\ e_q$	Armature voltage, direct and quadrature axis components
e_t	Terminal voltage
E_q	Voltage proportional to q-axis flux linkage
E_{FD}	Generator field voltage
T_e	Electrical or electromagnetic torque
T_m	Mechanical torque supplied by the prime mover
T_a	Acceleration torque
δ	The phase angle between the machine q-axis and reference (rotor angle)
v_s	The voltage measured at secondary bus of step-up transformer
θ_s	The angle of the voltage at secondary bus of step-up transformer

δ_s	The angle between the machine q-axis and high voltage of step-up transformer
E_{ref}	Reference input voltage
ω_r	Rotor speed (angular velocity) of a generator
ω_s	Synchronous speed
ω_0	Base angular speed
ω	Difference between rotor speed and synchronous speed in p.u
x_d	The machine d-axis synchronous reactance
x_q	The machine q-axis synchronous reactance
x'_d	The machine d-axis transient reactance
x'_q	The machine q-axis transient reactance
x_t	The transformer reactance
R_t	The transformer resistance
T'_{do}	Direct axis transient open circuit time constant
H	Inertia coefficient
K_D	Damping coefficient
Δ	Increment (small change)
P	real power
Q	reactive power
T_E	Exciter time constant
K_E	Exciter constant related to self-exciter field
K_A	Amplifier gain
T_A	Amplifier time constant
T_R	Rectifier time constant
K_F	Regulator stabilizing circuit gain
T_F	Regulator stabilizing circuit time constant
S_E	Exciter saturation function
T_g	Time constant of speed governing mechanism
T_T	Turbine time constant
T_V	Prime mover valve setting
R	The speed regulation due to generation action

SMIB	Single machine infinite bus system
FACTS	Flexible AC transmission system
AVR	Automatic voltage regulator
PSS	Power system stabilizer
CPSS	Conventional power system stabilizer
AC	Adaptive control
MRAC	Model reference adaptive control
INAC	Indirect adaptive control
ANN	Artificial neural networks
FLC	Fuzzy logic control
MFs	Membership functions
ANN-PSS	Neural Network Power System Stabilizer
FLPSS	Fuzzy Logic Power System Stabilizer
MMR-PID-PSS	Modified Multiresolution Proportional-Integral-Derivative Power System Stabilizer
T_W	Washout time constant for Lead-Lag PSS
T_1	First lead time constant for Lead-Lag PSS
T_2	First lag time constant for Lead-Lag PSS
T_3	Second lead time constant for Lead-Lag PSS
T_4	Second lag time constant for Lead-Lag PSS
K_S	PSS gain
GEP(s)	The ratio between electrical torque output and the reference voltage input of a generator
$G_{exc}(s)$	Transfer function of the exciter
FILT(s)	Transfer function of torsional filter
BPA	Back-propagation algorithm
CWT	Continuous wavelet transform
DWT	Discrete wavelet transform
WPT	Wavelet packet transform
MQF	Quadrature mirror filter
MR	Multi-resolution

$\psi(t)$	Wavelet function
$\varphi(t)$	Scaling function
$g[k]$	Digital low pass filter with impulse response
$h[k]$	Digital high pass filter with impulse response
MRA	Multiresolution analysis
$L^2(\mathbb{R})$	Hilbert space
$\oplus$	Direct orthogonal summation operation of the spaces
$V_j(\varphi)$	Subspace spanned by scaling function
$W_j(\psi)$	Space spanned by mother wavelet function
j	Level of the resolution
db3	Daubechies 3 mother wavelet

Chapter 1

1 Introduction

1.1 Power System Control

An electrical power system contains thousands of interconnected components. Many of these components are highly nonlinear and some are combinations of electrical and mechanical parts, such as synchronous and induction machines. Power systems have thus developed into complex operation and control systems with various kinds of unstable characteristics [1], [2]. Because these systems are spread over vast geographical areas, they are subject to several types of disturbances. Generators operating under these perturbations have less stability margins, making the systems even more fragile [3].

With the advent of the interconnection of large electrical power systems, a variety of problems have begun to emerge. Some of these problems involve the oscillations of the subsystems of a large interconnected electrical power against each other (inter-area oscillations). The definition of stability as applied to the power systems may be stated as follows [3]: If the oscillation in the power system caused by a disturbance stabilizes in a short period of time, then it can be said the system is stable. otherwise, the system is unstable. A typical power system is a multivariable system that is affected by a wide range of devices with different dynamic characteristics. Depending on system topology as well as the type of disturbance and operating mode, instability may occur in different ways. In most cases, automatic controls and/or human operator action will restore the system to normal operational status [4] [5] [6] [7] [8].

Figure 1.1 illustrates classification of power system stability, identifying its categories and subcategories [8]. As can be seen, the classification of power system stability better enables

identifying cases of instability, choosing the best way to deal with them, and using the appropriate analysis tools.

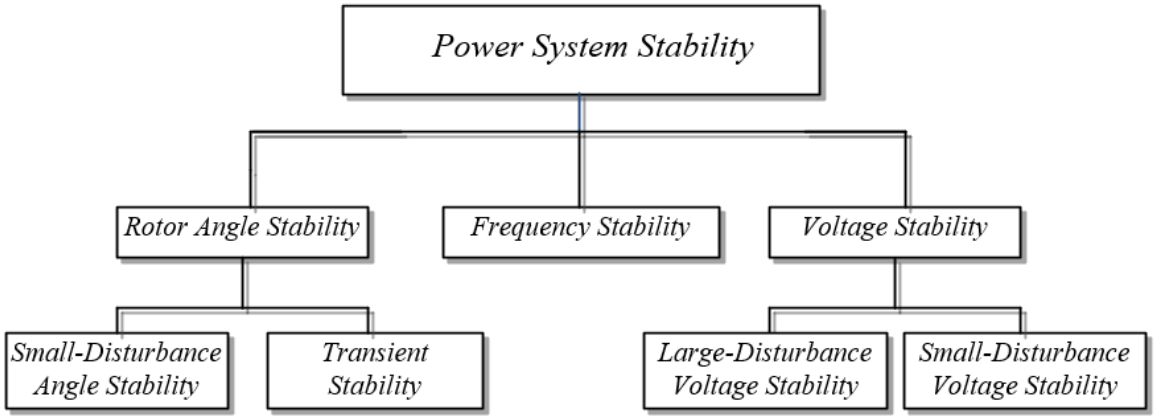

Figure 1.1 Classification of power system stability

Rotor angle stability is defined as the capability of a synchronous generator within an interconnected power system to restore equilibrium ($T_m = T_e$) after undergoing disturbances.

Figure 1.2 shows the mechanical and electrical torque direction applied to the shaft of a synchronous generator, where T_m is the mechanical torque, T_e is the electrical torque, P_e is output electrical power, and ω is the shaft speed. The synchronous generator mechanically connected to the turbine, and it is stable when the mechanical torque is equal to the electrical torque (synchronism). The change in electrical torque T_e of a synchronous machine following a disturbance can be resolved into two components: the synchronizing torque component and the damping torque component. System stability relies on the existence of both components of torque for each of the synchronous machines. An insufficient synchronizing torque causes a non-oscillatory instability issue, while the lack of damping torque produces an oscillatory instability problem [7] [8] [9].

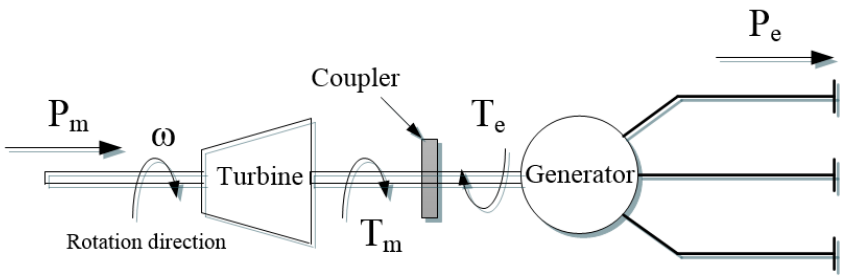

Figure 1.2 Mechanical and electrical torque applied to the shaft of synchronous machine

To simplify the analysis and for getting more understanding of stability problems, rotor angle stability can be divided into two subcategories: small disturbance stability and large disturbance stability or transient stability [7] [8].

Small signal stability can be defined as the capability of the power system to restore the synchronism after a small disturbance has occurred, such as minor changes in loads. In this case, the nonlinear equations of the system can be linearized around an equilibrium point. The time frame of interest for this type of stability is in the range of 10 to 20 seconds after a disturbance.

Transient stability is the ability of the power system to return to the steady-state after large disturbances have occurred. These disturbances may include faults on transmission lines, loss of a large load, loss of a generator, or loss of a system component, such as power transformers. The time frame of interest in transient stability studies is usually 3 to 5 seconds following the disturbance, though it may extend to 10 or 20 seconds for very large systems [7] [8] [9] [10] [11].

Voltage stability can be defined as the ability of the power system to preserve the voltage level of all busbars in a power system within an acceptable level under different operating conditions. Loss of load is the most common outcome of voltage instability along with tripping of transmission lines and other elements by their protective systems, leading to cascading outages. Based on the nature of the disturbances, voltage stability is also classified as a huge perturbation

in voltage stability or a slight disturbance in voltage stability. The time frame of interest for this kind of stability problem varies from a few seconds to ten minutes, so it is considered either a short- or long-term phenomenon [7] [8].

Frequency stability can be characterized as the ability of a power system to keep a stable frequency after large swings occur, leading to a significant imbalance between supply and demand. This is specified as either a short- or long-term phenomenon. There is some overlap between different types of instability because more than one type of instability may be observed in a power system [4] [7] [8].

A small signal perturbation model around an equilibrium point can be considered for dynamic stability studies, and linear differential equations can describe the system. However, for transient stability, the system must be described by nonlinear differential equations. Although there are several sources of positive damping in a power system (e.g., voltage regulator and speed governing), there is also negative damping when a power system has a small stability margin and any disturbance can cause the loss of synchronism.

Considerable efforts have been devoted over the years to improving power system stability in a variety of ways [7] [8] [9] [10] as shown in the block diagram of Figure 1.3 that illustrates the block diagram of power system control [7]. These attempts can be divided into two groups, as follows:

On the network side

- Clearing faults in a short time
- Reducing transmission lines reactance
- Shunt and series compensation
- Flexible AC transmission system (FACTS)

- Load shedding
- Energy storage systems

On the generation side

- Generator excitation control (automatic voltage regulator [AVR])
- Generator input power control (governor)

On the generation side, for a particular problem, any one of the above methods can be employed, but the excitation control method is preferred for the following reasons:

- Electrical systems generally have a smaller time constant than mechanical systems.
- Electrical control systems are economical and easier to implement than mechanical systems.
- Due to its short loop time constant, an electrical control system is effectively a continuously acting system, and thus gives a smooth system response.

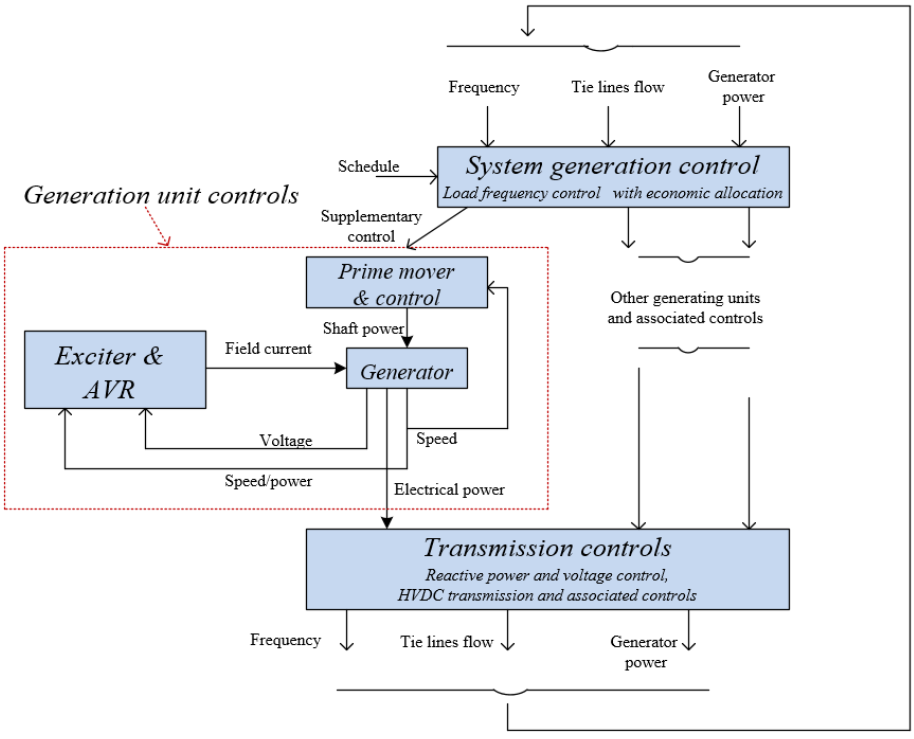

Figure 1.3. Block diagram of power system control

The voltage control loop has a significant impact on the dynamic stability of a power system. Oscillations of small magnitude and low frequency often persist for long periods of time and in some cases impose limitations on power transfer capability. Similar types of oscillations may also be observed when remote generating units are connected to a large power system through long transmission lines. Various methods have been proposed to enhance the dynamic performance of the power system. These can be divided into two main groups, as follows:

- Groups that design new excitation controller-based modern theory, and
- Groups that improve the performance of the excitation controllers by introducing a supplementary control signal.

A typical method within the second group is to utilize a power system stabilizer, (PSS) [12].

The effectiveness of damping produced by excitation control has been demonstrated both by computation and field test [10] [13] [14]. Today, many of the major electrical power plants in large interconnected power systems are equipped with an additional excitation control signal, commonly referred to as a power system stabilizer (PSS). Several kinds of PSS signals, (e.g., speed deviation, power angle deviation and voltage deviation), have been used as input signals.

1.2 Literature Review on Power System Stabilizers

Since the 1960s, power system stabilizers have been used to improve dynamic power system stability and thus have become an important auxiliary control when dealing with low-frequency oscillations. As the size of the interconnected power system grows, the possibility of withstanding unexpected disturbances without loss of power system stability is increased by using an additional excitation control signal, as shown in Figure 1.4 that describes the block diagram of excitation system and power system stabilizer (PSS) [9]. The essential function of a PSS is to extend the stability margin by modulation of the generator excitation system to dampen out the

oscillation in a power system. The oscillation of concern occurs in the frequency range of approximately (0.2-2.5 Hz). To provide damping, the stabilizer produces a component of electrical torque on the rotor shaft which is in phase with the speed variations. Independent of the type of excitation system, the generator and power system collectively determine the open loop transfer function. This transfer function is strongly influenced by the voltage regulator gain, generator power rating, and transmitted power level.

The primary characteristics of the control loop are high gain, short time constant, and high ceiling voltage excitation control. These increase both the steady-state and transient stability limit of the power system [3] [7] [10] [14].

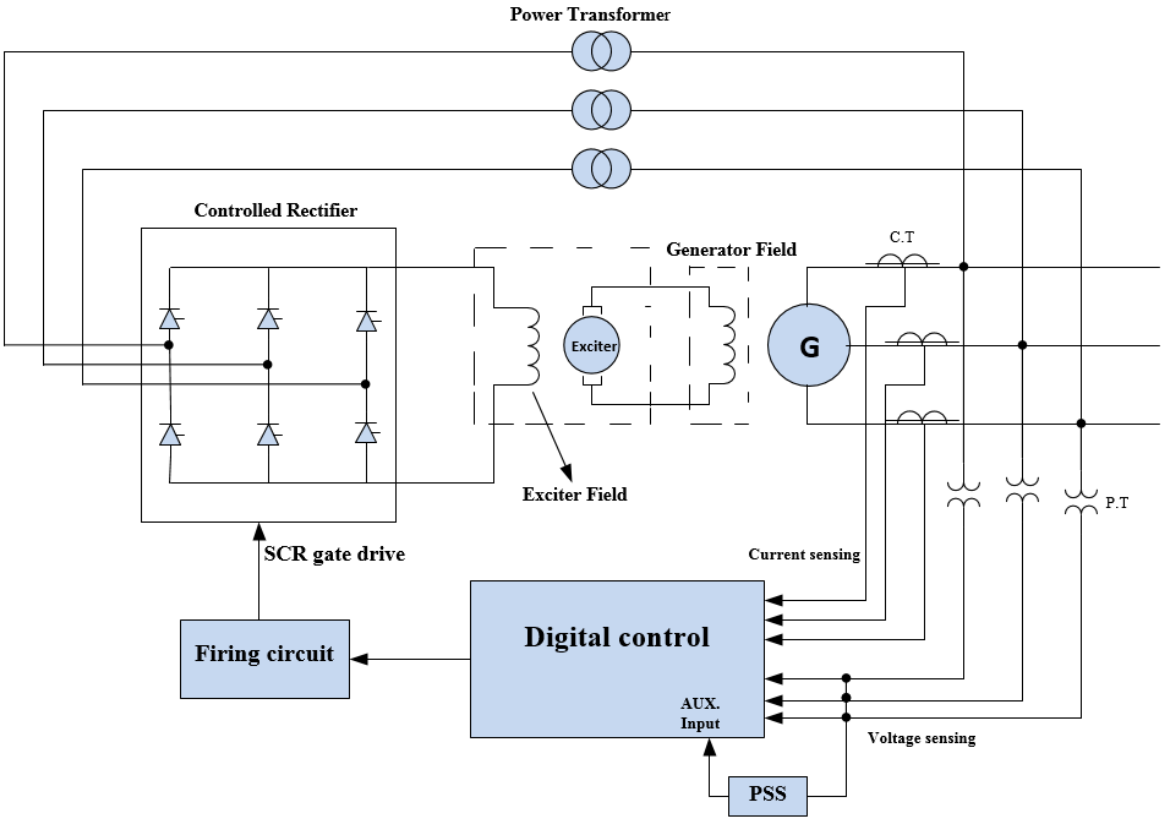

Figure 1.4 Block diagram of excitation system and PSS

1.2.1 Conventional Power System Stabilizer

Power system stabilizers are now in wide use on synchronous generators. In fact, PSSs have been used for over 30 years in the United States and Canada. Furthermore, PSS has been used in the United Kingdom to dampen the oscillations in tie lines connecting Scotland and England [10]. The conventional power system stabilizer (CPSS) is the type most commonly used and is typically presented as a network of cascaded lead-lag compensators. For instance, it can be a fixed parameter analog-type device, or it can be implemented as an algorithm by using digital control theory. The CPSS design is based on a transfer function GEP(s), which is the ratio of the developed electrical torque to the input reference voltage of the automatic voltage regulator (AVR), using classical control theory. It contains a phase compensation network for the phase difference between the excitation control input and the damping torque output. By appropriately tuning the phase and gain characteristics of the compensation network for the CPSS, it is possible to set the desired damping ratio. Conventional power system stabilizers are widely used in power systems today and have improved power system dynamic stability [3] [7] [10].

Demello and Concordia [4] explained the main concepts that influence the synchronous generator stability using excitation control. They presented a procedure to design a PSS based on a damping and synchronizing torque for a single machine infinite bus (SMIB) system, where the transfer function GEP(s) is supplied by the PSS transfer function. This technique forms the basic design of many PSSs in the field today. Dineley and Morris in [5] studied the effects of automatic excitation control on the interaction of two similar synchronous generators connected in parallel as well as connected to an infinite bus through transmission lines. Sherbiny and Mehta in [6] extended the method of analysis used in [4] by incorporating a realistic excitation system. Larsen and Swann also extended the technique introduced in [4] by applying an alternative input to the

PSS. They described a practical process, which included adjusting the PSS to reduce the effect of torsional oscillation and power system noise with various input signals to the PSS [12]. In [15] and [16] a proportional integral controller was introduced as a power system stabilizer instead of lead lag PSS (which was used in [4]) for single machine and multi-machine power systems. A study by Lam *et al.* in [17] described that in a multi-machine power system, the transfer function GEP(s) calculated for the SMIB system is satisfactory for designing PSS, and the frequency response of the GEP of one machine in a multi-machine system has two components. The first one relies only on an associated generator, and the second component depends on the connected generator and the network admittance matrix (external network and generator admittance). Thus, the most dynamic information required to design the PSS is mostly in the power plant.

In [18] Gibbard and Vowles discovered that the phase response of the transfer function (GEP), which is the ratio between terminal voltage V_t and voltage reference V_r with all shafts dynamically disabled (GEPSDD) agrees with the P-V_r transfer function under the same conditions. They also mentioned that the P-V_r phase compensation agrees with the method of residues for phase compensation. This technique, however, is not suitable for designing PSSs in interconnected power systems. In [19] Gurrala and Sen presented a decentralized PSS design based on the technique presented in [4], but using a different linearizing approach. In this strategy, the system dynamics of the i^{th} machine in a multi-machine environment system is linearized by taking the high voltage at the step-up transformer as a reference instead of an infinite bus system, as in the classical method. Thence, the model parameters are independent of the external system information. De Marco *et al.* in [20] designed PSS for i^{th} machine in a multi-machine environment system using a phase compensation method by changing the external reactance of a single machine connected to the infinite bus through a transmission line. The maximum value of the external

reactance in their system is determined by the lowest desired value of inter-area frequencies, while the minimum value is set by a step-up transformer next to the power plant. This technique consumed a significant amount of time for large connected networks with different operating conditions.

In [21], the author introduced a method to advance the PSS design procedure introduced in [19]. In this method local power plant information was used by adding an external reactance with the step-up transformer's reactance, which added a phase lead to the phase response of the GEP transfer function (TF) obtained in [19]. This technique closely agreed with the phase response of $P\text{-}V_r$ transfer function (TF) and provided more accurate information about the critical gain of PSS, whereas the $P\text{-}V_r$ design method does not give any information about the PSS critical gain.

It is important to note that the CPSS has an inherent drawback – namely, it is designed for a particular operating condition for the power system that is represented by a linearized transfer function, as mentioned above. The highly nonlinear parameters vary widely under different operating conditions and unpredictability of power system disturbances, which can lead to difficulties in maintaining the following properties:

- the accuracy of the linear model for the power system;
- the accuracy of the parameter for that model;
- the effective tuning of the CPSS parameters; and
- the tracking of the system nonlinearity.

However, because the CPSS is a linear controller that uses conventional filtering processes (washout filter), the response delays affect the performance of CPSS. Therefore, CPSS may not perform well in many practical applications and under different operating conditions. Extensive

research has been carried out to solve these problems, with numerous tuning techniques being introduced to tune the CPSS parameters effectively [22]

1.2.2 Adaptive Power System Stabilizer

The adaptive control theory provides a possible way to solve the problems mentioned above relating to power system stabilizers. There are two types of adaptive controller (AC) – model reference adaptive control (MRAC) and indirect adaptive control (INAC). The goal of the first adaptive controller, MRAC, is to adapt the parameters of the controller according to an adaptation law. This law is defined such that the behavior of the closed-loop control system maintains the performance specified by the reference model. It requires an appropriate reference model, controller and adaptive mechanism [23] [24], as shown in Figure 1.5. However, because the reference model of large systems is difficult to prove due to their complexity, MRAC is very difficult to apply when systems are large (such as interconnected power system).

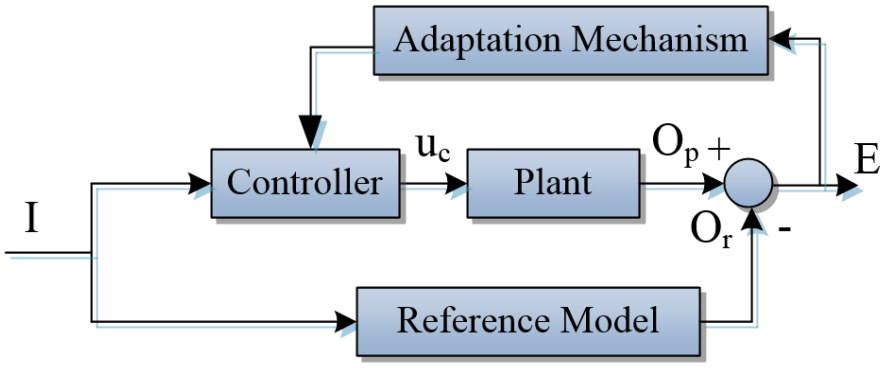

Figure 1.5. Block diagram of model reference adaptive control

The second control is an indirect adaptive control (INAC), which is shown in Figure 1.6. At each sampling instance, the input and the output of the generating unit are sampled.

Furthermore, the mathematical model is obtained by some online identification procedure, such as an artificial neural network technique or a fuzzy logic method [25] [26] [27], to represent the dynamic behaviour of the generating unit at that point in time. It is expected that the mathematical model obtained at each sampling period can track changes in the system. Following identification of the model, the necessary control signal for the generating unit is produced based on model identification. There are various control strategies, such as pole placement [28] [29], linear quadratic regulator (LQR) [30] [31], and linear quadratic Gaussian [22] [24] [32] [33] [34]. These strategies are developed by assuming that the identified model is the true mathematical description of the generating unit. However, since the power system is a high order nonlinear continuous system, it is difficult for the low order discretely identified model to precisely describe the dynamic behavior of the power system. As a result, a high order discrete model is used to represent the power system, which consumes a significant amount of computing time.

The computing time for an adaptive power system stabilizer is approximately proportional to the square of the order of the discrete model used in the identification. A longer computing time affects the control performance, and this becomes even more significant if the oscillation frequency is relatively high. There must be a compromise between the order of the discrete model and the computing time for the parameter identification and optimization. Some research tries to solve these problems by designing an adaptive power system stabilizer without an identification model and by using different techniques (e.g., model-free adaptive control) to design wide-area power system stabilizers [35].

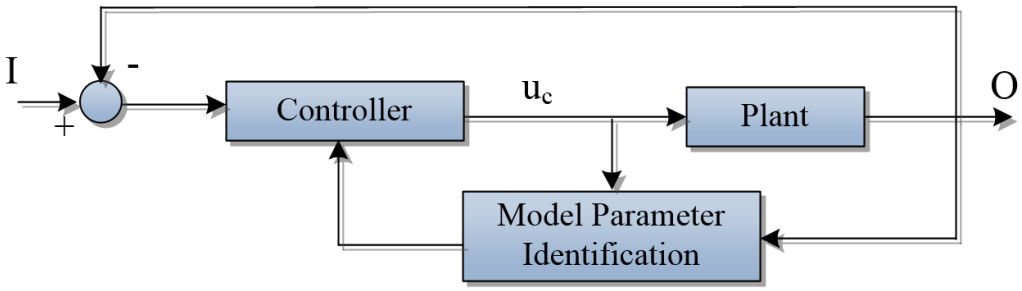

Figure 1.6. Block diagram of indirect adaptive control

1.2.3 Artificial Neural Network Based Power System Stabilizer

Artificial neural networks (ANN) attempt to achieve good performance via the dense interconnection of simple computational elements. Their structure is based on the present understanding of biological nervous systems. As mentioned in the preceding section, ANNs have been successfully implemented in identification systems, observers, and as adaptive controllers in non-linear dynamic systems. ANNs have the following advantages:

- capability of synthesizing complex and clear mapping;
- speed due to the parallel mechanism;
- robustness and fault tolerance; and
- adaptive adjustment to a new environment.

Based on its architecture, an artificial neural network has various types, such as a single layer feed-forward architecture, a multi-layer feed-forward architecture, and a recurrent network. The most common ANN used with the control system is the multi-layer feed-forward architecture [36] [37]. The ANN technique has been used for power system control as a power system stabilizer. Zhang *et al.* in [38] presented their PSS design based on the inverse input/output mapping of an artificial neural network. During the training, the output of the synchronous generator was desired

to store the reverse input and output mapping of the synchrony generator. After training the output of the synchronous generator was used as input to the PSS and the output of the PSS was the control signal. In [39], an ANN PSS design was presented for a multi-machine environment. The researchers used the accelerating power with delay as input to the controller and also used the multi-layer neural network with an error back propagation training method. The ANN PSS was trained based on the multi-layer perceptron with the error back propagation training method. Shamsollahi *et al.* in [40] introduced a neural network power system stabilizer design where the controller was applied directly to the power system without using a system identification technique to determine the states of the model using the back-propagation method. In [41], Changaroon *et al.* introduced a PSS-based neural network design approach. In order to reduce the time required to perform the standard method (multi-layer perceptron model) used to train the neural network, the authors employed a functional link network (FLN) instead of a hidden layer. They also used a recursive on-line training algorithm for the FLN model.

Segal *et al.* in [42] presented a method to design adaptive PSS based on a redial function neural network. The authors utilized this neural network to automatically tune the parameters of standard lead-lag PSS when the operating conditions are changed using an orthogonal least square algorithm. In [43], Chaturvedi et al. presented a generalized neuron based power system stabilizer in order to reduce the large training time of the ANN. The authors modified the generalized neuron (GN) model using fuzzy compensatory operators as collection operators. As aggregation functions, the generalized neuron GN has $\sum$, which utilizes a characteristic sigmoid function, and $\prod$, which uses a Gaussian characteristic function.

The authors in [25] extended the methodology that was used in [43] and applied it in a multi-machine environment. Baek *et al.* in [44] presented an ANN power system stabilizer-based

feed-forward neural network to calculate first-order derivatives required for the optimization of the nonlinear parameters of PSS output limits for a single machine infinite bus system and a multi-machine environment. In [27], the authors introduced an adaptive neurofuzzy power system stabilizer, which consists of an adaptive neuroidentifier to track the dynamic characteristic of the model and an adaptive neurofuzzy regulator. The neurofuzzy controller depends on both the fuzzy logic technique and the artificial neural network method. Kamalasadan and Swann in [45] introduced a model reference adaptive controller MRAC as a power system stabilizer, where the adaptation mechanism used the neural network identifier method and the controller is based on a feed-forward neural network technique. The authors used the controller in a multi-machine environment to reduce the power system oscillations. In [46], the authors used the same idea that was used in [45] to make the controller work effectively during normal operating conditions by using an explicit model reference adaptive control and full neural network outer loop control design. In [47], Farahani proposed a self-recurrent wavelet neural network controller to replace both the AVR and the power system stabilizer in the power system. The first derivative of a Gaussian function was used as a wavelet function in the hidden layer in the recurrent neural network. However, many of the above studies lack one or more factors that make the artificial neural network PSS perform well in real life such as uncomplicated structure, quick response (short computation time).

The success of ANNs to control unknown systems under significant uncertainties makes them highly attractive, yet there are some drawbacks in using them, as follows:

- Black box characteristics: It can be difficult for an outside observer to understand and modify the network decision-making process, as the initial value of the parameter is randomly chosen.

- ❖ Long training time: ANNs may require a long training time to obtain the desired performance. The time needed for training increases with the size of the ANN and with the complexity of the mapping.
- ❖ The large number of neurons and layers has an impact on the fault-tolerant capabilities of ANNs.

1.2.4 Fuzzy Logic-Based Power System Stabilizer

One of the methods used in controller design is fuzzy logic control (FLC) [36]. Fuzzy control systems are rule-based systems in which a set of fuzzy rules represents a control decision mechanism to adjust the effect coming from the system (fuzzification rule-based defuzzification). The following are some major features of FLC [48] [49]:

- ❖ Model-free: Unlike other classical control techniques, this method does not require the exact mathematical model of the system
- ❖ Nonlinear robust controller: FLC offers ways to implement simple but robust solutions that cover a broad range of system parameters and deal with major disturbances.
- ❖ Development time reduction: FLC works at two levels of abstraction: the symbol level and the compiled level. The symbol level is appropriate for describing application engineering strategies, while the compiled level is well understood by electronics engineers, since there is a well-defined translation between those levels. An FLC can help reduce communications problems.
- ❖ The FLC is knowledge based on the fuzzy control simulation strategy of the person controlling a process. Thus, the control strategy mimics a human way of thinking. The experience of the human operator can thus be implemented through an automatic control method, not through the slow response of a human controller.

The fuzzy logic technique-based controller has already been used as a power system stabilizer. In [50], the authors designed a power system stabilizer based on the fuzzy logic approach. Specifically, they used the speed and power output deviation as input signals for the controller. Toliyat *et al.* in [51] presented the design of a fuzzy logic power system stabilizer and tested it for both a single machine and a multi-machine power system. They selected the deviations of speed and acceleration to be inputs to the controller. As well as, they added signal, which is the modification of the terminal signal as a function of the acceleration power. The fuzzy controller decision was made using 49 rules, with each input fuzzified using seven triangle membership functions.

The authors in [52] introduced a global controller to coordinate the transient stability and small signal stability to make power systems more reliable. In this approach, the signal of the global controller is the average of the signals from local controllers, each weighted by an operating region membership function. In [53], the authors provided a fuzzy logic power system stabilizer based on the Takagi-Sugeno fuzzy logic control technique. The Takagi-Sugeno fuzzy system is described by fuzzy IF-THEN rules representing the local input-output relations of the nonlinear system. The controller has four input signals with a Gaussian membership function and one output going to the excitation system. In [54], the authors introduced simplified fuzzy logic PSS based on reducing the rules used in regular FLC (49-rule) (which are commonly employed in fuzzy control applications) to get a less complicated FLC based on its symmetry. The authors discovered that the simplified fuzzy logic PSS gives the same response as a fuzzy controller with the complete set of rules.

In [55], Vakula and Sudha designed a fuzzy logic power system stabilizer based on minimum rules. They used the differential evolution technique to tune the parameters of the

controller, discovering that the controller's input signals were rotor angle (δ), its first derivative (δ'), and second derivative (δ''). The inputs are scaled by three factors tuned using the differential evolution technique. As well, the output signal is scaled by a factor and optimized using the same method. The authors implemented their design for a single machine and a multi-machine power system. Cloughley *et al.* in [56], proposed an intelligent PSS based on Takagi-Sugeno fuzzy logic control and genetic algorithm optimization. The controller has two input signals – the deviation speed and its derivative. Each input is fuzzified using 7 membership functions and 49 fuzzy rules. A genetic algorithm was used to adjust the membership functions to dampen the oscillation in the power system. The authors in [57] extended the work proposed in [55] by using an evolutionary prisoner's dilemma, which is one of the classical games, to update the rules of the fuzzy linguistic model.

Designing stabilizers based on FLC is very attractive, and satisfactory results have been obtained. Although FLC introduces a useful tool to deal with complicated nonlinear and unlimited systems, it suffers from some major drawbacks, such as parameter tuning for the controller. At present, there is no systematic procedure for the design of FLC. The most straightforward approach is to define membership functions (MFs) and decision rules subjectively by studying the system or the existing controller. Therefore, there is a need for an efficient method to tune the MFs and decision rules to minimize the output error or to maximize the performance index. All the previous studies that proposed tuning MFs and adjusting the rules are very complicated and time-consuming methods that ultimately weaken the performance of the controller thus rendering them quite inefficient processes for the task at hand.

1.2.5 Wavelet Based Power System Stabilizer

Wavelet transforms have the capability to analyze non-stationary and non-periodic signals into time and frequency localized components simultaneously. The wavelet transforms focus on a signal with short time intervals for high-frequency components and a signal with long time intervals for low-frequency components. Wavelet transforms have been used for detecting transients in power system disturbances [58], fault diagnosis in induction machines [59], estimating the location of the fault [60], and in electrical motor drives [61]. Additionally, the wavelet technique can be used to detect electromechanical oscillations in power systems [62]. Hence, wavelet transforms can be used to compensate electromechanical disturbances in synchronous generators, thus indicating that they can be employed as a power system stabilizer. In [63], the authors proposed a power system stabilizer based on the wavelet technique. They used both the scaling coefficient and wavelet energy coefficient with border distortions of one cycle sliding window. The input of their proposed PSS was the real power and the first level of maximum overlap discrete wavelet transform (MODWT) was used to extract the electromechanical oscillations from the input signal which was used as input for the conventional lead-lag power system stabilizer.

Wavelet controllers have a few advantages over conventional and adaptive controllers. The following are some major features of a wavelet controller:

- Wavelet controllers are based on the filter-bank structure of orthogonal wavelet and scaling functions.
- A wide range of linear and nonlinear functions can be handled using wavelet controllers to obtain the desired degree of precision and conditions.
- Wavelet controllers are independent of an exact mathematical model of a system.

1.3 Problem Identification and Research Objectives

The late 20th century has seen a dramatic expansion of power systems around the world. Moreover, due in large part to their expansion, these systems have become increasingly complex and also feature a high system order. The more complicated the systems become, the more challenging it is to gauge their dynamic stability and adjust their controllers. To address these issues, the reduced model technique has been employed to mathematically define smaller system models from existing models, such that the properties of both systems are analogous properties. This study uses E. J. Davison's approach for decreasing the state space matrix (A) using dominant eigenvalues and eigenvectors. This strategic approach decreases the power system generation unit's matrix (A) order, while maintaining the identity of high bus voltage in the power generation unit. Therefore, current and voltage on the high bus voltage can be calculated and sent to another part of the power system either via fiber optic cables or by employing a phasor measurement unit (PMU). In order to implement this method, the dynamic model of the power system unit is linearized by taking the high voltage side of the generation unit as a reference instead of the infinite bus voltage as in the standard model. Thus, by applying this change, it is no longer necessary to estimate states, thereby reducing the amount of time required to make the measurements. Additionally, the model's parameters remain independent from those of the external system, so the PSS design remains likewise independent for all of the machines. In this way, a PSS can be developed for one machine and afterwards applied in a multi-machine system.

As electrical power systems contain thousands of interconnected elements, there are numerous categories of unpredictable issues that might occur. For example, faults in a transmission system with built-in protection system and small variations in the load might cause small signal disturbances within the electrical power system. These small signal fluctuations can persist for a

lengthy period, restricting the power transmitted through transmission lines. The probability of partial or complete blackouts is high when the power system is operating under stressed conditions. In other words, the system will be vulnerable. Standard control devices, such as governors and automatic voltage regulators (AVRs), might not be able to relieve these fluctuations in a short period. To mitigate these problems, most central power plants in interconnected grids have an additional control signal in the excitation system, known as a power system stabilizer (PSS). However, because the parameters of the standard PSS are fixed while the power system is highly nonlinear (i.e., it features configurations and parameters that change over time), a standard PSS might not be able to provide guaranteed optimal performance in many practical applications.

This study attempts to mitigate this limitation by implementing three types of smart power system stabilizers: an artificial neural network power system stabilizer (ANN-PSS), fuzzy logic power system stabilizer (FLPSS), and a modified multiresolution proportional-integral-derivative power system stabilizer (MMR-PID-PSS), based on the dynamic reduction of a power system model. These PSSs have been developed to refine the system's dynamic performance by adjusting the regulator's parameters in real time simulation with a broad range of operating conditions.

1.4 Outlines of the Dissertation

The remainder of this dissertation is arranged in the following order. Chapter 2 reviews linear techniques used to analyze small signal oscillations and extract information about system dynamic characteristics (state-space representation and linearization). It also performs a derivation of a linearizing model in a single synchronous generator connected to a network using a different linearization approach.

Chapter 3 discusses the model reduction approach to reduce the original higher order power system to a reduced order model. In this chapter, a comparison between the original model of the

power system and the reduced order one is given under several operating conditions and changes in parameters.

Chapter 4 presents the structure and tuning of the lead-lag power system stabilizer along with a brief explanation about the artificial neural network controller, and the design of an artificial neural network PSS (ANN-PSS) for a reduced order model. A comparison between the power system without PSS, with lead-Lag PSS, and with ANN-PSS is given for several different operating conditions and changes in parameters.

Chapter 5 presents a brief explanation about the fuzzy logic controller. Additionally, it includes the design of a novel fuzzy logic PSS (FLPSS) for a reduced order power system model. A comparison between the power systems without PSS, with ANN-PSS, with FLPSS is given under several different of operating conditions and changes in parameters.

Chapter 6 presents the proposed modified multiresolution proportional-integral-derivative power system stabilizer (MMR-PID-PSS) for a reduced order power system. At the beginning of the chapter, wavelet transforms and multi-resolution analysis are discussed. As well, mathematical analysis of the wavelet transforms is presented and principles of the multi-resolution PID controller are described. The design of the proposed MMR-PID-PSS is explained and then implemented for a single machine power system and a multi-machine environment. The stability analysis of the proposed MMR-PID-PSS is illustrated, and a comparison between the power system without PSS, with the proposed FLPSS and with the proposed MMR-PID-PSS is given under several different operating conditions for a single machine power system, 4-machine 10-bus power system, and 10-machine 39-bus power system. The conclusions and future work of this research are presented in Chapter 7, followed by references and appendices.

Chapter 2

2 Mathematical Analysis of the Power System

2.1 Introduction

Power systems consist of synchronous generators, power transformers, transmission lines (tie-lines and distribution lines), dynamic and static loads, and reactive energy sources, such as static var compensators (series capacitors, shunt capacitors, and shunt reactors). As defined in Chapter 1, a power system's ability to maintain synchronism following the occurrence small disturbances is referred to as dynamic stability. For small signal stability analysis, a dynamic model is required for the power system's major components (synchronous generator, excitation system, automatic voltage regulator [AVR], and others). This chapter reviews the linear techniques used to analyze small signal oscillations and to extract information about system dynamic characteristics [3] [7] [10].

2.2 State Space Representation

State-space representation is often used to describe the behavior of dynamic systems such as power systems. Hence, to model this particular behavior, a set of *n* first-order nonlinear ordinary differential equations is used, as follows [7] [10] [32] [36]:

$$\dot{x} = f(x, u, t) \tag{2.1}$$

where

$$x = [x_1 \ x_2 \ldots x_n]^T, \quad u = [u_1 \ u_2 \ \ldots u_r]^T, \quad f = [f_1 \ f_2 \ldots f_n]^T$$

The vector **x** refers to the state vector, and **u** is the vector of the inputs to the system. These are the external signals that affect system performance. The vector **f** is a nonlinear function, while *t* is time, *n* is system order, and *r* is number of inputs. If the derivatives of the state variables $\dot{\boldsymbol{x}}$ are

not explicit functions of time, the system is referred to as an autonomous system, in which case equation (2.1) becomes

$$\dot{x} = f(x, u) \tag{2.2}$$

The equation that relates the output vector to the state vector and the input variables can be written as:

$$y = g(x, u) \tag{2.3}$$

where

$$y = [y_1\ y_2 \dots y_m]^T, \quad g = [g_1\ g_2 \dots g_m\ ]^T$$

Vector **y** is the output vector, while vector **g** is the vector of nonlinear functions relating the state and input variables to the output variables

2.3 Linearization

For small signal disturbances, nonlinear differential equations that describe the behaviour of a dynamic system could be linearized for the purpose of analysis. The linearization process consists of initializing state vector $\mathbf{x}_0$ and input vector $\mathbf{u}_0$ around the equilibrium point. Equation (2.2) thus becomes

$$\dot{x}_0 = f(x_0, u_0) \tag{2.4}$$

For small perturbations in the state variables and input

$$x = x_0 + \Delta x, \quad u = u_0 + \Delta u \tag{2.5}$$

where Δ denotes a small deviation. Equation (2.2) then becomes

$$\dot{x} = \dot{x}_0 + \Delta\dot{x} = f[(x_0 + \Delta x), (u_0 + \Delta u)] \tag{2.6}$$

If the disturbances are small, system equations $f(x,u)$ can be expressed in terms of Taylor's series. With some simplification (e.g., neglecting the terms associated with second- and higher orders of power of Taylor's series), equation (2.2) can be expressed as follows:

$$\dot{x}_i = \dot{x}_{i0} + \Delta\dot{x}_i = f_i(x_0, u_0) + \frac{\partial f_i}{\partial x_1}\,\Delta x_1 + \cdots + \frac{\partial f_i}{\partial x_n}\Delta x_n + \frac{\partial f_i}{\partial u_1}\Delta u_1 + \cdots + \frac{\partial f_i}{\partial u_r}\Delta u_r \tag{2.7}$$

The above equation can then be divided into two equations:

$$\dot{x}_{i0} = f_i(x_0, u_0) \tag{2.8}$$

$$\Delta\dot{x}_i = \frac{\partial f_i}{\partial x_1}\Delta x_1 + \cdots + \frac{\partial f_i}{\partial x_n}\Delta x_n + \frac{\partial f_i}{\partial u_1}\Delta u_1 + \cdots + \frac{\partial f_i}{\partial u_r}\Delta u_r \tag{2.9}$$

By applying the same process to equation (2.3)

$$\Delta y_j = \frac{\partial g_j}{\partial x_1}\Delta x_1 + \cdots + \frac{\partial g_j}{\partial x_n}\Delta x_n + \frac{\partial g_j}{\partial u_1}\Delta u_1 + \cdots + \frac{\partial g_j}{\partial u_r}\Delta u_r \tag{2.10}$$

where i=1, 2, 3, … n, and j=1, 2, 3, …m

So, the linearized forms of equations (2.2) and (2.3) are

$$\Delta\dot{x} = A\,\Delta x + B\,\Delta u \tag{2.11}$$

$$\Delta y = C\,\Delta x + D\,\Delta u \tag{2.12}$$

$$A = \begin{pmatrix} \frac{\partial f_1}{\partial x_1} & \cdots & \frac{\partial f_1}{\partial x_n} \\ \vdots & \ddots & \vdots \\ \frac{\partial f_n}{\partial x_1} & \cdots & \frac{\partial f_n}{\partial x_n} \end{pmatrix}, \qquad B = \begin{pmatrix} \frac{\partial f_1}{\partial u_1} & \cdots & \frac{\partial f_1}{\partial u_r} \\ \vdots & \ddots & \vdots \\ \frac{\partial f_n}{\partial u_1} & \cdots & \frac{\partial f_n}{\partial u_r} \end{pmatrix}$$

$$C = \begin{pmatrix} \frac{\partial g_1}{\partial x_1} & \cdots & \frac{\partial g_1}{\partial x_n} \\ \vdots & \ddots & \vdots \\ \frac{\partial g_m}{\partial x_1} & \cdots & \frac{\partial g_m}{\partial x_n} \end{pmatrix}, \qquad D = \begin{pmatrix} \frac{\partial g_1}{\partial u_1} & \cdots & \frac{\partial g_1}{\partial u_r} \\ \vdots & \ddots & \vdots \\ \frac{\partial g_m}{\partial u_1} & \cdots & \frac{\partial g_m}{\partial u_r} \end{pmatrix} \tag{2.13}$$

Δx is the linearized state vector of dimension [n×1].

Δy is the linearized output vector of dimension [m×1].

Δu is the linearized input vector of dimension [r×1].

A is the system matrix of size [n×n].

B is the input matrix of dimension [n×r].

C is the output matrix of size [m×n].

D is the feed forward matrix size of [m×r].

By taking the Laplace transform for the equations (2.11) and (2.12), the state space equations can be obtained in the frequency domain as:

$$s\Delta X(s) - \Delta X(0) = A\Delta X(s) + B\Delta U(s) \tag{2.14}$$

$$\Delta Y(s) = C\Delta X(s) + D\Delta U(s) \tag{2.15}$$

The block diagram of the state-space representation can be obtained as shown in Figure 2.1. where, the initial condition $\Delta X(0)$ is assumed to be zero.

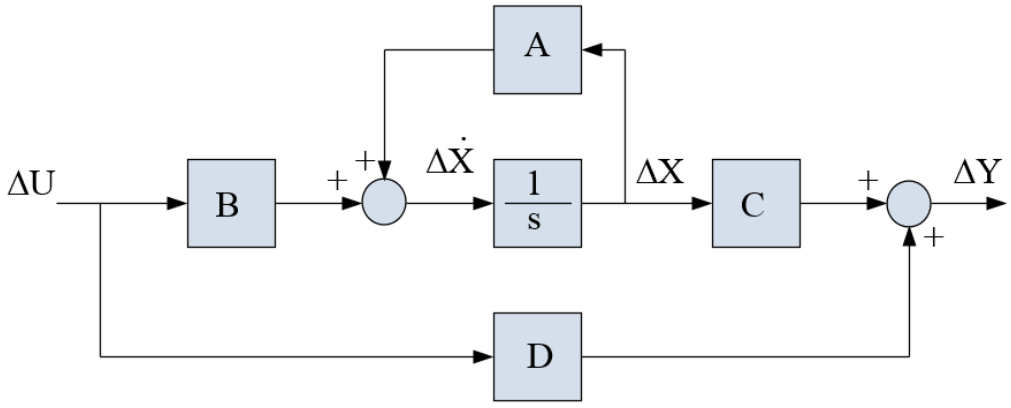

Figure 2.1 Block diagram of state space representation

2.4 Model Analysis

When the state space has been established, the stability of the system can be extracted and analyzed using eigenvalues, which can be obtained by solving the following equation [32] [36]

$$|A - \lambda I| = 0 \tag{2.16}$$

where (I) is the identity matrix and $\boldsymbol{\lambda}$ is the vector of eigenvalues.

The eigenvalues $\boldsymbol{\lambda}$ can be real or imaginary, as in $\lambda = \sigma \pm j\omega$. A system is said to be stable if the real parts of all eigenvalues are negative, and unstable if the real part of any eigenvalue is positive. If the real part of at least one eigenvalue is equal to zero while the real parts of all other eigenvalues are negative, then the system is borderline. The imaginary parts of the eigenvalues indicate a frequency of oscillation in rad/sec. The frequency of oscillation is calculated by $f = {}^{\omega}/_{2\pi}$, which is damped if the real part of the eigenvalue is negative. The damping coefficient (damping ratio) ζ, is defined as:

$$\zeta = \frac{-\sigma}{\sqrt{\sigma^2 + \omega^2}} \tag{2.17}$$

2.5 Modeling of the Power System

Assume that the external system is modeled as a reference bus at the secondary bus of a step-up transformer as shown in Figure 2.2. It consists of a synchronous generator represented by a two-axis model and equipped with IEEE type-1 excitation and governing turbine systems, instead of an infinite bus voltage in the classical method. This approach does not need to estimate or compute the value of the equivalent external reactance x_e, infinite bus voltage and rotor angle measured with respect to an external bus. Power system disturbances are determined based on information about power flow and the voltage at the secondary bus of the step-up transformer. The model shown in Figure 2.2 is used to obtain the modified linearized dynamic model (Heffron-Phillips or K-constant model [64]). The IEEE model 1.0 is used to model a synchronous generator [7] [10] [19] [21] [30].

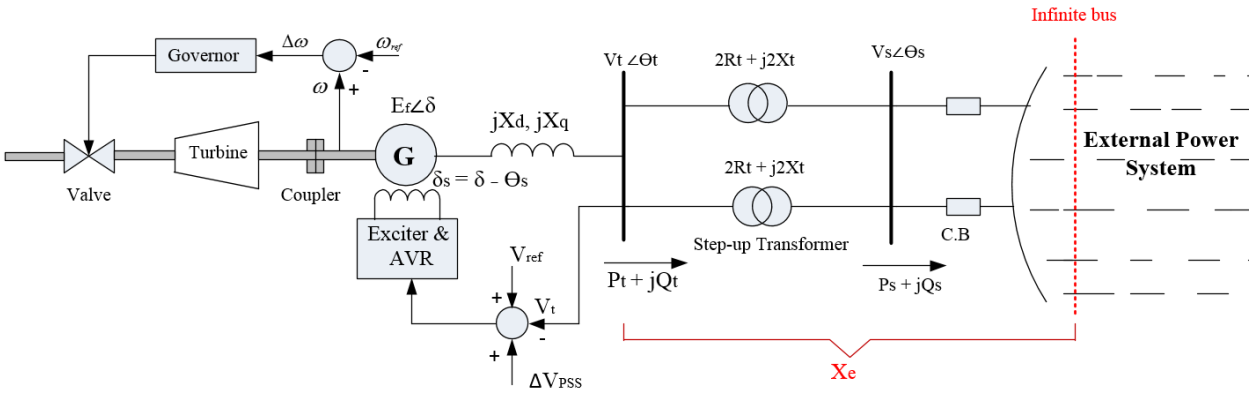

Figure 2.2 Single line diagram of the power system under study

The dynamic equations governing the system are as follows:

$$\frac{d\delta}{dt} = \omega_r - \omega_s \tag{2.18}$$

$$\dot{\delta} = \omega_0 \omega \tag{2.19}$$

where,

$\omega = (\omega_r - \omega_s)/\omega_0$ is the difference between rotor speed and synchronous speed in p.u, and

$\omega_0 = 2\pi f_0$ is the base angular speed

$$\dot{\omega} = \frac{1}{M}[T_m - T_e - K_D \omega] \tag{2.20}$$

$$\dot{E}'_q = \frac{1}{T'_{do}}[-E'_q + (x_d - x'_d) i_d + E_{fd}] \tag{2.21}$$

$$\dot{E}_{fd} = G_{exc}(s)\left(V_{ref} + V_{pss} - V_R\right) \tag{2.22}$$

$$T_e = E'_q i_q - (x_q - x'_d) i_d i_q \tag{2.23}$$

The stator algebraic equations are given by:

$$E'_q + x'_d i_d - R_a i_q = V_q \tag{2.24}$$

$$-x_q i_q - R_a i_d = V_d \tag{2.25}$$

From the phasor diagram in Figure 2.3 [65] [66], we can see that the rotor angle (with respect to the voltage $V_s\angle\theta_s$ of the high voltage bus) is defined as $\delta_s = \delta - \Theta_s$. The expressions of E_f, P_s, Q_s, i_d, i_q, and $\delta_{s,max}$ can be derived from the phasor diagram as follows:

$$|E_f| = |oa| + (i_s \sin(\theta + \delta_s))(x_d - x_q) \tag{2.26}$$

$$\overrightarrow{oa} = V_s\angle\Theta_s + i_s\left[(R_t + R_a) + j\left(x_q + x_t\right)\right] = |oa|\angle\delta \tag{2.27}$$

$$i_q = \frac{V_s \sin\delta_s}{x_q + x_t} \tag{2.28}$$

$$i_d = \frac{E_f - V_s \cos\delta_s}{x_d + x_t} \tag{2.29}$$

The complex power at the high voltage bus is:

$$S_s = 3 * V_S I_S^* = 3 * (V_s \cos\delta_s - jV_s \sin\delta_s)(i_q + ji_d) \tag{2.30}$$

Substituting equations (2.28) and (2.29) in equation (2.30), the real and reactive power equations at the high voltage bus are:

$$P_s = \frac{3E_f V_s}{(x_d + x_t)} \sin\delta_s + \frac{3V_s^2}{2(x_d + x_t)\left(x_q + x_t\right)}\left(x_d - x_q\right)\sin 2\delta_s \tag{2.31}$$

$$Q_s = \frac{3E_f V_S}{(x_d + x_t)} \cos\delta_s - \frac{3V_s^2}{2(x_d + x_t)\left(x_q + x_t\right)}\left[\left(x_d + x_q + 2x_t\right) - \left(x_d - x_q\right)\cos 2\delta_s\right] \tag{2.32}$$

From the phasor diagram in Figure 2.3, the power angle δ_s can be written as

$$\delta_s = \tan^{-1}\left[\frac{i_s\left(x_q + x_t\right)\cos\theta - i_s(R_a + R_t)\sin\theta}{V_s + i_s(R_a + R_t)\cos\theta + i_s\left(x_q + x_t\right)\sin\theta}\right] \tag{2.33}$$

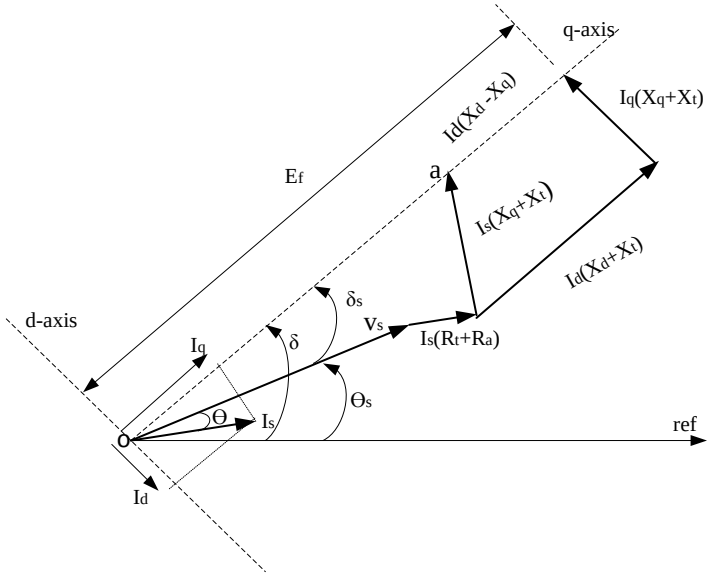

Figure 2.3 Phasor diagram for the system under study

2.6 Linearized Model

The standard linear model of a single machine infinite bus system (SMIB) (Heffron-Phillips- model [64]) can be obtained by linearizing system equations around an operating condition. The model details are provided in [7]. Here, the necessary modification will be to alter the linearizing system equation around the normal operating condition, since the system is linearized strictly from the secondary bus to the internal generator bus by defining the secondary bus of the step-up transformer as a reference bus instead of an infinite bus. By using this modification, one can design the power system stabilizer for a single machine system in a multi-machine environment depending on local measurements.

The synchronous generator is connected to the network by taking machine quantities from Park's transformation and transferring them to Kron's transformation rotating reference frame using a single transformation. In this way, a rotating reference frame with a single transformation

can provide a common reference frame. In the standard (Heffron-Phillips) model, the terminal voltage that illustrates these changes is given below [10] [13]:

$$v_Q + jv_D = (v_q + jv_d)e^{j\delta} = (i_q + ji_d)(R_e + jx_e)e^{j\delta} + E_b\angle 0 \tag{2.34}$$

This is Kirchhoff's voltage law between the generator terminal bus and the infinite bus. The subscripts *q* and *d* refer to the *q* and *d* axes in Park's reference frame, and *Q* and *D* refer to the *Q* and *D* axes in Kron's reference frame. The transformation from ABC to dq0 for a synchronous machine is

$$\begin{pmatrix} f_d \\ f_q \\ f_0 \end{pmatrix} = \frac{1}{\sqrt{3}} \begin{pmatrix} \sqrt{2}\cos\theta & \sqrt{2}\sin\theta & 1 \\ \sqrt{2}\cos\left(\theta - \frac{2\pi}{3}\right) & \sqrt{2}\sin\left(\theta - \frac{2\pi}{3}\right) & 1 \\ \sqrt{2}\cos\left(\theta + \frac{2\pi}{3}\right) & \sqrt{2}\sin\left(\theta + \frac{2\pi}{3}\right) & 1 \end{pmatrix}^{-1} \begin{pmatrix} f_a \\ f_b \\ f_c \end{pmatrix} \tag{2.35}$$

while the transformation from dq_0 to DQ_o can be obtained using:

$$\begin{pmatrix} f_D \\ f_Q \\ f_0 \end{pmatrix} = \begin{pmatrix} \cos\delta & \sin\delta & 0 \\ -\sin\delta & \cos\delta & 0 \\ 0 & 0 & 1 \end{pmatrix} \begin{pmatrix} f_d \\ f_q \\ f_0 \end{pmatrix} \tag{2.36}$$

where f could be any quantity of voltage, current, power, or flux.

The same equation for SMIB can be written between the high voltage bus of a step-up transformer and the terminal voltage bus of a synchronous generator, as follows. It is worth noting that this is the only modification proposed in this research to design a PSS independent of the external network.

$$v_Q + jv_D = (v_d + jv_d)e^{j\delta} = (i_q + ji_d)(R_t + jx_t)e^{j\delta} + v_s\angle\theta_s \tag{2.37}$$

From which:

$$v_q + jv_d = (i_q + ji_d)(R_t + jx_t) + v_s\angle\Theta_s e^{-j\delta} \tag{2.38}$$

From the phasor diagram $\delta = \delta_s + \Theta_s$, substituting in equation (2.38)

$$v_q + jv_d = (i_q + ji_d)(R_t + jx_t) + v_s\angle -\delta_s \tag{2.39}$$

Separating real and imaginary parts of this equation results in the modified stator algebraic equations referred to the high voltage bus of the step-up transformer, which is suitable for any synchronous generator in a multi-machine system.

$$v_q = R_t i_q - x_t i_d + v_s \cos\delta_s \tag{2.40}$$

$$v_d = R_t i_d + x_t i_q - v_s \sin\delta_s \tag{2.41}$$

Substituting Equation (2.25) when armature resistance is neglected in Equation (2.41) gives:

$$-R_t i_d - (x_t + x_q) i_q = -v_s \sin\delta_s \tag{2.42}$$

Substituting Equation (2.24) when armature resistance is neglected in Equation (2.40) gives:

$$(x'_d + x_t) i_d - R_t i_q = v_s \cos\delta_s - E'_q \tag{2.43}$$

Equations (2.42) and (2.43) can be rewritten in matrix form as:

$$\begin{pmatrix} (x'_d + x_t) & -R_t \\ -R_t & -(x_q + x_t) \end{pmatrix} \begin{pmatrix} i_d \\ i_q \end{pmatrix} = \begin{pmatrix} v_s \cos\delta_s - E'_q \\ -v_s \sin\delta_s \end{pmatrix} \tag{2.44}$$

The expressions for i_d, i_q are obtained by solving the above equation:

$$i_d = \frac{1}{A}\left[(x_q + x_t)(v_s \cos\delta_s - E'_q) + R_t v_s \sin\delta_s\right] \tag{2.45}$$

$$i_q = \frac{1}{A}\left[(x'_d + x_t)v_s \sin\delta_s - R_t\left(v_s \cos\delta_s - E'_q\right)\right] \tag{2.46}$$

where $A = (x'_d + x_t)\left(x_q + x_t\right) + R_t^2$

Equations (2.45) and (2.46) can be linearized by substituting $\delta = \delta_{s0} + \Delta\delta_s$, $v_s = v_{s0} + \Delta v_s$ and $E'_q = E'_{q0} + \Delta E'_q$, giving the following:

$$\Delta i_d = C_1\Delta\delta_S + C_2\Delta v_s + C_3 E'_q \tag{2.47}$$

$$\Delta i_q = C_4\Delta\delta_S + C_5\Delta v_s + C_6\Delta E'_q \tag{2.48}$$

where

$C_1 = \frac{1}{A}\left[R_t \cos\delta_{s0} - \left(x_t + x_q\right)\sin\delta_{s0}\right]v_{s0}$.

$C_2 = \frac{1}{A}\left[R_t \sin\delta_{s0} + \left(x_t + x_q\right)\cos\delta_{s0}\right]$.

$C_3 = \frac{1}{A}\left[-x_t - x_q\right]$.

$C_4 = \frac{1}{A}\left[(x_t + x'_d)\cos\delta_{s0} + R_t \sin\delta_{s0}\right]v_{s0}$.

$C_5 = \frac{1}{A}\left[(x_t + x'_d)\sin\delta_{s0} - R_t \cos\delta_{s0}\right]$.

$C_6 = \frac{R_t}{A}$.

By linearizing Equation (2.24) when armature resistance is neglected, one obtains

$$\Delta v_q = x'_d C_1\Delta\delta_S + x'_d C_2\Delta v_s + (1 + x'_d C_3)\Delta E'_q \tag{2.49}$$

Furthermore, by linearizing Equation (2.25) when armature resistance is neglected, one can obtain:

$$\Delta v_d = -x_q C_4 \Delta\delta_s - x_q C_5 \Delta v_s - x_q C_6 \Delta E'_q \tag{2.50}$$

Linearizing equation (2.23) gives:

$$\Delta T_e = K_1 \Delta\delta_S + K_{V1} \Delta v_s + K_2 \Delta E'_q \tag{2.51}$$

where

$K_1 = E_{q0} C_4 - (x_q - x'_d) i_{q0} C_1$, and $E_{q0} = E'_{q0} - (x_q - x'_d) i_{d0}$

$K_{v1} = E_{qo} C_5 - (x_q - x'_d) i_{q0} C_2$.

$K_2 = E_{q0} C_6 - (x_q - x'_d) i_{q0} C_3 + i_{q0}$.

By linearizing Equations (2.18) and (2.19) and applying the Laplace transform, we get:

$$\Delta\delta(s) = \frac{1}{s} \omega_0 \Delta\omega(s) \tag{2.52}$$

$$\Delta\omega(s) = \frac{1}{Ms} [\Delta T_m(s) - \Delta T_e(s) - K_D \Delta\omega(s)] \tag{2.53}$$

The equation of the field winding can be expressed as

$$T'_{do} \frac{dE'_q}{dt} = E_{fd} - E'_q + (x_d - x'_d) i_d \tag{2.54}$$

By linearizing this equation and taking the Laplace transform, we obtain

$$(1 + sT'_{do} K_3) \Delta E'_q(s) = K_3 \Delta E_{fd}(s) + K_3 K_4 \Delta\delta_s(s) + K_{v2} K_3 \Delta v_s(s) \tag{2.55}$$

where

$K_3 = \frac{1}{1 - (x_d - x'_d) C_3}$.

$K_4 = (x_d - x'_d) C_1$.

$K_{v2} = (x_d - x'_d)C_2.$

The disturbance in the terminal voltage can be expressed as follows [10] [12]

$$\Delta V_t = \frac{v_{d0}}{v_{t0}}\Delta v_d + \frac{v_{q0}}{v_{t0}}\Delta v_q \tag{2.56}$$

Substituting equations (2.49 and 2.50) in equation (2.56), gives:

$$\Delta V_t = K_5\Delta\delta_S + K_{v3}\Delta v_s + K_6\Delta E'_q \tag{2.57}$$

where

$$K_1 = \frac{v_{s0}}{A}[E_{q0}\{R_t \sin\delta_{s0} + (x'_d + x_t)\cos\delta_{s0}\} + (x_q - x'_d)i_{q0}\{(x_d + x_t)\sin\delta_{s0} - R_t \sin\delta_{s0}]$$

$$K_2 = \frac{E_{q0}\,R_t}{A} + i_{q0}(1 + \frac{i_{q0}(x_q - x'_d)(x_q + x_t)}{A})$$

$$K_3 = 1/\{1 + (x_q - x'_d)(x_q + x_t)/A\}$$

$$K_4 = \frac{(x_d - x'_d)}{A}\left[R_t \cos\delta_{s0} - \left(x_t + x_q\right)\sin\delta_{s0}\right]v_{s0}$$

$$K_5 = \frac{v_{s0}}{A * v_{t0}}[-v_{d0}\,x_q\{(x'_d + x_t)\cos\delta_{s0} + R_t \sin\delta_{s0}\} + v_{q0}\,x'_d\{R_t \cos\delta_{s0} - \left(x_t + x_q\right)\sin\delta_{s0}\}]$$

$$K_6 = \frac{-v_{d0}\,R_t\,x_q}{A * v_{t0}} + \frac{v_{q0}}{v_{t0}}(1 - \frac{x'_d\left(x_t + x_q\right)}{A})$$

$$K_{v1} = \frac{E_{q0}}{A}[(x'_d + x_t)\sin\delta_{s0} - R_t \cos\delta_{s0}] + \frac{(x_q - x'_d)(x_t + x_q)i_{q0}}{A}$$

$$K_{v2} = \frac{(x_d - x'_d)}{A}\left[R_t \sin\delta_{s0} + \left(x_t + x_q\right)\cos\delta_{s0}\right]$$

$$K_{v3} = \frac{x_q v_{d0}}{A * v_{t0}}[R_t \cos\delta_{s0} - (x'_d + x_t)\sin\delta_{s0}] + \frac{x'_d v_{q0}}{A * v_{t0}}[R_t \sin\delta_{s0} + \left(x_t + x_q\right)\cos\delta_{s0}]$$

The definitions of constants K_1 to K_6 are functions of v_s, δ_s , v_t, and machine currents. They are the same in the Heffron Phillips model except this model has references in δ, and E_b, and equivalent reactance X_e. As v_s is not constant in this research model; there are three new coefficients introduced, which are K_{v1}, K_{v2} and K_{v3}, as shown in Figure 2.4. If the voltage deviation is neglected and the angle voltage equals zero at the high bus voltage of the step-up transformer and transformer reactance is equal to equivalent, this model will be exactly the same as the Heffron-Phillips one [64].

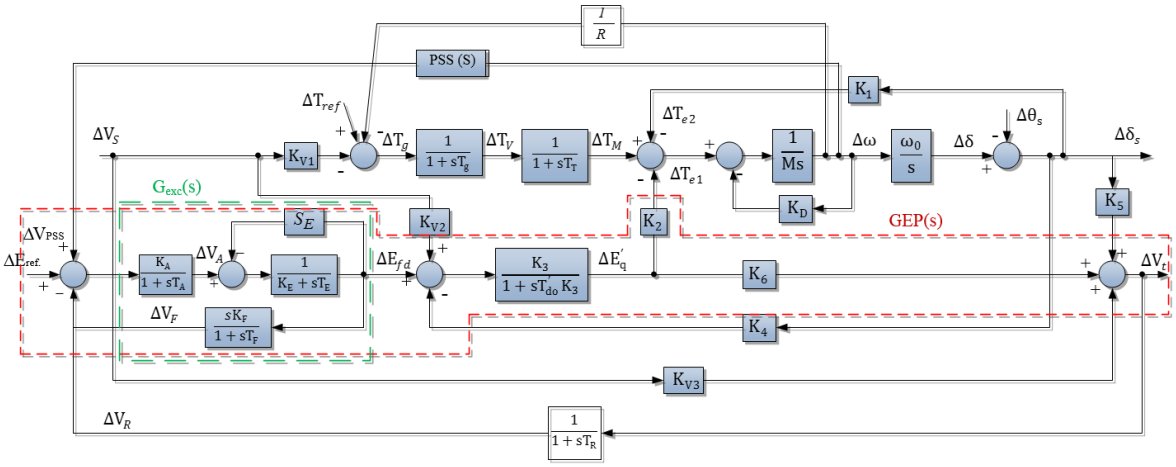

Figure 2.4 Linearizing model of a single synchronous generator connected to the network.

The linearized small disturbance equations for a system can be put in state variables, as follows:

$$\Delta\dot{X} = A\,\Delta X + B\,\Delta U \tag{2.58}$$

where

A and B are constant system matrices (depending on the parameters of the system) and have the dimensions of n×n and n×r, respectively,

ΔX is the state vector n×1

ΔU is the control vector r×1

$$\Delta X = [\Delta\delta \;\; \Delta\omega \;\; \Delta E'_q \;\; \Delta E_{fd} \, \Delta V_F \, \Delta V_A \, \Delta V_R \, \Delta T_m \, \Delta T_V \,]^T \tag{2.59}$$

$$\Delta U = [\Delta V_s \;\; \Delta T_{ref} \;\; \Delta E_{ref}]^T \tag{2.60}$$

$$A = \begin{bmatrix} 0 & \omega_\circ & 0 & 0 & 0 & 0 & 0 & 0 & 0 \\ \frac{-K_1}{M} & \frac{-K_D}{M} & \frac{-K_2}{M} & 0 & 0 & 0 & 0 & \frac{1}{M} & 0 \\ \frac{-K_4}{T'_{do}} & 0 & \frac{-1}{T'_{do}K_3} & \frac{1}{T'_{do}} & 0 & 0 & 0 & 0 & 0 \\ 0 & 0 & 0 & -\frac{S_E + K_E}{T_E} & 0 & \frac{1}{T_E} & 0 & 0 & 0 \\ 0 & 0 & 0 & -\frac{S_E K_F + K_E K_F}{T_E T_F} & \frac{-1}{T_F} & \frac{K_F}{T_E T_F} & 0 & 0 & 0 \\ 0 & 0 & 0 & 0 & \frac{-K_A}{T_A} & \frac{-1}{T_A} & \frac{-K_A}{T_A} & 0 & 0 \\ \frac{K_5}{T_R} & 0 & \frac{K_6}{T_R} & 0 & 0 & 0 & \frac{-1}{T_R} & 0 & 0 \\ 0 & 0 & 0 & 0 & 0 & 0 & 0 & \frac{-1}{T_T} & \frac{1}{T_T} \\ 0 & \frac{-1}{RT_g} & 0 & 0 & 0 & 0 & 0 & 0 & \frac{-1}{T_g} \end{bmatrix} \tag{2.61}$$

$$B = \begin{bmatrix} 0 & 0 & \frac{K_{V2}}{T'_{do}} & 0 & 0 & 0 & \frac{K_{V3}}{T_R} & 0 & \frac{-K_{V1}}{T_g} \\ 0 & 0 & 0 & 0 & 0 & 0 & 0 & 0 & \frac{1}{T_g} \\ 0 & 0 & 0 & 0 & 0 & \frac{K_A}{T_A} & 0 & 0 & 0 \end{bmatrix}^T \tag{2.62}$$

2.7 Summary

This chapter discussed the mathematical model of a power system consisting of a synchronous generator connected to a network. The behaviour of a dynamic power system was described by a set of *n* first-order nonlinear ordinary differential equations. This research is mainly concerned with the ability of a power system to maintain synchronism under small disturbances; thus, as the disturbances are considered to be sufficiently small, the linearization of the system equations is possible for the purpose of analysis. Although the power system is highly nonlinear, a wealth of information is obtained from the linearized model around an operating point. This permits the linear control system theory to be applied for system analysis, even though the system is inherently nonlinear. Some power system state variables are not measurable, and the external equivalent reactance has to be estimated. In addition, in multi-machine systems, full state feedback controllers require the feedback of other machine states.

This chapter utilized the recently proposed modified Heffron-Phillips model, which is derived by taking the secondary bus voltage of a step-up transformer as a reference instead of the infinite bus in order to solve the above problems. As a result, the linearizing model of a single generator connected to the network and the linearized state-space equation were obtained. These, will be used in the next chapters to test power system under a variety of operating conditions and design power system stabilizers.

Chapter 3

3 Reduced Order Model of the Power System

3.1 Introduction

Over the years, significant attention has been given to the development of simplified models primarily for the purpose of determining the dynamic behaviour of electrical machines during large excursions in some or all machine variables. The behaviour of synchronous machines was predicted by a set of steady-state voltage equations with modifications to account for transient conditions along with the dynamic relationship between rotor angle and torque. As mentioned in Chapter 2, the simplified model of a synchronous machine was obtained by neglecting the stator electrical transients and for all power system components connected to the stator (e.g., power transformer and transmission lines), this model is used widely in the industry as an analysis tool [7] [10] [13]. The basic generation unit of a power system consists of a synchronous generator, an automatic voltage regulator (AVR), a turbine, a governor, a power transformer and transmission lines, as shown in Figure 3.1.

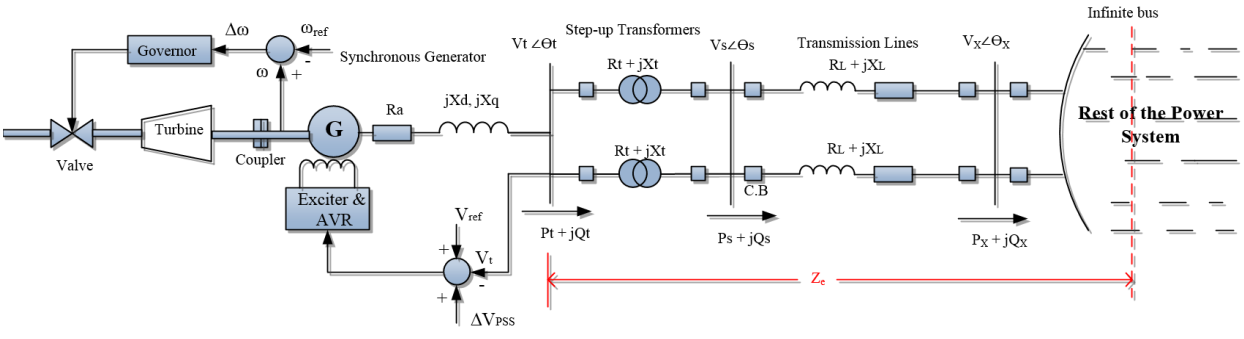

Figure 3.1. Power system generation unit connected to the network

In Figure 3.1, static representation of the external total impedance Z_T is given by the following equation:

$$Z_T = R_T + jx_T = \frac{R_L + jX_L}{2} + \frac{R_t + jX_t}{2} \tag{3.1}$$

In this chapter, the power system is linearized by taking high bus voltage X as a reference to include the effect of transmission lines. The dynamic behavior of this basic unit can be expressed by a set of first-order differential equations. The overall state-space matrix of the basic unit of the power system ends with a ninth order model. For a large interconnected power system consisting of 2500 power generation plants, for example, each power station contains four generators. This system will have a state-space matrix with $90{,}000^{th}$-order. The problems inherent in high-order models of power system are very time-consuming, occupy a massive amount of space in a computer's random-access memory (RAM), and lead to an unreliable controller. Also, ultra-high orders require a large number of states to be measured and a significant number of controller components. The reduction technique has been developed to overcome these difficulties.

Model reduction is a mathematical technique that is applied to the original model, high-dimensional full-order system in order to obtain a smaller system model with properties similar to the original model. Several authors have discussed methods of determining simplified models for dynamic power systems. One of these methods is called the state variable grouping technique, which involves dividing the system variables into two groups based on their speed and response [67] [68] [69]. Another method reduces the dynamic model for generators that are outside an interesting area and which can be replaced by a dynamic equivalent. In this approach, interconnected power systems are partitioned into two areas: an internal area that needs to be well-

represented, and an outside area that can be replaced by a dynamic equivalent [70], as shown in Figure 3.2. The construction of a dynamic equivalent involves the following three steps.

A. Identification of coherent generators.

B. Aggregation of generator terminal buses and elimination of the load buses.

C. Aggregation of coherent generators models and their control devices.

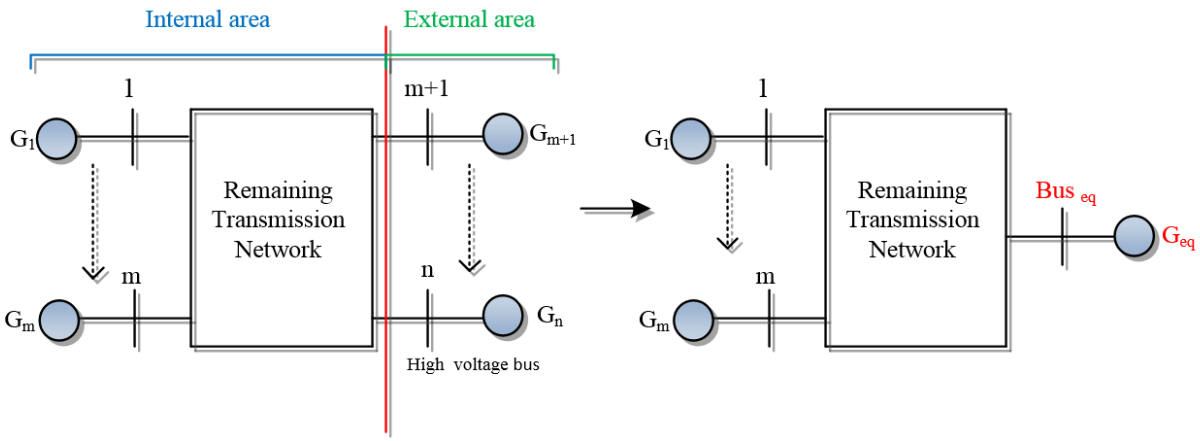

Figure 3.2. Dynamic model reduction for external area

As a result, the identities of all the generator terminal buses in a full-order model within the external area were lost in the reduced-order model. These types of reduced-order models are used only to estimate oscillation and assist small-signal stability. However, the models are not very useful to design control systems, as there is no clear way to implement a controller in the original system from a reduced-order model that does not maintain the identities of its buses [71].

E. J. Davison [72] provided a general method to reducing the state-space matrix (A) that depends on dominant eigenvalues and eigenvectors. The present research will use this method to minimize the order of matrix (A) of the power system under study while preserving the high bus voltage from the original system at each unit, whose voltage and injection current can be calculated

and sent to another part of the power system using PMUs or fiber optic cables. Figure 3.3 shows the block diagram of an interconnected power system, where each generation unit could represent one synchronous generator connected to the network or a group of non-overlap coherent synchronous generators.

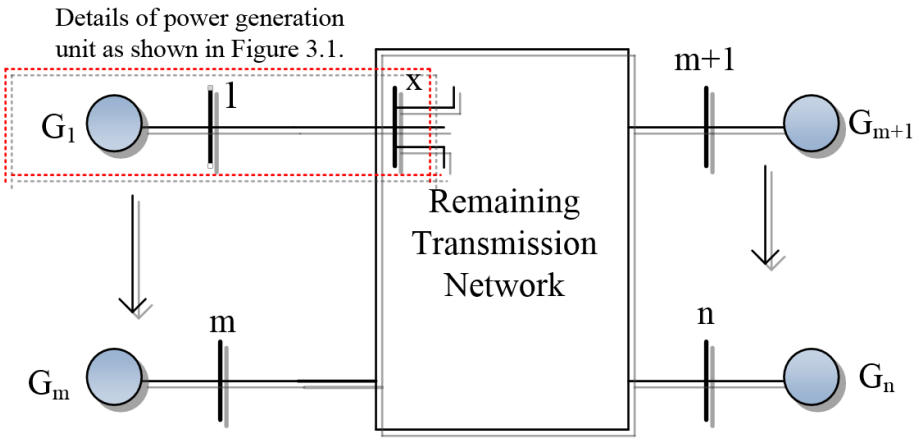

Figure 3.3. Block diagram of the entire power system

3.2 Analytical Process of the Reduction Approach

As mentioned above, this thesis will use E. J. Davison's methodology to obtain the reduced order model of the power system unit, depending on controlling eignvalues and eigenvectors. The linearized small disturbance equation for the power system unit can be written in a state variable, as follows:

$$\Delta\dot{X} = A\,\Delta X + B\,\Delta U \tag{3.2}$$

The matrix (A) of the system, which is given in the above equation, can be written as:

$$\Lambda = \mathrm{M}^{-1} * \mathrm{A} * \mathrm{M} \tag{3.3}$$

In equation (3.3), the product $(\mathrm{A} * \mathrm{M})$ may be written regarding eigenvalues and eigenvectors:

$$\mathrm{A} * \mathrm{M} = [\mathrm{Am}_1 | \mathrm{Am}_2 | \ldots . | \mathrm{Am}_\mathrm{n}] = [\lambda_1 \mathrm{m}_1 \, | \lambda_2 \mathrm{m}_2 \, | \ldots . \, | \lambda_\mathrm{n} \mathrm{m}_\mathrm{n}] \tag{3.4}$$

because $\mathrm{Am}_\mathrm{i} = \lambda_\mathrm{i} \mathrm{m}_\mathrm{i}$ is the relationship that defines eigenvalue λ_i. Equation (3.4) can be rearranged and written as follows:

$$\mathrm{A} * \mathrm{M} = [\mathrm{m}_1 | \mathrm{m}_2 | \ldots . | \mathrm{m}_\mathrm{n}] \begin{bmatrix} \lambda_1 & 0 & \cdots & 0 \\ 0 & \lambda_2 & \cdots & 0 \\ \vdots & \vdots & \ddots & \vdots \\ 0 & 0 & \cdots & \lambda_\mathrm{n} \end{bmatrix} = \mathrm{M} * \Lambda \tag{3.5}$$

where

$$\mathrm{M} = [\mathrm{m}_1 | \mathrm{m}_2 | \ldots . | \mathrm{m}_\mathrm{n}] = \begin{bmatrix} \mathrm{m}_{11} & \mathrm{m}_{12} & \cdots & \mathrm{m}_{1\mathrm{n}} \\ \mathrm{m}_{21} & \mathrm{m}_{22} & \cdots & \mathrm{m}_{2\mathrm{n}} \\ \vdots & \vdots & \ddots & \vdots \\ \mathrm{m}_{\mathrm{n}1} & \mathrm{m}_{\mathrm{n}2} & \cdots & \mathrm{m}_{\mathrm{nn}} \end{bmatrix} \tag{3.6}$$

Thus, equation (3.2) can be written as:

$$\Delta \dot{\mathrm{X}} = (\mathrm{M} * \Lambda * \mathrm{M}^{-1}) \, \Delta \mathrm{X} + (\mathrm{M}^{-1} * \, \mathrm{M} * \mathrm{B}) \Delta \mathrm{U} \tag{3.7}$$

where

A and B are constants of system matrices depending on the parameters of the system and have the dimensions [n×n] and [n×r], respectively,

ΔX is the state vector [n×1]

ΔU is the control vector [r×1]

M is the matrix of eigenvectors

Λ is the diagonal matrix of eigenvalues

Assuming initial conditions are zero, the time solution of equation (3.2) is as follows:

$$\Delta x(t) = \int_0^t \Phi(t-\tau) B \Delta u(\tau)\, d\tau \tag{3.8}$$

where

$\Phi(t)$ is the transition matrix of the system.

By assuming the following:

$$\begin{aligned} B\Delta u(t) &= 0, \qquad t < 0 \\ B\Delta u(t) &= B, \qquad t \geq 0 \end{aligned} \tag{3.9}$$

the transition matrix in equation (3.8) can be expressed by

$$\Phi(t-\tau) = M e^{\Lambda(t-\tau)} M^{-1} \tag{3.10}$$

In which case, equation (3.8) becomes

$$\Delta x(t) = \int_0^t M e^{\Lambda(t-\tau)} M^{-1} B \Delta u(\tau)\, d\tau \tag{3.11}$$

By considering the assumption above, the integration of equation (3.11) can be formulated as:

$$\Delta x(t) = M \begin{bmatrix} \frac{1-e^{\lambda_1 t}}{-\lambda_1} & 0 & \cdots & 0 \\ 0 & \frac{1-e^{\lambda_2 t}}{-\lambda_2} & \cdots & 0 \\ \vdots & \vdots & \ddots & \vdots \\ 0 & 0 & \cdots & \frac{1-e^{\lambda_n t}}{-\lambda_n} \end{bmatrix} M^{-1} B \tag{3.12}$$

Assuming that the inverse of the eigenvector matrix M is:

$$M^{-1} = [n_1|n_2| \dots .|n_n] = \begin{bmatrix} n_{11} & n_{12} & \cdots & n_{1n} \\ n_{21} & n_{22} & \cdots & n_{2n} \\ \vdots & \vdots & \ddots & \vdots \\ n_{n1} & n_{n2} & \cdots & n_{nn} \end{bmatrix} \quad (3.13)$$

Thus, the time solution for equation (3.2) can be written as follows:

$$\Delta x(t) = m_1 \left(\frac{1 - e^{\lambda_1 t}}{-\lambda_1}\right) n_1 B + m_2 \left(\frac{1 - e^{\lambda_2 t}}{-\lambda_2}\right) n_2 B + \cdots + m_n \left(\frac{1 - e^{\lambda_n t}}{-\lambda_n}\right) n_n B \quad (3.14)$$

where $\Delta x(t) = [\Delta x_1 \ \Delta x_2 \dots . \Delta x_n]^T \ B = [b_1 \ b_2 \dots b_n]^T$

Similarly, the time solution for a reduced system can be found, where the reduction has an order of z and ($z < n$)

$$\Delta x^r(t) = m_1^r \left(\frac{1 - e^{\lambda_1^r t}}{-\lambda_1^r}\right) n_1^r B^r + m_2^r \left(\frac{1 - e^{\lambda_2^r t}}{-\lambda_2^r}\right) n_2^r B^r + \cdots + m_z^r \left(\frac{1 - e^{\lambda_z^r t}}{-\lambda_z^r}\right) n_z^r B^r \quad (3.15)$$

By comparing equations (3.14) and (3.15), a reduced-order model can be found, which can be described by the following differential equation:

$$\Delta \dot{x}^r = A^r \Delta x^r + B^r \Delta U \quad (3.16)$$

where

$$A^r = M^r \Lambda^r (M^r)^{-1} \quad (3.17)$$

$$B^r = M^r (M^{-1} B)^r \quad (3.18)$$

and

A^r and B^r are reduced system matrices,

Δx^r is the reduced state vector corresponding to the retained state vector,

M^r is a square matrix representing a subset of the complete eigenvector matrix M (its columns are selected based on the dominant eigenvalue and its rows are selected based on the retained state variables),

Λ^r is a diagonal matrix of the dominant eigenvalues, and

$(M^{-1}B)^r$ is a diagonal matrix consisting of the retained rows of $(M^{-1}B)$ corresponding to Δx^r

3.3 Digital Simulation Results

The power system shown in Figure 3.1is used for digital simulation results and consists of a single equivalent machine connected to a network. The complete data for this system is given in Appendix A. The nominal operating condition is chosen as real power P = 0.75 p.u and reactive power Q = 0.0 p.u (unity power factor). The A and B matrices are given by:

$$A = \begin{bmatrix} 0 & 314 & 0 & 0 & 0 & 0 & 0 & 0 & 0 \\ -0.1131 & 0 & -0.1325 & 0 & 0 & 0 & 0 & 0.1 & 0 \\ -0.2826 & 0 & -0.4630 & 0.1667 & 0 & 0 & 0 & 0 & 0 \\ 0 & 0 & 0 & -0.8211 & 0 & 1.0526 & 0 & 0 & 0 \\ 0 & 0 & 0 & -0.0328 & -1.0 & 0.0421 & 0 & 0 & 0 \\ 0 & 0 & 0 & 0 & -2000 & -20 & -2000 & 0 & 0 \\ -0.6836 & 0 & 12.0765 & 0 & 0 & 0 & -33.3333 & 0 & 0 \\ 0 & 0 & 0 & 0 & 0 & 0 & 0 & -0.6667 & 0.6667 \\ 0 & -40 & 0 & 0 & 0 & 0 & 0 & 0 & -2.0 \end{bmatrix}$$

$$B = \begin{bmatrix} 0 & 0 & 0 \\ 0 & 0 & 0 \\ -0.1227 & 0 & 0 \\ 0 & 0 & 0 \\ 0 & 0 & 0 \\ 0 & 0 & 2000 \\ 14.0834 & 0 & 0 \\ 0 & 0 & 0 \\ -0.2543 & 2.0 & 0 \end{bmatrix}$$

3.3.1 Eigenvalue Analysis

In this dissertation, MATLAB software is used to determine the eigenvalues of the system under study during different operating conditions. The eigenvalues of the original system are either real or complex conjugate pairs, keeping in mind that the real part of every eigenvalue must be negative to create a stable system. The imaginary parts of complex conjugate pairs of eigenvalues with dimensions rad/sec indicate a frequency of the oscillation, which is damped if the real parts, called the damping coefficients, are negative.

Moreover, values of damping coefficients are a measure of system damping. The reciprocal of the absolute value of damping coefficient gives a corresponding time constant, and is a measure of the time required for the system to reach the steady-state condition. Generally, the eigenvalues of the original system (Λ) can be divided into three groups. The first group is those that are very close to the origin. They are called dominant eigenvalues, and the final transient of the system depends upon dominant eigenvalues. The second group is those that have intermediate values that play a dominant role in the transient response. The third group is those that are most distant from the origin, such that the group has an impact on the initial transient response. The eigenvalues can be calculated using the following equation:

$$|A - \lambda I| = 0 \tag{3.19}$$

Table 3.1. Eigenvalues of power system under study at normal operating condition

Modes	Eigenvalue
1	-0.1483 + j5.9251
2	-0.1483 - j5.9251
3	-6.0560
4	-14.6125
5	-0.7643 + j1.0037
6	-0.7643 - j1.0037
7	-0.641
8	-33.0775
9	-2.0721

3.3.2 Model Reduction Procedure

The model consisting of a synchronous generator connected to a network reduces from ninth-order model (A) to a third-order one (A^r). The resulting states are the rotor angle deviation ($\Delta\delta$) and the rotor speed deviation ($\Delta\omega$), which are the state variables representing the dominant eigenvalues. From the intermediate group of eigenvalues, the measurable state of the exciter voltage deviation (ΔE_{fd}) has been retained. At the nominal operating condition of P = 0.75 p.u and Q = 0.0 p.u, the reduced-order model is calculated using a MATLAB program, giving the following results:

$$A^r = \begin{bmatrix} 0 & 314 & 0 \\ -0.1125 & -0.263 & 0.0015 \\ -0.1631 & -370.26 & -14.6459 \end{bmatrix} \tag{3.20}$$

A comparison between the original model and the reduced model is carried out at different operating conditions to test the effectiveness and reliability of the third-order model. Firstly, the systems are tested at the unity power factor (Q = 0.0 p.u), after which the eigenvalues for the reduced-order model are calculated and compared with the complete model, as shown in Table 3.2. Figure 3.4 and Figure 3.5 show the time response of the rotor angle deviation and rotor speed deviation for both the original and reduced system due to a 1% step increase in the input reference voltage applied at time 1 sec.

Table 3.2. Eigenvalues of original and reduced systems at unity power factor

Real power P (p.u)	Eigenvalues	
	Original system	Reduced system
P = 0.50	-0.1505± j5.6653 -6.0560 -14.8780 -0.7835 ± j0.9774 -0.6321 -33.0348 -2.0635	-0.1505± j5.6653 -14.8780
P = 0.75	-0.1483 ± j5.9251 -6.0560 -14.6124 -0.7643 ± j1.0037 -0.641 -33.0775 -2.0721	-0.1483 ± j5.9251 -14.6124
P = 1.0	-0.1304 ± j5.8743 -6.0668 -14.3767 -0.8590 ± j1.0851 -0.6478 -33.1188 -2.0953	-0.1304 ± j5.8743 -14.3767
P = 1.15	-0.0995 ± j5.6769 -5.9243 -14.2826 -0.9838 ± j1.1506 -0.6505 -33.1379 -2.1219	-0.0995 ± j5.6769 -14.2826
P = 1.25	-0.0600 ± j5.4795 -5.7539 -14.2366 -1.1105 ± j1.1941 -0.6519 -33.1488 -2.1517	-0.0600 ± j5.4795 -14.2366

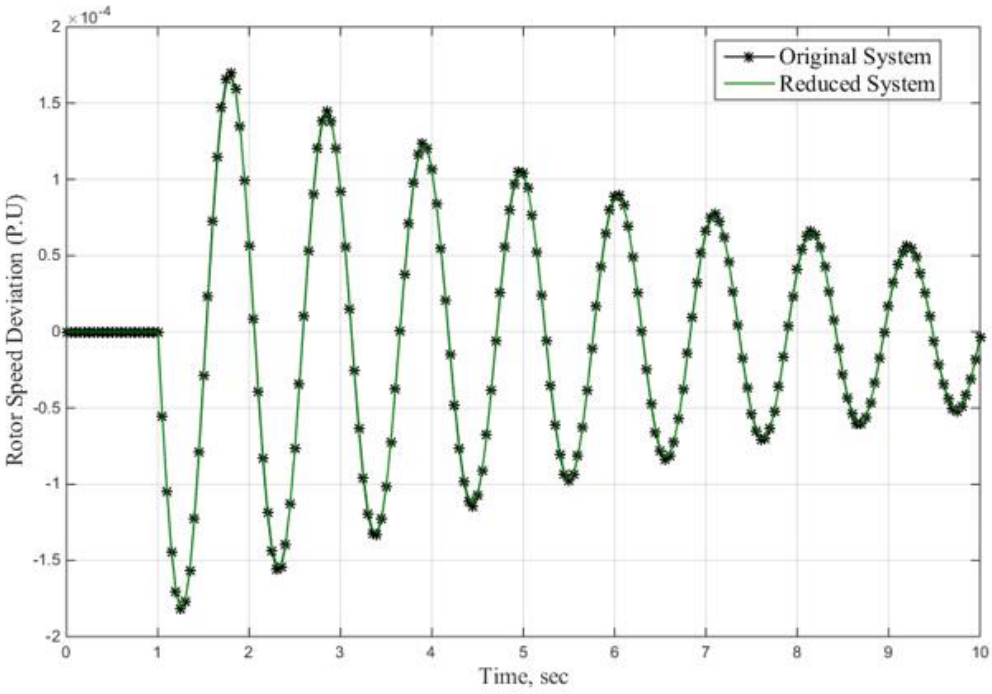

Figure 3.4. Time response of Δω due to disturbance at normal operating conditions

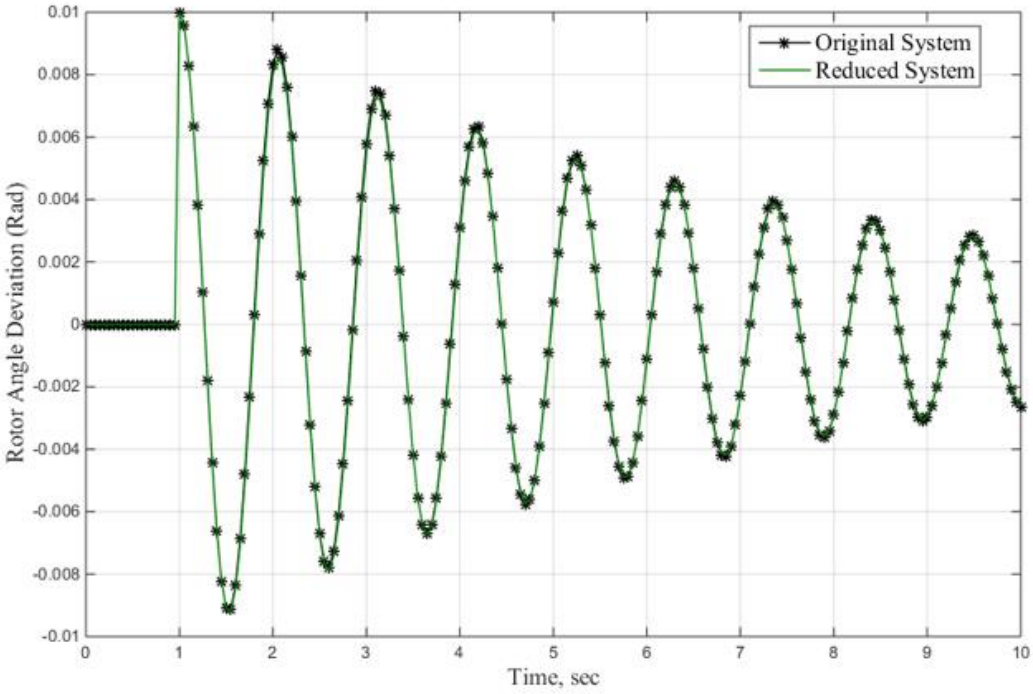

Figure 3.5. Time response of Δδ due to disturbance at normal operating conditions

Secondly, in comparing the original and reduced power systems at lagging and leading power factors, the eigenvalues of both systems are tabulated, as shown in Table 3.3. This is illustrated in Figures 3.6 to 3.9, which clearly demonstrate acceptable performance.

Table 3.3. Eigenvalues of original and reduced systems at lagging and leading power factors

(p.u)	Eigenvalues	
	Original system	Reduced system
P = 0.75 Q = 0.25	-0.0898 ± j5.6032 -5.4404 -14.9844 -0.9734 ± j1.0443 -0.6365 -33.0310 -2.0781	-0.1067± j5.6624 -14.9380
P = 0.75 Q = 0.5	-0.0614 ± j5.4567 -4.9433 -15.1327 -1.1795± j1.0488 -0.6336 -32.0021 -2.0906	-0.0614 ± j5.4567 -15.1327
P = 0.85 Q = 0.35	-0.0898 ± j5.6032 -5.2665 -14.9844 -1.0532± j1.0592 -0.6367 -33.0254 -2.0851	-0.0898 ± j5.6032 -14.9844
P = 1.25 Q = 0.6	0.0168 ± j 5.1361 -3.5258 -14.8905 -1.4859 ± j 1.1313 -0.6433 -33.0518 -2.2046	0.0168 ±j 5.1361 -14.8905
P = 0.75 Q = -0.25	-0.1745 ± j6.1816 -6.8177 -14.0596 -0.5925± j0.9453 -0.6479 -33.1507 -2.0741	-0.1745 ± j6.1816 -14.0596
P = 0.75 Q = -0.5	-0.1695 ± j 6.1257 -7.7936 -13.1287 -0.5096 ± j0.9307 -0.6567 -33.2554 -2.0914	-0.1695 ± j 6.1257 -13.1287
P = 0.85 Q = -0.35	-0.1658 ± j6.1095 -7.1182 -13.6704 -0.6094± j0.9882 -0.6533 -33.2026 -2.0890	-0.1658 ± j6.1095 -13.6704
P = 1.25 Q = -0.6	0.3498 ± j4.4803 -6.7631 -12.9522 -1.4594 ± j1.1945 -0.6623 -33.3070 2.3803	0.3498 ± j4.4803 -12.9522

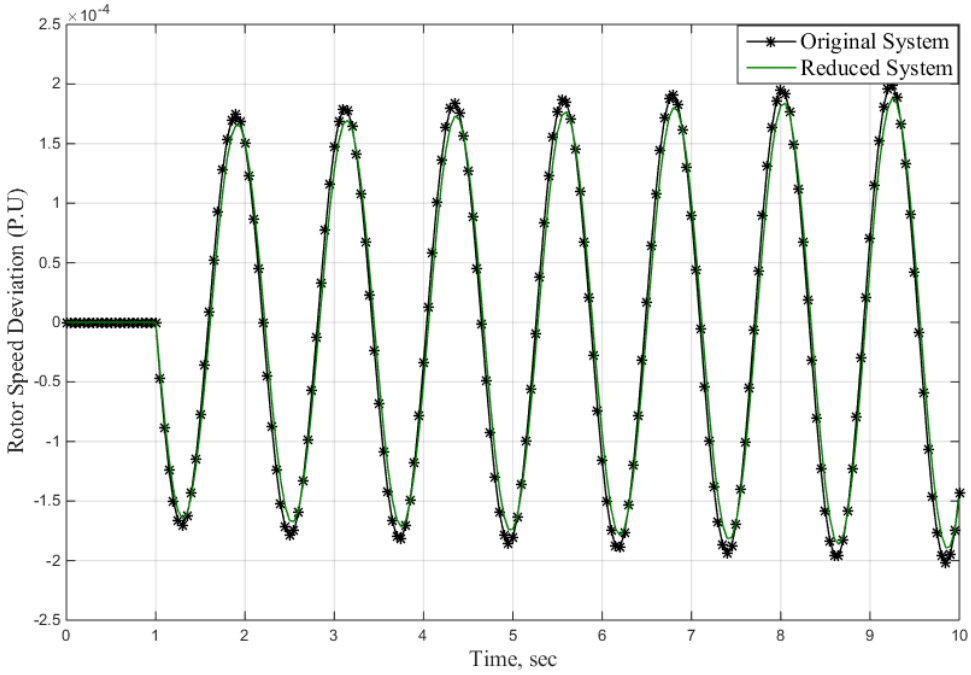

Figure 3.6. Time response of Δω due to disturbance at lagging power factor (P = 1.25 p.u, Q = 0.6 p.u)

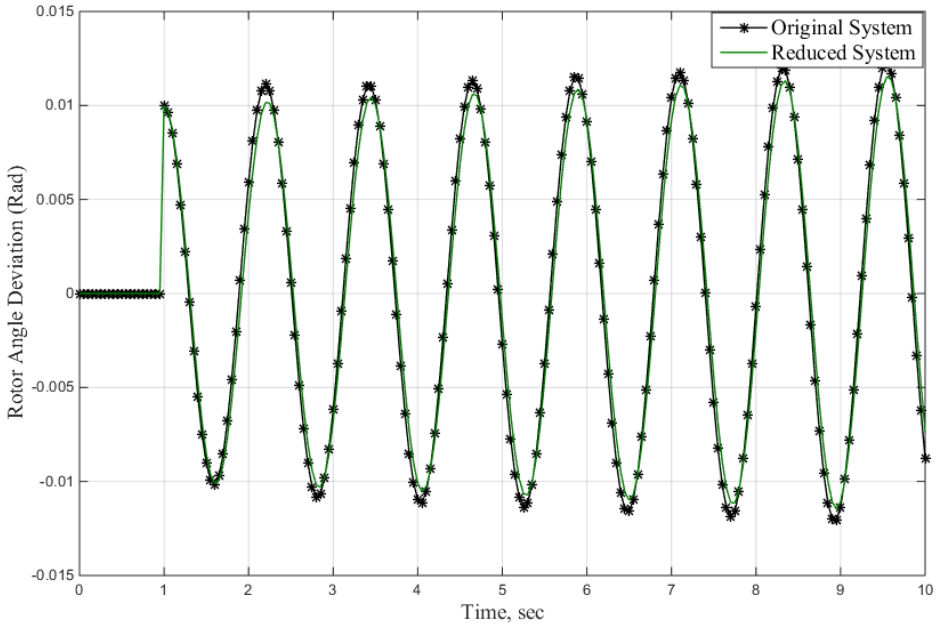

Figure 3.7. Time response of Δδ due to disturbance at lagging power factor (P = 1.25 p.u, Q = 0.6 p.u

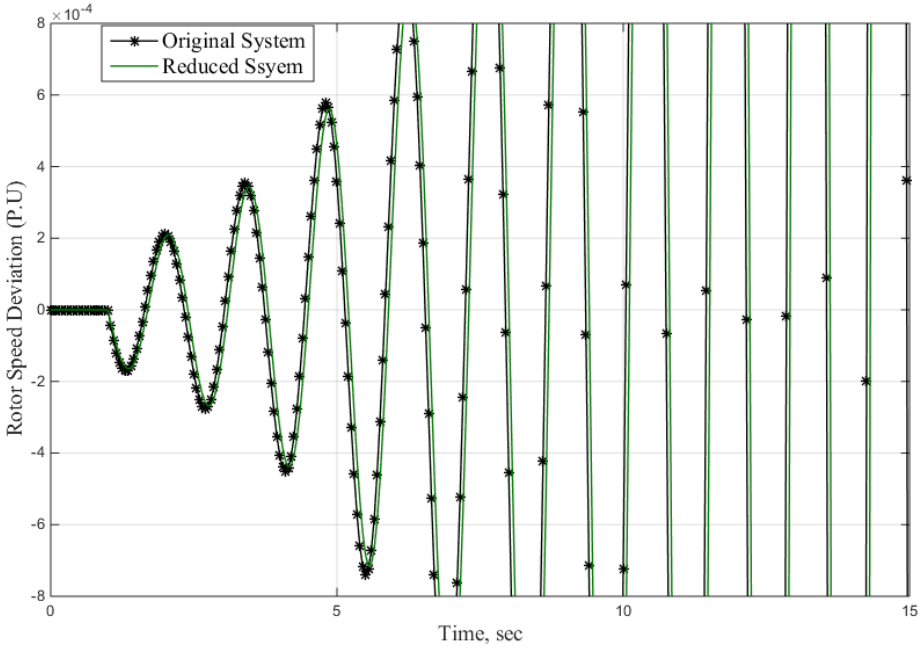

Figure 3.8. Time response of Δω due to disturbance at leading power factor (P = 1.25 p.u, Q = - 0.6 p.u)

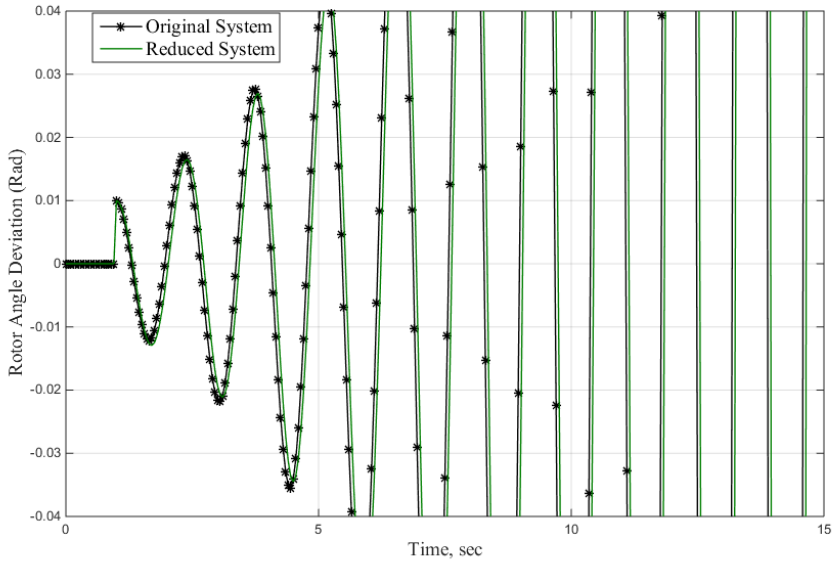

Figure 3.9 Time response of Δδ due to disturbance at leading power factor (P = 1.25 p.u, Q = - 0.6 p.u)

The third part of the comparison is achieved by changing the value of amplifier gain K_A and the value of the total external impedance ($R_T \neq 0$), as shown in Figure 3.1, whereas the previous results were with $R_T = 0$, and $x_T = 0.4$. Table 3.4 along with Figures 3.10 to 3.13, show the level of accuracy of the simplified method when the parameters of the system have been changed.

Table 3.4. Eigenvalues at nominal operating condition and ($R_T = 0.02$ p.u, $x_T = 0.8$ p.u)

K_A	Eigenvalues	
	Original system	Reduced system
70	-0.0622 ± j4.6591 -2.6595 -17.0196 -1.2157 ± j1.4128 -0.6313 -33.0906 -2.2213	-0.0622 ± j4.6591 -17.0196
80	-0.0371± j4.6411 -3.1369 -16.4653 -1.3090 ± j1.3563 -0.6313 -33.0598 -2.1925	-0.0371± j4.6411 -16.4653
90	-0.0109 ± j4.608 -3.7283 -15.8543 -1.3660 ± j1.2908 -0.6410 -33.0299 -2.1806	-0.1491 ± j5.9294 -15.8543
100	0.0263 ± j4.6105 -4.3774 -15.1701 -1.4443 ± j1.1779 -0.6316 -33.0007 -2. 1783	0.0519 ± j5.9251 -14.6124
110	0.0519 ± j4.6080 -5.2403 -14.3708 -1.4443 ± j1.1779 -0.6317 -32.9724 -2. 1783	0.0519 ± j4.6080 -14.3708
120	0.0612 ± j4.6187 -6.3568 -13.3723 -1.4144 ± j1.1464 -0.6313 -32.9450 -2.1663	0.0612 ± j4.6187 -13.3723

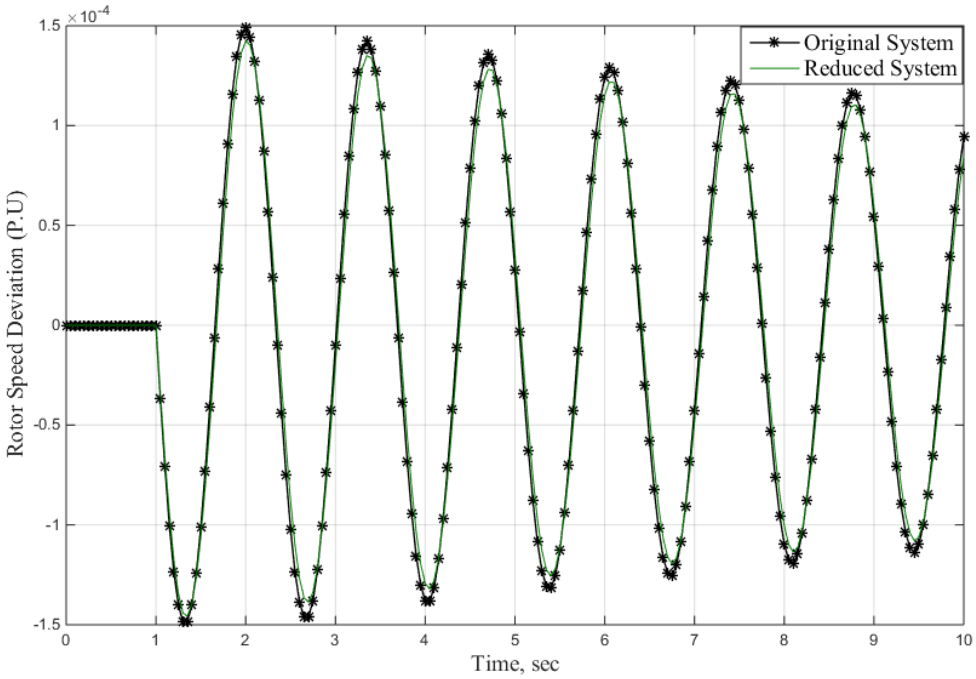

Figure 3.10 Time response of Δω due to disturbance at (P = 0.75 p.u, Q = 0.0 p.u, and $K_A = 80$)

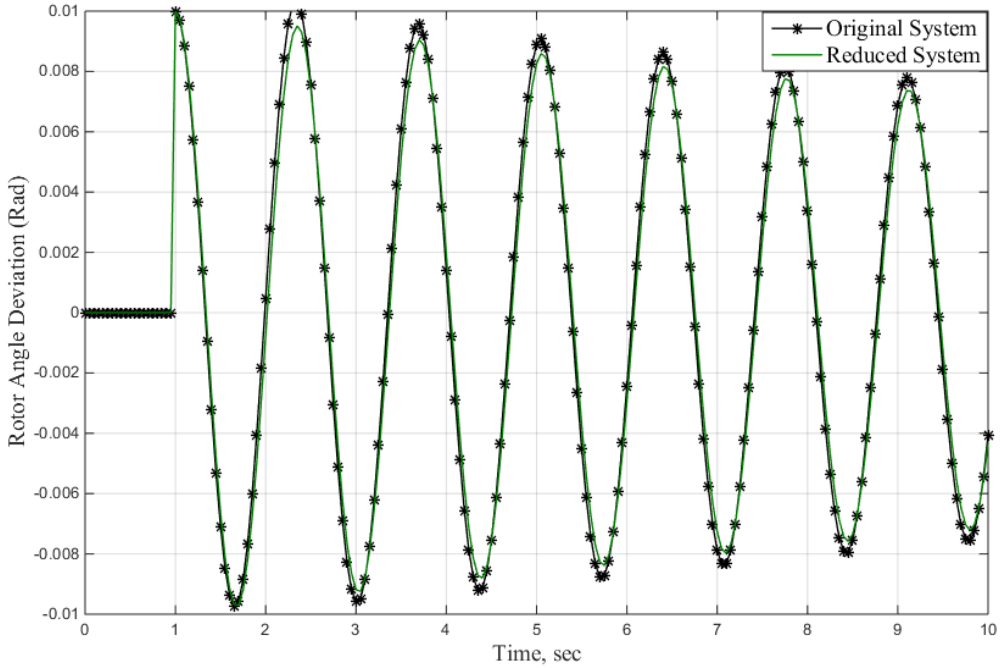

Figure 3.11 Time response of Δδ due to disturbance at (P = 0.75 p.u, Q = 0.0 p.u, and $K_A = 80$)

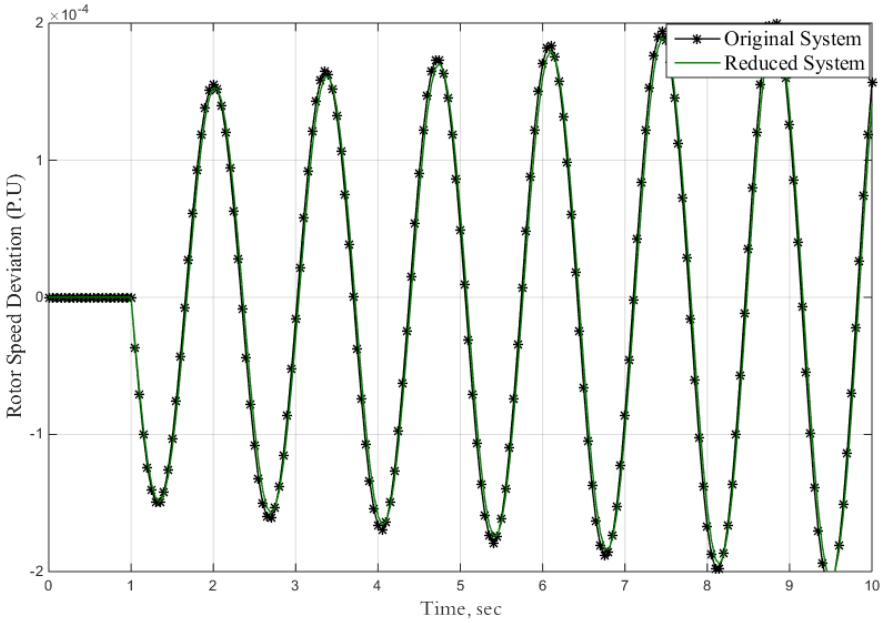

Figure 3.12 Time response of Δω due to disturbance at (P = 0.75 p.u, Q = 0.0 p.u, and $K_A = 110$)

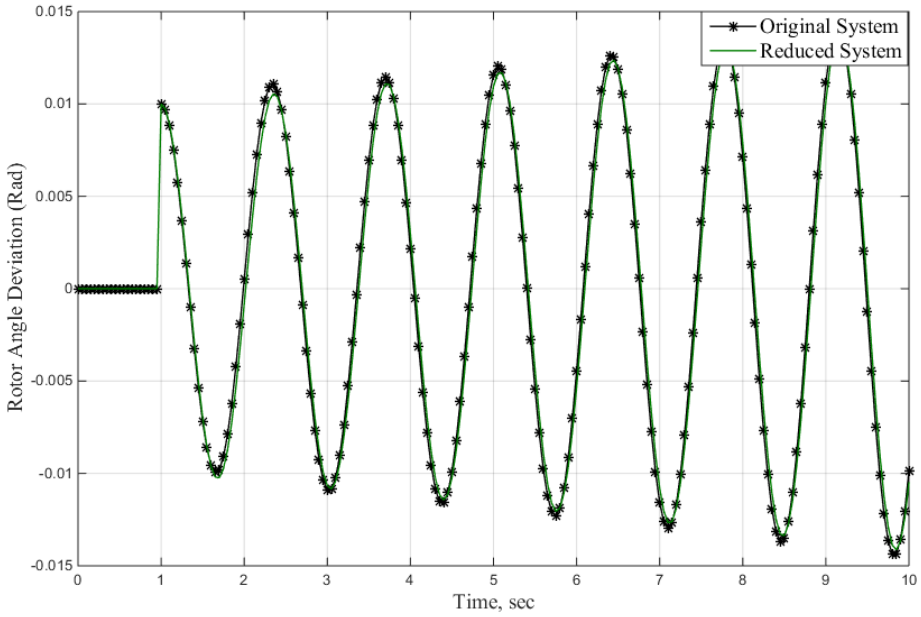

Figure 3.13 Time response of Δδ due to disturbance at P = 0.75 p.u, Q = 0.0 p.u, and $K_A = 110$

3.4 Summary

This chapter discussed the reduction technique that depends on dominant eigenvalues and eigenvectors, applying the technique to the power system consisting of a synchronous machine represented by a two-axis model and equipped with an IEEE type-1 excitation system and turbine governor system connected to the network. This approach used the method proposed in Chapter 2, which is to linearize the unit of the power system by taking the high voltage side (high bus voltage X) as a reference instead of the infinite bus, as shown in Figure 3.1. This concept will make it possible to represent each power generation unit independent of the entire power system using the reduction technique method, as shown in Figure 3.3. In this case, the identity of the high voltage bus at each unit of the original power system will not be lost. Thus, the controllers can be implemented to the original system from a reduced-order model, and the voltage and current at these buses can measure it and send it to another part of the power system using phasor measurement units PMUs or fiber optical cables. The main advantages of using the reduced dynamic model are decreasing the computational time and minimizing the space in a computer's random-access memory. The response will therefore be faster, which leads to superior controller performance. The reduction technique model was applied to a power system unit consisting of a synchronous generator connected to a network through a step-up transformer and transmission lines. The simulation tests of the original system and reduced-order model validate the reduced-order method. A comparison between the original power system and the reduced order model was carried out across a wide range of operating conditions and changes in parameters in order to test the effectiveness and reliability of the third-order model. This is illustrated in Figures 3.4 to 3.13, which clearly demonstrated acceptable performance. The simplified model can thus be considered equivalent to the original model.

Chapter 4

4 Design of Power System Stabilizers

4.1 Introduction

High-performance excitation systems are essential for maintaining a steady state and transient stability for modern synchronous generators, as well as for providing timely control of terminal voltage. Bus-fed static exciters with thyristor controllers, as shown in Figure 1.4, are increasingly being used for both hydraulic and thermal units. It is established that even using a fast acting exciter with a high gain automatic voltage regulator (AVR) can produce oscillatory instability in the power system. This type of oscillation is characterized by low frequency (0.2-2 Hz), which can persist or even grow in magnitude for no apparent reason. This type of instability can endanger system security and limits power transfer. The major factors that contribute to instability are the loading of a generator or tie line, power transfer capability of transmission lines, power factor of generator and automatic voltage regulator gain. One can avoid the instability by adding supplementary control to an excitation system, which is called the power system stabilizer (PSS). The main goal of designing a PSS is to provide additional damping torque without affecting the synchronizing torque at critical oscillation frequencies [10] [13] [12] [73]

4.2 Tuning of Lead-Lag PSS

Power system stabilizers have been used for over 30 years in the United States of America and in Canada. In the United Kingdom, PSSs have also been employed in Scotland to damp oscillations in the lines connecting Scotland and England. Lead-Lag power system stabilizers contain a washout circuit, dynamic compensator, torsional circuit, and limiter as shown in Figure 4.1.The major objective of Lead-Lag PSS is to introduce a damping torque that is in phase

with speed changes in order to increase the capability of the transmission line to deliver electrical power [10] [13] [73].

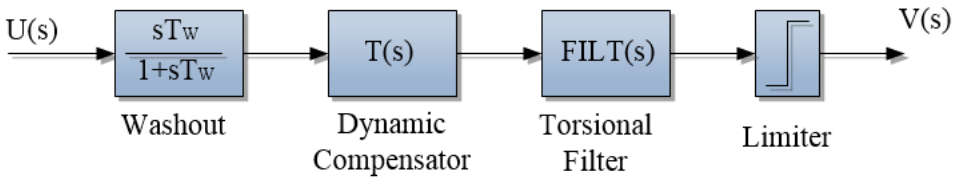

Figure 4.1 Block diagram of a lead-Lag PSS

4.2.1 Washout Circuit

A washout circuit is essentially working as a high pass filter. It removes DC offsets from the input signal and bias steady state from the output signal of PSS which will modify the terminal voltage of the generator because Lead-Lag PSS is expected to respond only to transient variation in the input signal, not to DC offsets in the signal. The value of T_W is not critical and it could be anywhere in the range between 1 to 20 seconds. For the local model oscillation in the range from 0.8 to 1.8 Hz, a washout time constant is satisfactory in 1.5 seconds. For inter-area oscillation in the range of 0.2 to 0.5 Hz, a washout time constant is 10 seconds or higher.

4.2.2 Dynamic Compensator

A two-stage lead-lag compensator is used as a dynamic compensator. It has a transfer function which is formulated as follows:

$$T(s) = \frac{K_s(1 + sT_1)(1 + sT_3)}{(1 + sT_2)(1 + sT_4)} \tag{4.1}$$

K_s is the gain of the power system stabilizer, while the amount of damping associated with rotor oscillation depends on stabilizer gain. To damp out rotor oscillations, a PSS must produce a damping component of electrical torque of a synchronous generator in phase with rotor speed deviation. This requires phase-lead circuits to be used to compensate the lag between the PSS output point and the resulting electrical torque developed. For design purposes of a Lead-Lag PSS, the effect of the washout circuit and torsional filter can be neglected but must be considered in evaluating PSS performance under various operating conditions. There are two design criteria: the time constants, T_1 to T_4, shown in equation (4.1), are to be chosen from the requirements of the phase compensation to achieve damping torque, and the Lead-Lag PSS gain is to be chosen to provide adequate damping torque across all criteria modes.

The basis for choosing time constants of the dynamic compensator can be explained with a reference to the block diagram when PSS is included, as shown in Figure 4.3. The GEP(s) is the transfer function between electrical torque output and the reference voltage input, with the deviation in the speed machine assumed to be zero. The expression of GEP(s) can be derived from Figure 4.2 as follows:

$$\mathrm{GEP}(s) = \frac{K_2 K_3 \, G_{exc}(s)}{\left(1 + sT'_{do} K_3\right) + K_3 K_6 \, G_{exc}(s)} \tag{4.2}$$

In this subsection, the transfer function of the excitation system is as follows:

$$G_{exc}(s) = \frac{K_E}{1 + sT_E} \tag{4.3}$$

Thus, equation (4.2) becomes:

$$\mathrm{GEP}(s) = \frac{K_2 K_3 K_E}{T_E T'_{do} K_3 s^2 + \left(T_E + T'_{do} K_3\right) s + (1 + K_3 K_6 K_E)} \tag{4.4}$$

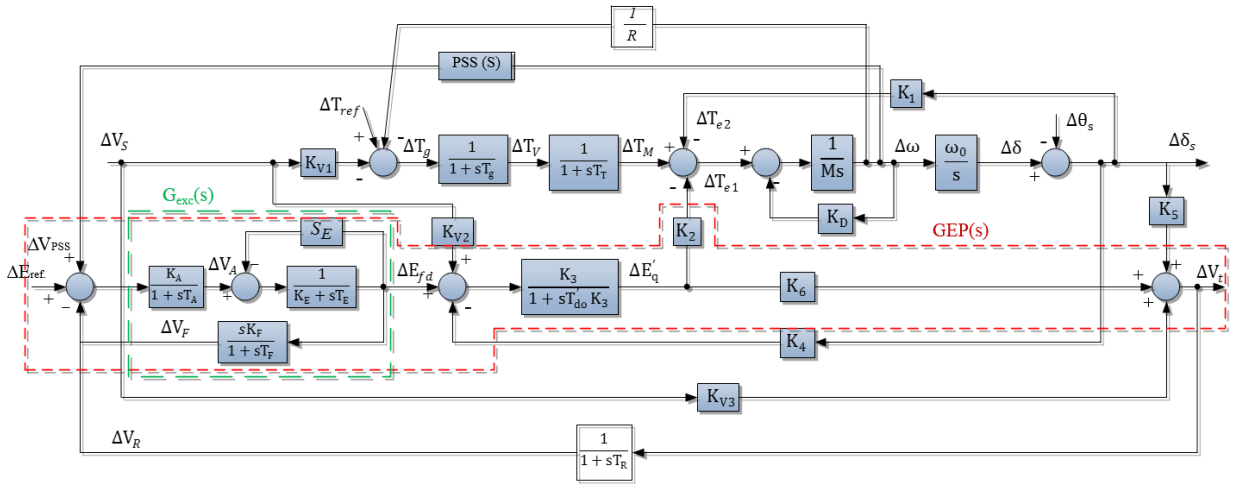

Figure 4.2. Linearizing model of a generation unit connected to the network

If the Lead-Lag PSS is providing pure damping torque at all frequencies, the phase characteristics must be balanced with the phase of GEP(s) at all frequencies. However, because this is not practical, the following steps are chosen to design the phase compensation of the PSS.

A. The compensation of phase lag (phase lag of P(s) = PSS(s) GEP(s)) should pass through 90° at a frequency of around 3.5 Hz (for input frequency, this can be reduced to 2 Hz).

B. The compensated phase lag at a local mode frequency of 7 rad/sec should be below 45° and preferably around 20°.

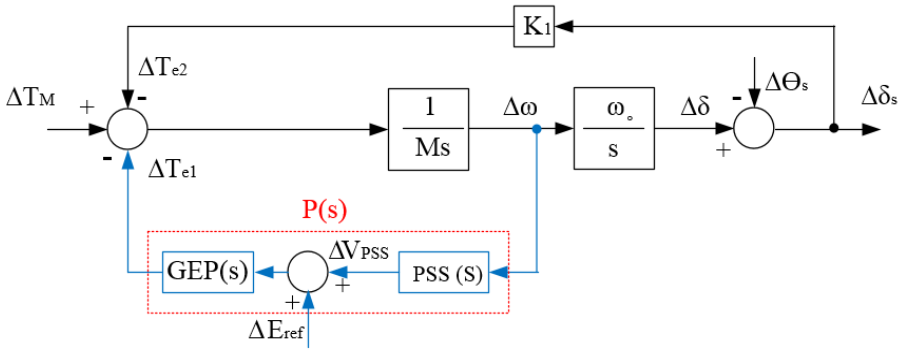

Figure 4.3. Block diagram of PSS with speed input

The plot of the phase angle $\angle(T(j\omega))$ of the compensator with variations in frequency will give different values for the center frequency (f_c), as follows:

$$f_c = \frac{1}{2\pi\sqrt{T_1 T_2}} \tag{4.5}$$

When the transfer functions, GEP(s), of the generators do not have a resonant peak, the guidelines given in [10] can be followed to determine the time constants of the compensator, as follows:

$$\alpha = \frac{T_2}{T_1} = \frac{1 - \sin\frac{\beta}{m}}{1 + \sin\frac{\beta}{m}} \tag{4.6}$$

where β is the required phase compensation, m is the number of stages, and

$$T_1 = \frac{1}{\omega_c\sqrt{\alpha}} \tag{4.7}$$

$$T_2 = \alpha T_1 \tag{4.8}$$

and $\omega_c = 2\pi f_c$

The gain of the PSS can be set by using root locus. Hence, for the speed deviation input, the PSS gain is set to one-third of the instability gain [10]. Using the bode plot for the transfer function, $GEP(j\omega)$, at the operating condition P = 0.75 and Q = 0.0 P.U, as shown in Figure 4.4, the phase lead at a frequency of 3.5 Hz (22 rad/sec) can be obtained ($\beta = 120^\circ - 90^\circ = 30^\circ$), as

shown in Figure 4.4. Substituting this into equations (4.4), (4.5) and (4.6) gives $\alpha = 0.333$ with time constants of $T_1 = 0.079$ sec, $T_2 = 0.0263$ sec, $T_1 = T_3$ and $T_4 = T_2 \times 10 = 0.263$.

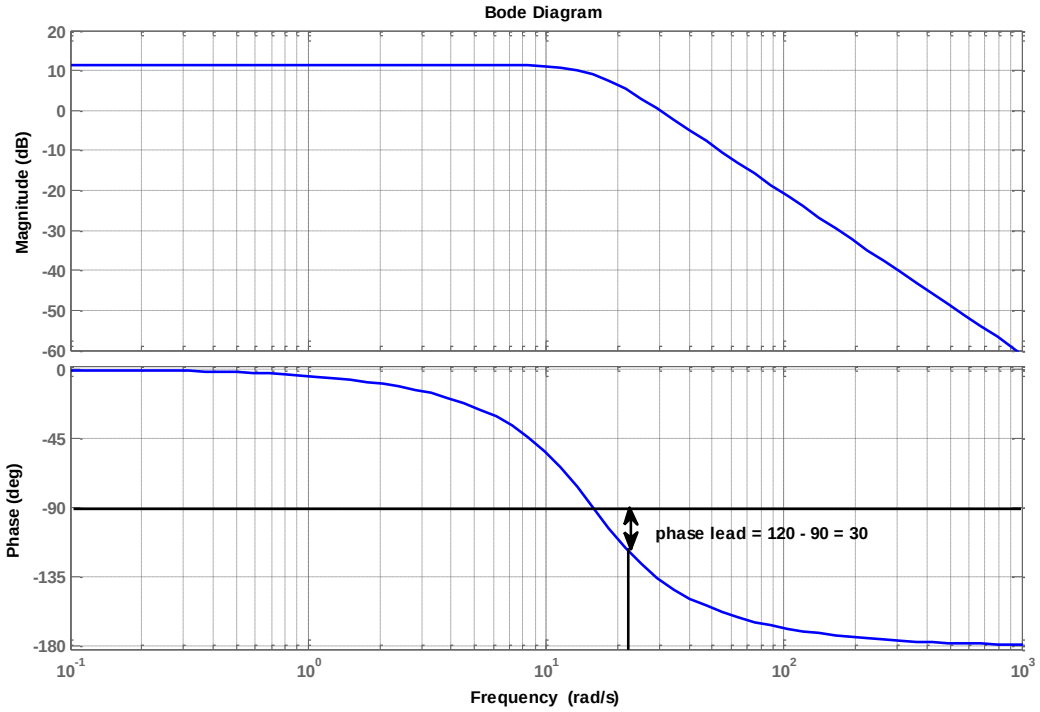

Figure 4.4 Magnitude and phase angle of GEP(jω)

4.2.3 Torsional Filter

The torsional filter in PSS is essentially a low pass filter to attenuate the first torsional mode frequency. Such a filter is necessitated by the adverse interaction of the PSS with torsional oscillation. This can damage the shaft, particularly at light generator loads when inherent mechanical damping is small. Even if shaft damage does not occur, PSS output can go into saturation (due to torsional frequency components) making it ineffective. The filter's transfer function can be expressed as [10] [13]:

$$\mathrm{FILT}(s) = \frac{\omega_n^2}{s^2 + 2\zeta\omega_n s + \omega_n^2} \tag{4.9}$$

4.2.4 Limiter

The output of the PSS must be restricted to prevent the PSS countering the action of the automatic voltage regulator when load rejection takes place. The AVR acts to reduce the terminal voltage when PSS action calls for high terminal voltage due to increases in speed or frequency. It may even be desirable to trip PSS in the case of load rejection. The positive output is limited if the stabilizer is set at a relatively large value between 0.1 and 0.2 p.u. This allows a high level of contribution from the PSS during the swing.

With such a high value of stabilizer output limit, it is essential to have a means of limiting the generator terminal voltage to its maximum allowable value. The negative limit of the PSS output is important during the rotor's back swing, such that negative side limits are raised to prevent the PSS from reducing the generator's terminal voltage excessively following a fault. Furthermore, AVR action is necessary to maintain the voltage and thus prevent loss of synchronism after the angular separation has increased. Typically, -0.2 to -0.5 p.u is used for the negative limit.

4.3 Artificial Neural Network Controller

The key to artificial neural networks (ANNs) is that their design enables them to process information in a way that is similar to a human (biological) brain, which is comprised of many millions of interconnected units of cells attached at several input (dendrites) and output (axon) signals. The axon connects with many other neurons via connection points called synapses. A synapse produces a chemical reaction in response to an input. The biological neuron fires if the sum of the synaptic reactions is sufficiently large. This makes humans able to remember, think,

learn and reason [36] [37]. Artificial neural networks are already being used in the industry with nonlinear procedures and human operator modeling. Additionally, for fault detection and monitoring as well as control process and optimization, ANN has been used as power system stabilizer [37] - [42] [74]. A brief review of ANN analysis will be discussed in this chapter.

4.3.1 Basic Elements of an Artificial Neural Network

An artificial neural network is a computational or mathematical model that mimics biological neural networks. It consists of processing elements called neurons which are linked together to create a network structure. Nonlinear function approximation uses process inputs to evaluate process outputs. An important feature of ANNs is their ability to adjust connections through an adaptive learning process called, appropriately enough, "learning", which can be achieved using a series of examples and patterns. Information achieved through learning is retained and represented by a set of connection weights within the neural network structure. Figure 4.5 shows a simple neural network consisting of a linear combiner and nonlinear active function. The input signals $I_1, I_2, \dots, I_n$ are multiplied by weights $W_1, W_2, \dots, W_n$ and then collected together to generate the net input to the nonlinear active function. Thus, the output signal can be expressed as follows [36] [37] [38]:

$$O_j = f_j(x_j) \tag{4.10}$$

$$x_j = \sum_{i=1}^{N} W_{ji} I_i + b_j \tag{4.11}$$

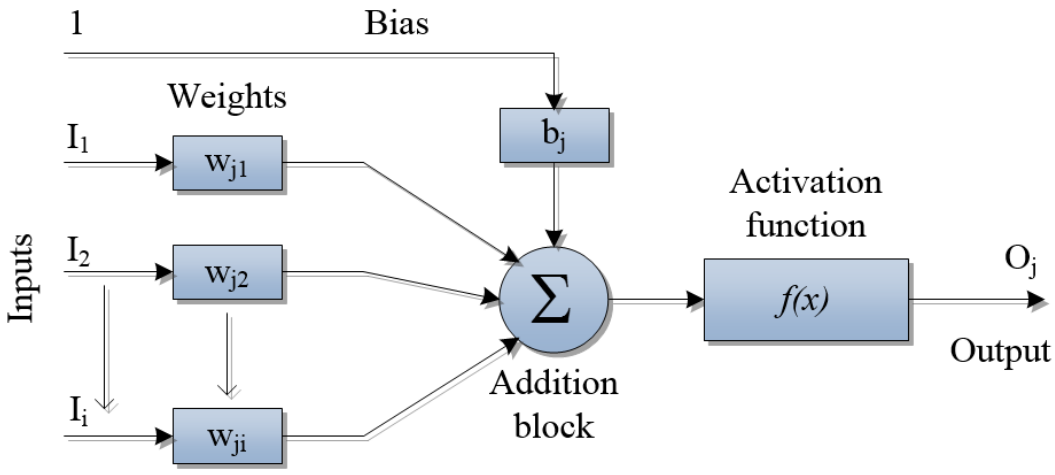

Figure 4.5. Simple model of an ANN

In determining an ANN's output, the weights are the most important coefficients. Weights are used to adjust connections between the neurons according to a modification rule. The bias (b) is utilized to increase or decrease the input to the nonlinear active function. The nonlinear active function is applied to transfer the activity level of the neuron to the output signal. There are many types of nonlinear active functions that have been used to build ANNs such as the sigmoid function, hard limit function, hyperbolic tangent function and Gaussian function, as shown in Figure 4.6 [36] [37]. The choice of the active function is dependent on the application using the ANN; in multi-layer neural networks, the active functions most commonly used are sigmoid and hyperbolic tangent functions.

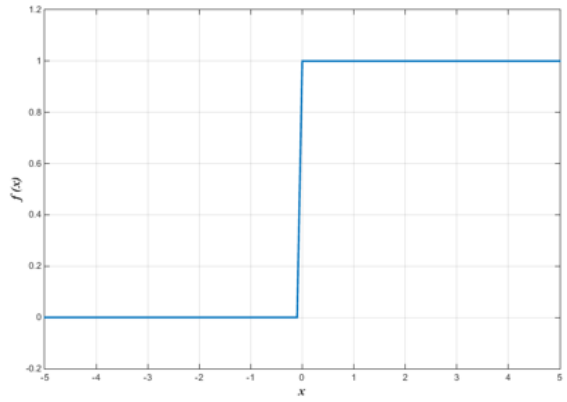

Hard limit function

$$f(x) = \begin{cases} 1 & if\ x \geq 0 \\ 0 & if\ x < 0 \end{cases}$$

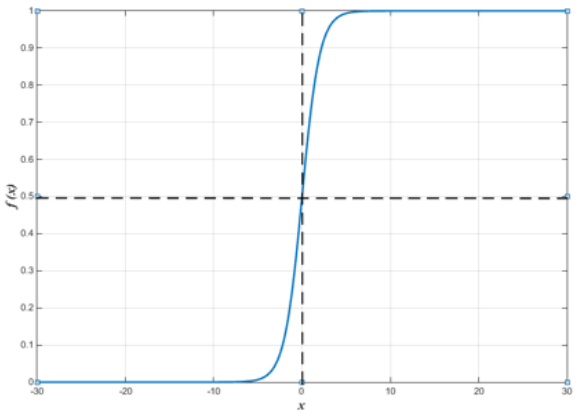

Sigmoid function

$$f(x) = \frac{1}{1 + e^{-x}}$$

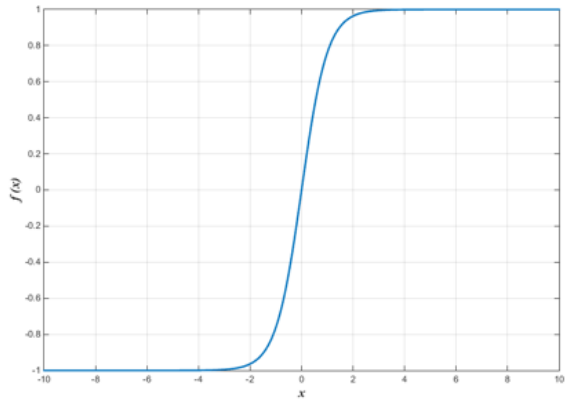

Hyperbolic tangent function

$$f(x) = \tanh(x) = \frac{e^{x} - e^{-x}}{e^{x} + e^{-x}}$$

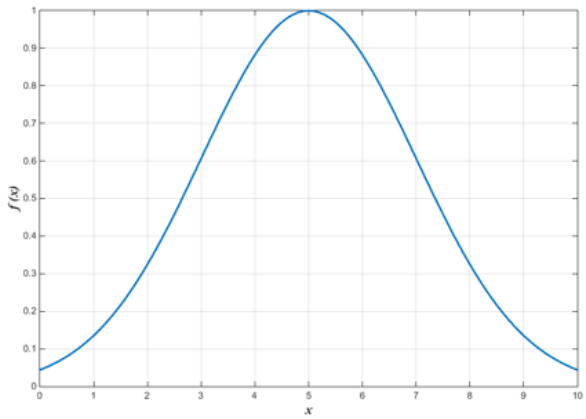

Gaussian function

$$f(x) = ae^{-(x-b)^2/2c^2}$$

Figure 4.6. Types of activation function

There are different types of neural network architectures, which are based on the way neurons are connected. One of these is *a single-layer feed-forward network* consisting of one computational layer and multi-input and multi-output signals, as shown in Figure 4.7. The input signals are connected with each neuron in the network. This type of the architecture can only

approximate a linear function. In the input layer, no computation process has taken place, so it is not accounted as a layer.

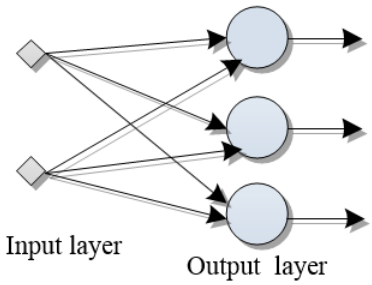

Figure 4.7. Single layer feed-forward network

The second type of network architecture is *a multi-layer feed-forward network*. It consists of two or more layers connected together to make one network, as shown in Figure 4.8. By using this type of neural network, the approximation of a non-linear function can be obtained.

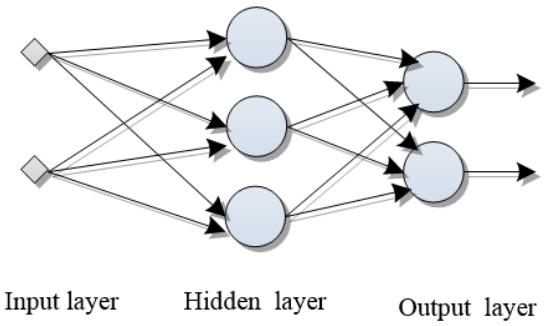

Figure 4.8. Multi-layer feed-forward network

The third type is *a recurrent neural network*. This type of network contains feedback connections between the network's outputs and inputs. Thus, the signals flow in both forward and backward directions, adding dynamic memory to the network and are useful to emulate dynamic

systems. This design can be either a single-layer or multi-layer recurrent network, as shown in Figure 4.9 and Figure 4.10, respectively.

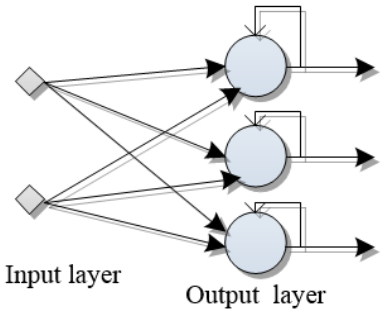

Figure 4.9. Single-layer recurrent network

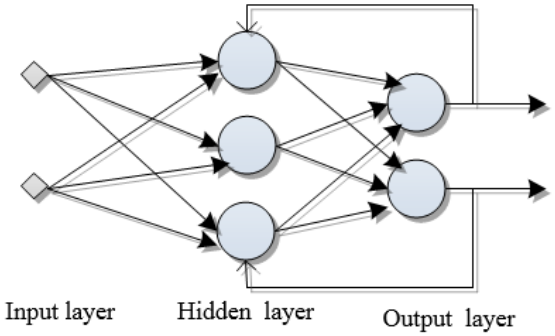

Figure 4.10. Multi-layer recurrent network

4.3.2 Neural Network Learning Algorithms

One of the most important features of ANNs is their ability to learn, which can be defined as the procedure of adjusting the neural network parameters (weights and biases). Therefore, outputs can be predicted based on a given number of inputs and within acceptable limits of error. Learning algorithms include the following [36] [37] [38]:

- *Supervised Learning*: The network is presenting with training data that represent the range of input possibilities, together with associated desired outputs. The weights are adjusted until the differences between the actual and desired outputs become a minimal acceptable value.
- *Unsupervised Learning*: Because the technique does not use feedback information to update the network's parameters, it is also called open-loop adaption. This approach is used in some applications such as speech recognition and image comparison.

4.3.3 Back-Propagation Algorithm

The back-propagation algorithm (BPA), which is one of the most common algorithms used to train ANNs. It is a supervised learning approach. It uses a gradient-descent optimization method. It is also called the delta rule, when applied to feed-forward networks. A feed-forward network that uses the delta rule for training is called a multi-layer perceptron (MLP). If the performance index of the cost function (J) takes the form of a summed squared error function, then

$$\mathrm{J} = \frac{1}{\mathrm{M}} \sum_{\mathrm{j}=1}^{\mathrm{M}} (\mathrm{d_j} - \mathrm{O_j})^2 \tag{4.12}$$

where $\mathrm{O_j}$ is the actual output while $\mathrm{d_j}$ is the desired output. Using gradient-descent, the weight increment, ΔW_{ji}, is proportional to the negative slope, as follows:

$$\Delta \mathrm{W_{ji}} = -\mu \frac{\partial \mathrm{J}}{\partial \mathrm{W_{ji}}} \tag{4.13}$$

where μ is a constant. From equations (4.12) and (4.13), one can obtain:

$$\frac{\partial \mathrm{J}}{\partial \mathrm{W_{ji}}} = \frac{1}{\mathrm{M}} \sum_{\mathrm{j}=1}^{\mathrm{M}} \frac{\partial}{\partial \mathrm{W_{ji}}} (\mathrm{d_j} - \mathrm{O_j})^2 \tag{4.14}$$

Using the chain rule, equation (4.14) can be written as follows:

$$\frac{\partial J}{\partial W_{ji}} = -\frac{2}{M}\sum_{j=1}^{M}(d_j - O_j)\frac{\partial O_j}{\partial W_{ji}} \tag{4.15}$$

If the active function is the sigmoid function, then:

$$\frac{\partial f}{\partial x_j} = f(x)[1 - f(x)] \tag{4.16}$$

Since the neuron output O_j is f(x), equation (4.16) can be written as follows

$$\frac{\partial O_j}{\partial x_j} = O_j[1 - O_j] \tag{4.17}$$

From equation (4.15), we can again use the chain rule:

$$\frac{\partial O_j}{\partial W_{ji}} = \frac{\partial O_j}{\partial x_j} * \frac{\partial x_j}{\partial W_{ji}} \tag{4.18}$$

In equation (4.11), the bias b_j is called W_{jo}. Thus equation (4.11) can be written as follows:

$$x_j = \sum_{i=0}^{N} W_{ji} I_i \tag{4.19}$$

$$\frac{\partial x_j}{\partial W_{ji}} = \frac{\partial}{\partial W_{ji}}\sum_{i=0}^{N} W_{ji} I_i = I_i \tag{4.20}$$

Substituting equations (4.17) and (4.20) in equation (4.18), we get:

$$\frac{\partial O_j}{\partial W_{ji}} = O_j[1 - O_j] I_i \tag{4.21}$$

Substituting equation (4.21) in equation (4.15), one obtains:

$$\frac{\partial J}{\partial W_{ji}} = -\frac{2}{M}\sum_{j=1}^{M}(\mathrm{d_j} - \mathrm{O_j}) * \mathrm{O_j}[1 - \mathrm{O_j}]\mathrm{I_i} \tag{4.22}$$

Equation (4.22) can be rewritten as follows:

$$\frac{\partial \mathrm{J}}{\partial \mathrm{W_{ji}}} = -\frac{2}{\mathrm{M}}\sum_{\mathrm{j=1}}^{\mathrm{M}}\delta_\mathrm{j}\mathrm{I_i} \tag{4.23}$$

where

$$\delta_\mathrm{j} = (\mathrm{d_j} - \mathrm{O_j}) * \mathrm{O_j}[1 - \mathrm{O_j}] \tag{4.24}$$

Substituting equation (4.23) in equation (4.13) leads to:

$$\Delta W_{ji} = \eta\sum_{\mathrm{j=1}}^{\mathrm{M}}\delta_\mathrm{j}\mathrm{I_i} \tag{4.25}$$

where $\eta = \frac{2\mu}{\mathrm{M}}$

This leads to weight increment, called the delta rule, for a particular neuron

$$\Delta\mathrm{W_{ji}(kT)} = \eta\delta_\mathrm{j}\mathrm{I_i} \tag{4.26}$$

where η is the learning rate and has a value between 0 and 1. Therefore, the new weight becomes:

$$\mathrm{W_{ji}(kT)} = \mathrm{W_{ji}([k-1]T)} + \eta\delta_\mathrm{j}\mathrm{I_i} \tag{4.27}$$

In other words, if the sensitivity of the squared error to a particular weight is that increasing the weight causes an increase in the squared error, during a training step the weight is slightly reduced. If the error is increased by decreasing the weight, the weight is increased. When fed many times with each data point in an input/output training set, this iteration, when stable, usually backs down the global E^2 versus weight bowl in hyperspace towards the global minimum. A small value of η

promotes iteration stability. To avoid convergence to local minima, noise added to the weights could be used to periodically shake up the iteration.

Generally, many thousands of iterations are needed to reach the global minimum. When one considers the many directions in weight hyperspace, this is not surprising. Other training methods such as those which try to mimic genetic algorithms are supposed to be faster but are not as well developed. Mapping a neural network could also be used to get the overall dynamics of a system or for error-driven control in order to mitigate the downside of ANN controllers, which is that they require extensive offline training and can react unpredictably when encountering operating conditions outside of their original training sets. This thesis presents an untrained ANN controller to use in a PSS.

4.4 Proposed Untrained Artificial Neural Network

The proposed method uses a multi-layer feed-forward network, consisting of an input layer, a hidden layer, and an output layer, as shown in Figure 4.11. The active function is a nonlinear sigmoid function.

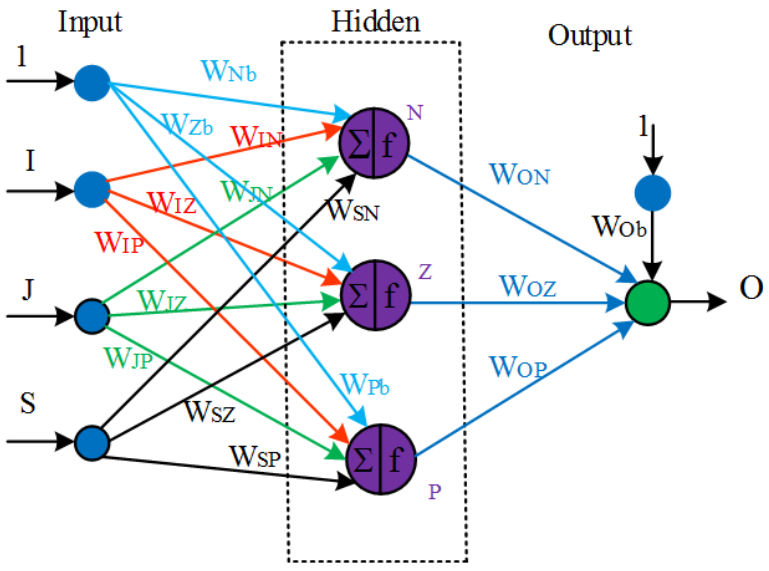

Figure 4.11. Multi-layer feed-forward neural network

From Figure 4.6, it can be noted that, in the sigmoid, when x tends to ∞, the value of f(x) tends to +1, while when x tends to -∞, f(x) tends to zero. When x is equal to zero the value of the sigmoid function is equal to 0.5. The derivative of the sigmoid function is given below. From equation (4.28), it can be noted that as x tends to ∞ or -∞, the value of $df(x)/dx$ tends to zero. However, when $x = 0$, the value of $df(x)/dx$ achieves its greatest value of 0.25, as shown in Figure 4.12.

$$\frac{df(x)}{dx} = \frac{e^{-x}}{(1+e^{-x})^2} \tag{4.28}$$

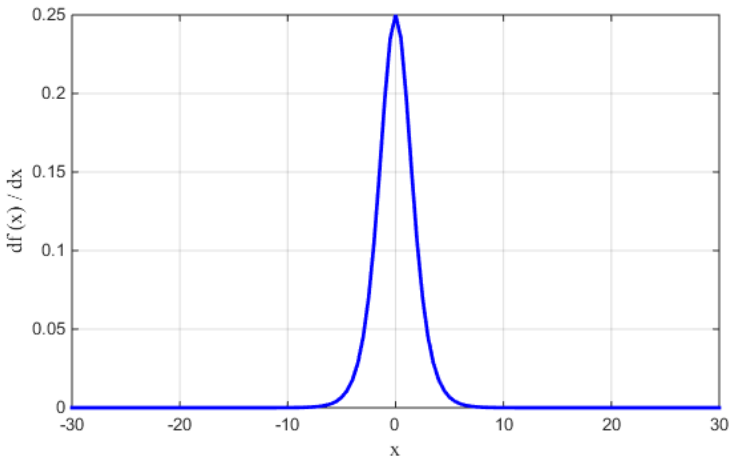

Figure 4.12. Derivative of sigmoid function

This research uses only three hidden neurons (N, Z and P) resulting in a network that is easy and less time-consuming to train. The network has three inputs (I), (J) and (S). These, respectively, represent the error (deviation speed Δω), the integral of the error ($\int \Delta\omega$), and the

derivative of the error (acceleration $\Delta\dot{\omega}$). The network is shown in Figure 4.11. The output is the control signal as given below:

$$\begin{aligned} O = W_{Ob} &+ W_{ON} f\left(IW_{IN} + JW_{JN} + SW_{SN} + W_{Nb}\right) \\ &+ W_{OZ} f\left(IW_{IZ} + JW_{JZ} + SW_{SZ} + W_{Zb}\right) \\ &+ W_{OP} f\left(IW_{IP} + JW_{JP} + SW_{SP} + W_{Pb}\right) \end{aligned} \tag{4.29}$$

Equation (4.29) shows how the weights (W) can be used in a map to scale and shift the squashing function horizontally and vertically. In this research, the artificial network mimics the PID controller, the output signal of which is shown in following equation [75] [76]:

$$O = K_P I + K_I J + K_D S \tag{4.30}$$

For an artificial neural network to mimic a PID controller, the following assumptions are made:

$$W_{JN} = W_{SN} = W_{IZ} = W_{SZ} = W_{IP} = W_{JP} = 0, \;\; W_{Nb} = W_{Zb} = W_{Pb} = 0 \tag{4.31}$$

along with:

$$W_{Ob} = -\frac{1}{2} * (W_{ON} + W_{OZ} + W_{OP}) \tag{4.32}$$

The saturation limits of the controller are set to be the values of W_{ON}, W_{OZ} and W_{OP}, which are determined by the hardware. Therefore, the value of W_{Ob} would be known. The ANN controller reduces to:

$$O = W_{ON} f(IW_{IN}) + W_{OZ} f\left(JW_{JZ}\right) + W_{OP} f(SW_{SP}) + W_{Ob} \tag{4.33}$$

The differentiation of the output signal of the PID controller with respect to input I gives the proportional gain, K_p, while the output signal with respect to the input, J, gives the integral gain, K_I, and that of the output signal of with respect to the input, S, provides the derivative gain,

K_D. Therefore, differentiation of the reduced ANN controller with respect to I, J and S, when they are equal to zero, gives:

$$W_{IN} = \frac{4K_P}{W_{ON}} \tag{4.34}$$

$$W_{JZ} = \frac{4K_I}{W_{OZ}} \tag{4.35}$$

$$W_{SP} = \frac{4K_D}{W_{OP}} \tag{4.36}$$

4.4.1 Design of Fixed Gain Proportional-Integral-Derivative Regulator (PID-PSS)

As mentioned above, determining the parameters of the proposed untrained ANN regulator requires the PID regulator gains first to be evaluated. To design a fixed-gain PID-PSS, the gains K_P, K_I and K_D can be calculated by selecting a pair of specified eigenvalues (dominant eigenvalues) $\lambda = \lambda_1$ and $\lambda = \lambda_2$ for the electromechanical mode of the synchronous generator connected to the network [77].

The linearized mode of the power system that is obtained around the operating condition is given as follows:

$$\Delta\dot{x}(t) = A\Delta x(t) + B\Delta u(t) \tag{4.37}$$

$$\Delta y(t) = C\,\Delta x(t) \tag{4.38}$$

By taking the Laplace transform for the equations (4.37) and (4.38)

$$\Delta X(s) = (sI - A)^{-1}B\Delta U(s) \tag{4.39}$$

and,

$$\Delta Y(s) = C\Delta X(s) \tag{4.40}$$

The output signal of the PID controller with washout circuit can be written as follows:

$$\Delta U(s) = H(s)\Delta Y(s) = \frac{sT_W}{1+sT_W}\left(K_P + \frac{K_I}{s} + sK_D\right) C\Delta X(s) \tag{4.41}$$

where H(s) is the transfer function of the PID controller and washout circuit, $\Delta Y(s)$ is the output of the power system and the input of the controller (which has been selected to be rotor speed deviation, $\Delta\omega$), T_W is the washout time constant and, K_P, K_I and K_D are the gains of the PID regulator.

Substitution of equation (4.41) into equation (4.39), gives:

$$\frac{sT_w}{1+sT_w}\left(K_{P+}\frac{K_I}{s} + sK_D\right) = \frac{I}{C(sI-A)^{-1}B} \tag{4.42}$$

If λ is the assigned eigenvalue of the closed-loop system equipped with the PID controller, then:

$$\frac{\lambda T_w}{1+\lambda T_w}\left(K_{P+}\frac{K_I}{\lambda} + \lambda K_D\right) = \frac{I}{C(\lambda I-A)^{-1}B} \tag{4.43}$$

Thus, by substituting a pair of pre-specified eigenvalues $\lambda = \lambda_1$ and $\lambda = \lambda_2$ for the electromechanical mode into equation (4.43), three algebraic equations with three unknowns will result as follows: K_P, K_I, and K_D. These gain settings can then be obtained by solving the algebraic equations.

The fixed gains of PID-PSS are a function of the power system parameters K_1-K_6 and K_{V1}-K_{V3}, and these parameters are functions of a generator's operating conditions. Therefore, the eigenvalues of the system will be changed from specified values as long as the loading conditions of the generator are changed. In actual practical case, the loading conditions for any generator in

a power system will continue to change. The operating conditions of the generators will also change when faults occur in the power system, adding new loads to the power system and disconnecting some equipment such as power transformers and transmission lines in order to repair them. These contingencies make a fixed-gain PID-PSS unable to provide a good response under a wide range of operating conditions. In order to mitigate these problems, an artificial neural network power system stabilizer (ANN-PSS) that mimics a PID regulator is proposed. The design of ANN-PSS is the subject of the next subsection.

4.4.2 Design of an Artificial Neural Network PSS (ANN-PSS) for a Reduced Order Model

Although traditional control structures could improve the power system stability, they cannot guarantee adequate performance in many practical applications because their parameters are determined at a particular operating point. Moreover, the power systems are highly non-linear and potentially subjected to unpredictable disturbances. Increasing the demand as well as the complexity of power systems has led to making them unreliable controllers. To offset these issues, an artificial intelligent controller is proposed. The basic structure of this proposed artificial neural network power system stabilizer (ANN-PSS) is shown in Figure 4.13. The inputs of the controller are selected to have a speed deviation, $\Delta\omega$, an integral speed change, $\int \Delta\omega$, and a derivative speed deviation $\Delta\dot{\omega}$. From Figure 4.13, it is clear that the values of speed deviation, $\Delta\omega$, the integral of the speed change and the acceleration, $\Delta\dot{\omega}$, pass through three layers, namely the input layer, a hidden layer, and an output layer of neurons. In practice, the input data are received from the electronic sensors, while the neuron's output layer gives the control signal. Within the hidden layer, the summed inputs are processed by a nonlinear squashing function when they pass through the neurons.

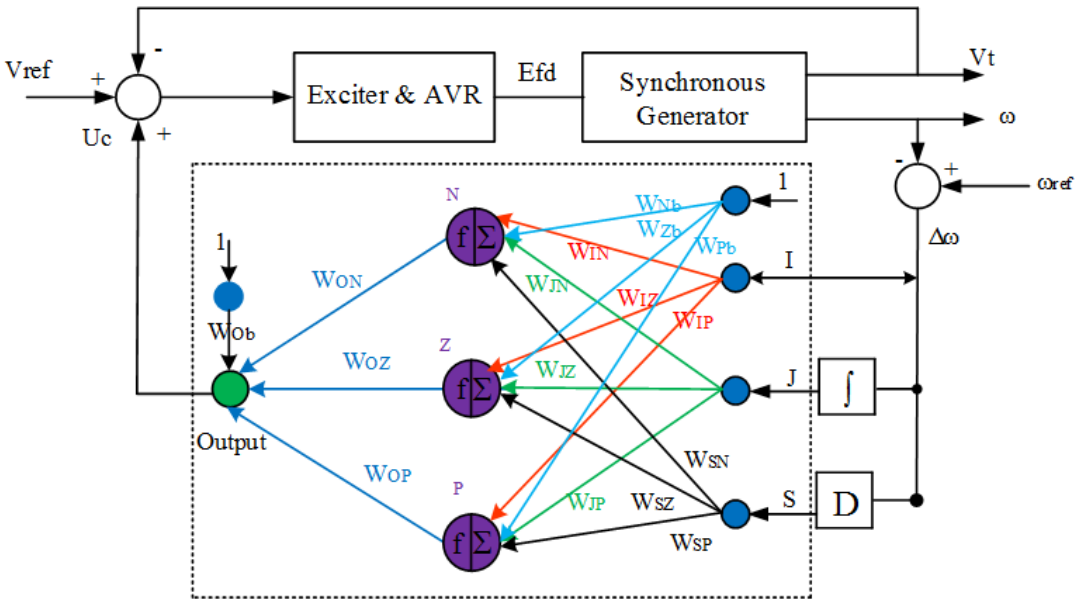

Figure 4.13. Schematic diagram of the power system model with proposed ANN-PSS

In this dissertation, an ANN-PSS will be applied to a reduced order power system model, as shown in Figure 4.14. The original system is first formed, after which a proposed reduction technique is used, and the roots of the reduced order model matrices are found. The ANN-PSS technique thus uses another control signal based on reduced order response.

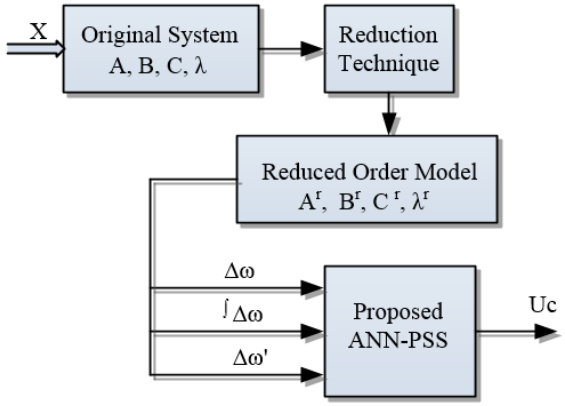

Figure 4.14. Block diagram of ANN-PSS

4.5 Numerical Results

Numerical results are carried out on the power system shown in Figure 2.2, which consists of a synchronous machine represented by a two-axis model and equipped with an IEEE type-1 excitation system and turbine governor system connected to a network. The artificial neural network techniques are applied as discussed above and compared with a conventional Lead-Lag controller to obtain a proper dynamic performance over a wide range of operating conditions. The effectiveness of the ANN-PSS approach is characterized through ±1% step change in the input reference voltage applied at times of 1 sec, 11 sec, and 21 sec.

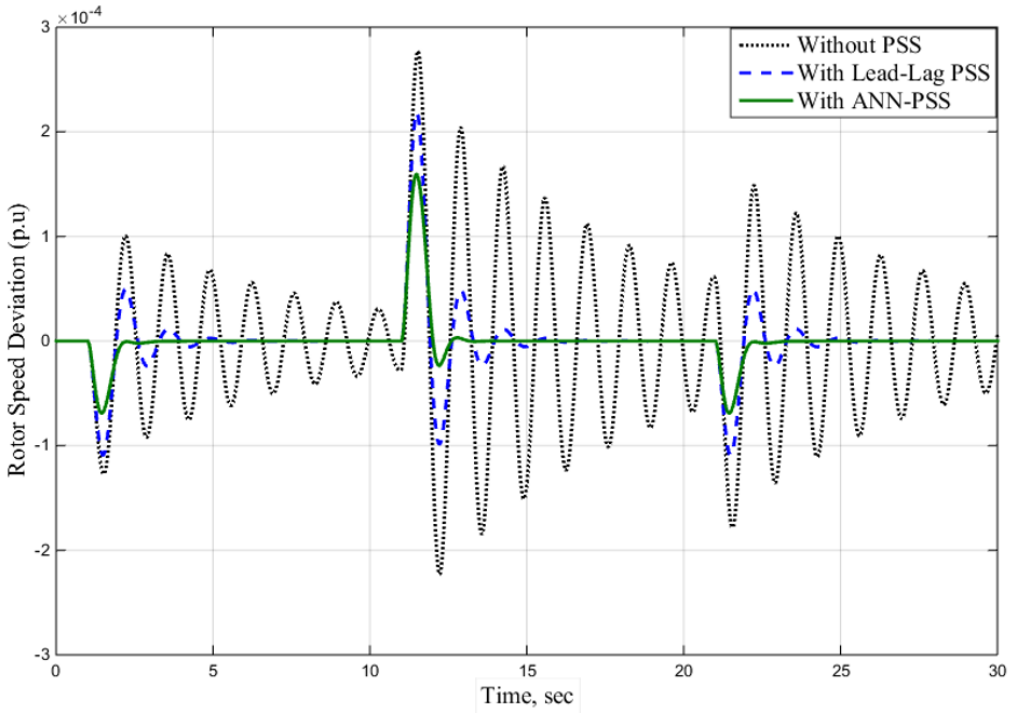

Figure 4.15. Time response of Δω due to disturbances at P = 0.25 and Q = 0.0 pu

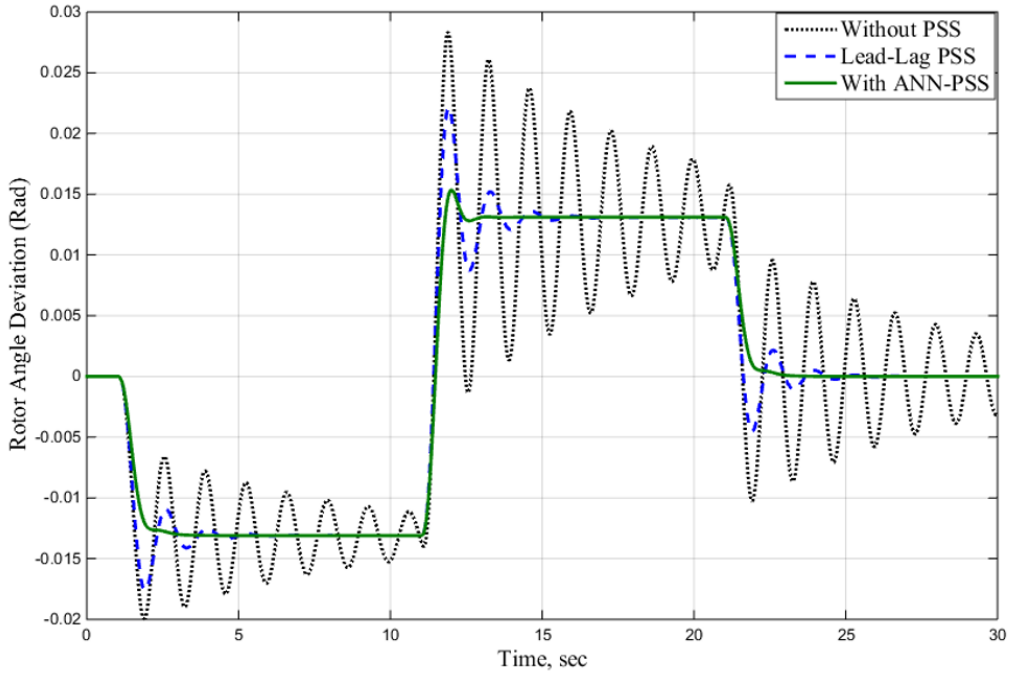

Figure 4.16. Time response of Δδ due to disturbances at P = 0.25 and Q = 0.0 pu

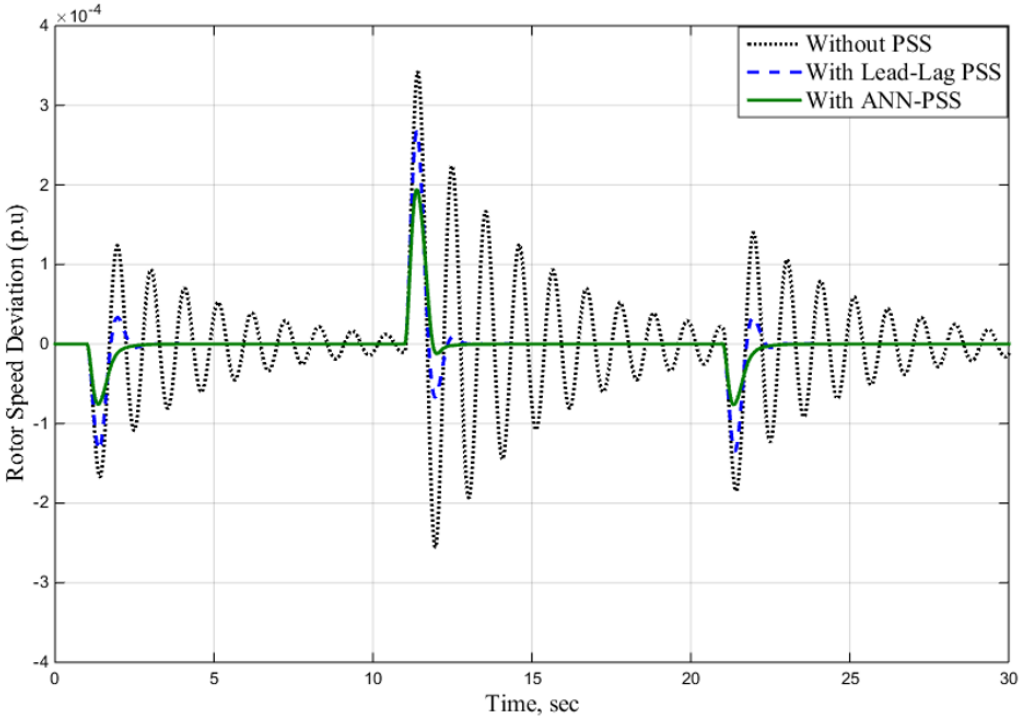

Figure 4.17. Time response of Δω due to disturbances at normal operating condition

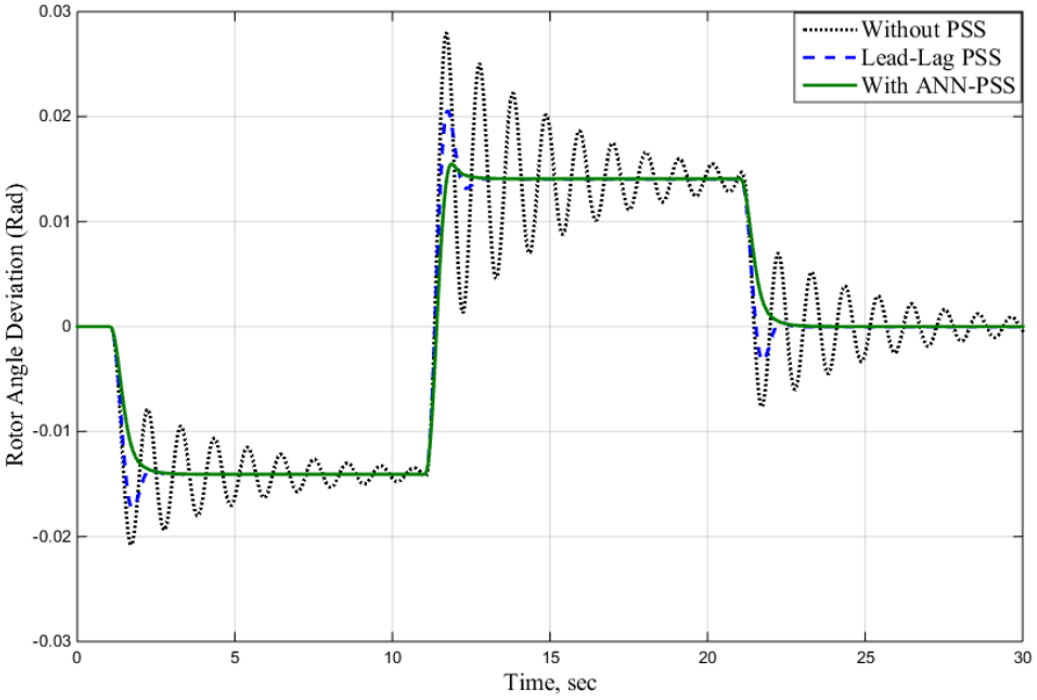

Figure 4.18. Time response of $\Delta\delta$ due to disturbances at normal operating condition

In the results shown above in Figures 4.15 to 4.18, it is assumed that the transformer reactance is fixed at $X_t = 0.4$ P.U. From the figures, it is evident that the system at the unity power factor, due to the ±1% step change in input reference voltage applied at times 1, 11 and 21 seconds, caused persistent oscillations over a relatively long time. By using the PSS approach this oscillation damps extremely fast, especially with the proposed controller, of ANN-PSS. However in real life the power transformer is connected in series with the transmission lines, the reactance in the next study cases will be changed at lagging and leading power factors to gauge the efficacy of the proposed controller under changes in parameters and operating conditions.

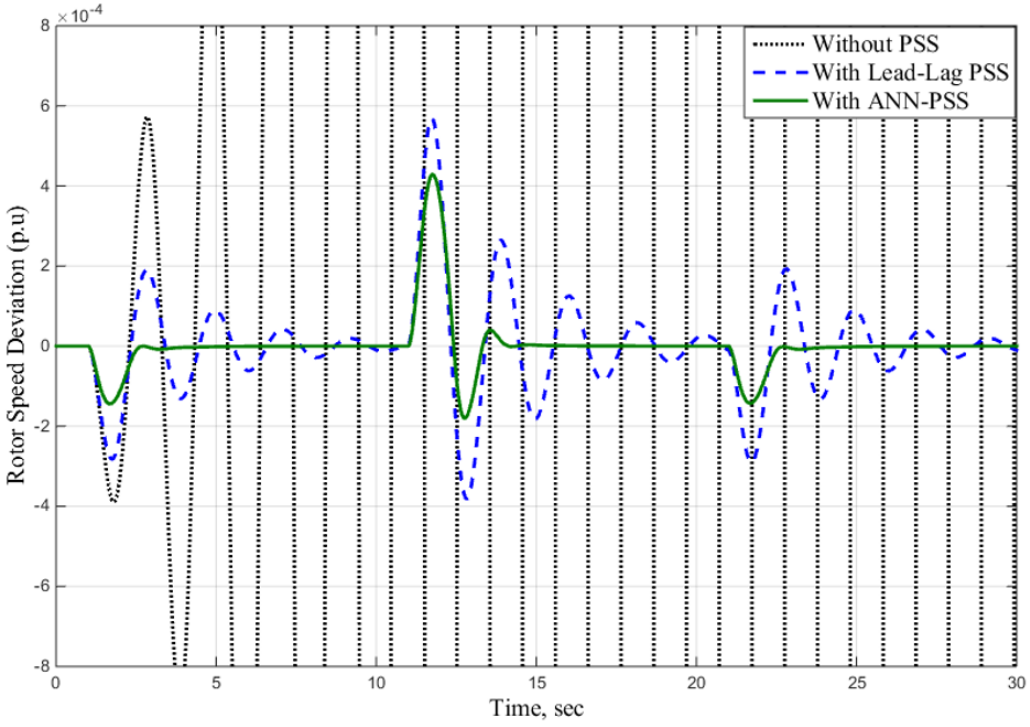

Figure 4.19. Time response of Δω due to disturbances at P = 0.85, Q = 0.65 and X_t = 0.8 pu

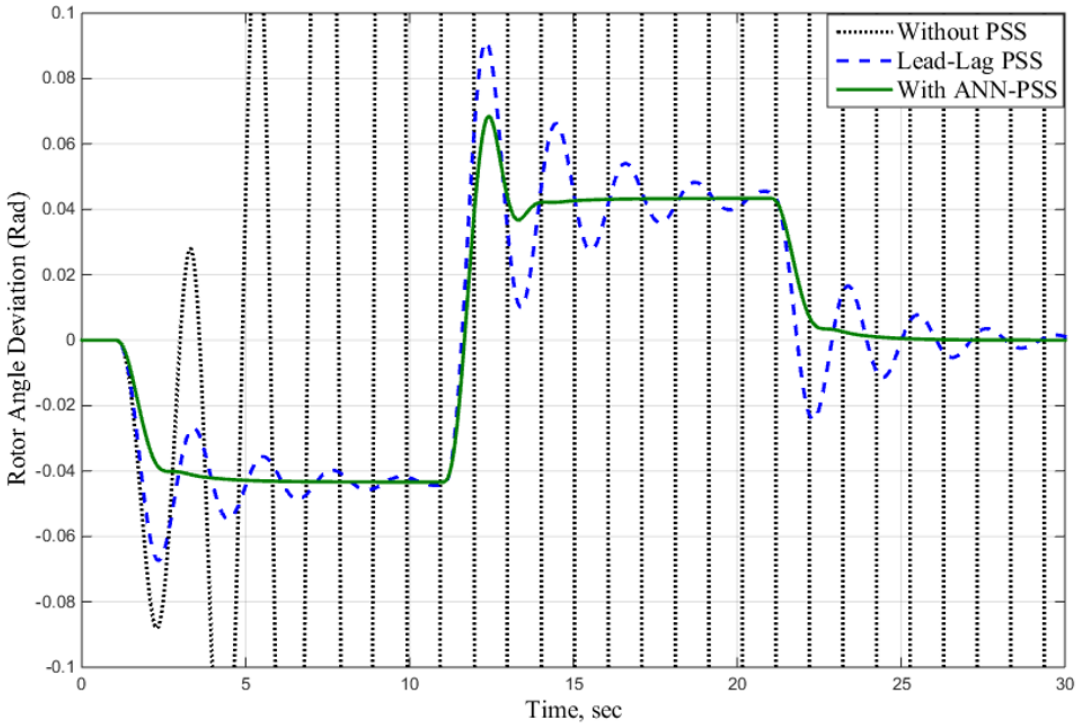

Figure 4.20. Time response of Δδ due to disturbances at P = 0.85, Q = 0.65 and X_t = 0.8 pu

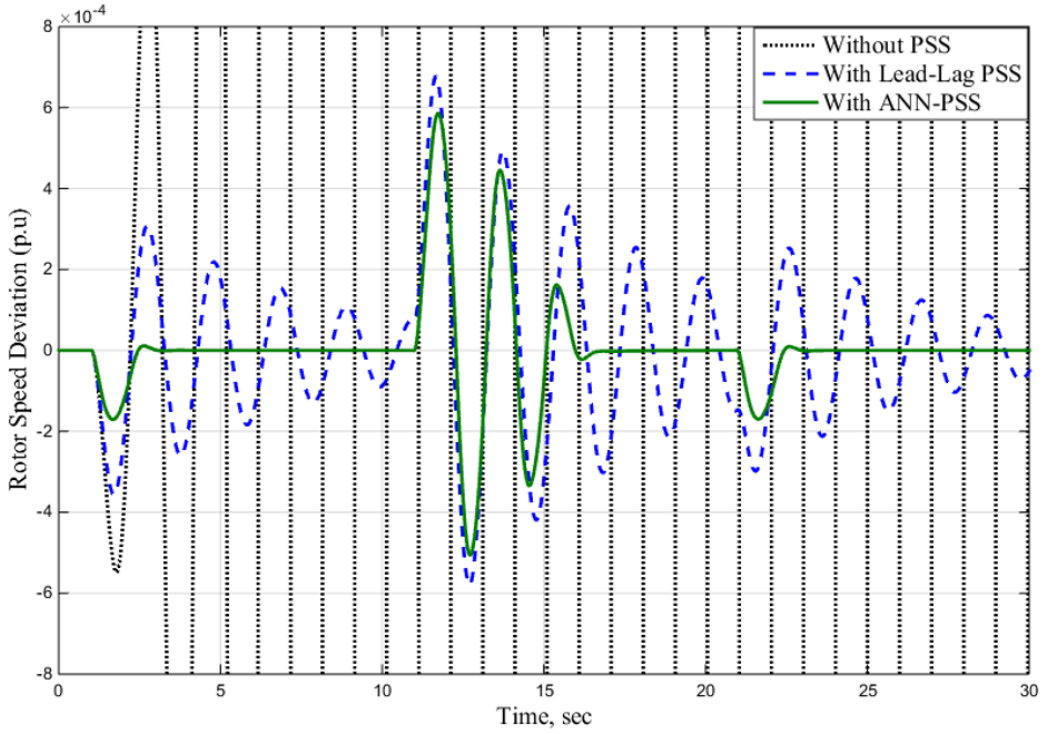

Figure 4.21. Time response of Δω due to disturbances at P = 1.25, Q = 0.6 and X_t = 0.65 pu

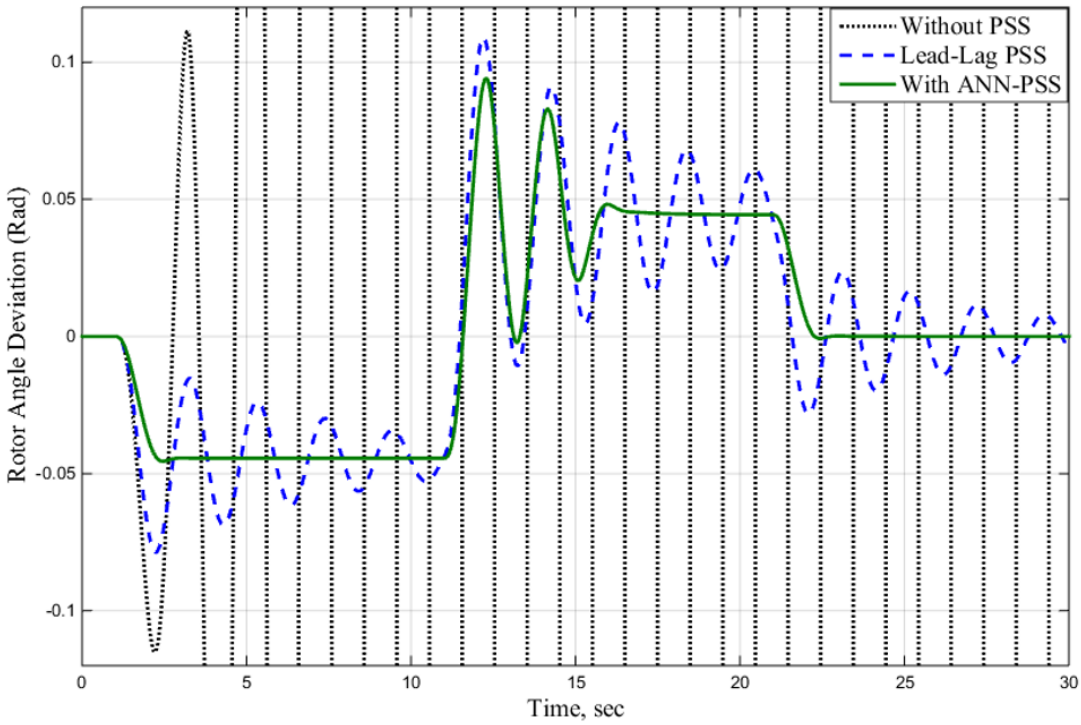

Figure 4.22. Time response of Δδ due to disturbances at P = 1.25, Q = 0.6 and X_t = 0.65 pu

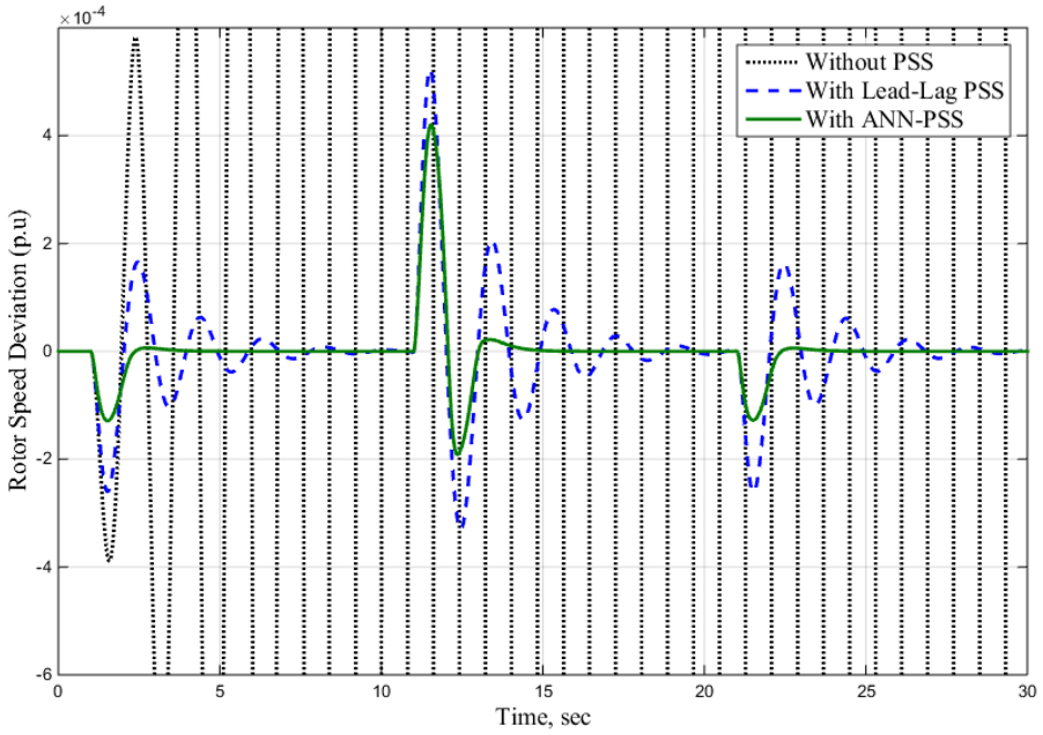

Figure 4.23. Time response of Δω due to disturbances at P = 0.85, Q = -0.6 and X_t = 0.8 pu

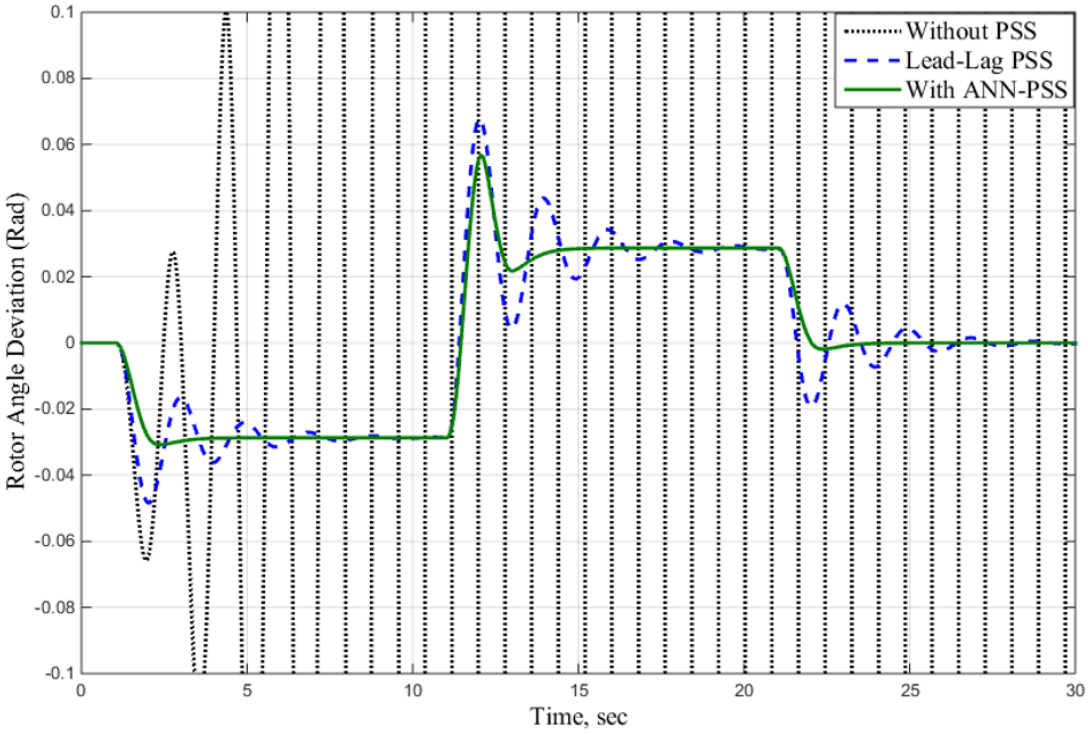

Figure 4.24. Time response of Δδ due to disturbances at P = 0.85, Q = -0.6 and X_t = 0.8 pu

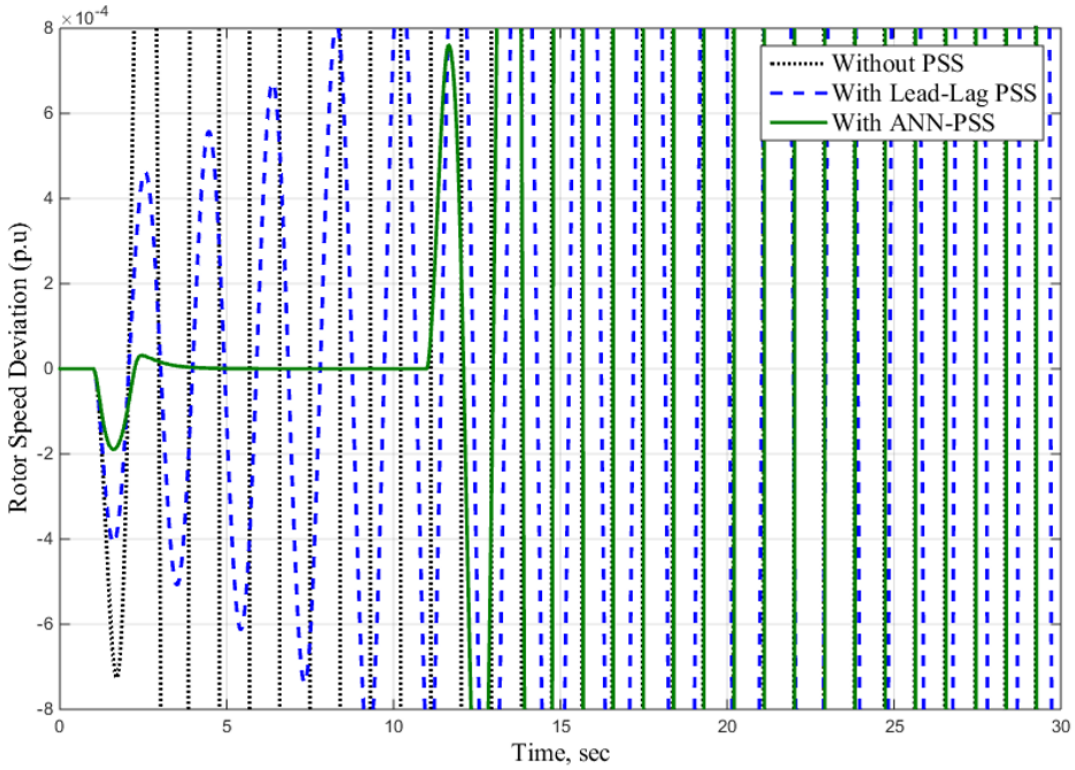

Figure 4.25. Time response of Δω due to disturbances at P = 1.05, Q = -0.6 and X_t = 0.8 pu

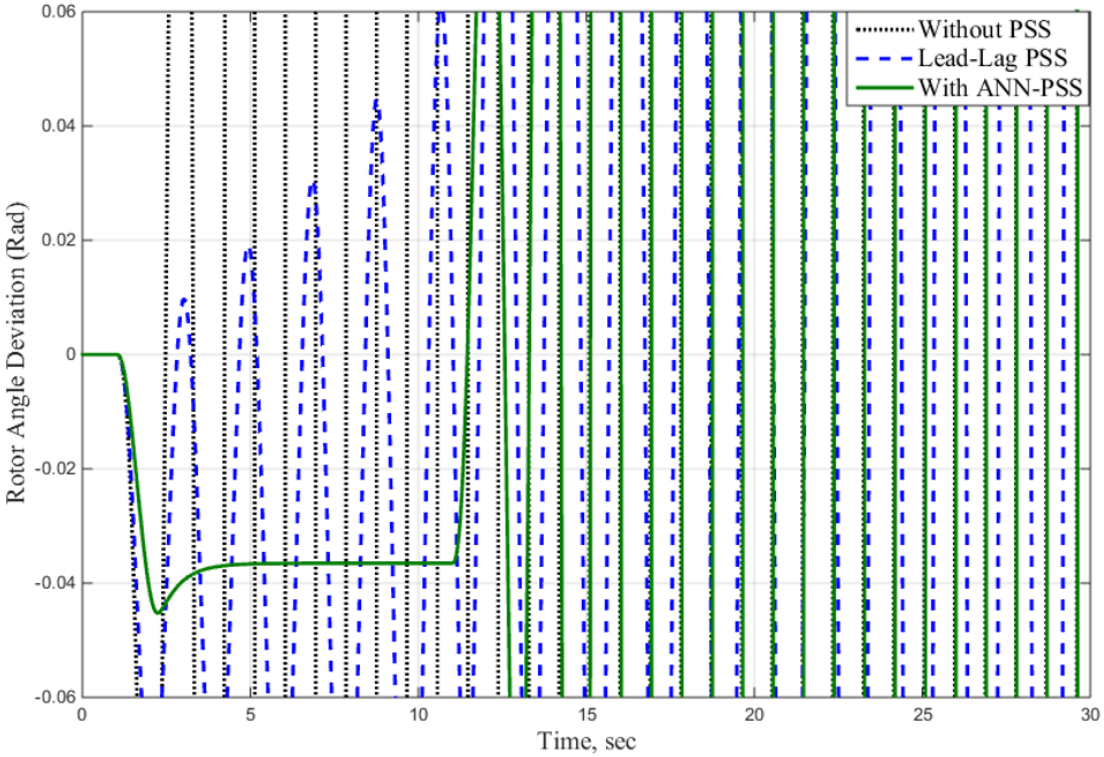

Figure 4.26. Time response of Δδ due to disturbances at P = 1.05, Q = -0.6 and X_t = 0.8 pu

4.6 Comparative Study

To indicate the superiority of the proposed controller (ANN-PSS) over the traditional controller (Lead-Lag PSS), Tables 4.1 to 4.4 present a comparative study between the controllers using calculations of the maximum peak value and the settling time for rotor speed response at different operating conditions. Changes in transformer reactance and in the amplifier gain, K_A, in the excitation system are also compared. From the tables, it is evident that the proposed ANN-PSS shows good time response with better maximum peak value and less settling time compared to the Lead-Lag PSS. The power system is stable with most of the operating conditions having been tested. Under a few of the more severe operating conditions, when the disturbance is caused by $\pm 1\%$ change in voltage reference (which is the input for the AVR), the power system with the proposed controller ANN-PSS is unstable.

Table 4.1. Comparative study between conventional PSS and proposed controllers with different operating conditions and ($X_t = 0.4,\ K_A = 100$)

	With Lead- lag PSS		With ANN-PSS	
Operating conditions	Max. peak value (P.U)	Settling time (sec)	Max. peak value (P.U)	Settling time (sec)
P = 0.85, Q = 0.65	$3 * 10^{-4}$	4.2	$2.12 * 10^{-4}$	3.1
P = 0.75, Q = 0.55	$2.85 * 10^{-4}$	4	$2.08 * 10^{-4}$	3.4
P = 0.75, Q = 0.0	$3 * 10^{-4}$	3.84	$2.2 * 10^{-4}$	3.2
P = 0.75, Q = -0.55	$3.3 * 10^{-4}$	4.1	$2.5 * 10^{-4}$	3.5
P = 0.85, Q = -0.65	$3.5 * 10^{-4}$	4.37	$2.7 * 10^{-4}$	3.8
P = 1.25, Q = 0.6	$3.6 * 10^{-4}$	4.5	$2.73 * 10^{-4}$	3.9
P = 1.25, Q = - 0.6	$4.8 * 10^{-4}$	6.47	$3.9 * 10^{-4}$	4.53

Table 4.2. Comparative study between conventional PSS and proposed controllers with different operating conditions and ($X_t = 0.6,\ K_A = 100$)

	With Lead- lag PSS		With ANN-PSS	
Operating conditions	Max. peak value (P.U)	Settling time (sec)	Max. peak value (P.U)	Settling time (sec)
P = 1.45, Q = 0.25	$3.9 * 10^{-4}$	> 10	$1.8 * 10^{-4}$	3.75
P = 1.25, Q = 0.5	$6.3 * 10^{-4}$	9.2	$5.1 * 10^{-4}$	5.5
P = 1.05, Q = 0.6	$5 * 10^{-4}$	6.67	$3.8 * 10^{-4}$	5.07
P = 0.85, Q = 0.6	$3.7 * 10^{-4}$	5.6	$2.7 * 10^{-4}$	3.55
P = 0.85, Q = - 0.6	$4.1 * 10^{-4}$	5.6	$3.2 * 10^{-4}$	3.9
P = 1.05, Q = - 0.6	$5.7 * 10^{-4}$	9.8	$4.7 * 10^{-4}$	5.15
P =1.45, Q = - 0.25	$6.1 * 10^{-4}$	7.6	$5 * 10^{-4}$	5

Table 4.3. Comparative study between conventional PSS and proposed controllers with different operating conditions and ($X_t = 0.8,\ K_A = 100$)

	With Lead- lag PSS		With ANN-PSS	
Operating conditions	Max. peak value (P.U)	Settling time (sec)	Max. peak value (P.U)	Settling time (sec)
P = 1.05, Q = 0.5	$7.5 * 10^{-4}$	> 10	$6 * 10^{-4}$	6.4
P = 0.85, Q = 0.6	$5.8 * 10^{-4}$	> 10	$4.5 * 10^{-4}$	5.1
P = 0.85, Q = - 0.6	$5.2 * 10^{-4}$	> 10	$4.1 * 10^{-4}$	5.05
P = 1.05, Q = -0.6	∞	∞	∞	∞
P = 1.45, Q = 0	$7.1 * 10^{-4}$	> 10	$6.2 * 10^{-4}$	5.6

Table 4.4. Comparative study between conventional PSS and proposed controllers with different operating conditions and ($X_t = 0.6$)

	With Lead- lag PSS		With ANN-PSS	
Operating conditions	Max. peak value (P.U)	Settling time (sec)	Max. peak value (P.U)	Settling time (sec)
P = 1.25, Q = 0.45 $K_A = 120$	$6.5 * 10^{-4}$	10	$5.5 * 10^{-4}$	5.4
P = 1.05, Q = 0.5 $K_A = 110$	$4.9 * 10^{-4}$	5.43	$3.7 * 10^{-4}$	4.8
P = 0.85, Q = 0.6 $K_A = 100$	$5.8 * 10^{-4}$	> 10	$4.5 * 10^{-4}$	5.1
P = 0.85, Q = - 0.6 $K_A = 90$	$3.8 * 10^{-4}$	6.3	$2.9 * 10^{-4}$	4.6
P = 1.05, Q = -0.6 $K_A = 90$	$5.5 * 10^{-4}$	9.5	$4.3 * 10^{-4}$	5.55
P = 1.25, Q = - 0.45 $K_A = 80$	$6.5 * 10^{-4}$	> 10	$5.4 * 10^{-4}$	4.7

4.7 Summary

In this chapter, two types of power system stabilizers were designed. One is a Lead-Lag power system stabilizer, and the other is an intelligent controller (ANN-PSS). The main goal in designing a Lead-Lag PSS is to understand the construction and tuning of this type of stabilizer, as it is still frequently used in the power systems. Additionally, the Lead-Lag PSS has been used in this chapter comparatively to show the effectiveness of the proposed controller and to demonstrate that, designing methodologies based on classical conventional control techniques do not formally guarantee driver robustness at the design stage. However, the advances achieved in computer processing speed and memory capacity over the past few years have allowed the use of robust control techniques for the design of damping controllers, such as the proposed controller (ANN-PSS). The proposed ANN-PSS is designed based on a reduced order model of the power

system, which consists of a synchronous generator represented by a two-axis model and equipped with IEEE type-1 excitation and turbine governor systems connected to the network, to improve the system's dynamic performance and to adapt real-time controller parameters due to changes in the loading conditions.

In order to reduce the lengthy time required to train the network in ANN-PSS, this research used a neural network with only three hidden neurons and three inputs to mimic a PID controller, as explained above. The input signals to the ANN-PSS were the aberration speed, $\Delta\omega$, the integral of speed change, $\int \Delta\omega$, and the derivative of the speed deviation, $\Delta\dot{\omega}$. The digital simulation results show that the system with the proposed ANN-PSS produces proper damping characteristics at different operating conditions. The digital simulation results showed that the system with Lead-Lag PSS and ANN-PSS yielded proper damping characteristics under some operating conditions, whereas the system with the ANN-PSS gave better dynamic response compared with the Lead-Lag PSS controller under the same operating conditions. These improved parameters increase a power system's reliability. Under severe operating conditions as is shown in Figure 4.25 and Figure 4.26 when the disturbance caused by -1% change in voltage reference (which is the input for the AVR), the power system with the proposed controller ANN-PSS was unstable. Thus, the proposed ANN-PSS can be said to provide good dynamic response only under limited operating conditions, but it is still better than conventional Lead-Lag PSS.

Chapter 5

5 Design of a Novel Fuzzy Logic PSS (FLPSS) for a Reduced-Order Power System

5.1 Fuzzy Logic Control Principles

A brief review of some basic concepts of fuzzy logic and fuzzy control will be presented in this chapter. A more comprehensive review of the subject is covered in detail in [36] [78] [79].

Unlike the classical control approach, which requires an in-depth understanding of a power system along with exact equations and precise numerical values, the philosophy behind fuzzy logic control is applicable for a power system. It allows for the modeling of a complex system using a higher-level abstraction originating in accumulated knowledge and experience. Fuzzy logic also allows for the expression of knowledge in linguistic commands rather than crisp values in control systems. This linguistic concept can be reflected in certain (*if……..then*) production rules. Fuzzy logic theory is attractive to some operators in that it gives computers the ability to make flexible and highly responsive control, which in the past had to be performed by human judgment. In the previous methodology, a condition could be judged by the computer as being only either correct or incorrect, but this theory permits to judging something to be almost correct or very correct. The applications of fuzzy logic control techniques appear to be suitable for a power system in light of the following factors:

- Improved robustness over that obtained using conventional linear controllers.
- Simplified control design for difficult-to-model systems (to design fuzzy logic controllers, there is no need for an accurate model of the power system).
- Low computational burden and simplified computer implementation.

5.2 Basic Concept of Fuzzy Logic

The following summarizes the basic concepts of fuzzy set theory that will be used in control signal algorithms [36] [78] [80].

5.2.1 Fuzzy Sets

A fuzzy set is a generalization of concepts of an ordinary bivalent set or crisp set. If C is a crisp set defined in universe U, then for any element u of U, either u ∈ C [$\mu_C(u) = 1$] or u ∉ C [$\mu_C(u) = 0$]. For any crisp set C it is possible to define a characteristic function as follows:

$$\mu_C(u) = \begin{cases} 1 & \text{if } u \in C \\ 0 & \text{if } u \notin C \end{cases} \tag{5.1}$$

The central concept of the fuzzy set theory is that the membership function, (μ), can have a value between 0 and 1. The membership function (μ) has a relationship with the x-axis called the universe of discourse or domain of discourse (U). In fuzzy logic theory, the characteristic function is generalized to a membership function (MF) that assigns u ∈ U a value from the unit interval [0, 1] instead of a two-element set {0, 1}. The set defined on the basis of such an extended membership function is called a fuzzy set $\mu_C: U \rightarrow [0,1]$. The fuzzy set is represented as follows:

$$C = \mu_1/u_1 + \cdots + \mu_n/u_n = \sum_{i=1}^{n} \mu_C(u_i)/u_i \tag{5.2}$$

In equation (5.2), the symbol (+) is not an addition as in the normal algebraic sense, but instead denotes a fuzzy arithmetic union operation and the symbol (/) is a delimiter. Thus, the numerator of each term is the membership value in fuzzy set C associated with the element of the universe indicated in the denominator.

The membership function has different shapes such as triangular, trapezoidal and Gaussian membership function [79]:

- Triangular membership function: the triangular curve is a function of vector x and depends on three parameters (a, b and c), as given below:

$$f(x,a,b,c) = \begin{cases} 0, & x \le a \\ \dfrac{x-a}{b-a} & a < x \le b \\ \dfrac{c-x}{c-b} & b \le x < c \\ 0, & c \le x \end{cases} \tag{5.3}$$

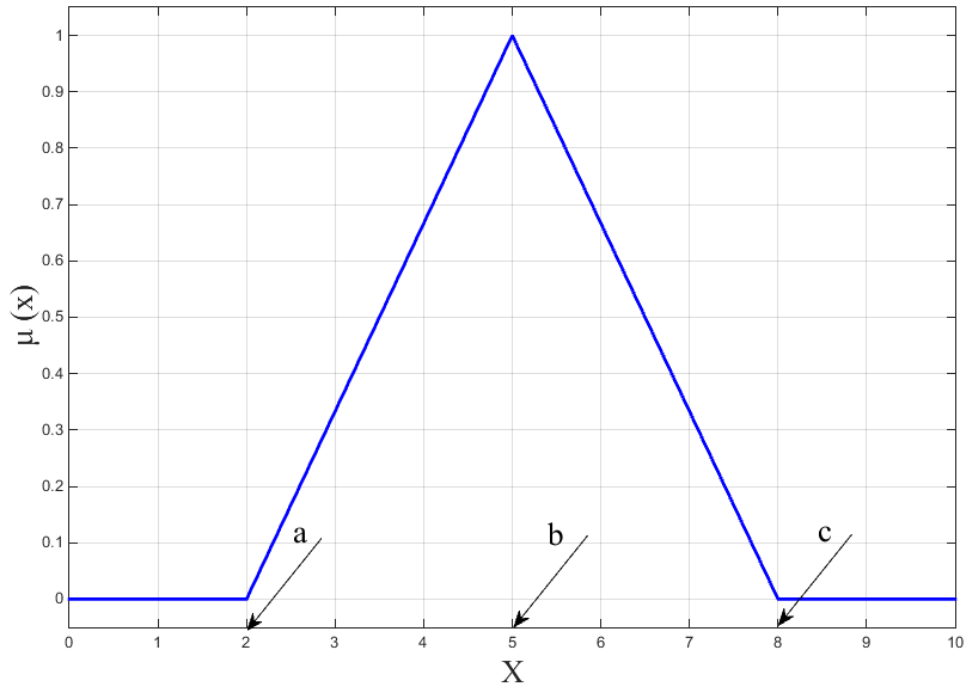

Figure 5.1. Triangular membership function of fuzzy set

- Trapezoidal membership function: the triangular curve is a function of a vector x, and depends on four parameters (a, b, c and d), as given below:

$$f(x,a,b,c,d) = \begin{cases} 0, & x \le a \\ \dfrac{x-a}{b-a} & a < x \le b \\ 1, & b \le x \le c \\ \dfrac{d-x}{d-c} & c < x < d \\ 0 & x \ge d \end{cases} \tag{5.4}$$

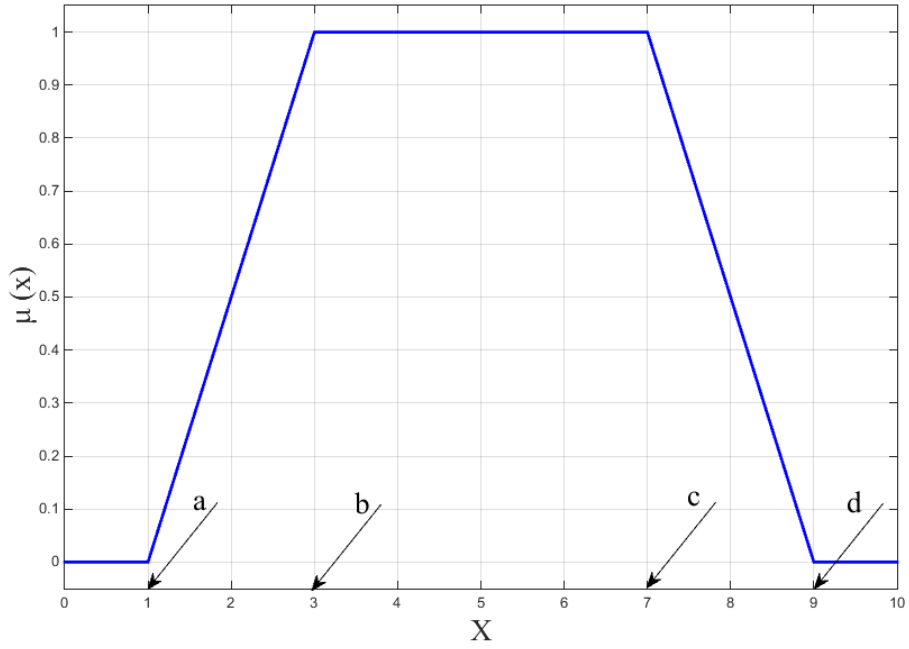

Figure 5.2. Trapezoidal membership function of fuzzy set

❖ Gaussian membership function: the symmetric Gaussian function depends on two parameters (a and b), as shown in the following equation:

$$f(x,a,b) = e^{\left[\frac{-(x-b)^2}{2*a^2}\right]} \tag{5.5}$$

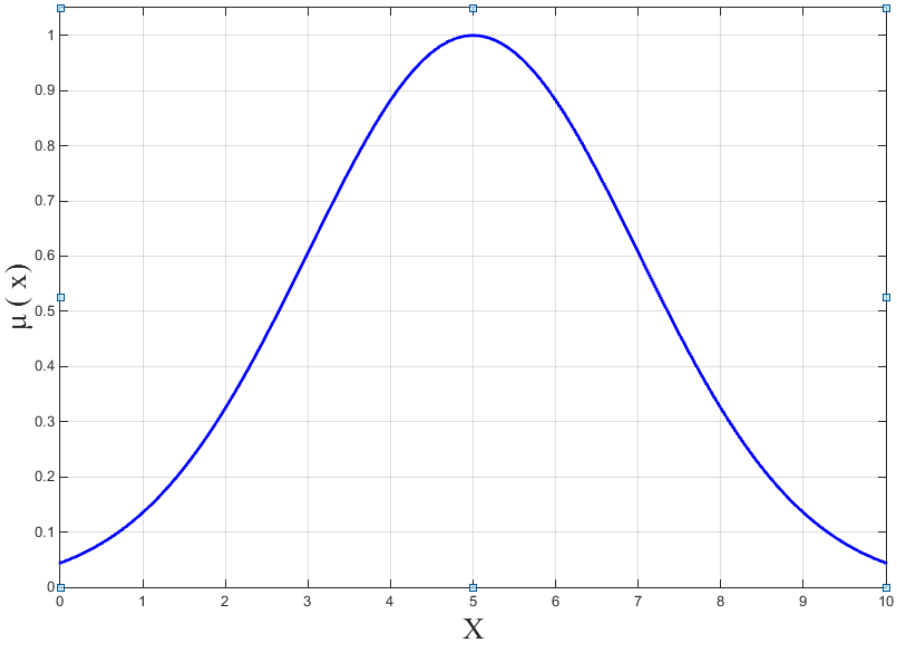

Figure 5.3. Gaussian membership function of fuzzy set

The selection of the membership function is up to the designer of the controller and application. Fuzzy sets represented by a symmetrical triangular are most commonly used because their computation is quite simple and give good results.

5.2.2 Fuzzy Set Operations

Fuzzy sets theory involves very complicated theorems, most of which are not related to the development of fuzzy control applications. The following definition is used in control system algorithms for fuzzy sets. Let A and B be two fuzzy sets within classical set X with the membership functions of μ_A and μ_B, respectively. The following fuzzy set operations, shown in Figure 5.4, can be defined as [80]:

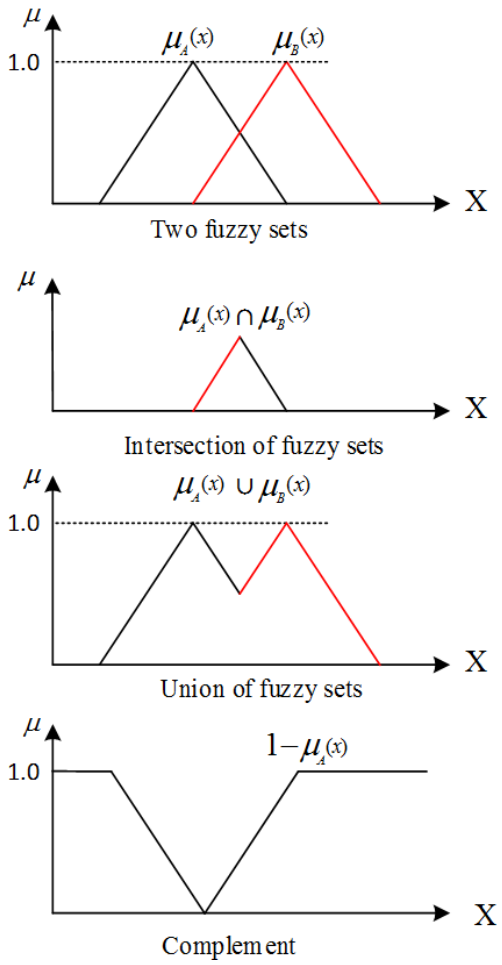

Figure 5.4. Operators on fuzzy sets

❖ Equality of fuzzy sets:

Two fuzzy sets A and B, are equal if they have the same membership function on the classical set X

$$\mu_A(x) = \mu_B(x) \quad \forall x \in X \tag{5.6}$$

❖ Union of fuzzy sets:

The union of two fuzzy sets, A and B, corresponding to the Boolean OR function, is given by the following equation:

$$\mu_{A\cup B}(x) = \mu_{A+B}(x) = \max\big(\mu_A(x), \mu_B(x)\big) \quad \forall\, x \in X \tag{5.7}$$

❖ Intersection of fuzzy sets:

The intersection of two fuzzy sets, A and B, corresponding to the Boolean AND function, is given by:

$$\mu_{A\cap B}(x) = \min\big(\mu_A(x), \mu_B(x)\big) \quad \forall\, x \in X \tag{5.8}$$

❖ Complement of fuzzy sets:

The complement of fuzzy set, A, corresponding to the Boolean NOT function, is given as follows:

$$\mu_{-A}(x) = 1 - \mu_A(x) \quad \forall\, x \in X \tag{5.9}$$

5.3 Fuzzy Logic Control (FLC)

The basic construction of a fuzzy logic control (FLC) system is shown in Figure 5.5. It consists of three stages: the fuzzification stage, the rule and inference stage, and defuzzification stage. The fuzzification stage is a process of mapping inputs to the FLC into fuzzy set membership values, with decisions needed to be made regarding number of inputs, size of the x-axis of the fuzzy sets, and number and shape of the fuzzy sets. A FLC that mimics a proportional derivative controller (PD) will be required to minimize the error E (t) and the rate of change of the error $dE(t)/dt$ [36] [80].

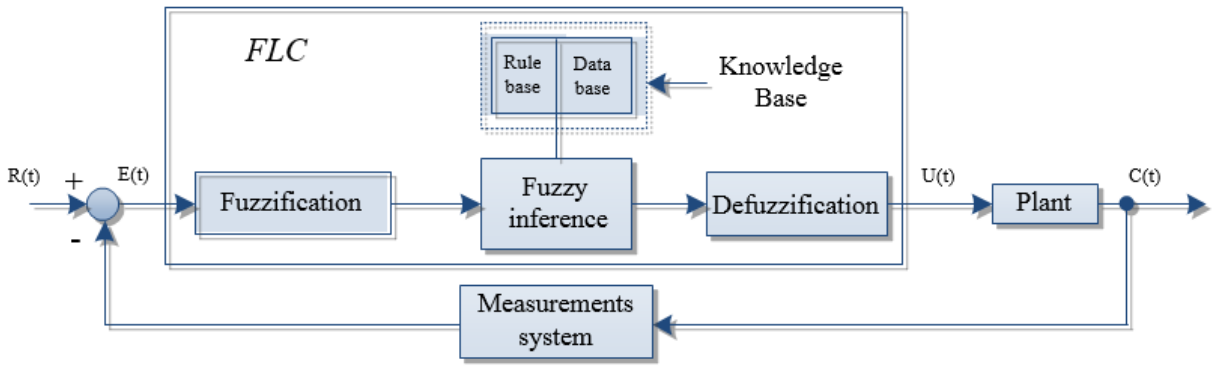

Figure 5.5. Fuzzy logic control system

The number and shape of fuzzy sets is a compromise between the accuracy of control action and real-time computational complications. For seven linguistic variables, the input domain can be described by appropriate linguistic terms, such as positive large (PL), positive medium (PM), positive small (PS), about zero (Z), negative small (NS), negative medium (NM), and negative large (NL). A fuzzy rule base consists of a set of antecedent-consequent linguistic rules of the form as in equation (5.10). A typical set of fuzzy interface rules is shown in Table 5.1 [80] [81]

$$\text{IF} \quad E \quad \text{is} \quad PS \quad \text{AND} \quad dE \quad \text{is} \quad NS \quad \text{THEN} \quad U \text{ is } Z \tag{5.10}$$

The rule-base is constructed using prior knowledge from either one or all of the following sources: the physical laws that govern plant dynamics, data from existing controllers, and knowledge obtained from experience experts. Defuzzification is the process of mapping a set of inferred fuzzy control signals contained within a fuzzy output window to a non-fuzzy (crisp) control signal. The center of the area method is the most known defuzzification technique, which can be expressed as:

$$\text{Crisp control signal} = \frac{\text{sum of the first moments of area}}{\text{sum of areas}} \tag{5.11}$$

Table 5.1. Typical fuzzy logic control rules [80]

dE \ E	NL	NM	NS	Z	PS	PM	PL
NL	NL	NL	NL	NM	NM	NS	Z
NM	NL	NL	NM	NM	NS	Z	PS
NS	NL	NM	NS	NS	Z	PS	PM
Z	NM	NM	NS	Z	PS	PM	PM
PS	NM	NS	Z	PS	PS	PM	PL
PM	NS	Z	PS	PM	PM	PL	PL
PL	Z	PS	PM	PM	PL	PL	PL

5.4 Fuzzy Logic Power System Stabilizer FLPSS

Most current electrical power systems have long transmission lines and remote sources of generation. Such systems typically have high series impedance, which reduces system stability. The application of a conventional power system stabilizer (CPSS) to improve the dynamic performance power system has been the focus of extensive studies for some time. These have a fixed structure, constant parameters, and are tuned for one operating point. Due to power system drifts that arise due to continuous load changes or unpredictable major disturbances such as three-phase faults, it is desirable (and, in fact, preferable) to adapt a power stabilizer parameters in real

time based on online measurement in order to maintain good dynamic performance over a wide range of operating conditions.

The desirable performance has motivated the development of a self-tuning power system stabilizer. Although the self-tuning power system stabilizer is capable of offering better dynamic performance than a conventional power system stabilizer, it requires model identification in real time, which can be very time-consuming. The nonlinear behaviour of a power system can be approximated by linear models and additional information must be supplied in order to design reliable and well-performing controllers. An important source of such information is the knowledge of plant operators, control engineers and process designers. A FLC technique has been found to be a good replacement for conventional power system stabilizer techniques [53] [55] - [57] [81] [82].

5.5 Design of a Novel Fuzzy Logic PSS (FLPSS) for a Reduced Order Power System

A common way to damp electromechanical low-frequency oscillations in a power system is to use additional control signals with an automatic voltage regulator (AVR) fed by a speed deviation signal. Conventional design techniques use a single machine infinite bus system (SMIB) to design a power system stabilizer based on the transfer function between the AVR's input and the resultant torque. In this technique, the external equivalent reactance and the voltage at the infinite bus or their estimation value must be known. Other conventional design methods require all of the system information such as P-Vr characteristic and residue [20].

The proposed method uses the information at the secondary side of a step-up transformer to deduce a power system model, and the order of which is then reduced to design the PSS. The basic schematic of a proposed fuzzy logic power system stabilizer (FLPSS) is shown in Figure 5.6.

The inputs of such a controller are selected to be the generator speed deviation, $\Delta\omega$, and the derivative of the speed deviation $\Delta\dot{\omega}$. In practice, only speed variation can be sampled at regular intervals defined by a sampling period. The rate of speed deviation (acceleration) can be derived from the speed signals measured at two successive sampling intervals using the following equation:

$$\Delta\dot{\omega} = (\Delta\omega(k) - \Delta\omega(k-1))/\Delta T \tag{5.12}$$

where ΔT is the sample interval.

The decisions in the fuzzy logic approach are made by forming a series of control rules to cover all possible combinations of input variables (n) with membership functions (z). The number of control rules (F) will be ($F = z^n$). Most researchers have used fuzzy logic control as a power system stabilizer with two inputs, where each input has seven membership functions (typical control rules). The number of rules in this case will be the 49-rule [53] [56] [57] [82] [83]. However, increasing the number of rules requires more memory storage and processing time. To avoid these problems, only three membership functions for each input are used in this research. Thus, the number of rules will be 9 instead of the 49 used in the classical design.

As shown in Figure 5.6, it is clear that the values of speed deviation, $\Delta\omega$, and the acceleration, $\Delta\dot{\omega}$, pass through three stages: fuzzification, rule and inference, and defuzzification.

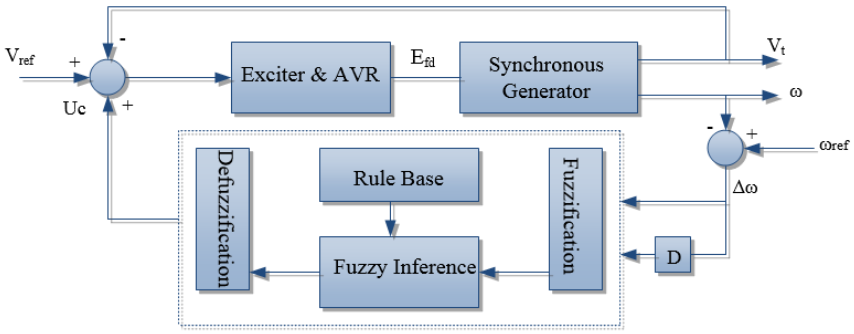

Figure 5.6. Schematic diagram of power system model configuration

In the fuzzification stage, the input crisp variables, $\Delta\omega(k)$ and $\Delta\dot{\omega}(k)$, are converted into fuzzy variables, $\Delta\omega$ and $\Delta\dot{\omega}$, by the triangular membership functions, as shown in Figure 5.7. Each input is divided into three fuzzy sets rather than seven fuzzy sets (seven being the dividing range of choice in most published research) [53] [56]; the three fuzzy sets are negative (N), about zero (Z) and positive (P). Each fuzzy variable is a number of subsets with a degree of membership $\mu(\Delta\omega)$ and $\mu(\Delta\dot{\omega})$ varying between zero (no membership) and one (full membership). The fuzzy variables $\Delta\omega$ and $\Delta\dot{\omega}$ produced by the fuzzification stage are then processed by an inference engine that executes a set of control rules, as shown in Table 5.2, where VLN is a very large negative, LN is a large negative, MN is medium negative, SN is small negative, Z is about zero, SP is small positive, MP is medium positive, LP is a large positive, and VLP is a very large positive. Figure 5.8 shows the output of the membership function. To simplify the calculations, these output membership functions do not overlap.

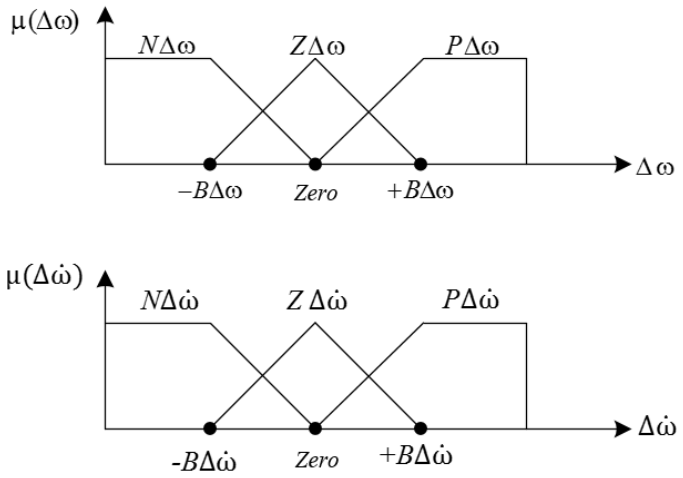

Figure 5.7. Fuzzy logic input triangular membership functions

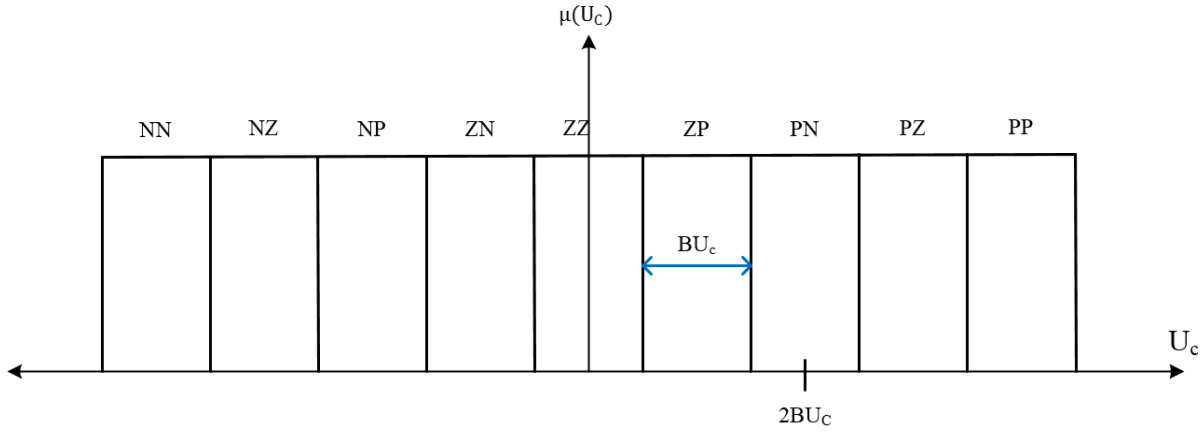

Figure 5.8. An output membership function

Table 5.2. Decision table

Δω	Δω̇		
	N	Z	P
N	VLN	LN	MN
Z	SN	Z	SP
P	MP	LP	VLP

For a system with two control variables and three linguistic variables, this leads to a 3×3 decision matrix. In Table 5.2, each fuzzy variable represents a fuzzy rule. The knowledge required to generate the fuzzy rules can be derived from understanding the behavior of the dynamic system under control. Each rule contributes to the output. The contribution is the minimum between the memberships $\mu(\Delta\omega)$ and $\mu(\Delta\dot{\omega})$. A typical rule has the following structure:

$$R: \text{if } (\Delta\omega) \text{ is } P \text{ AND } (\Delta\dot{\omega}) \text{ is } Z \text{ THEN } U_c \text{ is } LP \tag{5.13}$$

Because a crisp control signal is needed for the excitation system, the numerical value of the fuzzy controller is obtained from the output contributions using the centroid of area method as shown in equation (5.11).

In this dissertation, the FLPSS will be applied to a reduced order power system model, as shown in Figure 5.9. The original system is first formed, after which a proposed reduction technique is used and the roots of the reduced order model matrices are found. The FLPSS technique thus uses another control signal based on reduced order response:

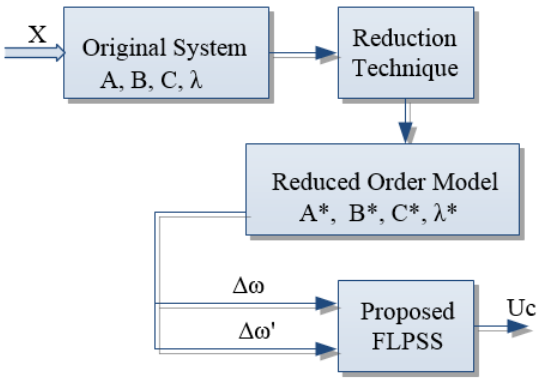

Figure 5.9. Block diagram of fuzzy logic power system stabilizer (FLPSS)

5.6 Determination of Fuzzy Logic Controller Parameters

As mentioned above, a fuzzy logic controller (FLC) that mimics a proportional derivative controller (PD) will be required to minimize the error, E (t), and the rate of change of the error, dE (t)/dt. The break points in a simplified fuzzy logic rule-based controller can be related to the PD gains. Therefore, in order to determine the parameters of an FLC that mimics a PD controller, the gains of the PD controller should be determined.

5.6.1 Design of Proportional-Derivative Controller

In the design of a fixed gain proportional-derivative controller (PD-PSS), the gain setting, K_P and K_D, can be computed by assigning a set of specified eigenvalues, $\lambda = \lambda_1$, $\lambda = \lambda_2$ and $\lambda = \lambda_3$, for the electromechanical mode of the synchronous generator connected to the network. This is referred to as the pole assignment technique. First, the linearized model of the power system is obtained around the operating condition. This model is given as [84]:

$$\Delta\dot{x}(t) = A\Delta x(t) + B\Delta u(t) \tag{5.14}$$

$$\Delta y(t) = C\,\Delta x(t) + D\,\Delta u(t) \tag{5.15}$$

The Laplace transform is then applied to the equations (5.14) and (5.15)

$$\Delta X(s) = (sI - A)^{-1}B\Delta U(s) \tag{5.16}$$

$$\Delta Y(s) = C\,\Delta X(s) + D\,\Delta U(s) \tag{5.17}$$

Next, by substitution of equation (5.16) into equation (5.17), the transfer function of the system can be obtained as follows:

$$TF(s) = \frac{\Delta Y(s)}{\Delta U(s)} = C(sI - A)^{-1}B + D = \frac{n(s)}{d(s)} \tag{5.18}$$

where n(s) is the numerator and d(s) is the denominator of the open loop transfer function.

The closed loop transfer function of the system that includes the PD controller can be obtained as follows:

$$\mathrm{TF}_{c.l}(\mathrm{s}) = \frac{\mathrm{n(s)} * (\mathrm{K_P} + \mathrm{sK_D})}{\mathrm{d(s)} + \mathrm{n(s)} * (\mathrm{K_P} + \mathrm{sK_D})} \tag{5.19}$$

The characteristic equation of the closed loop transfer function is:

$$\mathrm{d(s)} + \mathrm{n(s)} * (\mathrm{K_P} + \mathrm{sK_D}) = 0 \tag{5.20}$$

Comparing the characteristic equation of the closed loop transfer function with the characteristic equation that has the desired eigenvalues, the proportional gain, K_P, and the derivative gain, K_D, can be found.

5.6.2 Design of Fuzzy Logic Controller

After the PD controller gain has been obtained, the parameters of a simplified fuzzy logic controller can be found. Consider the case, where the derivative input $\Delta\dot{\omega}$ of a fuzzy logic controller is 100% positive and 0% negative. As the error input, $\Delta\omega$, of the fuzzy logic controller goes from 100% positive to 100% negative between the break points, $+B\Delta\omega$ and $-B\Delta\omega$, as shown in Figure 5.10, the output of the fuzzy logic controller, U_C, goes from $+4BU_C$ to $+2BU_C$ as shown in Figure 5.11.

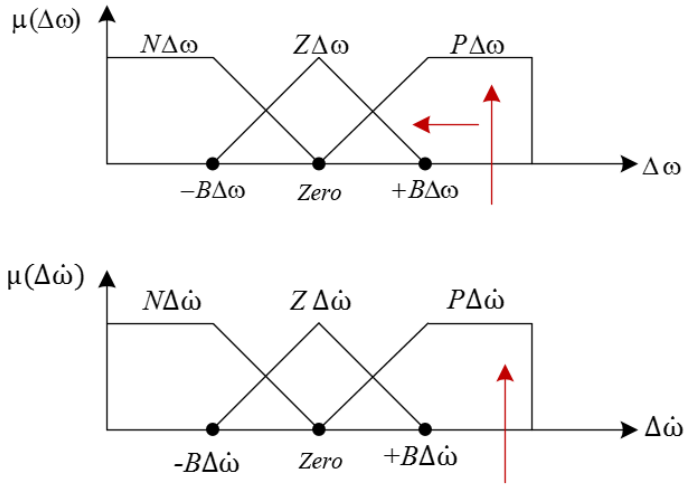

Figure 5.10. Fuzzy input membership functions (the error Δω is varied while Δω̇ is fixed)

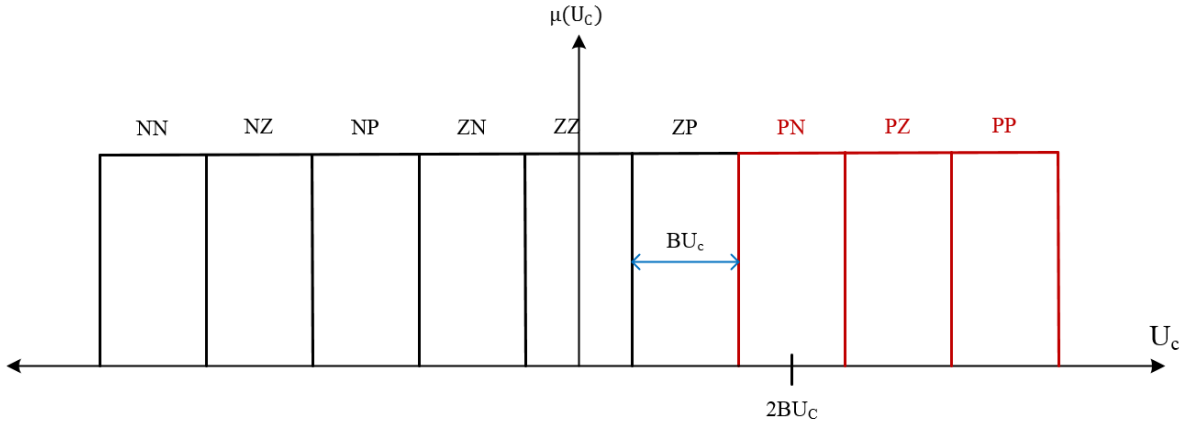

Figure 5.11. Output membership function generated by changed Δω and fixed Δω̇.

The relationship between changes in error break point BΔω and the resultant output controller's break points, BU_C, are found to be a straight line as shown in Figure 5.12.

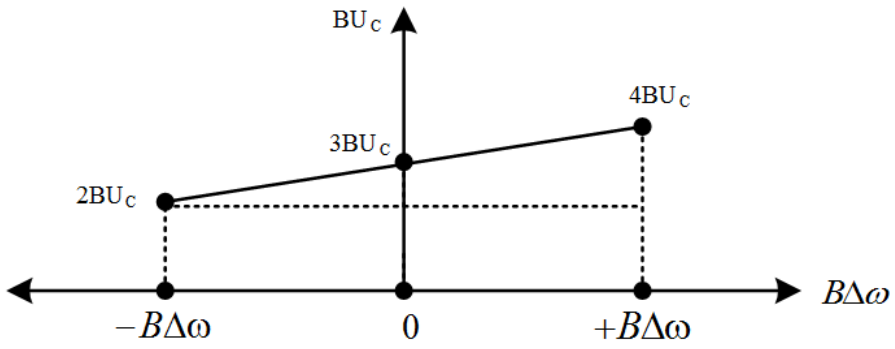

Figure 5.12. Relationship between changes in error break point, BΔω, and the resulting output controller's break points BU_C

The slope of the line is $BU_C/B\Delta\omega$ and is like the proportional gain K_P.

$$\text{Slope} = K_p = BU_C/B\Delta\omega \tag{5.21}$$

Similarly, the derivative gain can be found as follows:

$$\text{slope} = K_D = BU_C/B\Delta\dot{\omega} \tag{5.22}$$

A conventional PD controller (4BΔω) is equal to the saturation level of half of a control signal $U_{C\,s}/2$, while the other half is the derivative signal (4BΔω̇). This gives the equation for B U_C, where the gains, K_P and K_D, would also be known. Hence, the equations for BΔω and BΔω̇ are as follows:

$$BU_C = \frac{U_{CS}}{8} \rightarrow B\Delta\omega = \frac{U_{CS}}{8 * K_P} \tag{5.23}$$

and,

$$B\Delta\dot{\omega} = \frac{U_{CS}}{8 * K_D} \tag{5.24}$$

5.7 Digital Simulation Results

Numerical results are carried out on the power system as shown in Figure 2.2, which consists of a synchronous machine represented by a two-axis model and equipped with an IEEE type-1 excitation system and turbine governor system connected to the network. The fuzzy logic technique is applied as discussed above and compared with the artificial neural network power system stabilizer (ANN-PSS) designed in Chapter 4. The proposed ANN-PSS provides a better dynamic response compared to those of the Lead-Lag PSS for obtaining good dynamic performance over a wide range of operating conditions. The effectiveness of both FLPSS and ANN-PSS are characterized for a ±1% step change at input reference voltage applied at time 1, 11, and 21 seconds.

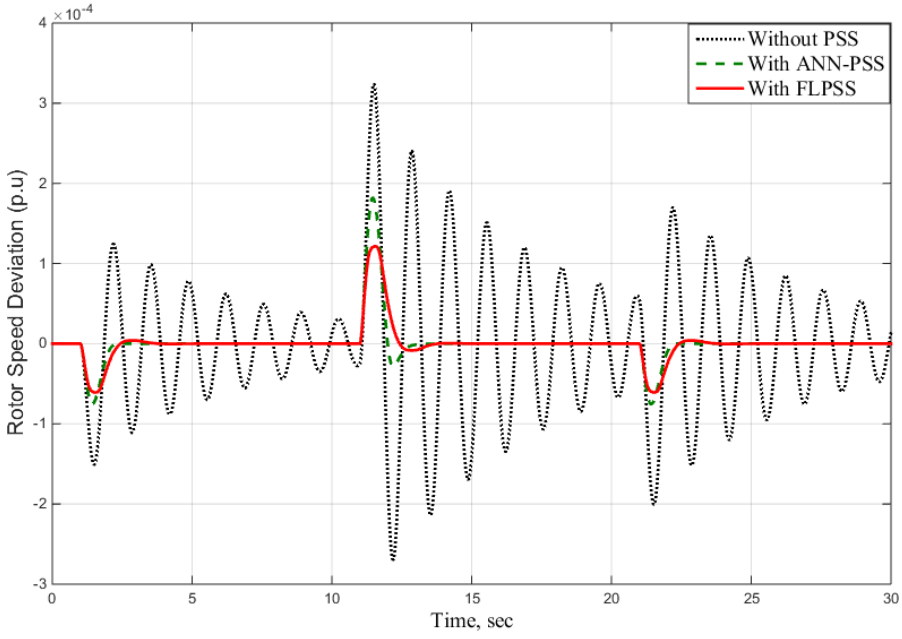

Figure 5.13. Time response of Δω due to disturbances at P = 0.25 and Q = 0.0 pu

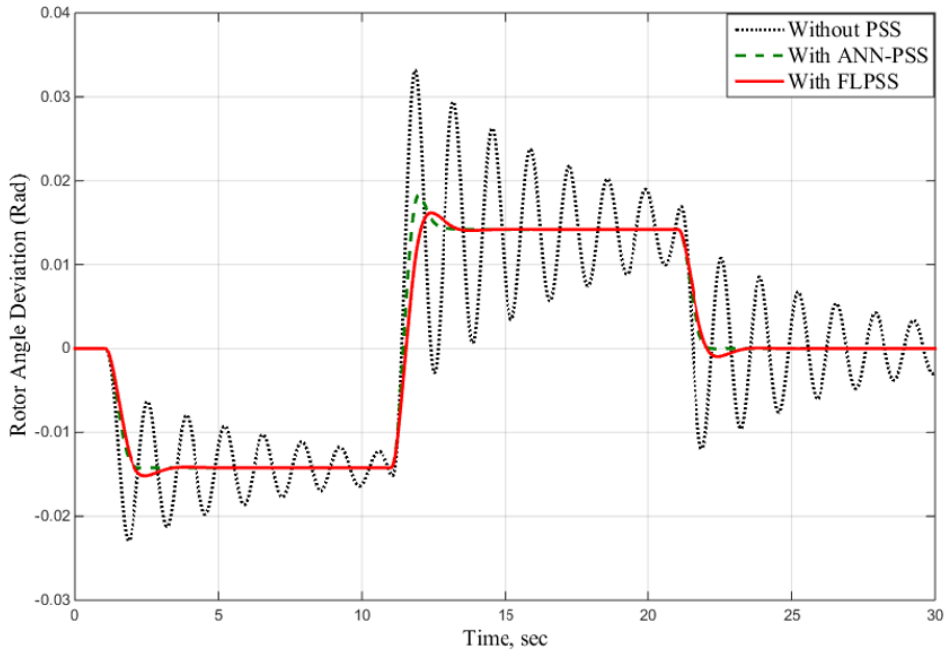

Figure 5.14. Time response of Δδ due to disturbances at P = 0.25 and Q = 0.0 pu

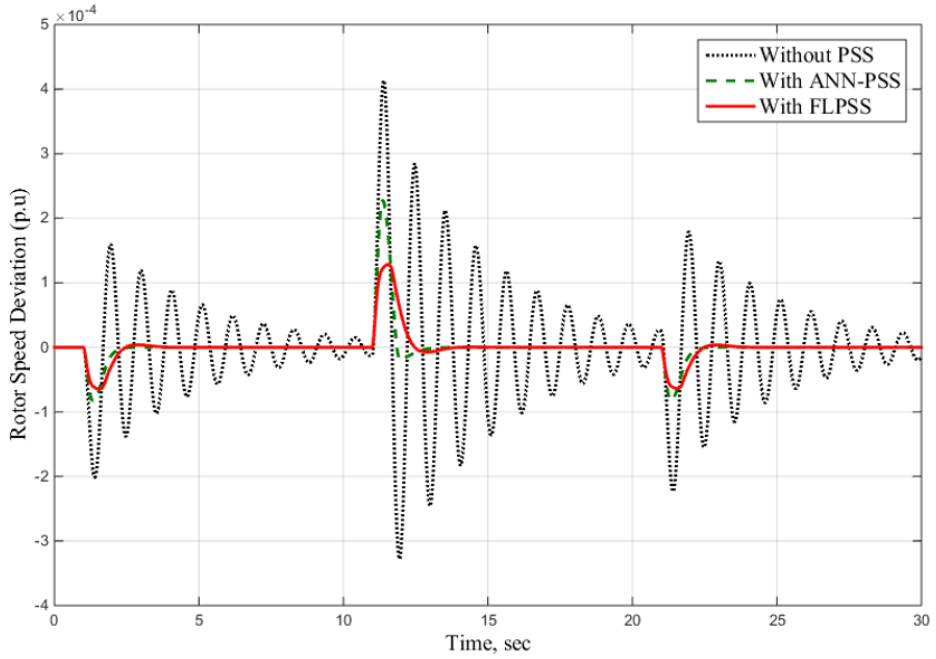

Figure 5.15. Time response of Δω due to disturbances at the normal operating condition

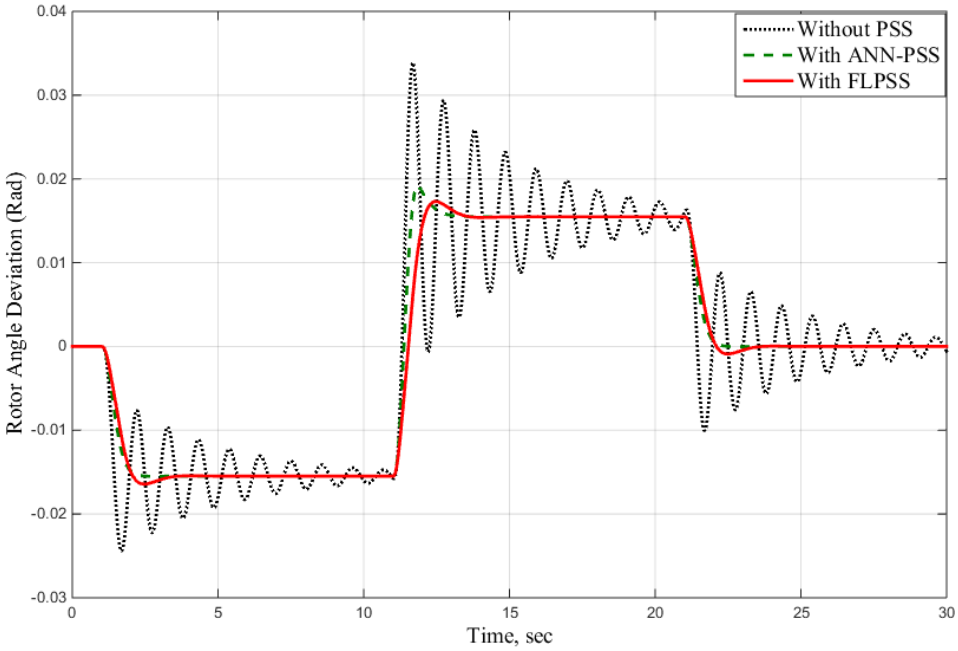

Figure 5.16. Time response of Δδ due to disturbances at the normal operating condition

In the results shown in Figures 5.13 to 5.16, it is assumed that the power transformer reactance is fixed at $X_t = 0.4$ P.U. The figures make it evident that the system at unity power factor due to a ±1% step change in input reference voltage (which is the input of AVR), applied at time 1, 11 and 21 seconds. caused persistent oscillations for a relatively long period. These oscillations were damping very fast in both proposed controllers for ANN-PSS and FLPSS. However, in practical cases the power transformers are connected in series with the transmission lines. The following examples (Figures 5.17 to 5.24) will show the reactance changing at lagging and leading power factors cases in order to gauge the efficacy of the proposal controller of FLPSS for changes in parameters and operating conditions

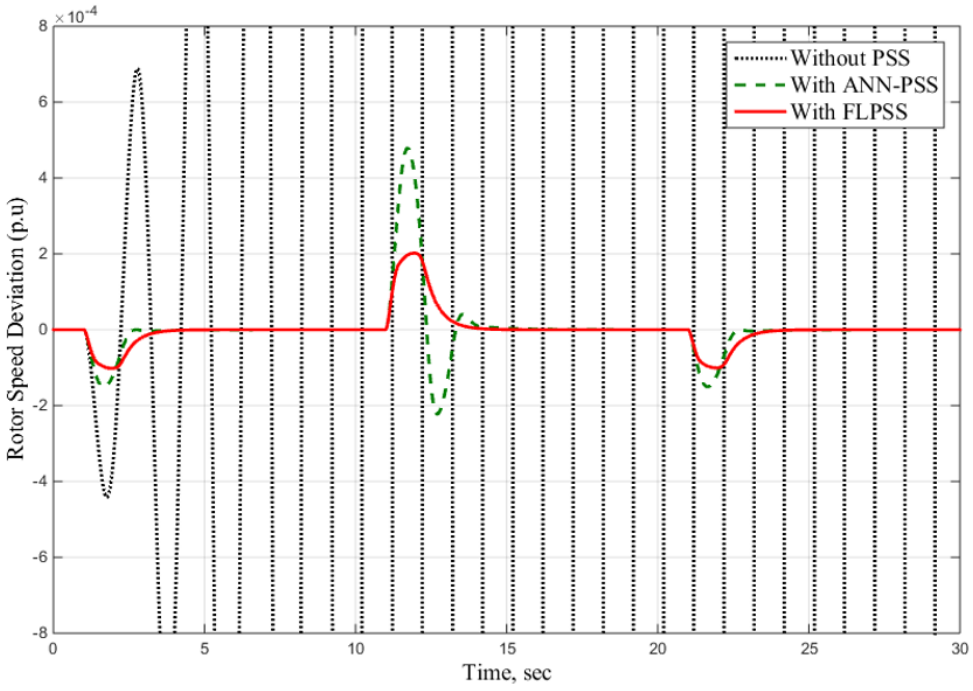

Figure 5.17. Time response of $\Delta\omega$ due to disturbances at P = 0.85, Q = 0.65 and X_t = 0.8 pu

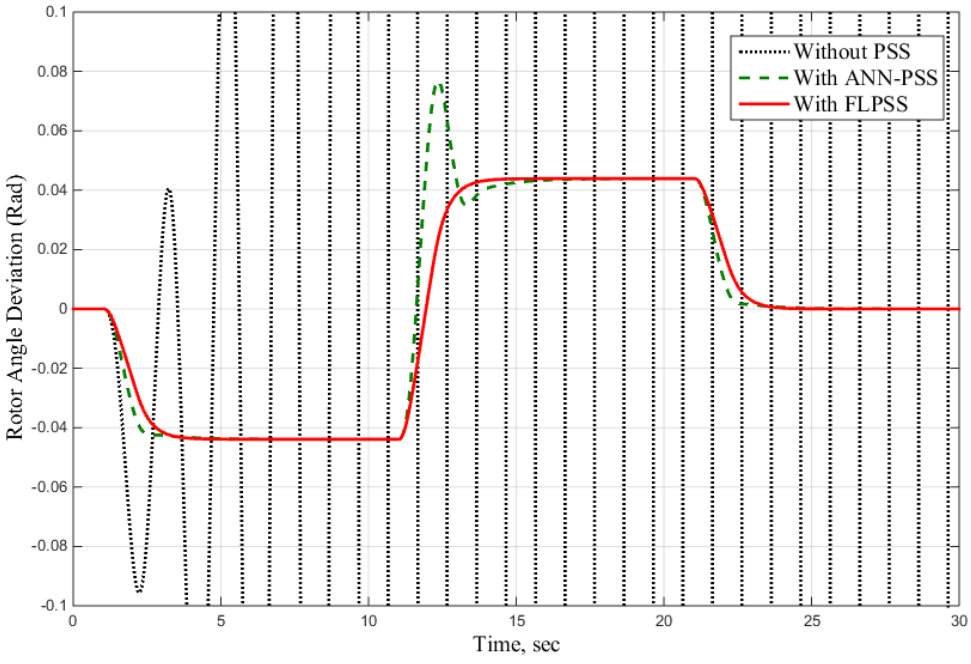

Figure 5.18. Time response of $\Delta\delta$ due to disturbances at P = 0.85, Q = 0.65 and X_t = 0.8 pu

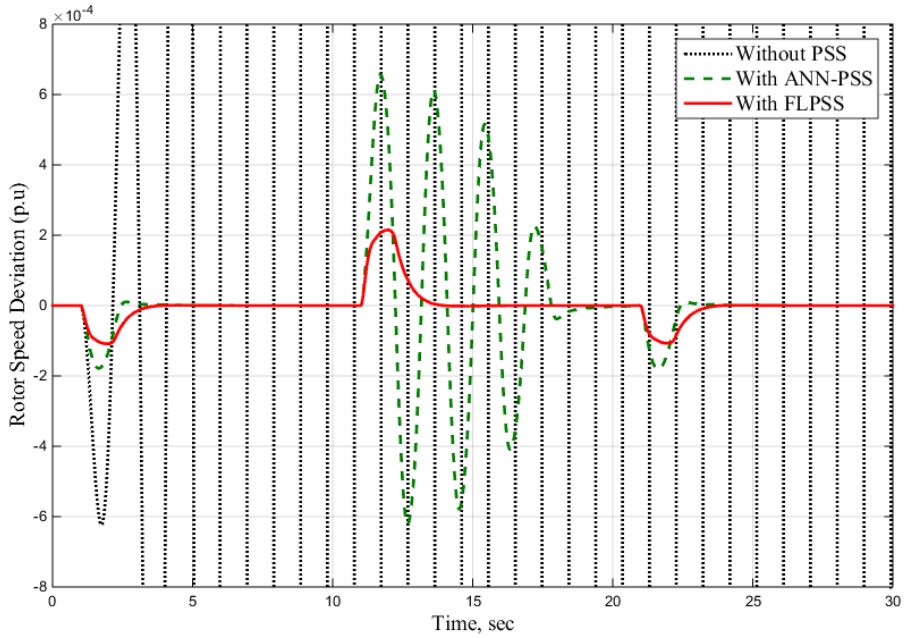

Figure 5.19. Time response of $\Delta\omega$ due to disturbances at P = 1.25, Q = 0.6 and X_t = 0.65 pu

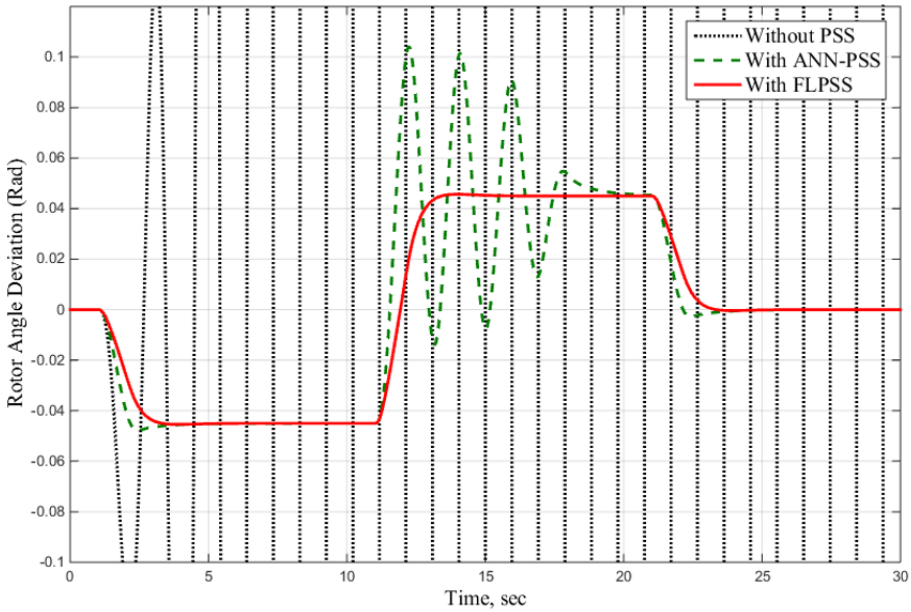

Figure 5.20. Time response of $\Delta\delta$ due to disturbances at P = 1.25, Q = 0.6 and X_t = 0.65 pu

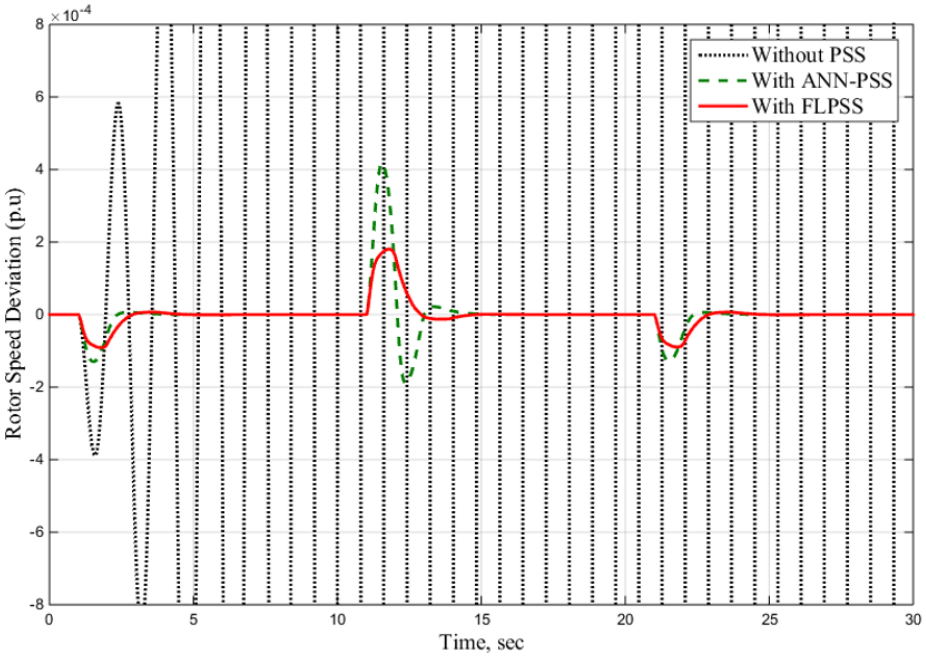

Figure 5.21. Time response of $\Delta\omega$ due to disturbances at P = 0.85, Q = -0.6 and X_t = 0.8 pu

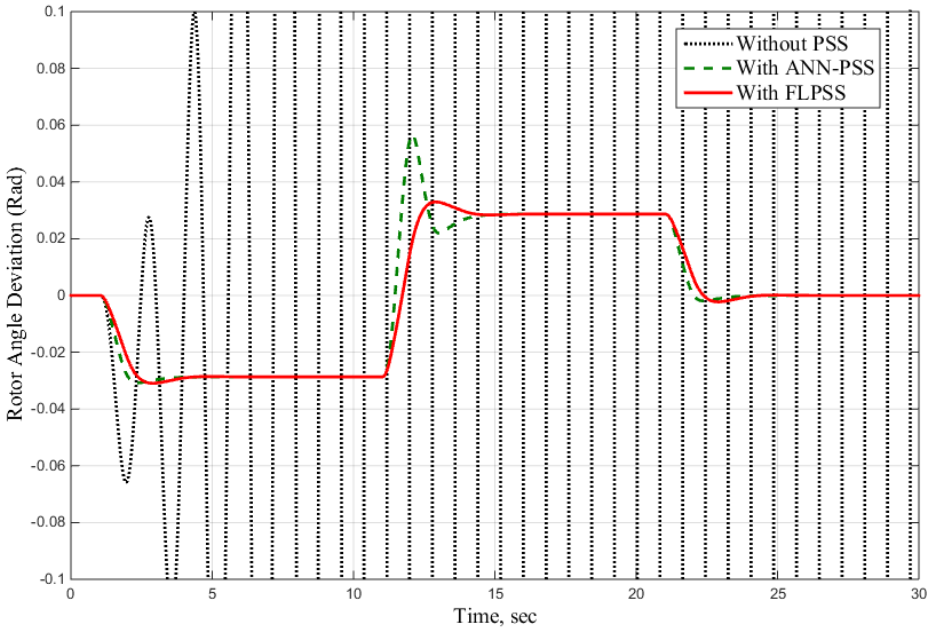

Figure 5.22. Time response of $\Delta\delta$ due to disturbances at P = 0.85, Q = -0.6 and X_t = 0.8 pu

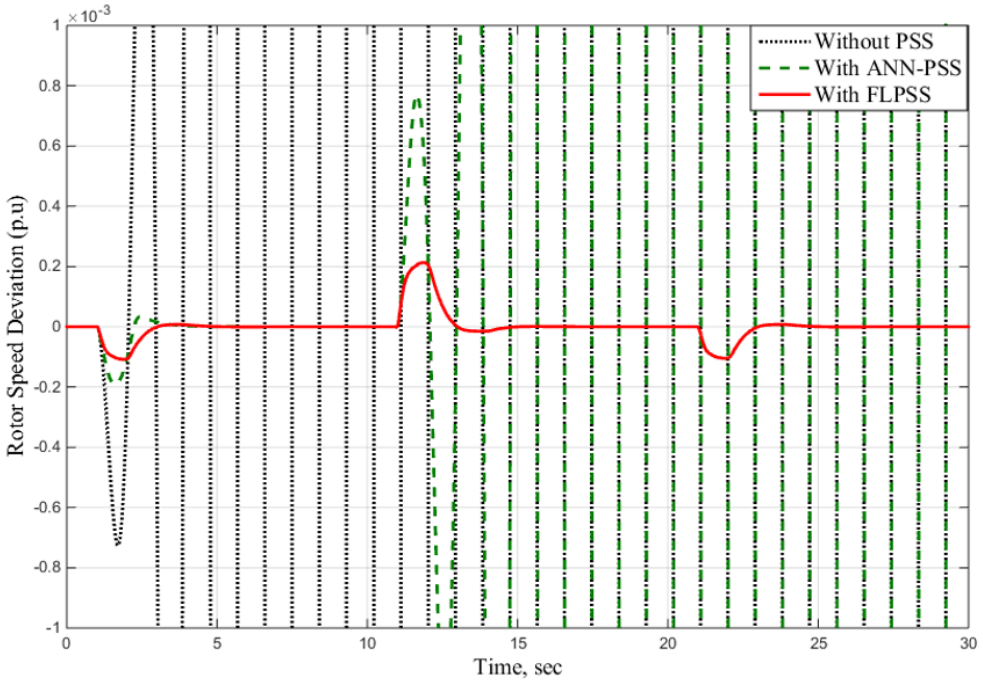

Figure 5.23. Time response of $\Delta\omega$ due to disturbances at P = 1.05, Q = -0.6 and X_t = 0.8 pu

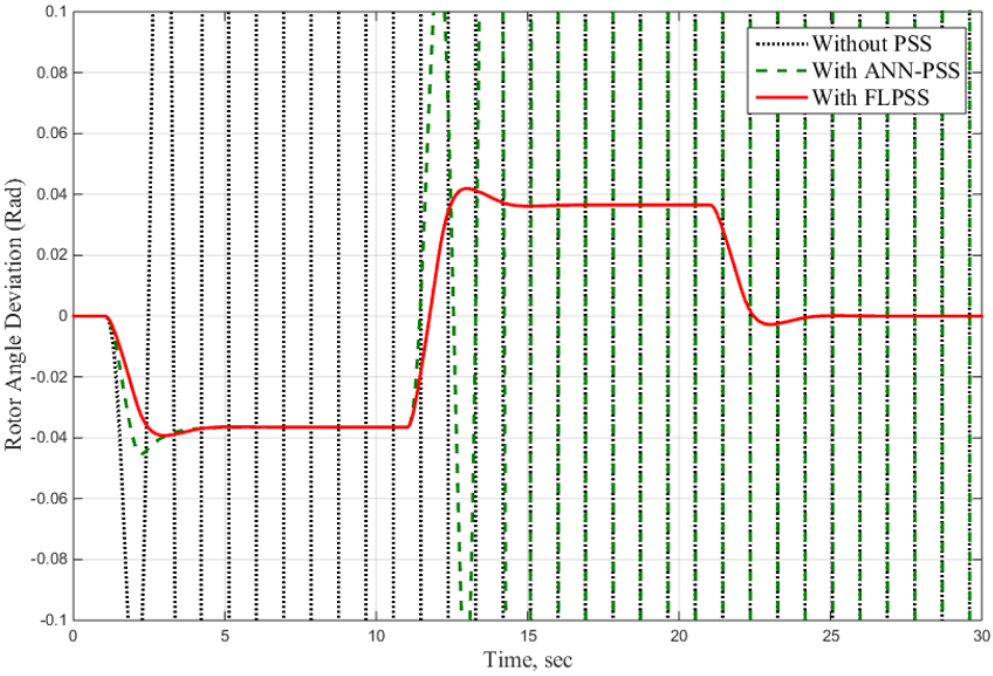

Figure 5.24. Time response of $\Delta\delta$ due to disturbances at P = 1.05, Q = -0.6 and X_t = 0.8 pu

5.8 Comparative Study

The purpose of the following comparison is to demonstrate the superiority of the proposed controller, FLSS, over the artificial neural network, ANN-PSS, introduced in Chapter 4. The ANN-PSS gives better performance than the lead-lag power system stabilizer (Lead-Lag PSS). Table 5.3 to Table 5.6, contain a comparative study of the proposed controllers for maximum peak value and the settling time for rotor speed response at different operating conditions and changes in power transformer reactance. From these tables, it is clear that the proposed fuzzy logic power system stabilizer has good time response in terms of better maximum peak values and less settling time compared to those of the artificial neural network power system stabilizer (ANN-PSS). The power system remains stable under FLPSS for all the operating conditions that have been tested, whereas the power system with the ANN-PSS suffered from instability issues under some operating conditions.

Table 5.3. Comparative study between proposed controllers (ANN-PSS and FLPSS) with different operating conditions and ($X_t = 0.4$)

	With ANN-PSS		With FLPSS	
Operating conditions	Max. peak value (P.U)	Settling time (sec)	Max. peak value (P.U)	Settling time (sec)
P = 0.85, Q = 0.65	$2.12 * 10^{-4}$	3.1	$0.6 * 10^{-4}$	3.1
P = 0.75, Q = 0.55	$2.08 * 10^{-4}$	3.4	$1.2 * 10^{-4}$	3.4
P = 0.75, Q = 0.0	$2.2 * 10^{-4}$	3.2	$1.1 * 10^{-5}$	3.2
P = 0.75, Q = -0.55	$2.5 * 10^{-4}$	3.5	$1.35 * 10^{-4}$	3.5
P = 0.85, Q = -0.65	$2.7 * 10^{-4}$	3.8	$1.4 * 10^{-4}$	3.8
P = 1.25, Q = 0.6	$2.73 * 10^{-4}$	3.9	$1.46 * 10^{-4}$	3.9
P = 1.25, Q = - 0.6	$3.9 * 10^{-4}$	4.53	$1.73 * 10^{-4}$	4

Table 5.4. Comparative study between proposed controllers (ANN-PSS and FLPSS) with different operating conditions and ($X_t = 0.6$)

	With ANN-PSS		With FLPSS	
Operating conditions	Max. peak value (P.U)	Settling time (sec)	Max. peak value (P.U)	Settling time (sec)
P = 1.45, Q = 0.25	$1.8 * 10^{-4}$	3.75	$1 * 10^{-4}$	3.1
P = 1.25, Q = 0.5	$5.1 * 10^{-4}$	5.5	$1.9 * 10^{-4}$	4.2
P = 1.05, Q = 0.6	$3.8 * 10^{-4}$	5.07	$1.78 * 10^{-4}$	4.01
P = 0.85, Q = 0.6	$2.7 * 10^{-4}$	3.55	$1.35 * 10^{-4}$	3.55
P = 0.85, Q = - 0.6	$3.2 * 10^{-4}$	3.9	$1.6 * 10^{-4}$	3.1
P = 1.05, Q = - 0.6	$4.7 * 10^{-4}$	5.15	$1.9 * 10^{-4}$	4.1
P = 1.25, Q = - 0.5	∞	∞	$2.1 * 10^{-4}$	3.4
P =1.45, Q = - 0.25	$5 * 10^{-4}$	5	$3.7 * 10^{-4}$	4.1

Table 5.5. Comparative study between proposed controllers (ANN-PSS and FLPSS) with different operating conditions and ($X_t = 0.8$)

	With ANN-PSS		With FLPSS	
Operating conditions	Max. peak value (P.U)	Settling time (sec)	Max. peak value (P.U)	Settling time (sec)
P = 1.15, Q = 0.45	∞	∞	$2.1 * 10^{-4}$	3.7
P = 1.05, Q = 0.5	$6 * 10^{-4}$	6.4	$2.1 * 10^{-4}$	3.8
P = 0.85, Q = 0.6	$4.5 * 10^{-4}$	5.1	$1.9 * 10^{-4}$	4.3
P = 0.85, Q = - 0.6	$4.1 * 10^{-4}$	5.05	$1.8 * 10^{-4}$	4.6
P = 1.05, Q = -0.6	∞	∞	$2.1 * 10^{-4}$	5.2
P = 1.25, Q = - 0.45	∞	∞	$2.05 * 10^{-4}$	4
P = 1.45, Q = 0	$6.2 * 10^{-4}$	5.6	$2.02 * 10^{-4}$	3.7

Table 5.6. Comparative study between proposed controllers (ANN-PSS and FLPSS) with different operating conditions and ($X_t = 0.6$)

	With ANN-PSS		With FLPSS	
Operating conditions	Max. peak value (P.U)	Settling time (sec)	Max. peak value (P.U)	Settling time (sec)
P = 1.25, Q = 0.45 $K_A = 120$	$5.5 * 10^{-4}$	5.4	$2 * 10^{-4}$	3.8
P = 1.05, Q = 0.5 $K_A = 110$	$3.7 * 10^{-4}$	4.8	$1.7 * 10^{-4}$	4
P = 0.85, Q = 0.6 $K_A = 100$	$4.5 * 10^{-4}$	5.1	$1.9 * 10^{-4}$	4.3
P = 0.85, Q = - 0.6 $K_A = 90$	$2.9 * 10^{-4}$	4.6	$1.5 * 10^{-4}$	4.1
P = 1.05, Q = -0.6 $K_A = 90$	$4.3 * 10^{-4}$	5.55	$1.8 * 10^{-4}$	3.6
P = 1.25, Q = - 0.45 $K_A = 80$	$5.4 * 10^{-4}$	4.7	$2.* 10^{-4}$	3.85
P = 1.45, Q = 0 $K_A = 80$	∞	∞	$2.07 * 10^{-4}$	3.8

5.9 Summary

In this chapter, a brief review of basic concepts of fuzzy logic theory and fuzzy logic control was presented. As well, a fuzzy logic power system stabilizer was designed based on the dynamic reduction of power system model. However, as shown in Chapter 4 through the comparison of Lead-lag PSS and artificial neural network power system stabilizer, the design methodologies based on conventional control techniques do not adequately guarantee robustness of the controller for a power system stabilizer. However, advances have been made in computer processing speed and memory capacity over recent years. These allow for the use of advanced control techniques for the design of robust damping controllers, such as the proposed regulator for fuzzy logic power system stabilizer. The fuzzy logic power system stabilizer is designed based on the dynamic reduction of a power system model aimed to improving the system dynamic performance due to changes in loading conditions. A fuzzy logic power system stabilizer was

introduced, with the input signals to the fuzzy logic power system stabilizer being the speed deviation, $\Delta\omega$, and derivative of the speed deviation $\Delta\dot{\omega}$. Additionally, the number of the rules was decreased from 49 to 9, significantly reducing the computational burden.

The numerical simulation results showed that the system with the proposed fuzzy logic power system stabilizer (FLPSS) improved damping characteristics across a broad spectrum of operating conditions. Furthermore, the digital simulation results indicated that the system with the artificial neural network power system stabilizer (ANN-PSS) and FLPSS produced good damping characteristics under some operating conditions. Specifically, the system with ANN-PSS suffered instability problems under some operating conditions, while the system with the FLPSS provided better dynamic response compared to those of the ANN-PSS controller for the same operating conditions. This improvement serves to increase the overall reliability of the power system.

Chapter 6

6 A Wavelet-based Power System Stabilizer for the Dynamic Reduction of a Power System Model

6.1 Introduction

In this chapter, a wavelet-based multi-resolution control technique algorithm is used to design a power system stabilizer (PSS) to overcome small signal stability problems in power systems. A brief review of the wavelet transforms including the multi-resolution analysis and, filter bank analysis is discussed below.

Many mathematical techniques are used to analyze signals. The Fourier transform breaks the signal into its harmonics by weighting it with sine and cosine functions and integrating it from $-\infty$ to $+\infty$, as shown in Figure 6.1. Because data samples have a finite duration, the Fourier transform will not be from $-\infty$ to $+\infty$ and the harmonic content can be varied with time event within the sampling range. To overcome this issue, the short time Fourier transform breaks the signal duration into non-overlapping segments and analyzes each section using the Fourier transform, which can localize in time where harmonics exist and can generate a three-dimensional plot of amplitude versus frequency and time as shown in Figure 6.2. This procedure runs into resolution problems when the number of segments is increased. A wavelet transforms, shown in Figure 6.3, attempts to get around this problem by using wavelets instead of sine and cosine waves to weight the signal. These are said to have compact support, in that they are non-zero only over a small segment of time, which can be shifted in time and squeezed or stretched in time. Squeezing allows them to identify high-frequency harmonics in the signal, while stretching allows them to identify low-frequency harmonics in a signal. Wavelet transforms have been used for analysis of non-stationary, non-periodic, and transient signals [85] [86].

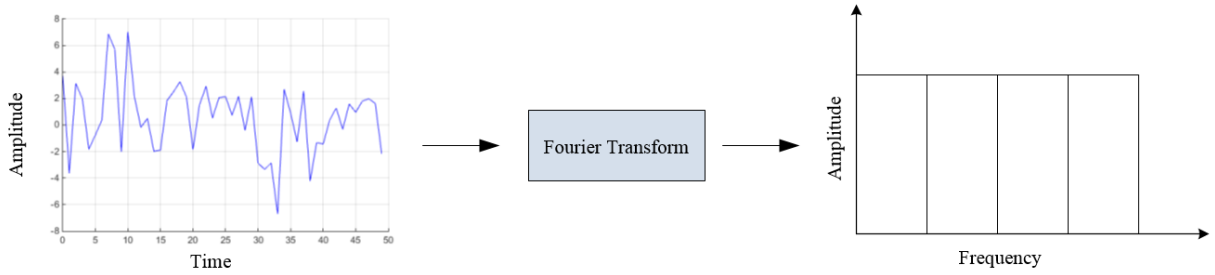

Figure 6.1. Fourier transform

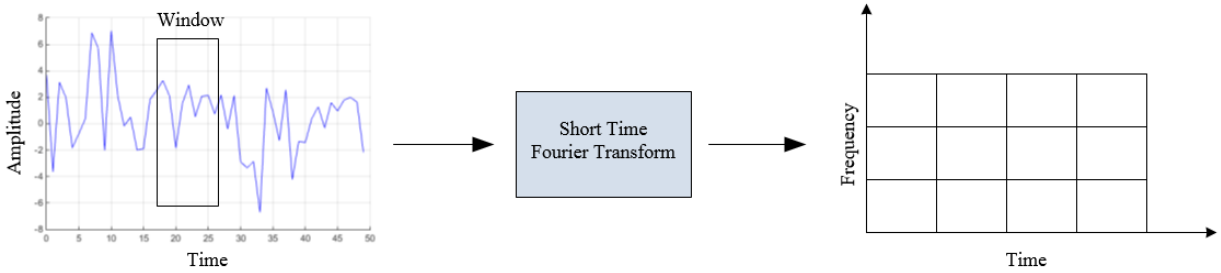

Figure 6.2. Short-time Fourier transform

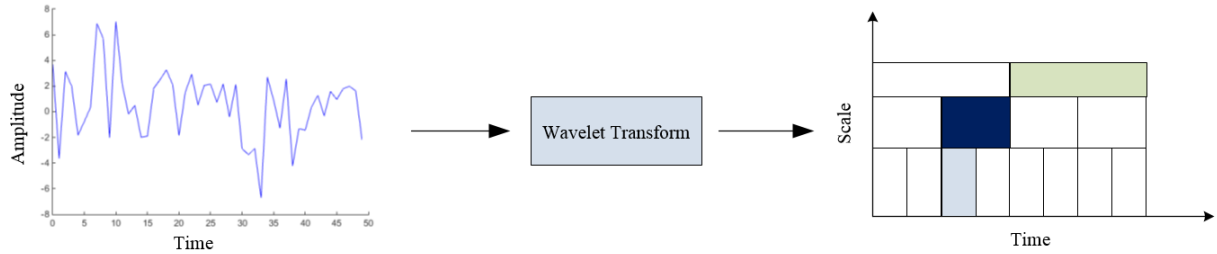

Figure 6.3. Wavelet transform

6.2 Wavelets and Scaling Functions

Wavelets are described by a wavelet function $\psi(t)$ (mother wavelet) and a scaling function $\varphi(t)$ (father wavelet) in a time domain. Different regions of support are derived from the mother wavelet function during the transformation process. The wavelets are nonzero only over a small segment period, which is known as the support period. The scaling function is required to create basis functions, which represent the analyzed signals, using shifting, scaling or rotating. The scaling functions are able to produce a number of polynomials of degree that will be equal to or less than the disappearance moment of the mother wavelet. The translation of the wavelet function is known as the level of resolution, where the resolution generates another wavelet function called the daughter wavelet by shifting and scaling the mother wavelet. At each level of resolution, the basis functions will be produced by the scaling function, which can be expressed by the following equation.

$$\varphi_{j,k}(t) = 2^{-j/2}\varphi(2^{-j}t - k); \quad j, k \in \mathbb{Z} \tag{6.1}$$

The orthogonal wavelet basis function is generated from the mother wavelet function $\psi(t)$, which can be expressed as:

$$\psi_{j,k}(t) = 2^{-j/2}\psi(2^{-j}t - k); \quad j, k \in \mathbb{Z} \tag{6.2}$$

where,

j represents the level of resolution, k represents the dimension of the function space at the level of resolution j, and t is time [85] [87] [88] [89] [90] [91].

6.2.1 Orthogonal and Non-Orthogonal Wavelets

Wavelets are categorized into two types: orthogonal and non-orthogonal. When the wavelet function overlaps with the next wavelet function, it is called a non-orthogonal wavelet function.

Examples include Morlet, Mexican Hat and complex Shannon, which provide too much unwanted information. Figure 6.4 shows the non-orthogonal Morlet function, while Figure 6.5 shows the non-orthogonal complex Shannon function. This type of wavelet is used with continuous wavelet transform (CWT) to guarantee the continuity of the procedure. However, when the mother wavelet and scaling function are able to produce an orthogonal basis function at each level of resolution, it is known as an orthogonal wavelet. There are many types of orthogonal wavelet families, such as the Daubechies family, the Meyer family, and others. Figure 6.6 and Figure 6.7 show the orthogonal Daubechies function and orthogonal Meyer function, respectively. For control applications, detection and classification of disturbances in power systems, the Daubechies family of orthogonal wavelets is more commonly used [86] [92].

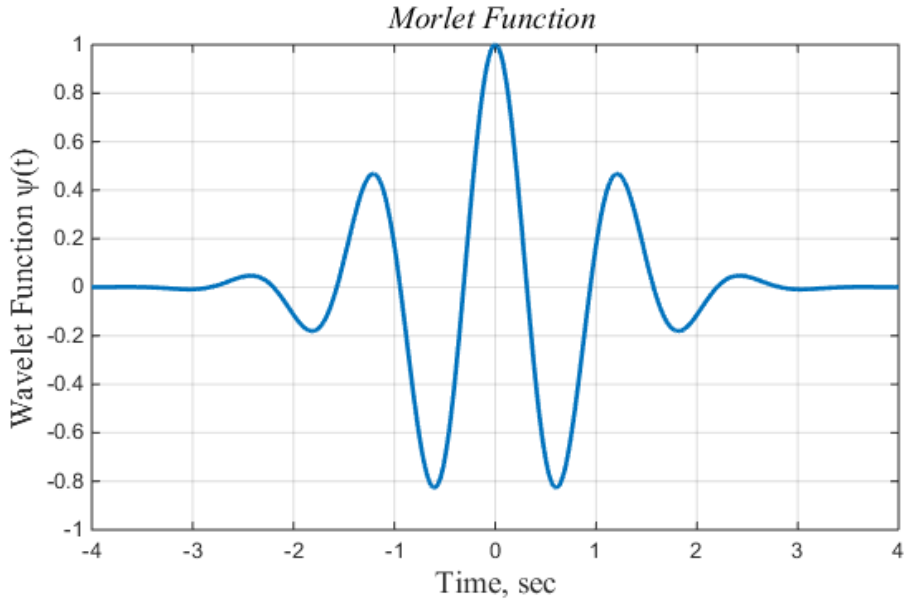

Figure 6.4. Non-orthogonal Morlet function

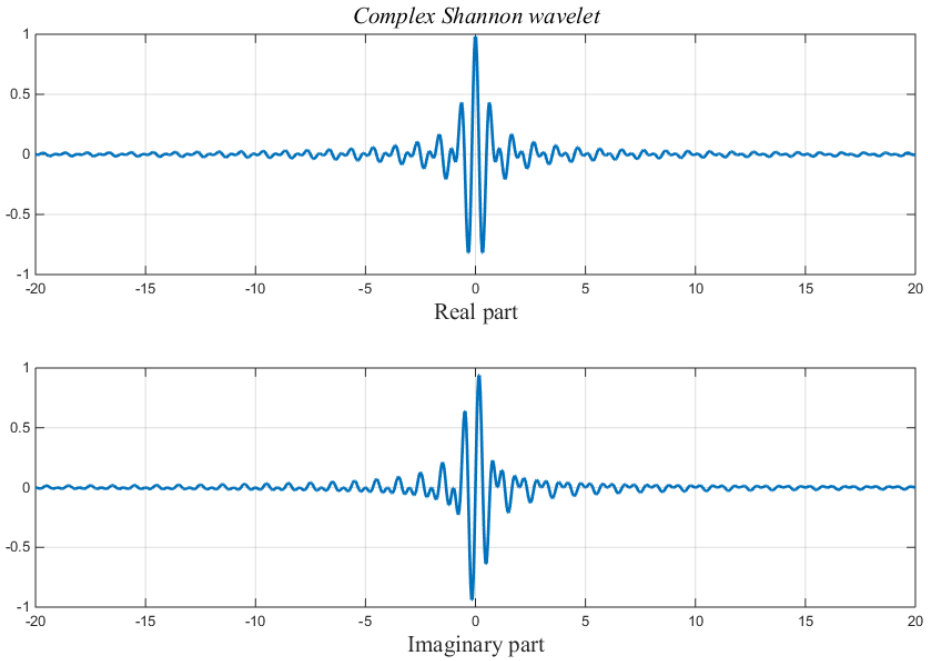

Figure 6.5. Non-orthogonal complex Shannon function

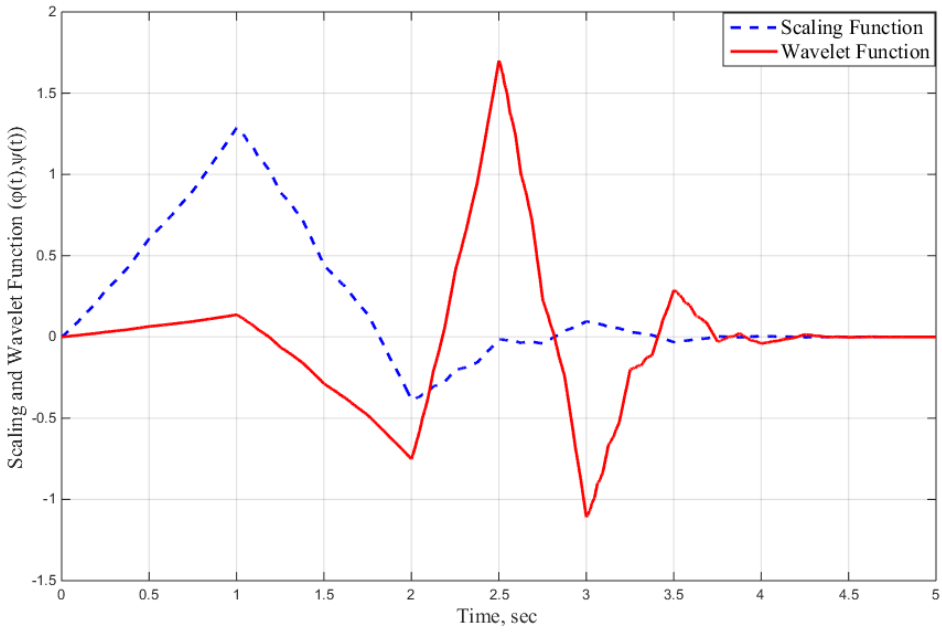

Figure 6.6. The Daubechies (db_3): Wavelet function and its scaling function

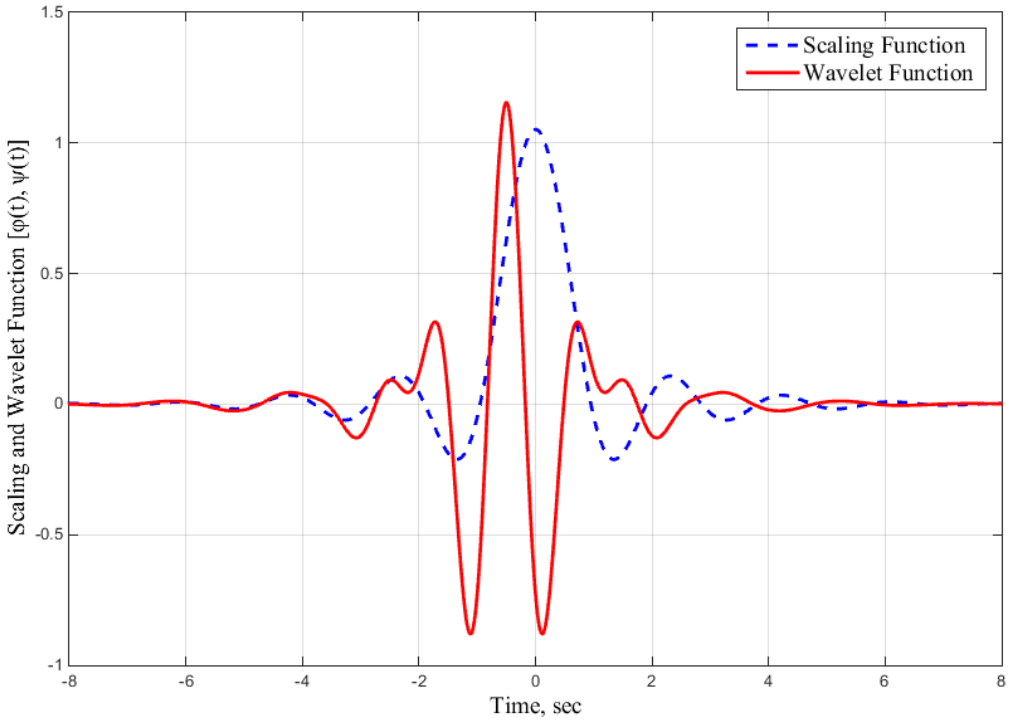

Figure 6.7. The Meyer: Wavelet function and its scaling function

6.3 Wavelet Transform

A wavelet transform uses small waves, called wavelets, to weight the signals in order to obtain better time resolution. There are different types of wavelet transforms such as continuous wavelet transform (CWT), discrete wavelet transform (DWT), and packet wavelet transform (PWT) [92] [93]

6.3.1 Continuous Wavelet Transform (CWT)

This type of transform is defined as the sum over all time of the signal multiplied by scaled and shifted versions of the mother wavelet function $\psi(t)$. It deals with non-orthogonal wavelet functions such as the Morlet function and the complex Shannon function [94], which are shown in

Figure 6.4 and Figure 6.5, respectively. The wavelet transform of a continuous signal $f(t)$ can be expressed as:

$$CWT_{\psi}[f](a\ (scale), b(position)) = \langle f, \psi_{a,b} \rangle = \frac{1}{\sqrt{a}} \int_{-\infty}^{+\infty} f(t) \psi^{*} \left(\frac{t-b}{a} \right) dt \qquad (6.3)$$

In equation (6.3), the symbol * denotes the complex conjugate. The integrand contains the scaled and shifted mother wavelet function. This can be written as follows:

$$\psi_{a,b}(t) = \frac{1}{\sqrt{a}} \psi^{*} \left(\frac{t-b}{a} \right), a, b\ \in \mathbb{R}, a \neq 0 \qquad (6.4)$$

where *a* is a scaling factor that determines the degree of resolution, and *b* is a shifting parameter that determines the time location of the wavelet, as shown in Figure 6.8. Thus, equation (6.3) can be rewritten as:

$$CWT_{\psi}[f](a, b) = \langle f, \psi_{a,b} \rangle = \int_{-\infty}^{+\infty} f(t)\ \psi_{a,b}(t)\ dt \qquad (6.5)$$

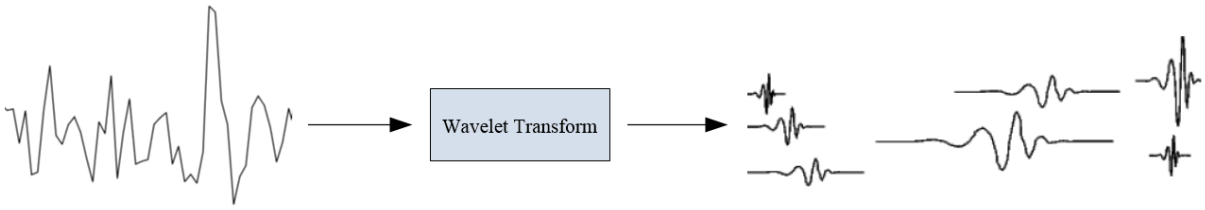

Figure 6.8. CWT for different scales and locations

6.3.2 Discrete Wavelet Transform (DWT)

A discrete wavelet transform (DWT) is any wavelet transform for which the wavelets are discretely sampled. In a continuous wavelet transform, the mother wavelet is scaled and shifted over a real continuous number region $L^2(\mathbb{R})$, which requires a fair amount of work and contains unwanted information. Therefore, by using a discrete wavelet transform, the analysis of the signals will be more efficient and accurate. The wavelet function can be scaled and shifted discretely by replacing $a = a_0^m$, and $b = nb_0a_0^m$, where a_0 and b_0 are fixed constants with $a_0 > 1$, $b_0 > 1$ and $m, n \in \mathbb{N}$, where $\mathbb{N}$ is a positive integer. In this way, the mother wavelet function becomes [95] [96]:

$$\psi_{m,n}(t) = a_0^{-m/2}\psi(a_0^{-m}t - nb_0) \tag{6.6}$$

For $f \in L^2(\mathbb{R})$, the discrete wavelet transform can be expressed as:

$$DWT_\psi[f](m,n) = \langle f, \psi_{m,n} \rangle = \int_{-\infty}^{+\infty} f(t)\psi_{m,n}^*(t)\, dt \tag{6.7}$$

The DWT analyzes a signal at different frequency bands with various resolutions by decomposing the signal into an approximation and information details. The DWT applies two sets of functions, which are scaling function $\varphi(t)$ and wavelet function $\psi(t)$. The scaling function is associated with a low-pass filter while the wavelet function is associated with a high-pass filter. The time scale representation of a digital signal is obtained using a digital filtering technique. The filter bank realization of the discrete wavelet transform DWT is similar to the wavelet decomposition by the continuous wavelet transform CWT, which is computed by changing the scale of the analysis window of the wavelet function. The analysis window shifts in time, multiplies the signal, and then integrates over all the time.

In the DWT, filter banks, which are filters of cut-off frequencies, are used to analyze the signal at different scales. The signal is passed through a series of high-pass filters to analyze the high frequencies, and it is passed through a series of low-pass filters to analyze the low frequencies [97]. The resolution of the signal, which is a measure the amount of information detail in the signal, is changed by filtering operations, and the scale is changed by up-sampling or down- sampling. Down sampling a signal reduces the sampling rate by removing some of the samples from the signal, whereas, up-sampling increases the sampling rate of the signal by adding a new sampling to it [98].

The DWT process starts by passing the discrete signal $f[n]$ of length N through a digital low pass filter with impulse response $g[k]$ and a digital high pass filter with impulse response $h[k]$. The digital low pass filter is determined from a scaling filter while the digital high pass filters is determined from a wavelet filter. The output of the low pass digital filter is the approximation coefficient (a^1) of the discrete signal at the first level of the DWT resolution. The output of the high pass filter is the detail coefficient (d^1) of the discrete signal at the first level of the DWT resolution. The first level of DWT decomposition can be expressed as follows [89] [99]:

$$a^1[n] = \sum_{k=0}^{N-1} g[k]\, f[N-k] \tag{6.8}$$

$$d^1[n] = \sum_{k=0}^{N-1} h[k]\, f[N-k] \tag{6.9}$$

The approximation coefficient (a^1) at the first level of resolution is used as input into another pair of wavelet filters after being down-sampled by two. The filters at the second level of

resolution produce sets of approximation and detail coefficients (a^2) and (d^2), respectively, of length N/2. These coefficients of the second level can be expressed mathematically as:

$$a^2[n] = \sum_{k=0}^{(N/2)-1} g[k]\, a^1\left[\frac{N}{2} - k\right] \tag{6.10}$$

$$d^2[n] = \sum_{k=0}^{(N/2)-1} h[k]\, a^1\left[\frac{N}{2} - k\right] \tag{6.11}$$

Figure 6.9 illustrates the two-level decomposition block diagram of a discrete wavelet transform for a digital signal $f[n]$. In the decomposition process, both high-pass (h) and low-pass (g) filters have been used.

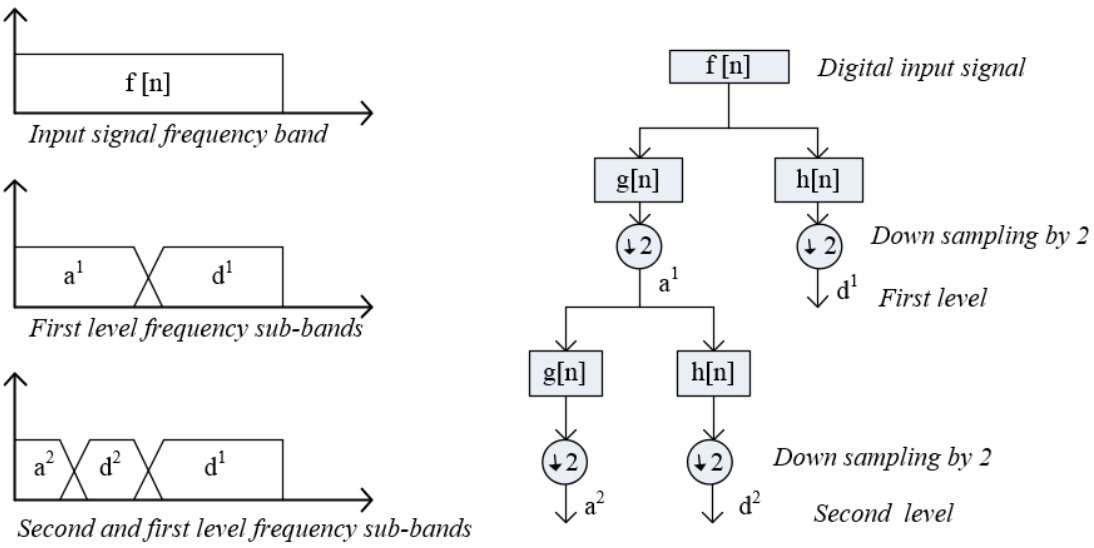

Figure 6.9. Two level DWT of digital signal f [n]

6.3.3 Wavelet Packet Transform (WPT)

As explained above, the wavelet transform gives excellent time and frequency resolution. It has one possible disadvantage: weak frequency resolution on the high-pass filter side, which makes it difficult to differentiate between signals that have nearby high-frequency components. The WPT has alternative bases, which can found from the linear combinations of standard wavelet functions. These bases inherit properties such as orthonormality and time-frequency localization from their corresponding wavelet function. The WPT is a function of three indicates j, k, and n, which can be expressed as in equation (6.12) [96] [100] Thus, the wavelet packet transform WPT is an extension of the discrete wavelet transform DWT. Figure 6.10 illustrates a block diagram of the WPT decomposition.

$$W_{j,k}^{n}(t) = 2^{j/2} W^{n}\left(2^{j}t - k\right), j, k, n \in \mathbb{Z} \tag{6.12}$$

where j is the index of the scale operation, k refers to the shift process, and the index n is defined as the modulation or oscillation parameter. The first two wavelet packet functions are the scaling function and the wavelet function, which are expressed as:

$$W_{0,0}^{0}(t) = \varphi(t) \tag{6.13}$$

$$W_{0,0}^{1}(t) = \psi(t) \tag{6.14}$$

The wavelet packet functions for $n = 2, 3, \ldots$ can be written as:

$$W_{0,0}^{2n}(t) = 2^{1/2} \sum_{k} g(k) W_{1,k}^{n}(2t - k) \tag{6.15}$$

$$W_{0,0}^{2n+1}(t) = 2^{1/2} \sum_{k} h(k) W_{1,k}^{n}(2t - k) \tag{6.16}$$

where g(k) and h(k) are the quadrature mirror filters QMF associated with the predefined scaling and mother wavelet functions.

The first level of decomposition of the digital signal $f\ [n]$ of length N in WPT produces two-frequency sub-bands as in DWT, which are approximation coefficients $a_n^1 = [a_0^1\ a_1^1\ a_2^1 \ldots . a_{N-1}^1]$ and detail coefficients $b_n^1 = [b_0^1\ b_1^1\ b_2^1 \ldots . b_{N-1}^1]$ as given in equation (6.8) and equation (6.9). The second level of resolution produces two-frequency sub-bands using the same filters as the first level of resolution, which are defined as:

$$aa^2[n] = \sum_{k=0}^{(N/2)-1} g[k]\ a^1\left[\frac{N}{2} - k\right] \tag{6.17}$$

$$ad^2[n] = \sum_{k=0}^{(N/2)-1} h[k]\ a^1\left[\frac{N}{2} - k\right] \tag{6.18}$$

$$da^2[n] = \sum_{k=0}^{(N/2)-1} g[k]\ d^1\left[\frac{N}{2} - k\right] \tag{6.19}$$

$$dd^2[n] = \sum_{k=0}^{(N/2)-1} h[k]\ d^1\left[\frac{N}{2} - k\right] \tag{6.20}$$

The frequency sub-band aa^2 is the second level low frequency approximation of the discrete signal $f[n]$, while the frequency sub-band ad^2 is the second level low-frequency details of the discrete signal $f[n]$. The frequency sub-band da^2 is the second level high-frequency

approximation of the discrete signal $f[n]$, and the frequency sub-band dd^2 is the second level high frequency details of the discrete signal $f[n]$, as shown in Figure 6.10.

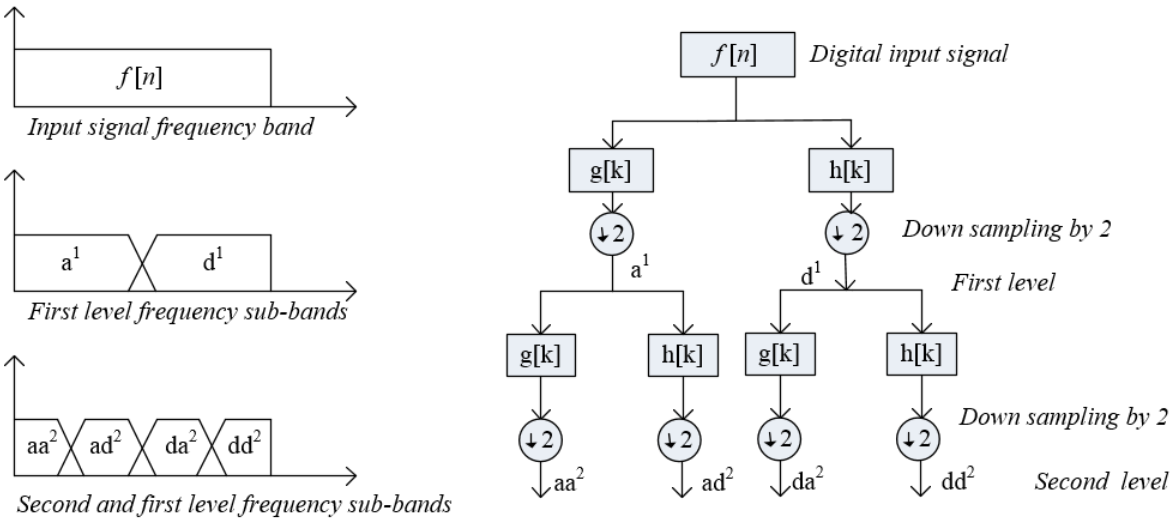

Figure 6.10. Two level decomposition of WPT for a discrete wavelet function $f[n]$

6.4 Multi-resolution Analysis (MRA)

The idea of the multi-resolution analysis (MRA) or multi-scale approximation (MSA) was introduced by Meyer and Mallet in 1986. The MRA is a convenient framework for hierarchical representation of functions at different scales. The MRA represents a signal as a boundary of the subsequent approximations and has a smoother form and more precise details of the original signal. The multiresolution analysis maps a one-dimensional signal of time into a two-dimensional signal of time and frequency. The aim of MRA is to represent a continuous function $f(t)$ in terms of its orthonormal bases (scaling $\varphi(t)$ and wavelet $\psi(t)$ functions). A function $f(t) \in L^2(\mathbb{R})$ (Hilbert space) can be described by the N-level of a wavelet series as follows [93] [101]:

$$f(t) = \sum_{k} a_{j0,k}\, \varphi_{j0,k}(t) + \sum_{j=j0}^{\infty} \sum_{k} b_{j,k} \psi_{j,k}(t) \quad , j \geq j0 \tag{6.21}$$

where,

$$a_{j0,k} = \int f(t) \varphi_{j0,k}(t) dt \tag{6.22}$$

$$b_{j,k} = \int f(t) \psi_{j,k}(t) dt \tag{6.23}$$

For the discrete function S[n] the N-level of the discrete wavelet series will be as follows:

$$S[n] = \frac{1}{\sqrt{m}} \left\{ \sum_{k} W_{\varphi}(j0,k)\, \varphi_{j0,k}[n] + \sum_{j=j0}^{\infty} \sum_{k} W_{\psi}(j,k) \psi_{j,k}[n] \right\} \tag{6.24}$$

where, $n = 1, 2, 3, \ldots, m-1$

$1/\sqrt{m}$ is a normalizing term, as typically $j0 = 0$ and $m = 2^{j}$ and j = 0, 1,…, J-1

$$W_{\varphi}(j0,k) = \frac{1}{\sqrt{m}} \sum_{k} S[n]\, \varphi_{j0,k}[n] \tag{6.25}$$

$$W_{\psi}(j,k) = \frac{1}{\sqrt{m}} \sum_{k} S[n]\, \psi_{j,k}[n] \tag{6.26}$$

The multi-resolution analysis in Hilbert space $L^2(\mathbb{R})$ consists of a nested sequence of subspaces V_j in which $V_j \subset V_{j+1}$, where $j \in \mathbb{Z}$. The multiresolution analysis MRA has properties that can be described as follows [102]:

❖ The MRA decomposes a function space into a sequence of subspaces, each subspace contains a lower subspace, as illustrated in equation (6.27) and as is shown in Figure 6.11.

$$V_{-\infty} \subset \cdots \subset V_{-1} \subset V_0 \subset V_1 \ldots \subset V_{\infty} \tag{6.27}$$

❖ Because each subspace contains a lower space, thus a new level of a resolution can be created by dilating the mother wavelet function without losing the information of the decomposing function, which can be expressed as follows

$$V_j = V_0 \oplus W_0 \oplus W_1 \oplus W_2 \oplus \ldots \oplus W_j \tag{6.28}$$

Multi-resolution analysis can be mathematically expressed as:

$$MRA(\varphi, \psi) = \bigcup_{j \in \mathbb{Z}} (V_j(\varphi) \oplus W_j(\psi)) \tag{6.29}$$

where, $V_j(\varphi)$ is the subspace spanned by the scaling function $\varphi(t)$, the sign $\oplus$ is the direct orthogonal summation operation of the spaces, and $W_j(\psi)$ is the space spanned by the mother wavelet function $\psi(t)$.

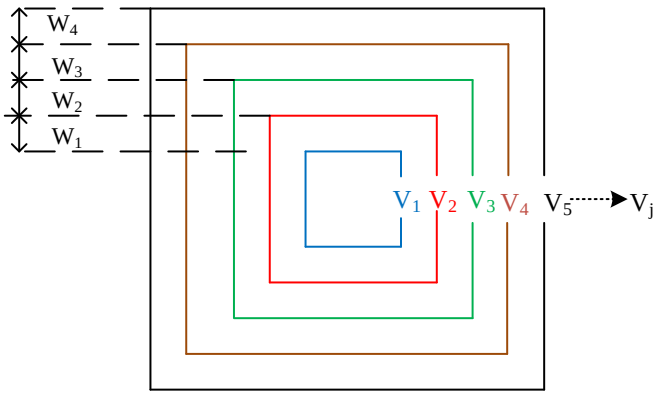

Figure 6.11. Scaling and wavelet spaces

❖ As the resolution becomes coarser and coarser, more and more details are removed in such a way that when $j \to \infty$, then only a constant frequency component remains. Here, j is the level of the resolution

❖ If the signal $f(t)$ does not have any oscillations at scales smaller than $1/2^j$, then $f(2t)$ will not have any oscillations at scales smaller than $1/2^{j+1}$.

6.4.1 Quadrature Mirror Filter (QMF)

A multi-resolution analysis can be constructed by using quadrature mirror filter (QMF) banks. As shown in Figure 6.12, QMF consists of two stages: an analysis stage and a synthesis stage. Both stages have high-pass filters (h) and low-pass filters (g) and are separated by up- and down-sampling operations. The selected wavelet and scaling functions, which are defined in equation (6.30) and equation (6.31), respectively, are used to generate the QMF coefficients [91] [102]:

$$\psi[n] = \sqrt{2} \sum_k h[k]\varphi[2n - k] \tag{6.30}$$

$$\varphi[n] = \sqrt{2} \sum_k g[k]\varphi[2n - k] \tag{6.31}$$

QMF is used to provide multi-resolution analysis of the input signal by decomposing the signal into multi-level resolutions. If C_h and C_g are considered to be convolution coefficients of the high-pass filter and low-pass filter respectively, both should satisfy the orthogonal and perfect reconstruction conditions to get good QMF, which are $C_h C_g = C_g C_h = 0$ and $C_h C_h + C_g C_g = I$, where I is the identity operator.

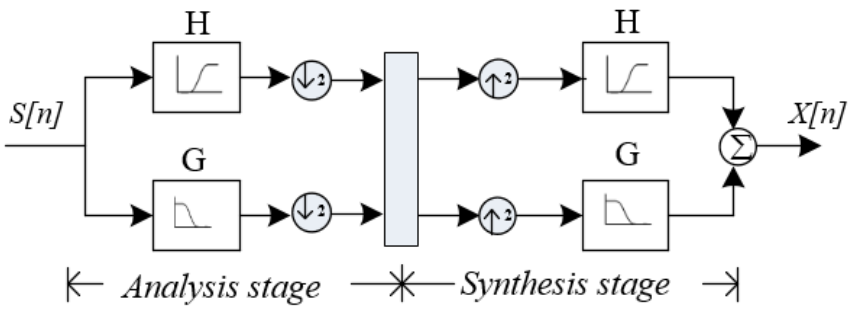

Figure 6.12. Block diagram of quadrature mirror filter

6.5 Selection of Wavelet

The mother wavelet function selection depends on the signal and the type of information that needs to be extracted from the signal. The best mother wavelet function is one that can analyze and synthesize the signal by shifting and scaling the wavelet function and keep the energy of the signal constant throughout the transformation process. The choice of an optimum wavelet function can be described as a selection of an orthonormal basis function. Detecting the frequency components that are present in a signal is one of the most important properties provided by the mother wavelet function. This property can be used to design power system controllers such as the power system stabilizer, where the speed deviation of synchronous generators can be rapidly identified [103].

The best mother wavelet function candidate that has been found in control applications is the Daubechies (db3), because it shows minimum attenuation in the pass band and stops band frequencies. This property is helpful for removing high-frequency noise from the control signal so that can be concentrated on specific frequency components. As a result, the mother wavelet filter (db3) will be used to perform multi-resolution analysis of the rotor speed deviation signal for the

proposed controller, which is the modified multi-resolution proportional-integral-derivative controller (MMR-PID), to use it as the power system stabilizer (MMR-PID-PSS).

The six non-zero scaling coefficients of the Daubechies db3 wavelet for the low-pass and high- pass filters are:

$$g = [0.0352 \quad -0.0854 \quad -0.1350 \quad 0.4599 \quad 0.8069 \quad 0.3327]$$

$$h = [-0.3327 \quad 0.8069 \quad -0.4599 \quad -0.1350 \quad 0.0854 \quad 0.0352]$$

The first-level magnitude response of the half-band digital filters G and H associated with the db3 wavelet is shown in Figure 6.13, while the second-level magnitude response of the half-band digital filters GG and GH associated with db3 wavelet is shown in Figure 6.14.

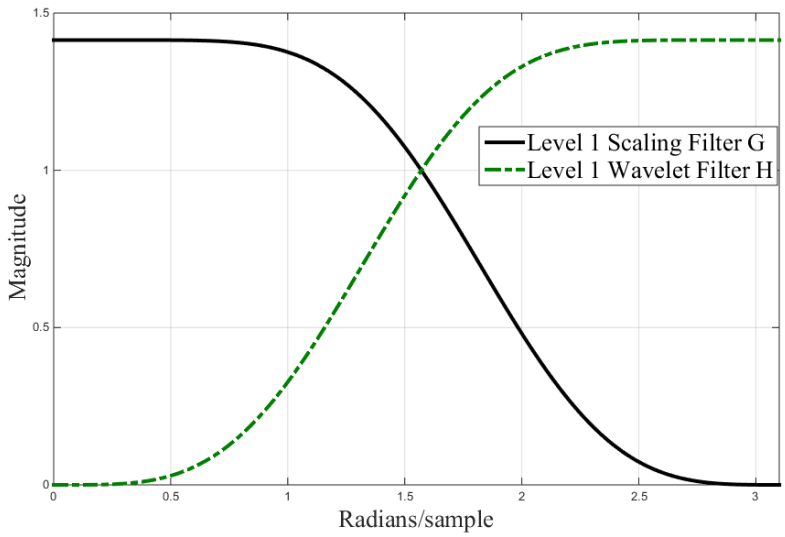

Figure 6.13. First level magnitude response of half-band digital filters G and H associated with db3 wavelet

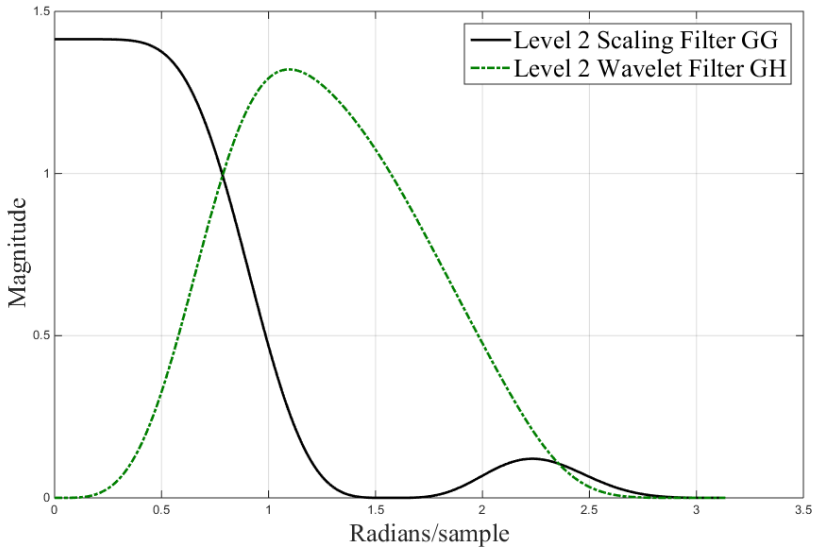

Figure 6.14. Second level magnitude response of half-band digital filters GG and GH associated with db3 wavelet

6.6 Wavelet-based Multi-resolution PID Controller

The proportional-integral-derivative (PID) controller has been effectively used in industrial control systems for nearly a century. A PID controller continually computes the error ($e(t)$), which is the difference between the measured value and the reference value, and adjusts the control signal depending on the proportional, integral and derivative terms as shown in Figure 6.15. The proportional deals with the error's present value, the integral corrects the errors past value, so the error will accumulate over time, and the derivative calculates the error's possible future value (derivative value). The control signal of a PID controller can be described as in equation (6.32) [32] [104]:

$$u_c(t) = k_p e(t) + k_i \int e(t)dt + k_d \frac{de(t)}{dt} \tag{6.32}$$

where k_p is the proportional gain, k_i is the integral gain, and k_d is the derivative gain.

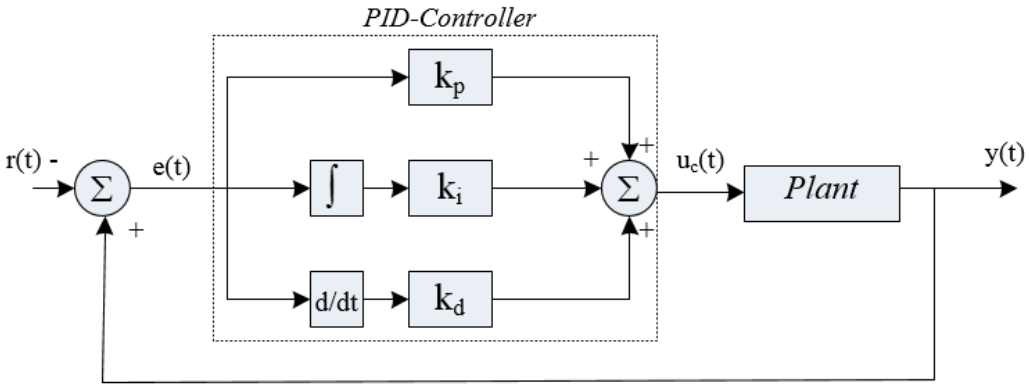

Figure 6.15. Block diagram of PID controller

In terms of frequency information, the proportional and integral capture the low-frequency information of the error signal, while the derivative captures the high-frequency information of the error signal. Using the multi-resolution analysis technique, the error signal can be decomposed to its high-, small- and middle-frequency components, as in equation (6.33):

$$e(t) = e_L(t) + e_{M_1}(t) + \cdots + e_{M_{N-1}}(t) + e_H(t) \tag{6.33}$$

where $e_L(t)$ means the error signal that has a low-frequency component, $e_{M_1}(t) \ldots\ldots e_{M_{N-1}}(t)$ indicates the error signals that have a middle-frequency component, and $e_H(t)$ denotes the error signal that has a high-frequency component. In the MR controller, which is shown in Figure 6.16, each frequency component of the error signal is scaled by its gain and then added together to generate the control signal, as defined in equation (6.34) [103] [105]:

$$u_c(t) = k_L e_L(t) + k_{M_1} e_{M_1}(t) + \cdots + k_{M_{N-1}} e_{M_{N-1}}(t) + k_H e_H(t) \tag{6.34}$$

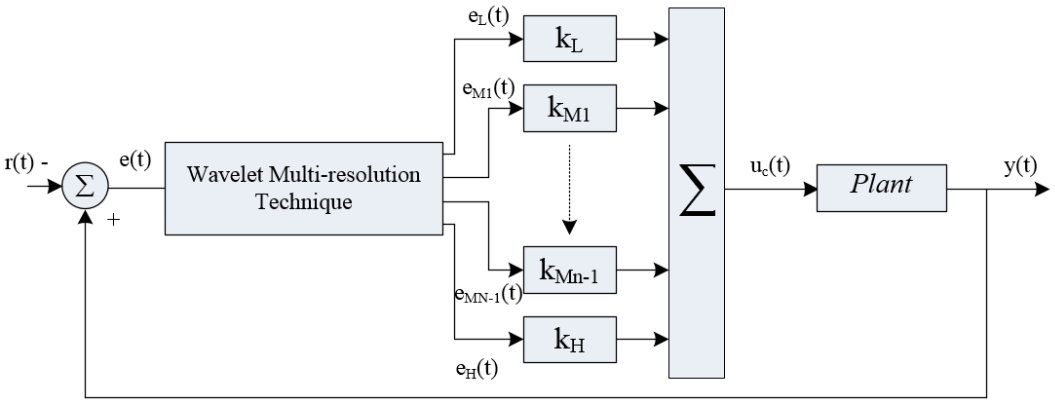

Figure 6.16. Block diagram of multiresolution controller [103]

In the MR-PID controller, the controller decomposes the error signal into its low-frequency components (approximation) and its high-frequency components (details), using DWT up to the second level of resolution and the selected mother wavelet db3, as shown in Figure 6.9. The selected mother wavelet function db3 is used to produce sets of approximations and details coefficient using high-pass filter h[k], and the low-pass filter g[k], as in equations (6.35) to (6.38) [89] [99]:

$$e_{a^1}[n] = \sum_{k=0}^{N-1} g[k]\, e[n-k] \tag{6.35}$$

$$e_{d^1}[n] = \sum_{k=0}^{N-1} h[k]\, e[n-k] \tag{6.36}$$

$$e_{a^2}[n] = \sum_{k=0}^{(N/2)-1} g[k]\, e_{a^1}\left[\frac{N}{2} - k\right] \tag{6.37}$$

$$e_{d^2}[n] = \sum_{k=0}^{(N/2)-1} h[k]\; e_{a^1}\left[\frac{N}{2} - k\right] \tag{6.38}$$

In previous studies, researchers claimed that the high-frequency component of the error signal $e_{d^1}[n]$ in the first-level of the resolution is the derivative signal that should be scaled by a gain k_{d^1}. The integral signal is $e_{d^2}[n]$, which can be obtained from the second-level resolution of the error signal, should be scaled by a gain k_{d^2} and the proportional signal is $e_{a^2}[n]$, which can be obtained from the second-level resolution of the error signal, should be scaled by a gain k_{a^2}, as shown in Figure 6.17. Thus, the control signal will be as follows [61] [99] [103] [105] [106]:

$$u_{MR-PID} = k_{a^2}\, e_{a^2} + k_{d^2}\, e_{d^2} + k_{d^1}\, e_{d^1} \tag{6.39}$$

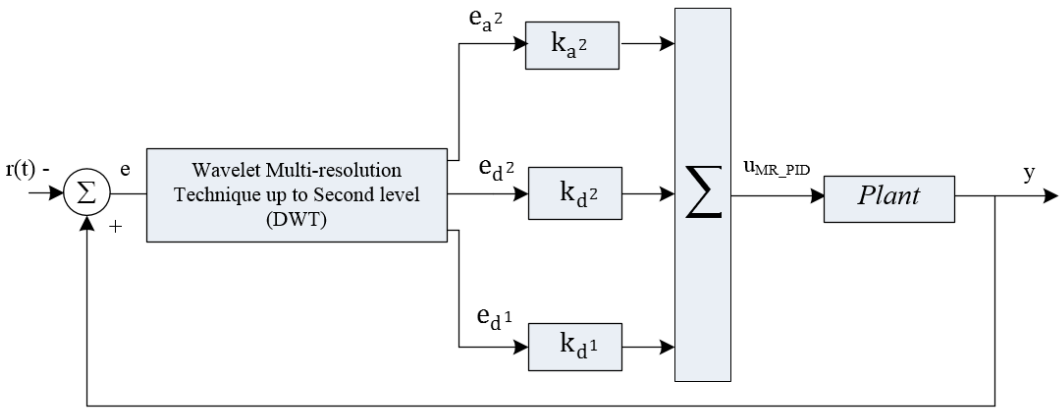

Figure 6.17. MR-PID controller

In order to obtain PID controller requirements, multiply the integral of the error signal by the gain k_{d^2} to correct the past value of the error value, and multiply the derivative of the error signal by gain k_{d^1} to correct the possible future value of the error. This dissertation adds a new modification to the MR-PID controller, which is that the high frequency component of error signal in the first level of DWT e_{d^1} should be derivative (derivative error signal), and the signal e_{d^2} should be integrated, as shown in Figure 6.18. Therefore, the output control signal of the modified multi-resolution MMR-PID controller will be as follows:

$$u_{MMR-PID}[n] = k_{a^2}\, e_{a^2}[n] + k_{d^2} \sum_{n=1}^{k} e_{d^2}[n]\, \Delta T \quad + k_{d^1} \left(\frac{e_{d^1}[n] - e_{d^1}[n-1]}{\Delta T} \right) \qquad (6.40)$$

where, ΔT is the sample interval

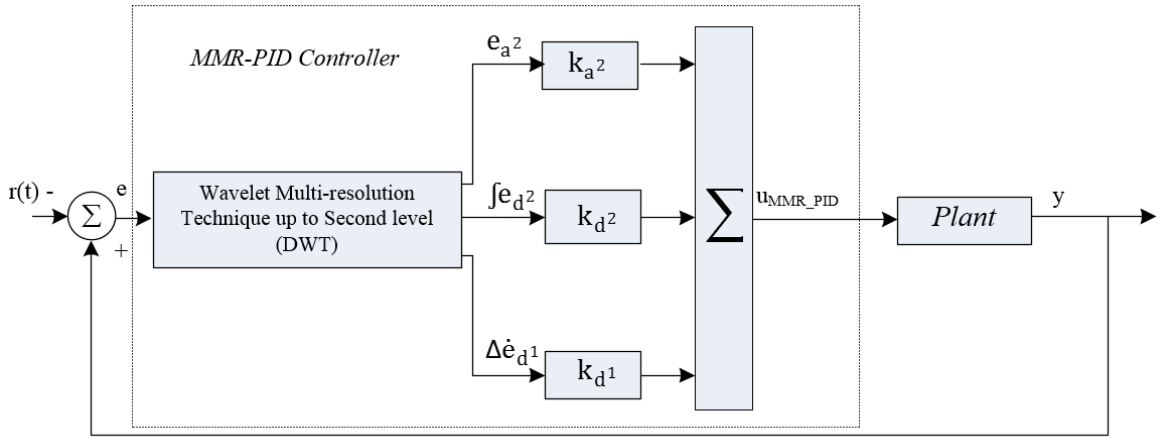

Figure 6.18. Block diagram of MMR-PID controller

6.7 Design of a Modified Multi-resolution Proportional-Integral-Derivative Power System Stabilizer (MMR-PID-PSS) for a Reduced-order Power System

This dissertation uses the MMR-PID controller as the power system stabilizer MMR-PID-PSS in a power system to enhance small signal power system stability, where the input of such a controller is selected to be the generator speed deviation Δω. As was mentioned previously, the proposed method uses the information at the secondary bus of a step-up transformer to derive the power system model, the order of which is then reduced to the design PSS. The basic structure of the proposed modified multiresolution proportional-integral-derivative power system stabilizer (MMR-PID-PSS) is shown in Figure 6.20. The proposed MMR-PID-PSS has three gains which are k_{a^2}, k_{d^2} and k_{d^1} where the rotor speed deviation signal is decomposed into its detail (high-frequency) components and approximation (low-frequency) components using the DWT technique as shown in Figure 6.19 and selected mother wavelet function db3, as follows:

$$\Delta\omega_{a^1}[n] = \sum_{k=0}^{N-1} g[k]\,\Delta\omega[n-k] \tag{6.41}$$

$$\Delta\omega_{d^1}[n] = \sum_{k=0}^{N-1} h[k]\,\Delta\omega[n-k] \tag{6.42}$$

$$\Delta\omega_{a^2}[n] = \sum_{k=0}^{(N/2)-1} g[k]\,\Delta\omega_{a^1}\left[\frac{N}{2}-k\right] \tag{6.43}$$

$$\Delta\omega_{d^2}[n] = \sum_{k=0}^{(N/2)-1} h[k]\,\Delta\omega_{\,a^1}\left[\frac{N}{2}-k\right] \tag{6.44}$$

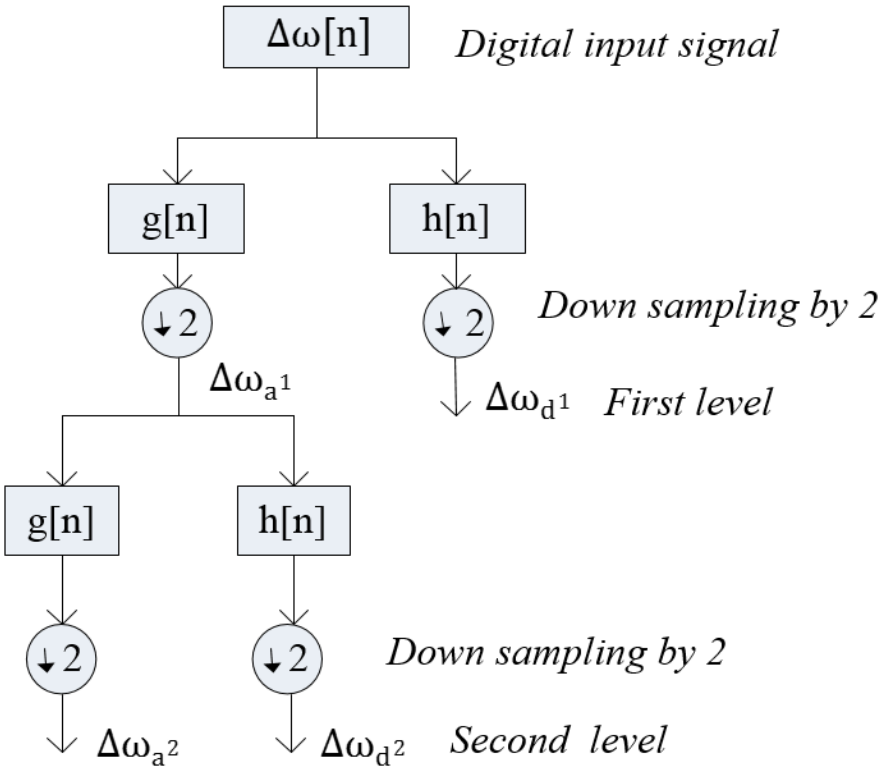

Figure 6.19. Decomposition of rotor speed deviation signal up to second level using DWT

The gain k_{a^2} is used to adapt the low-frequency component of the rotor speed deviation signal $\Delta\omega_{a^2}$ in the DWT. The gain k_{d^1} is used to correct the derivative of the high frequency component of the speed deviation signal $\Delta\dot{\omega}_{d^1}$ in the DWT, while the gain k_{d^2} is used to correct the integral of the medium frequency component of the speed deviation signal $\int \Delta\omega_{d^2}$ in the DWT. It has been found that the low frequency component of the error signal using multi-resolution decompensation DWT up to the second level is identical to the proportional error using a standard PID controller. Therefore, to reduce the settling time and enhance the disturbance rejection of the power system stabilizer, the gain k_{a^2} can be increased. Also, the integral of the medium frequency component of the error signal using multi-resolution decompensation (DWT) up to the second

level is identical to the integral of the error signal using a standard PID controller. Thus, the gain k_{d^2} that is used to weight the integral of the medium-frequency component of the speed deviation signal can be increased to minimize the steady state error. The derivative of the high-frequency component of the error signal using multi-resolution decompensation DWT up to the first level is identical to the derivative error signal using a standard PID controller. Accordingly, the gain k_{d^1} might be increased to decrease the overshoot/undershoot of the control signal and to improve the transient response. The output control signal of the proposed MMR-PID-PSS will be as follows:

$$u_{MMR-PID-PSS}[n] = k_{a^2}\,\Delta\omega_{a^2}[n] + k_{a^2}\sum_{n=1}^{k}\Delta\omega_{d^2}[n]\,\Delta T + k_{d^1}\left(\frac{\Delta\omega_{d^1}[n] - \Delta\omega_{d^1}[n-1]}{\Delta T}\right) \quad (6.45)$$

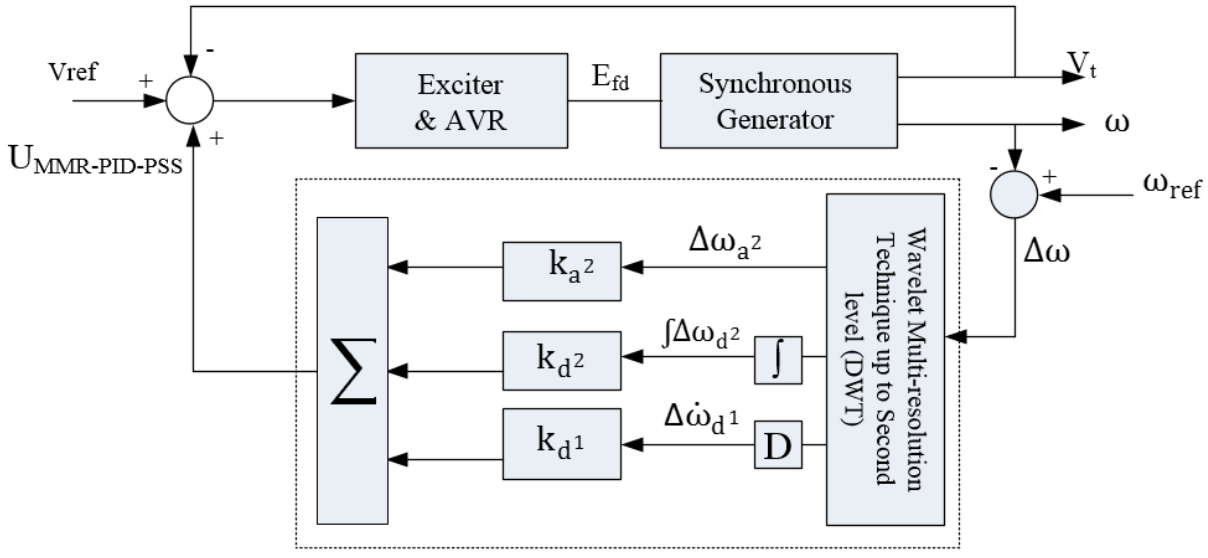

Figure 6.20. Block diagram of power system with proposed MMR-PID-PSS

The performance of the proposed MMR-PID-PSS can be affected by supplementary disturbances or harmonics during the operation. Thus, the effects of the disturbances or harmonics must be considered in the design of an optimal control system of the proposed MMR-PID-PSS. Because the disturbances are low-frequency signals and the harmonics are high-frequency signals, it is challenging to reduce the effects of these unpredictable signals simultaneously, but the proposed MMR-PID-PSS performs well under these circumstances.

In this thesis, the proposed MMR-PID-PSS is used in a reduced-order power system, as shown in Figure 6.21. The original system is first formed and then a proposed reduction technique is used. The roots of the reduced order model matrices are found. The proposed MMR-PID-PSS technique has therefore produced a control signal based on a reduced-order response.

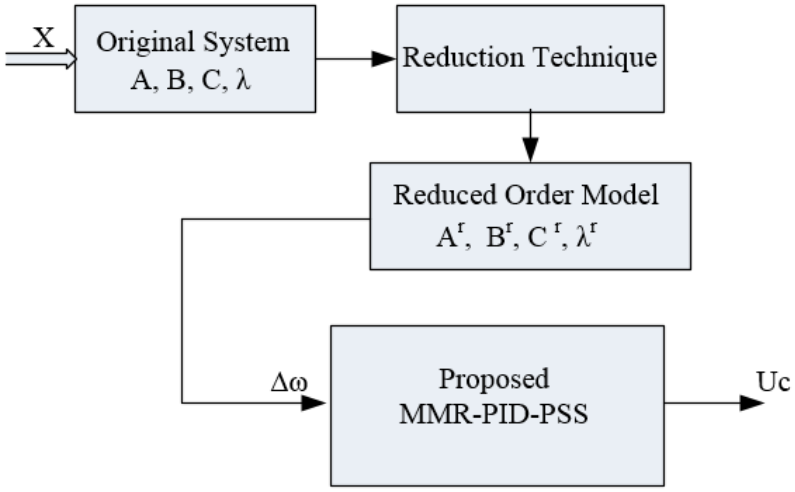

Figure 6.21. Block diagram of proposed MMRPID-PSS

6.8 Digital Simulation Results

6.8.1 Single Machine Connected to the Network

Digital simulation runs were carried out on the power system under study, which consists of a synchronous generator connected to the network through step-up transformers. The synchronous generator is represented by a two-axis model and equipped with IEEE type-1 excitation and governing turbine systems. The data for this scheme are given in Appendix A. The reduced-order model was established, as per Chapter 3, and gave acceptable performance compared with the original model. The proposed MMR-PID-PSS is then applied with altered operating conditions. To validate the performance of the proposed regulator, the MMR-PID-PSS is compared with the fuzzy logic power system stabilizer (FLPSS) presented in Chapter 5, giving better performance compared to ANN-PSS.

The validation is characterized by studying the time response for a ±1% change in mechanical torque at 1, 11, and 21 seconds in a MATLAB environment [107]. These responses are given in Figure 6.22 to Figure 6.33.

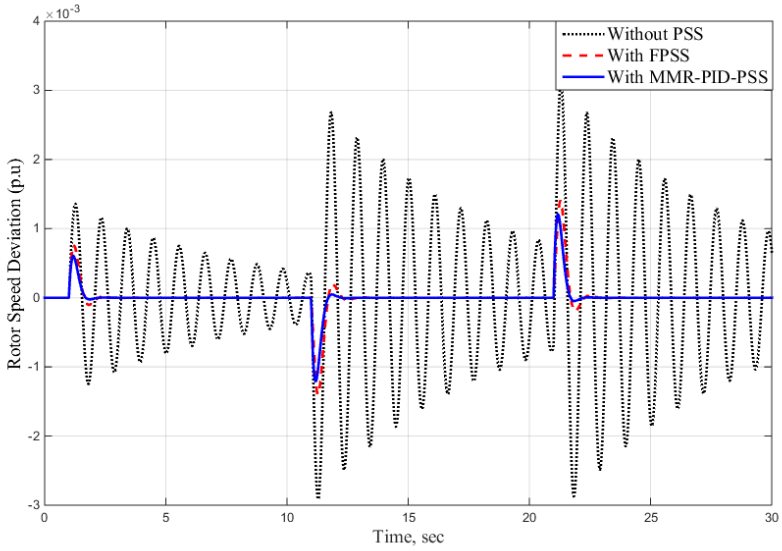

Figure 6.22. Time response of Δω due to disturbances at the normal operating conditions

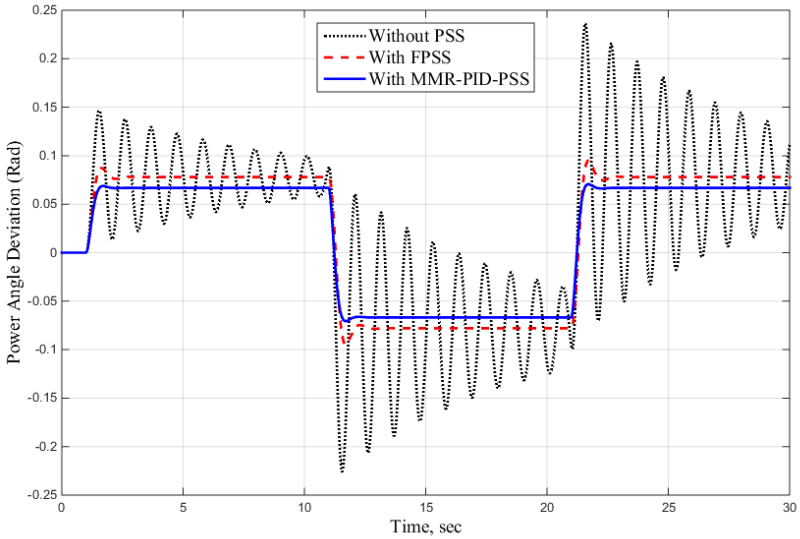

Figure 6.23. Time response of Δδ due to disturbances at the normal operating conditions

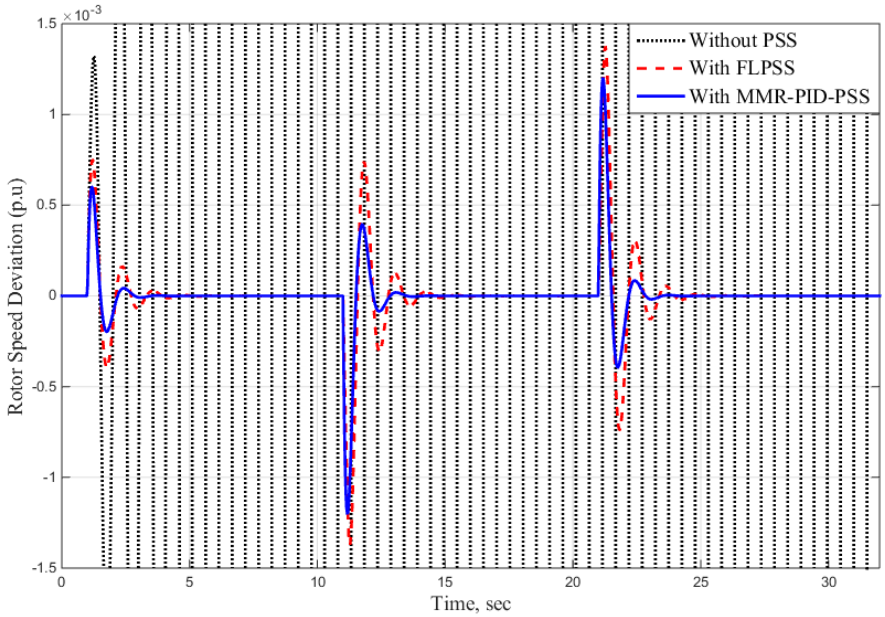

Figure 6.24. Time response of Δω due to disturbances at P = 1.25 and Q = 0.0 pu

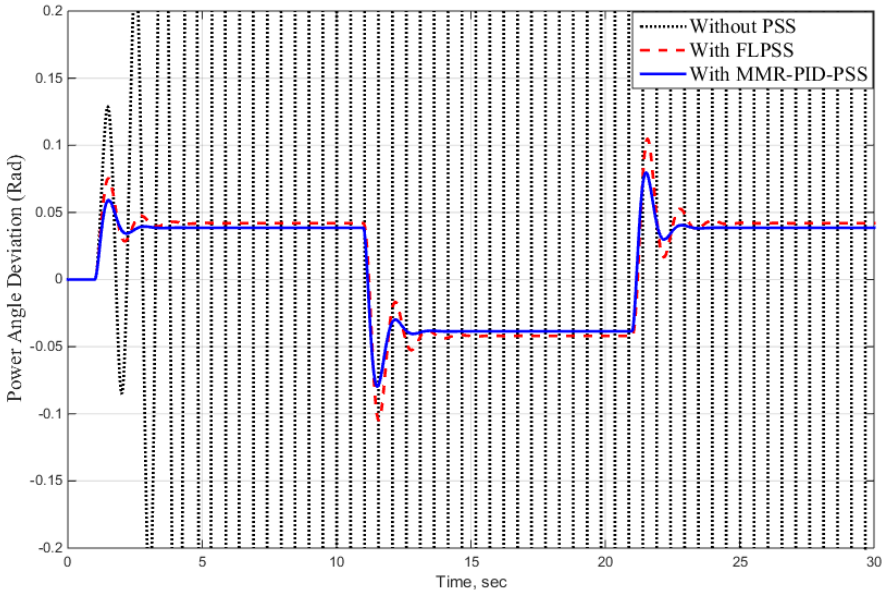

Figure 6.25. Time response of $\Delta\delta$ due to disturbances at P = 1.25 and Q = 0.0 pu

In the results shown above in Figures 6.22 to 6.25, it is assumed that the transformer reactance is fixed at $X_t = 0.4$ P.U at a unity power factor. From these figures, it is evident that the system at unity power factor due to a ±1% step change in the mechanical torque applied at time 1, 11, and 21 seconds caused persistent oscillations for a relatively long time at normal operating conditions. Furthermore, at heavy load, the power system with real power P = 1.25 and reactive power Q = 0.0, is unstable. By using the proposed PSSs, which are MMR-PID-PSS and FLPSS, the oscillation is damped out quickly. However, the power system with the proposed MMR-PID-PSS is more stable under heavy loads. The proposed MMR-PID-PSS gave a better dynamic response compared to those of the FLPSS.

In the next cases of study, the power transformer reactance will be added in series with the transmission line, and the power system will be operated at different lagging and leading power factors to observe the efficiency changes. For both the FLPSS and MMR-PID-PSS controllers,

Figures 6.26 to 6.29 show the time response of the rotor speed deviation and rotor angle change under disturbance at lagging power factors for various loading values. The results indicate that the power system is more stable using both the proposed regulators FLPSS and MMR-PID-PSS. However, the power system with MMR-PID-PSS gives a better dynamic response compared to those of the FLPSS. Specially, the responses give a better settling time and less under/over shoot for the MMR-PID-PSS. Using both proposed power system stabilizers, the power system will be stable but with different power angle positions. The new rotor angle value using MMR-PID-PSS will be less than the new rotor angle value using FLPSS. Thus, the power system with MMR-PID-PSS provide greater stability margin than the FLPSS. This allows the generation unit to send more power to the transmission lines.

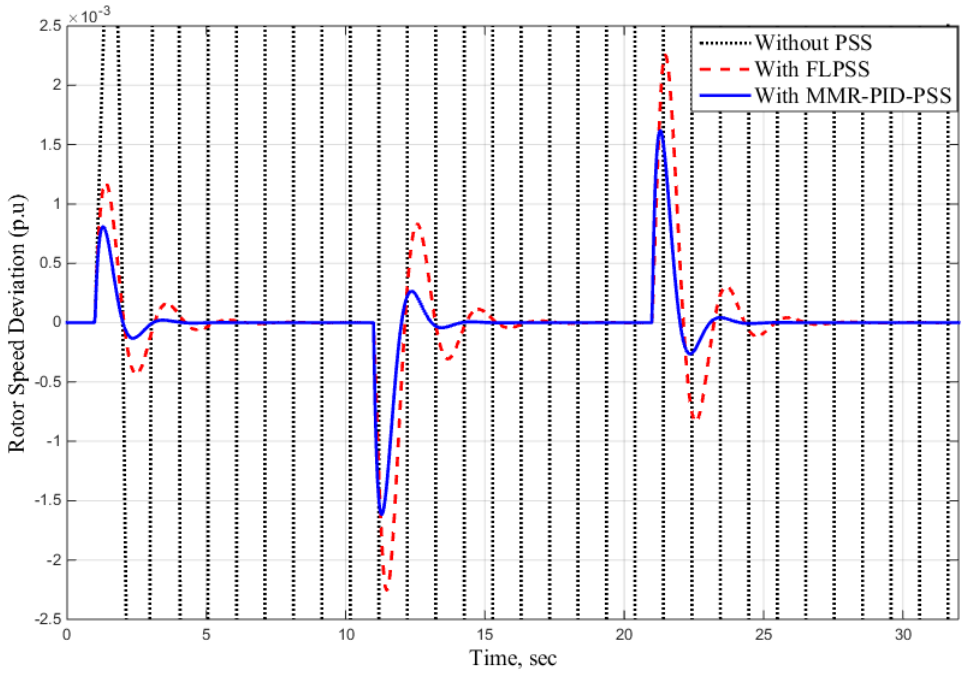

Figure 6.26. Time response of $\Delta\omega$ due to disturbances at P = 1.25, Q = 0.85 and X_t = 0.8 pu

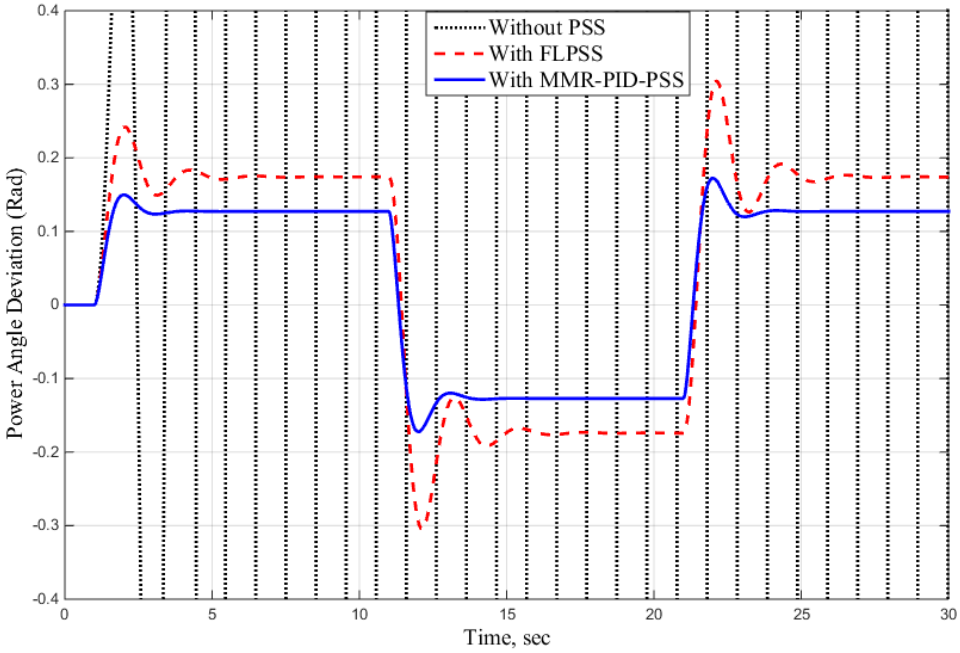

Figure 6.27. Time response of Δδ due to disturbances at P = 1.25, Q = 0.85 and X_t = 0.8 pu

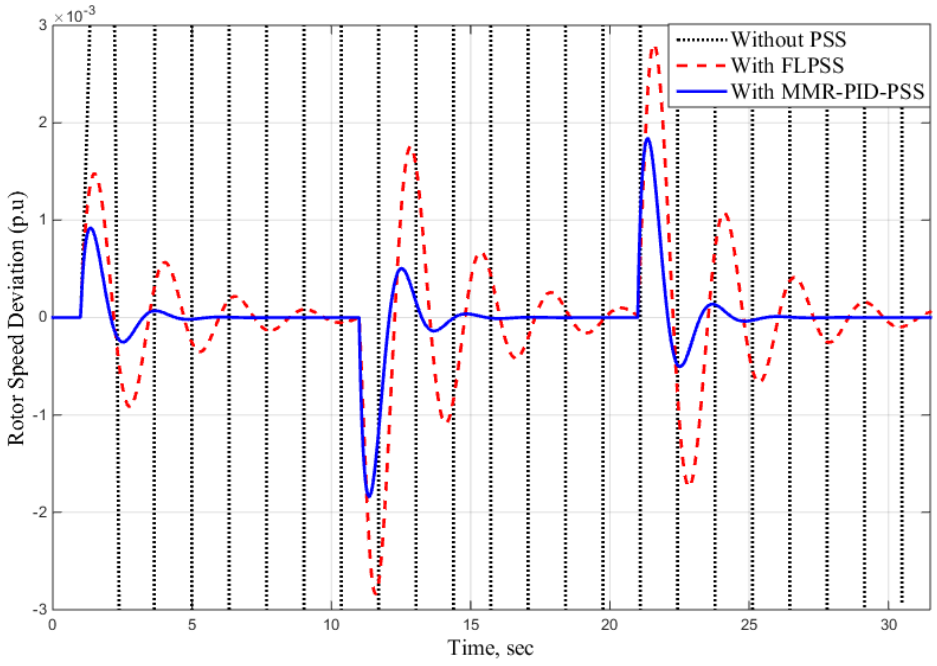

Figure 6.28. Time response of Δω due to due to disturbances at P = 1.45, Q = 0.95 and X_t = 0.8 pu

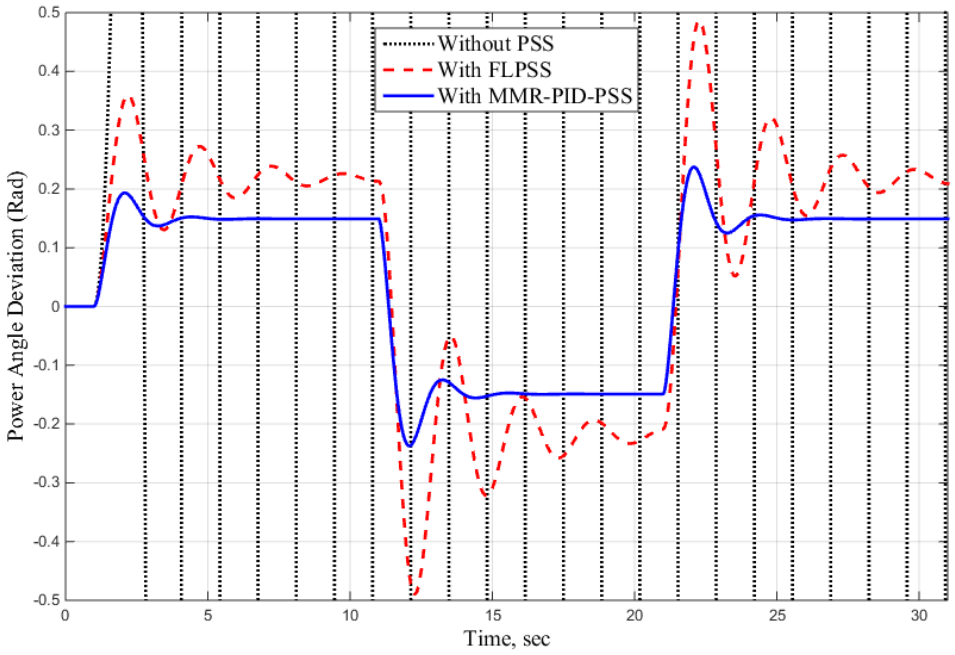

Figure 6.29. Time response of Δδ due to disturbances at P = 1.45, Q = 0.95 and X_t = 0.8 pu

The time response for a ±1% change in mechanical torque at 1, 11, and 21 sec. of rotor speed deviation Δω and power angle variation Δδ at different leading power factors and different reactance is shown in Figures 6.30 to 6.33. The results show that the power system without PSS is unstable, whereas the power system with both regulators (FLPSS and MMR-PID-PSS) is stable. The power system with the suggested MMR-PID-PSS gives a better dynamic response compared to those of FLPSS. Specially, it gives a better settling time and less under/over shoot. From Figures 6.32 and 6.33, it is clear that the power system with FLPSS has oscillations that persist for a long time, while the power system with MMR-PID-PSS damps out the oscillations over a short time.

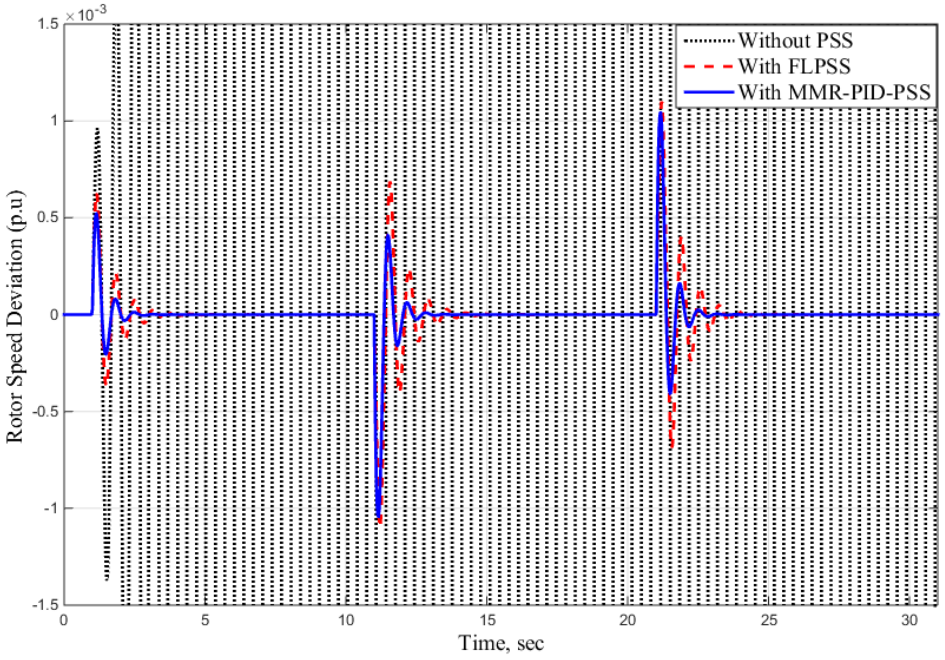

Figure 6.30. Time response of $\Delta\omega$ due to disturbances at P = 1.25, Q = - 0.6 and X_t = 0.45 pu

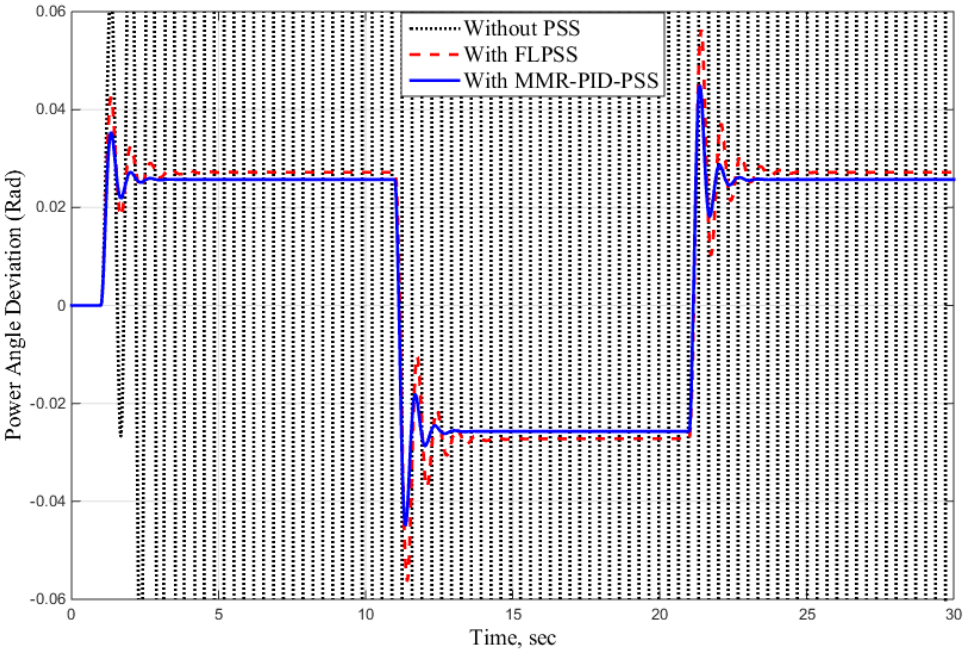

Figure 6.31. Time response of $\Delta\delta$ due to disturbances at P = 1.25, Q = - 0.6 and X_t = 0.45 pu

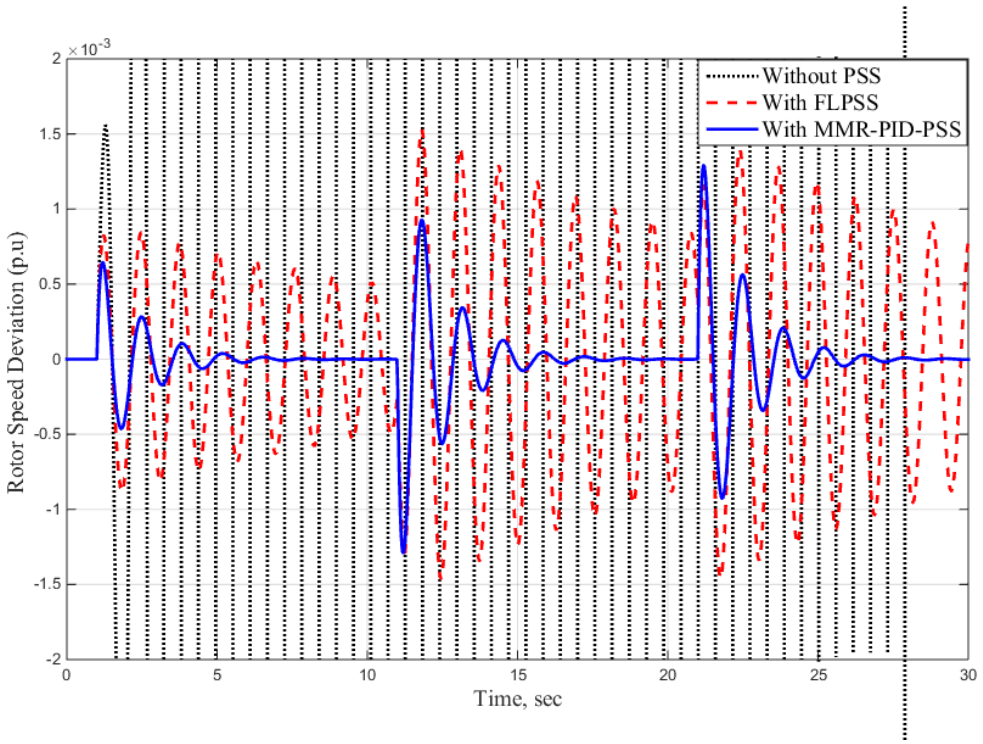

Figure 6.32. Time response of Δω due to disturbances at P = 1.25, Q = - 0.65 and X_t = 0.65 pu

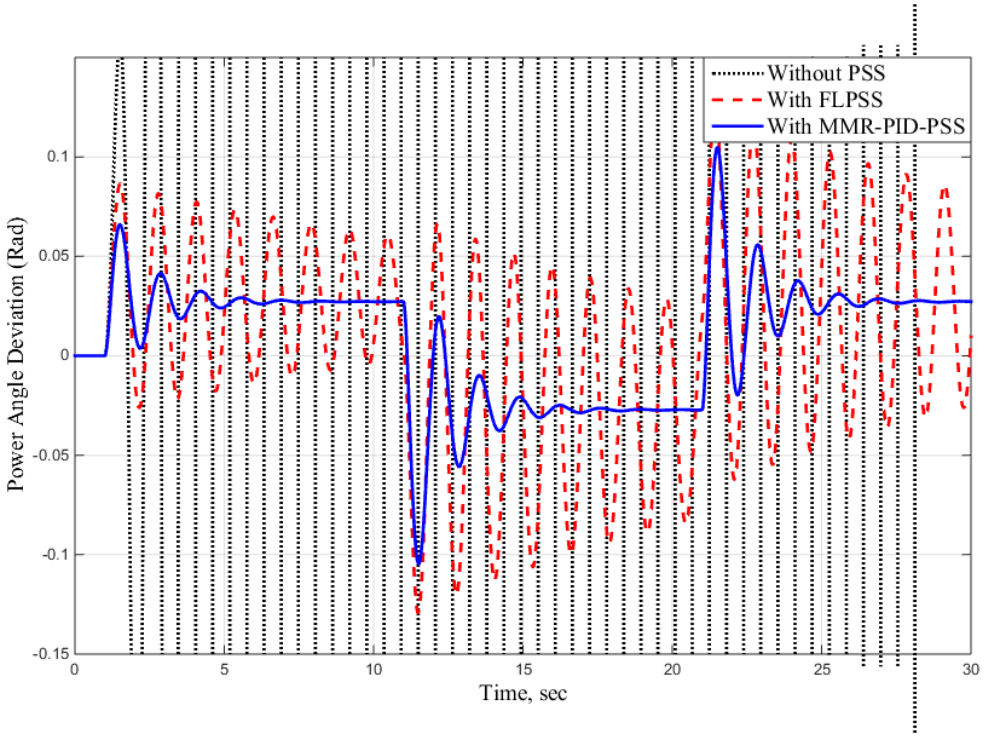

Figure 6.33. Time response of Δδ due to disturbances at P = 1.25, Q = - 0.65 and X_t = 0.5 pu

6.8.2 Multi-machine Power System

6.8.2.1 Four-Machine Ten-Bus Power System

Figure 6.34 shows a single-line diagram of a two-area power system. It has four machines, ten buses and eleven transmission lines, with a total connected load of 2734 MW [10] [108] [109]. The system data, including all the equipment, are given in Appendix B. The proposed MMR-PID-PSS has been applied to the four-machine ten-bus power system under different operating conditions to test its effectiveness of damping out power system oscillations after disturbances occur. The design is performed in MATLAB [107] and simulated with Power System Toolbox [110].

The first test was applied with a self-clearing three-phase fault at bus 9 at 0.5 second and cleared after 100 ms without line clearing. In this case, some of the system states were chosen to check system behaviour under the fault condition. Figure 6.35 to Figure 6.39 illustrate rotor speed deviation and rotor angle deviation of generator G_1, magnitude value of voltage change on bus 9, changes in real power generated from generator G_4, and changes in the absolute value of terminal current at generator G_4.

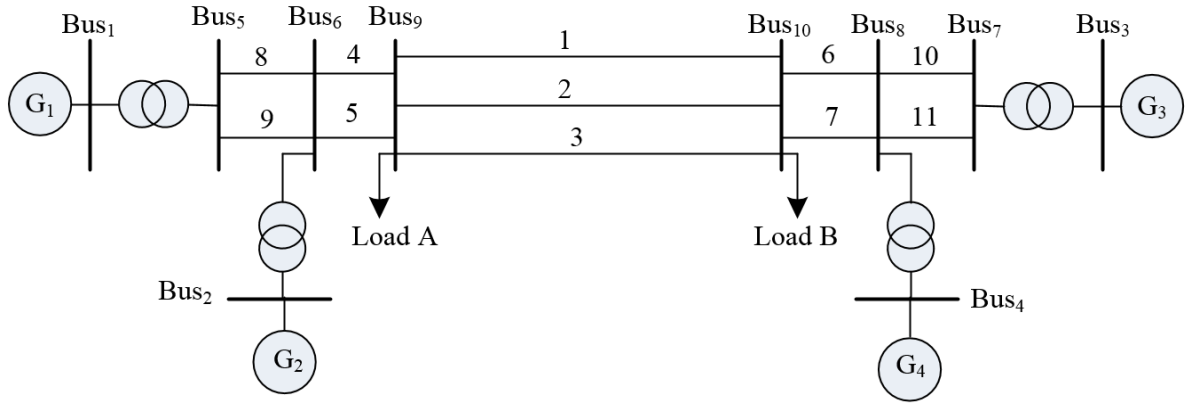

Figure 6.34. Single line diagram of four-machine ten-bus power system

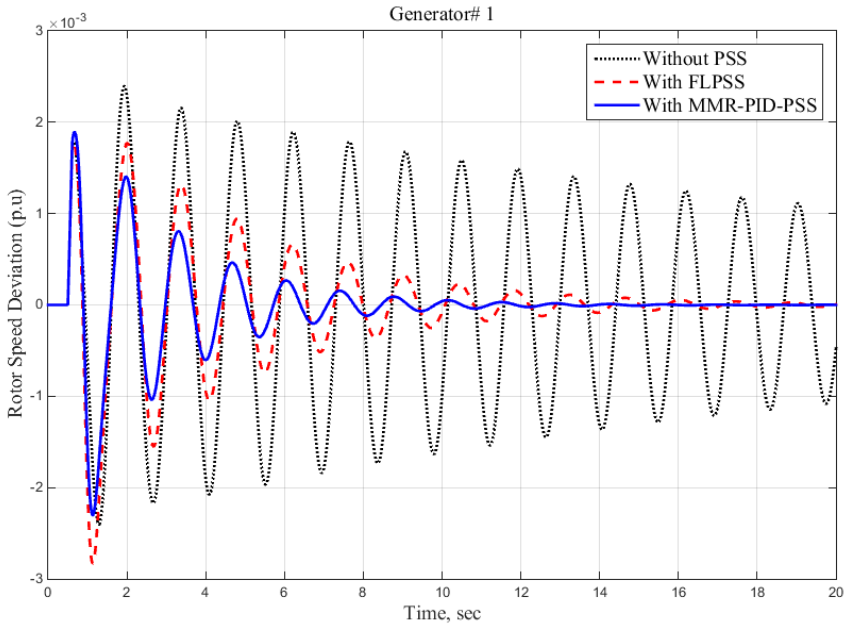

Figure 6.35. Time response of rotor speed deviation of generator 1 when 3-ph fault applied at bus 9

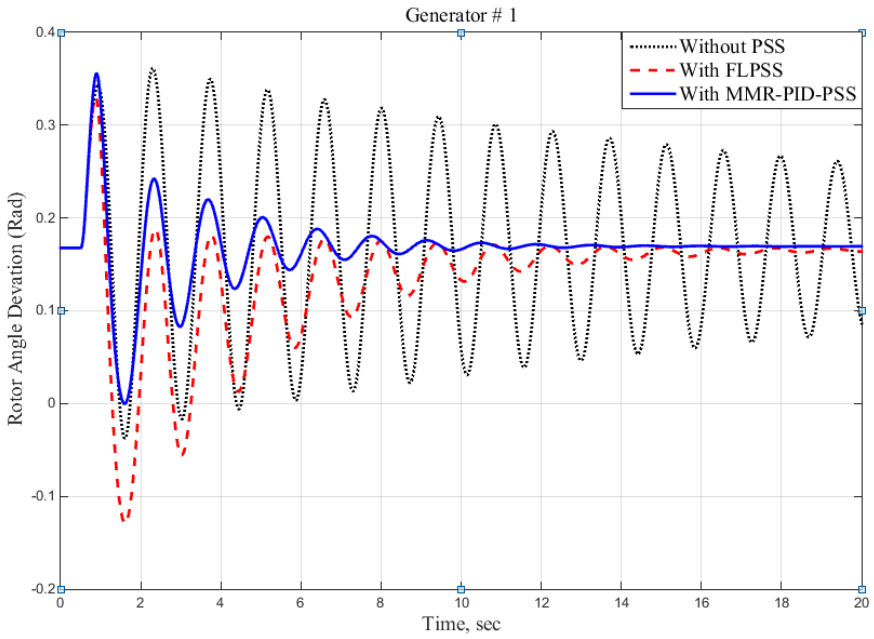

Figure 6.36. Time response of rotor angle deviation of generator 1 when 3-ph fault applied at bus 9

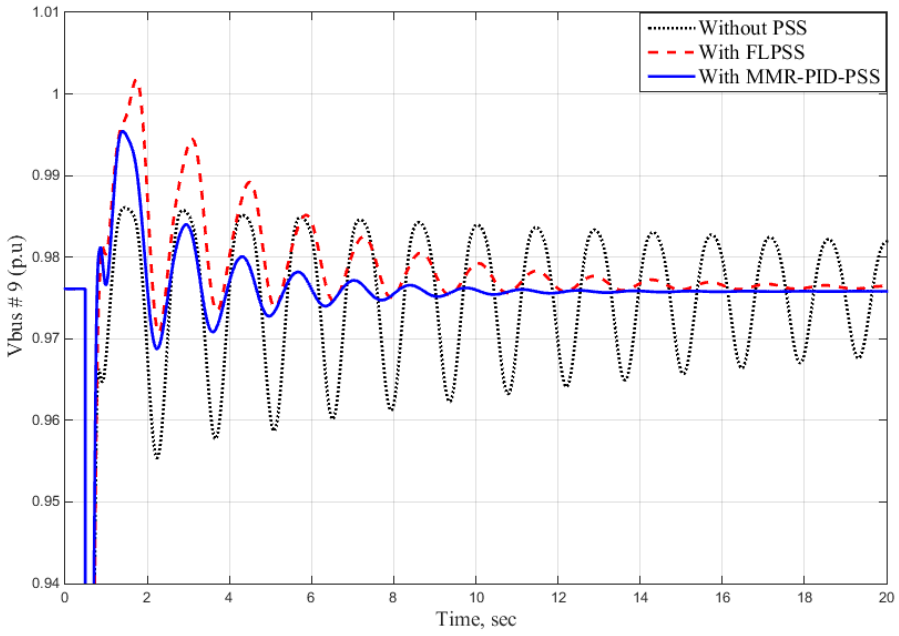

Figure 6.37. Time response of voltage change of bus 9 when 3-ph fault applied at bus 9

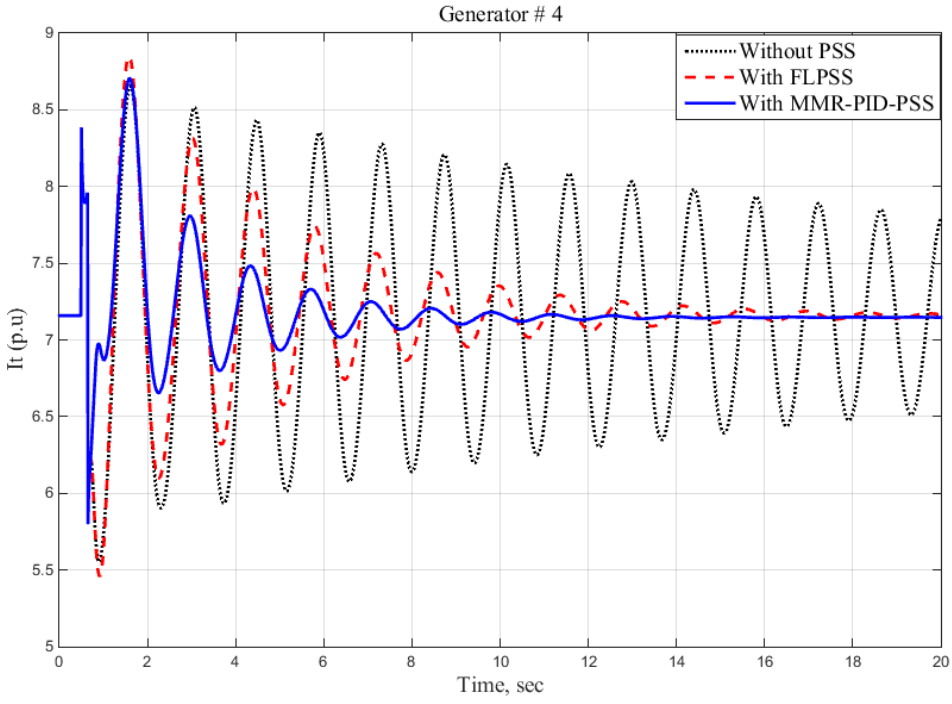

Figure 6.38. Time response of terminal current deviation of generator 4 when 3-ph fault applied at bus 9

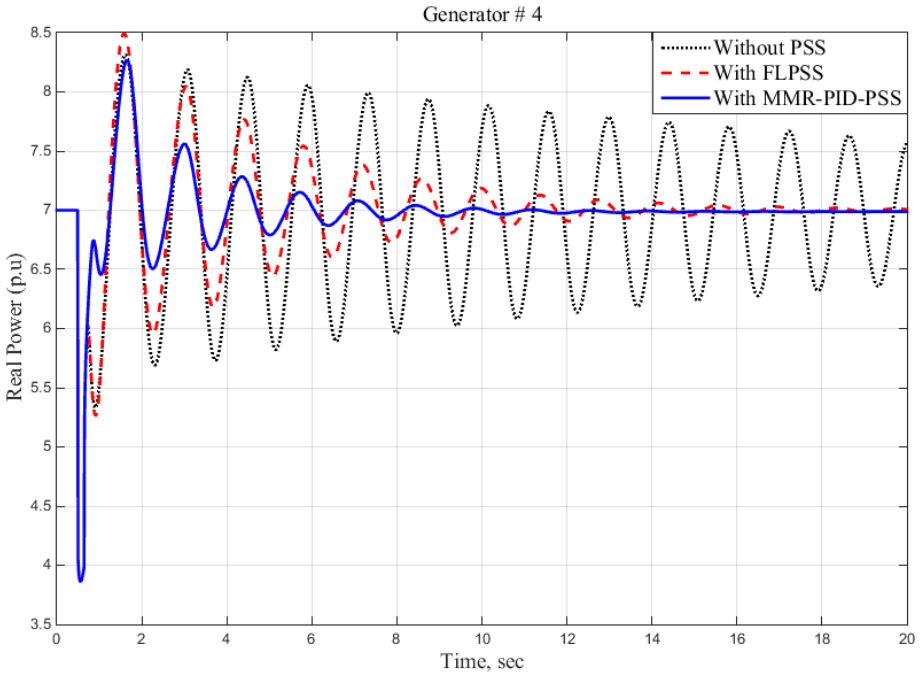

Figure 6.39. Time response of real power deviation of generator 4 when 3-ph fault applied at bus 9

From Figure 6.35 to Figure 6.39, it is evident that, after the fault clears, the system will suffer from an oscillation problem that persists for a long time, making it fragile. Using the proposed MMR-PID-PSS, these oscillations will be quickly damped out. Therefore, the power system with the proposed PSS will be more stable and have a better stability margin. As well, it will be able to send more power through transmission lines to cover the increasing demand for electrical energy. The second scenario of the case study changes the voltage reference of generator G_1 by a 10% step increase. In this case, the time response of the rotor speed deviation for generator G_1 and generator G_4 are shown in Figure 6.40 and Figure 6.41, from which it is clear that both generators swing against each other, for the power system without PSS, with FLPSS, and with MMR-PID-PSS. The power system without PSS oscillates for a long time, while for the power system with the proposed PSSs, the oscillations are damped in a short time. However, the power

system with MMR-PID-PSS has better dynamic response as compared to the power system with FLPSS.

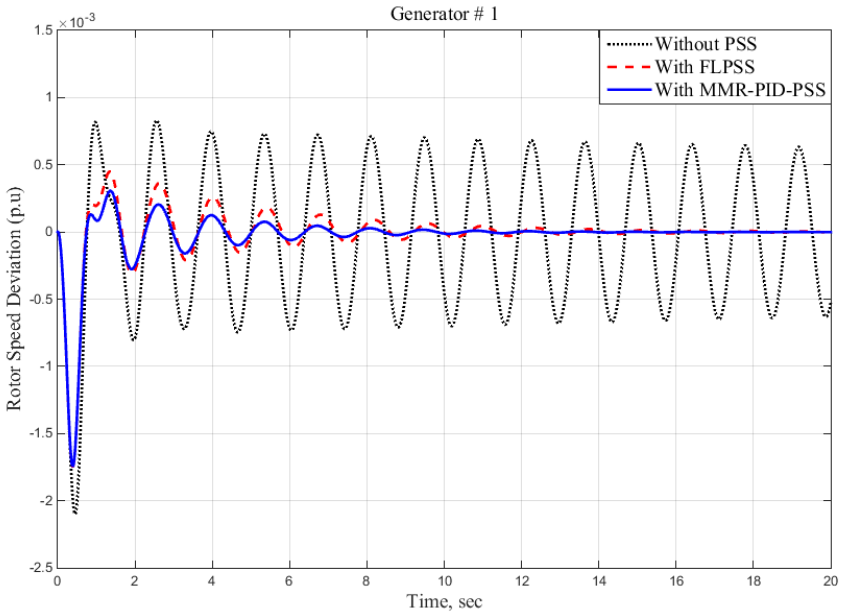

Figure 6.40. Time response of rotor speed deviation of generator 1 for perturbation of V_{ref}

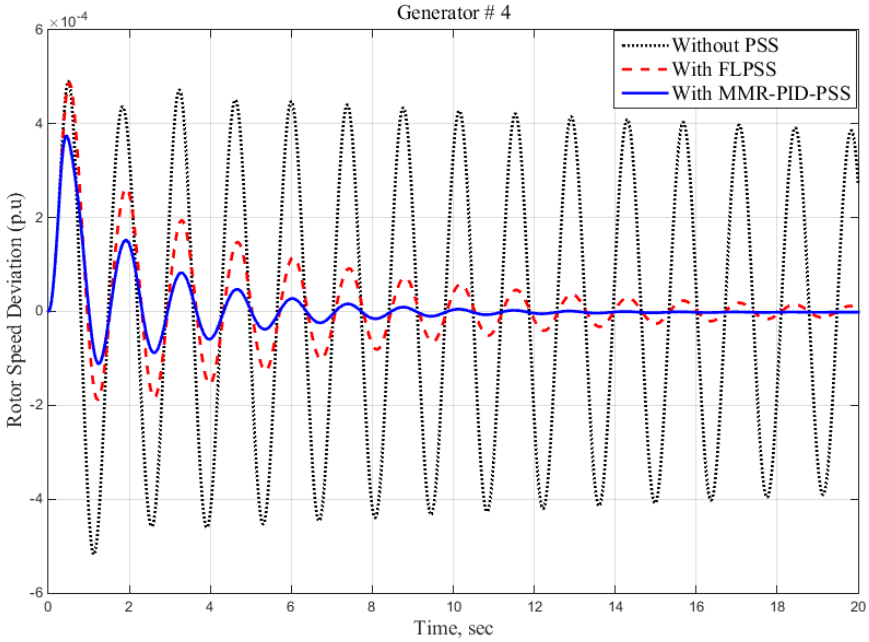

Figure 6.41. Time response of rotor speed deviation of generator 4 for perturbation of V_{ref}

The third test for the power system with the proposed regulator is to increase the output mechanical torque from the turbine mechanically coupled with generator G_1 by 0.7 p.u step increase ($\Delta T_{m1} = 0.7\,\text{p.u}$) applied at 0.5sec. From Figure 6.42, it is evident that when the mechanical torque increases the rotor speed will also increase. To maintain the synchronism, the electrical torque should increase which is clear in Figure 6.43. As a result, the acceleration torque will be zero. In order to perform this process, the power system without PSS will have oscillations that continue for a long time, and the system under this situation could lose synchronism (blackout). The system with MMR-PID-PSS has a better dynamic response compared as compared to the FLPSS. Thus, the acceleration torque will reach zero within a short time, which means the power system is safer, and the system has a better stability margin. Moreover, the possibility of the system losing its synchronism or even losing part of the power system is quite low.

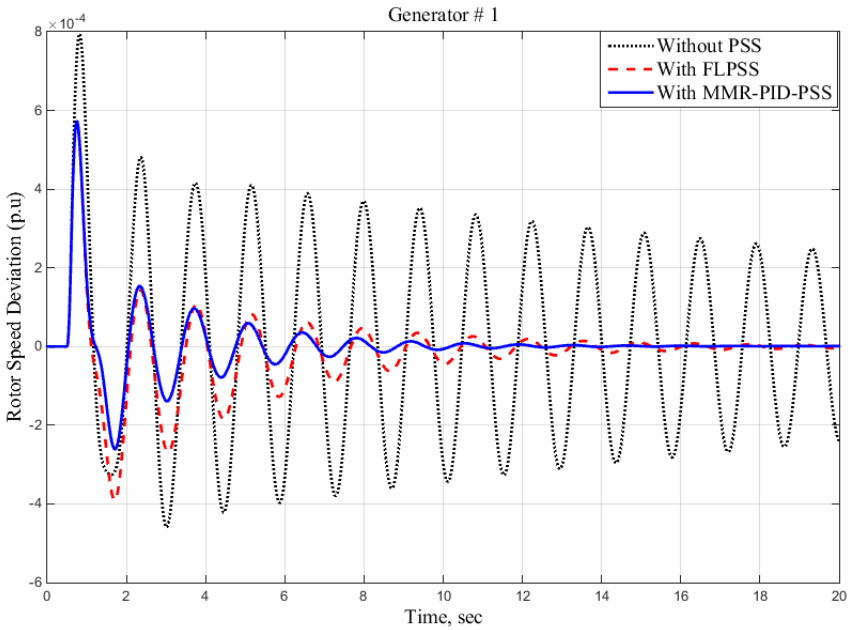

Figure 6.42. Time response of rotor speed deviation of generator 1 for perturbation of T_{m1}

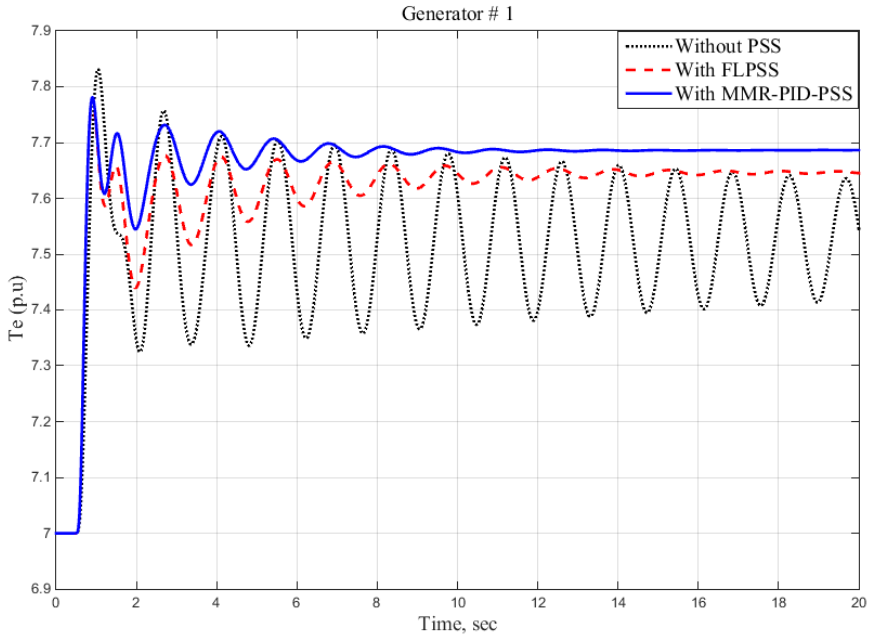

Figure 6.43. Time response of electrical torque deviation of generator 1 for perturbation of T_{m1}

6.8.2.2 Ten-Machine 39-Bus New England Power System

In this thesis, a New England power system, which contains 10 machines and 39 buses, has been used to test the proposed power system stabilizers. A single-line diagram of the 10-generator and 39-bus power system is shown in Figure 6.44 [10] [108] [109]. The loads are modeled as constant impedances and the power system data are given in Appendix C. The design is performed in MATLAB [107] and simulated with Power System Toolbox [110]. The first test applied is a self-clearing three-phase fault at bus 26 at 0.5 sec. and cleared after 10 ms without line clearing. The chosen state variables are rotor speed deviation of generator G_1, rotor angle deviation of generator G_1, real power change of generator G_1 and voltage change on bus 26.

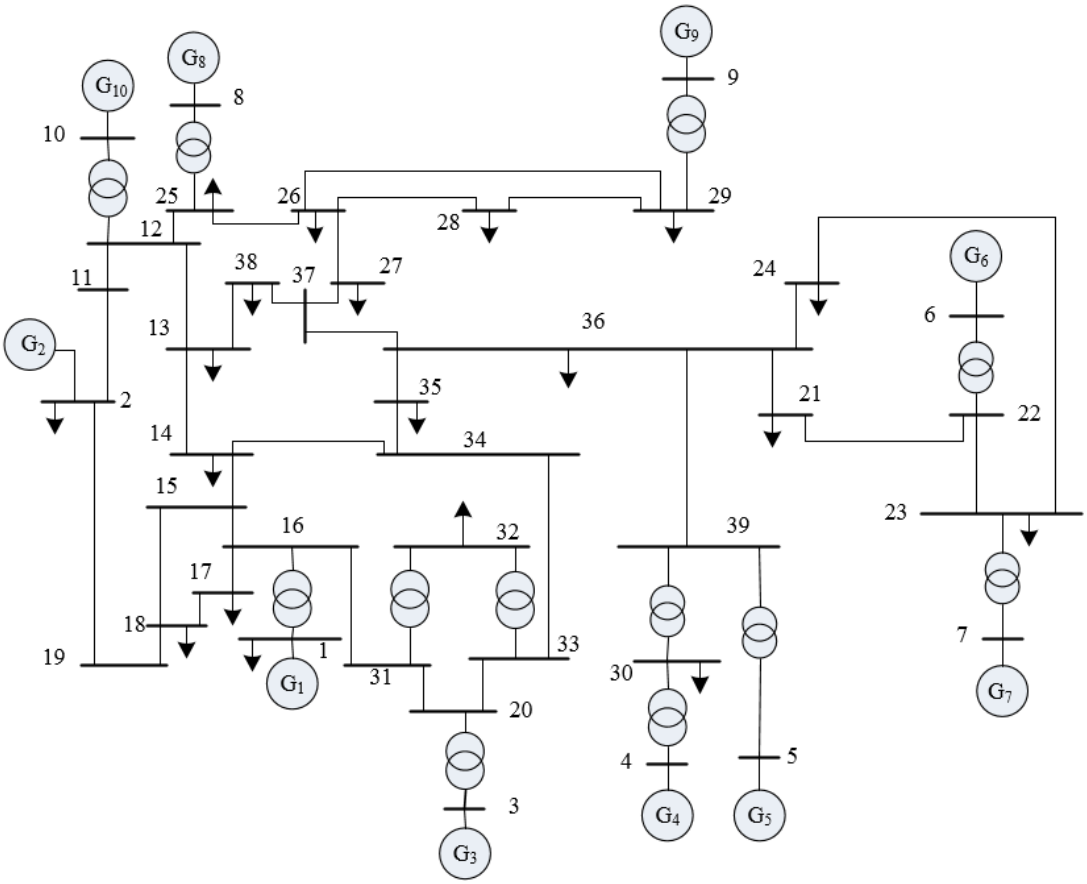

Figure 6.44. Single-line diagram of 10-generator 39-bus power system

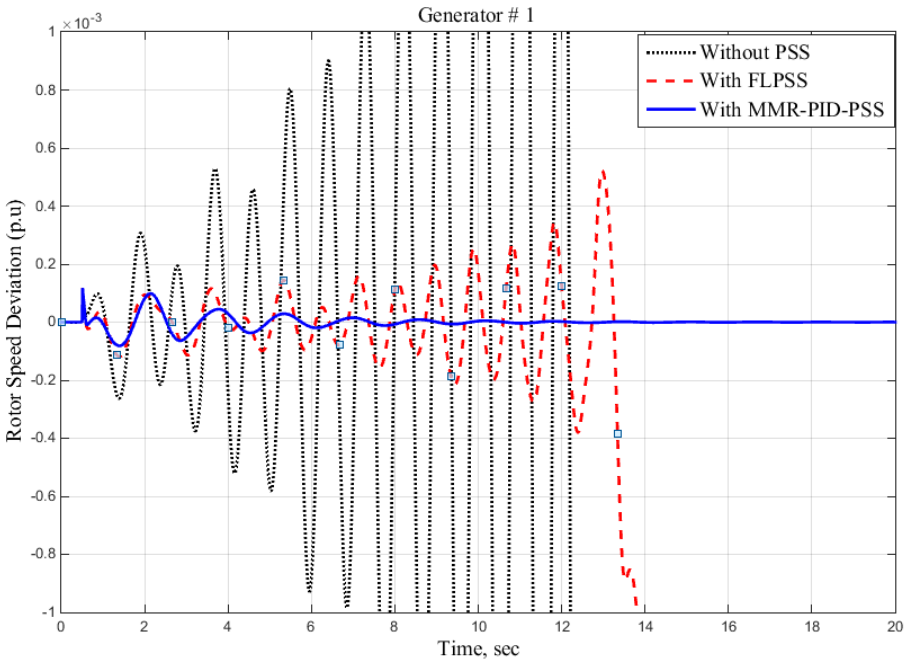

Figure 6.45. Time response of rotor speed deviation of generator 1 with 3-ph fault applied at bus 26

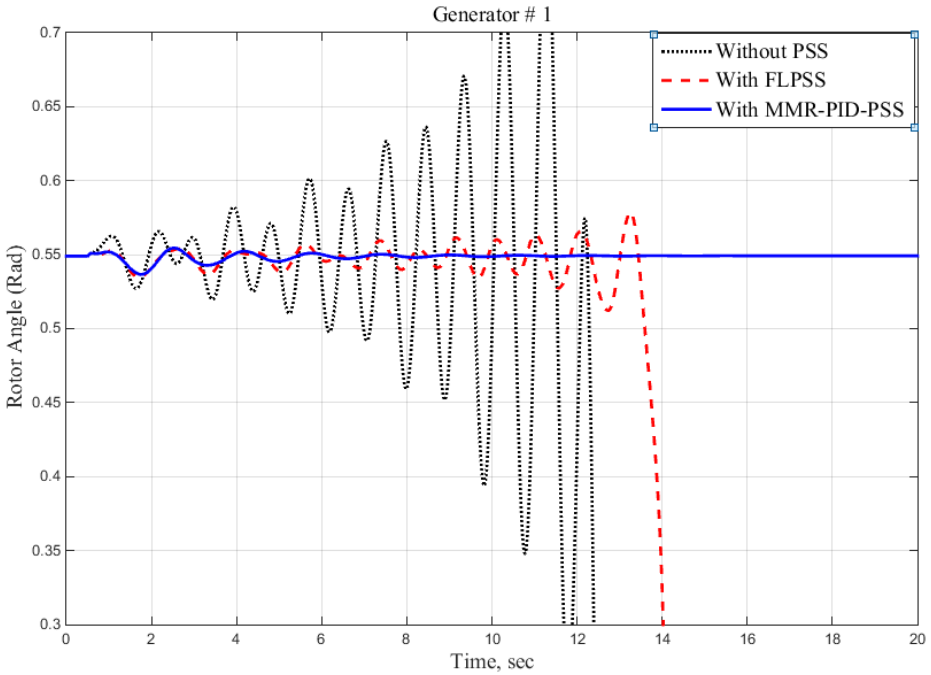

Figure 6.46. Time response of rotor angle deviation of generator 1 with 3-ph fault applied at bus 26

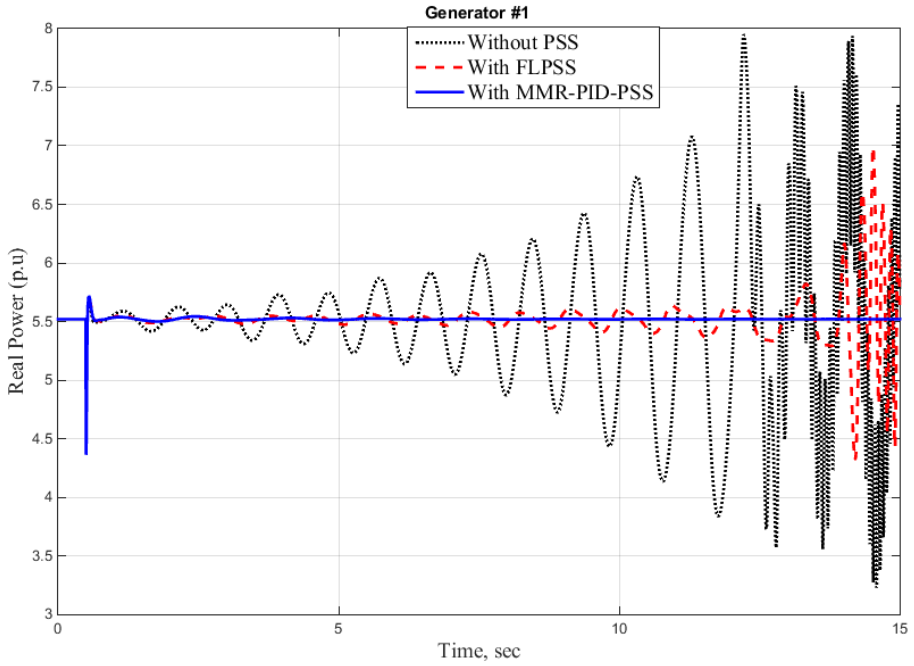

Figure 6.47. Time response of real power deviation of generator 1 with 3-ph fault applied at bus 26

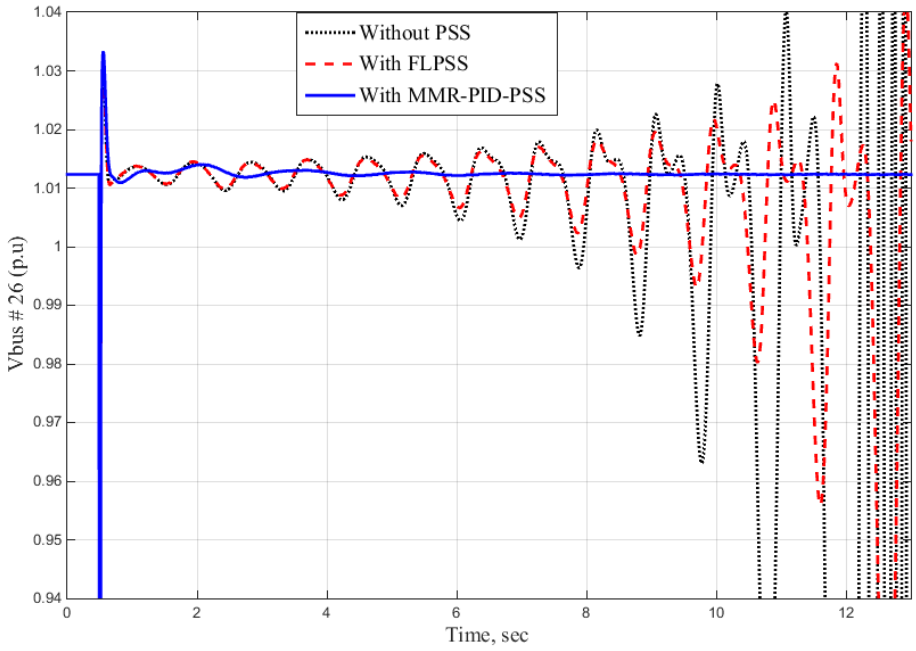

Figure 6.48. Time response of voltage change of bus 26 with 3-ph fault applied at bus 26

Figure 6.45 to Figure 6.48 show that the system under network disturbance, which is a three-phase fault at bus 26, without PSS and with FLPSS, is unstable, while the system with the suggested MMR-PID-PSS is stable. When the fault occurs at 0.5 second, the voltage at bus 26 drops to zero, which will lead to a reduction of real power generated from generator G_1, as shown in Figure 6.47 (reduction in electromechanical torque). Thus, the acceleration torque will increase ($T_a = T_m - T_e$) and both the rotor speed and the rotor angle will increase as well, as shown in Figure 6.45 and Figure 6.46, respectively. To maintain equilibrium the acceleration torque should be zero, which can be achieved by controlling the excitation voltage using the automatic voltage regulator (AVR) and power system stabilizer (PSS).

The second scenario of case study is to change the voltage reference of generator G_1 by a 10% step increase. Increasing the voltage reference leads to increases in the electromechanical torque and terminal current as shown in Figure 6.51, which then decreases the rotor speed and rotor angle as illustrated in Figure 6.49 and Figure 6.50, respectively. Results show that the power system without PSS will be unstable within a short time under this disturbance, while the power system with FLPSS will be unstable after a period of time. Meanwhile, the power system with MMR-PID-PSS is stable and will eliminate the system oscillations within a short time. As a result, the power system under study without PSS and with FLPSS will be unsafe under this type of disturbance and will lose synchronism, whereas the power system with the proposed MMR-PID-PSS will be secure.

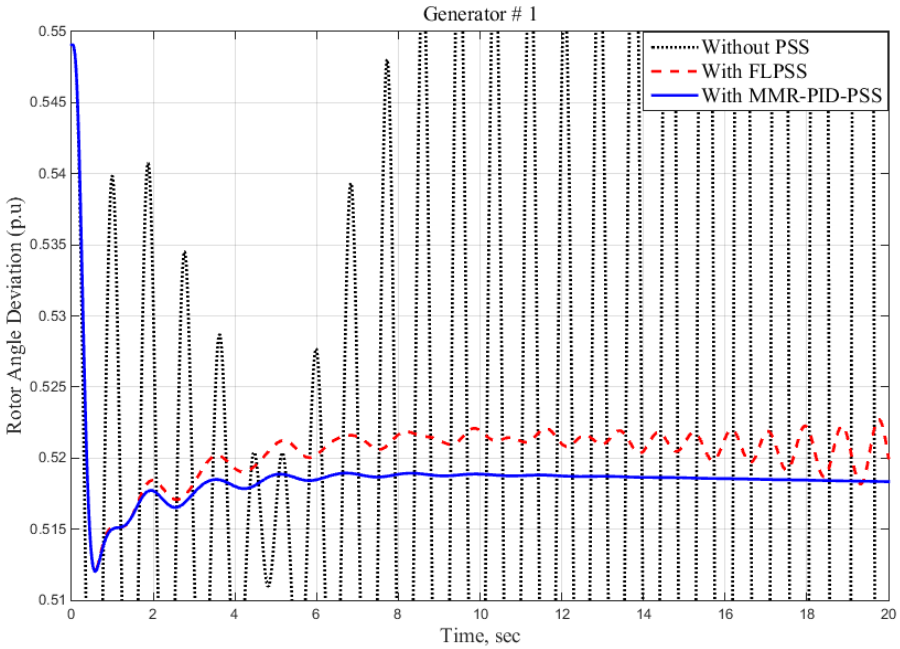

Figure 6.49. Time response of rotor speed deviation of generator 1 for perturbation of V_{ref}

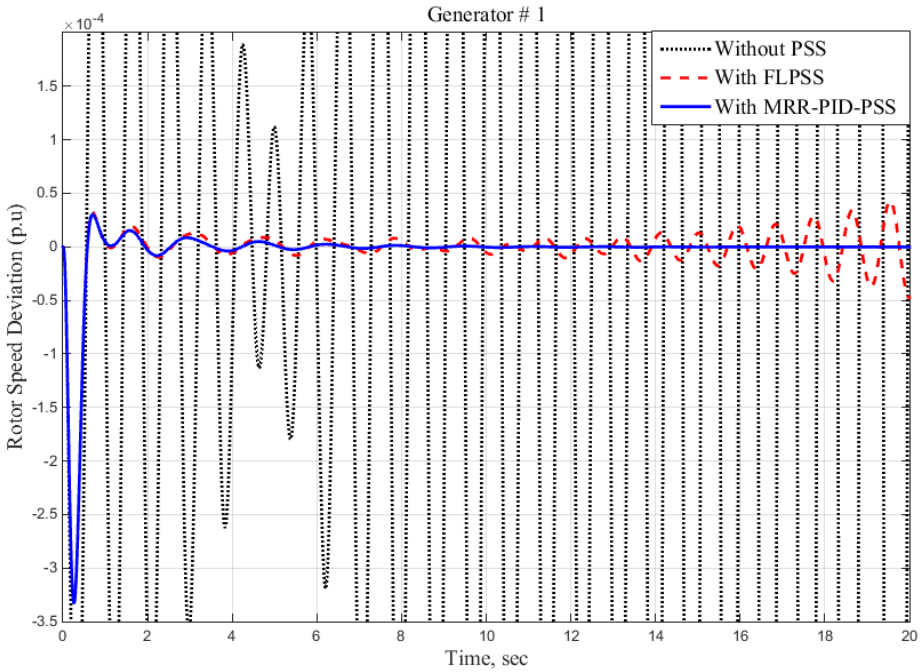

Figure 6.50. Time response of rotor angle deviation of generator 1 for perturbation of V_{ref}

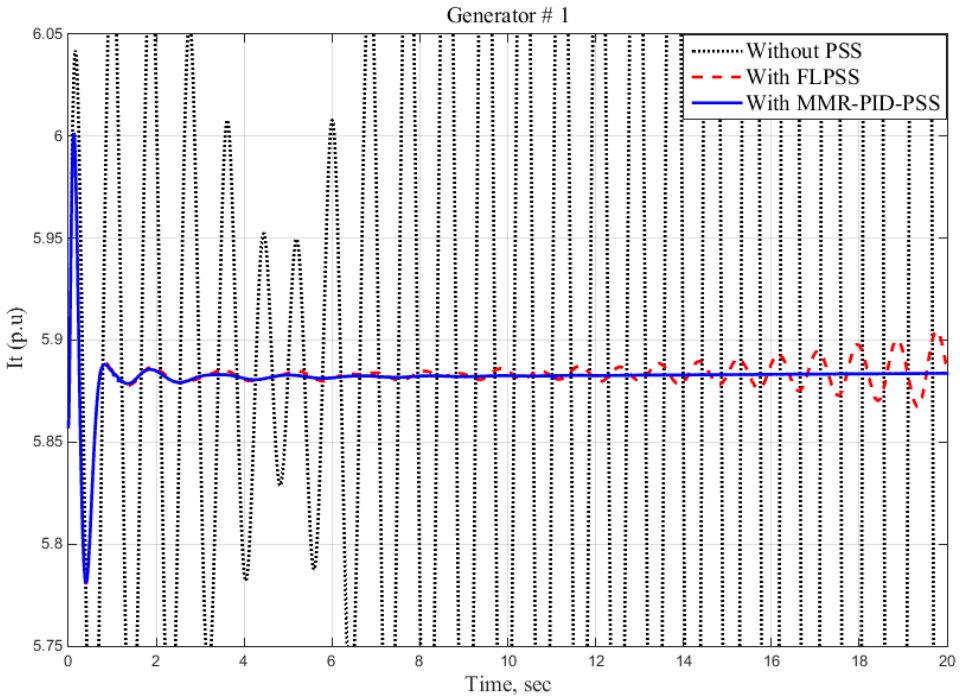

Figure 6.51. Time response of terminal current deviation of generator 1 for perturbation of V_{ref}

6.9 Summary

In this chapter, a wavelet-based modified multi-resolution PID power system stabilizer (MMR-PID-PSS) was developed to improve power system stability under various cases of disturbance. At the beginning of this chapter, wavelet transforms, multi-resolution analysis and optimum mother wavelet selecting were briefly explained. Then, the MMR-PID-PSS was designed based on a reduced-order power system, which consists of one synchronous generator with IEEE type-1 excitation and turbine governor systems connected to the network. The proposed MMR-PID-PSS has three gains (k_{a^2}, k_{a^2} and k_{d^1}) where the rotor speed deviation signal is chosen to be the input of the proposed regulator. The rotor speed deviation is decomposed up to the second level of resolution using the discrete wavelet technique. The gain k_{a^2} is used to adjust the low-frequency component of the rotor speed deviation signal at the second level of resolution $\Delta\omega_{a^2}$. The gain k_{d^1}

is used to correct the derivative of the high-frequency component of the rotor speed deviation at the first level of resolution $\Delta\dot{\omega}_{d^1}$, and the gain k_{d^2} is used to weight the integral of rotor speed deviation at the second level of resolution $\int \Delta\omega_{d^2}$. The proposed regulator was tested for a single machine connected to the network and compared with FLPSS, designed in Chapter 5, under different operating conditions.

Also in this chapter, the proposed MMR-PID-PSS was tested with a four-machine ten-bus power system and with the New England ten-machine 39-bus power system under different operating conditions, such as the application of a self-clearing three-phase fault; a change in the voltage reference of one generator by a 10% step increase; and an increase in the output mechanical torque from the turbine that is mechanically coupled with a generator by a 0.7 p.u step increase. With all types of disturbances tested either for a single-machine or a multi-machine system, the power systems with the proposed MMR-PID-PSS gave a better dynamic response. As a result, the power system with the proposed controller has a greater stability margin.

Chapter 7

7 Conclusions

7.1 Summary of the Thesis

Modern electrical power systems have many interconnected components. Therefore, they can encounter variety unpredictable problems. For instance, faults occur on transmission lines that have built-in protection systems and small variations in the load cause small signal perturbations within the electrical power system. Such unwanted variations may continue for a lengthy period and cause restrictions on the power transmitted through transmission lines. The probability of outage or complete blackouts (Ohio blackout 2003, Arizona-California 2011) is relatively high when the power system is operating under stressed conditions. In other words, the system will be vulnerable. Standard control devices such as governors and automatic voltage regulators (AVRs) might not be sufficient to relieve these fluctuations within a short period.

In order to solve these problems, most central power stations in interconnected power systems have an additional control signal in the excitation system, known as a power system stabilizer (PSS). However, the parameters of standard PSS are fixed while the power system is highly nonlinear as it features configurations and parameters that change over time. Moreover, the design of a standard PSS is typically based on an accurate mathematical model of system dynamics, and even though the system model is well-known, building an accurate mathematical model is a very difficult task due to unavoidable conditions such as system noise, saturation, etc. Therefore, a standard PSS might not be able to provide good performance in many practical applications.

This thesis attempts to mitigate this limitation by implementing smart power system stabilizers: a neural network power system stabilizer (ANN-PSS), a novel fuzzy logic power

system stabilizer (FLPSS), and a modified multi-resolution proportional-integral-derivative power system stabilizer (MMR-PID-PSS), based on the dynamic reduction of a power system model. These power system stabilizers have been developed to refine the system dynamic performance under a broad range of operating conditions.

Chapter 1 provided a general description of power system stability and control (introduction, basic concepts, definitions, classifications) and also presented a literature review on conventional PSS, adaptive PSS, artificial neural network PSS, fuzzy logic PSS and wavelet techniques in power systems.

Chapter 2 looked at some linear techniques that have been utilized for the analysis of small signal perturbations and for obtaining information on dynamic system features such as linearization approach and state-space representation. As well, this chapter provided a linearizing model as a derivation for a single synchronous generator connected in a network by taking a high voltage bus of the generation unit as a reference rather than the commonly used infinite bus for standard models.

Chapter 3 introduced a model reduction method for changing a higher-order power system into a reduced-order model. The original model of power system was compared to the reduced-order model under several different operating conditions and parameter alterations.

Chapter 4 provided an explanation of the structure and tuning of a Lead-Lag power system stabilizer. Additionally, it provided an overview of artificial neural network (ANN) controllers and introduced a design for an artificial neural network PSS (ANN-PSS) for a reduced-order power system model. Power systems without PSS, with Lead-Lag PSS, and with ANN-PSS were then compared for a broad range of operating conditions and parameter variations.

Chapter 5 presented an overview of fuzzy logic theory as well as the principle of fuzzy logic controllers. Also, this chapter introduced the design of an improved fuzzy logic PSS (FLPSS) based on a reduced-order power system model. With a range of operational conditions and changed in the parameters, power system without PSS, with ANN-PSS and then using FLPSS were compared.

Chapter 6 introduced the proposed modified multi-resolution proportional-integral-derivative power system stabilizer (MMR-PID-PSS) for a reduced-order power system model. The chapter began with a discussion of wavelet transforms and multi-resolution analysis, along with a more in-depth mathematical analysis of wavelet transforms and a brief summary of the principles of the multi-resolution PID controller. Next came an explanation of the proposed MMR-PID-PSS design, followed by the implementation of MMR-PID-PSS in both single- and multi-machine power systems. A stability analysis followed, together with comparisons of power systems without PSS, with the proposed FLPSS, and with the proposed MMR-PID-PSS. These comparisons were made for different operating conditions in a single-machine power system, a 4-machine 10-bus power system, and a 10-machine 39-bus power system.

7.2 Laboratory Experimental Layout and Results

As an integral part of the work in this thesis, a verification of the simulation results of the proposed technique is provided experimentally using Lab-Volt equipment. This experimental implementation includes the software and hardware setup of the proposed controller.

Experimental tests were carried out for different loads and rotor speeds. Figure 7.1shows the excremental layout using Lab-Volt modules. The 0.2 kW three-phase synchronous generator is connected with three-phase resistive load and coupled with a DC-motor, which is used as a prime mover. The DC voltage supplies the rotor winding of the synchronous generator during

IGBT DC-DC converter, where its gates are firing utilizing the control signal that generated from the control circuit. The rotor speed change is used as an input signal. The speed sensor consists of a permanent generator, while an analog meter was employed to measure the rotor speed that was filtered with a low-pass filter. The control circuit uses a 16F876 PIC. The code is downloaded into the PIC from the computer through an RS232 chip, after which the PIC reads a speed sensor through one of its analog inputs in the 0-5 volt range. The sensor signal gives 1 volt per 500 RPM. A voltage divider is used to get the signal in the proper range, while the PIC calculates a control signal and sends it to the DC-DC converter. The control signal then fires the gate of the DC-DC converter using pulse width modulation (PWM) in order to control the excitation voltage.

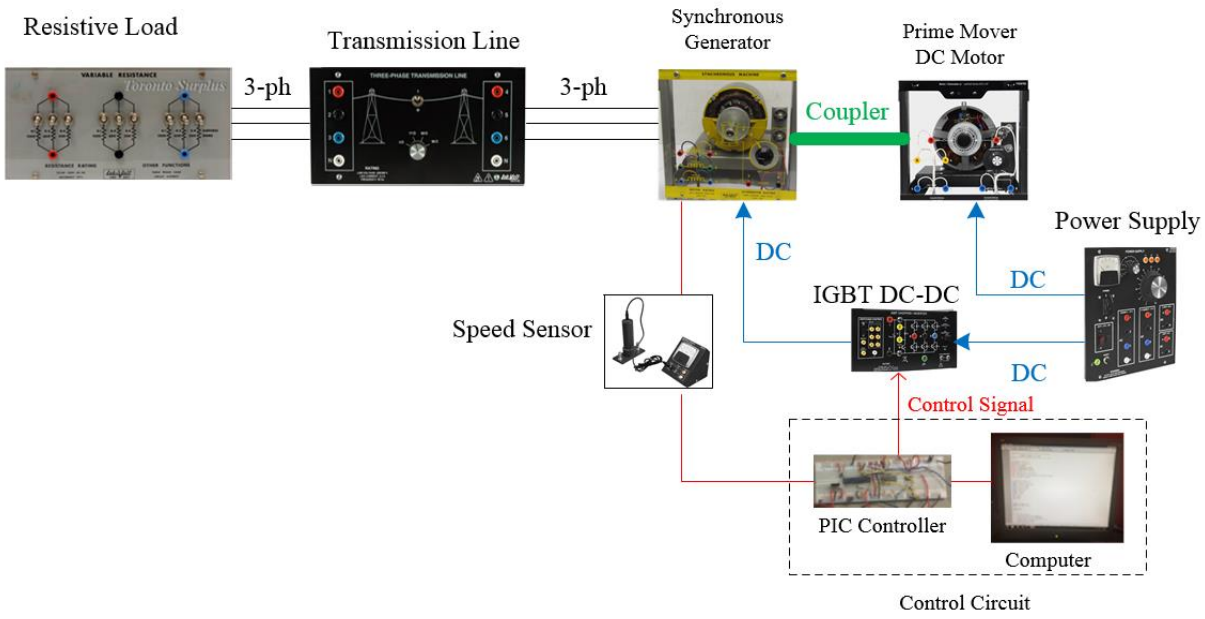

Figure 7.1. Experimental layout using Lab-Volt modules

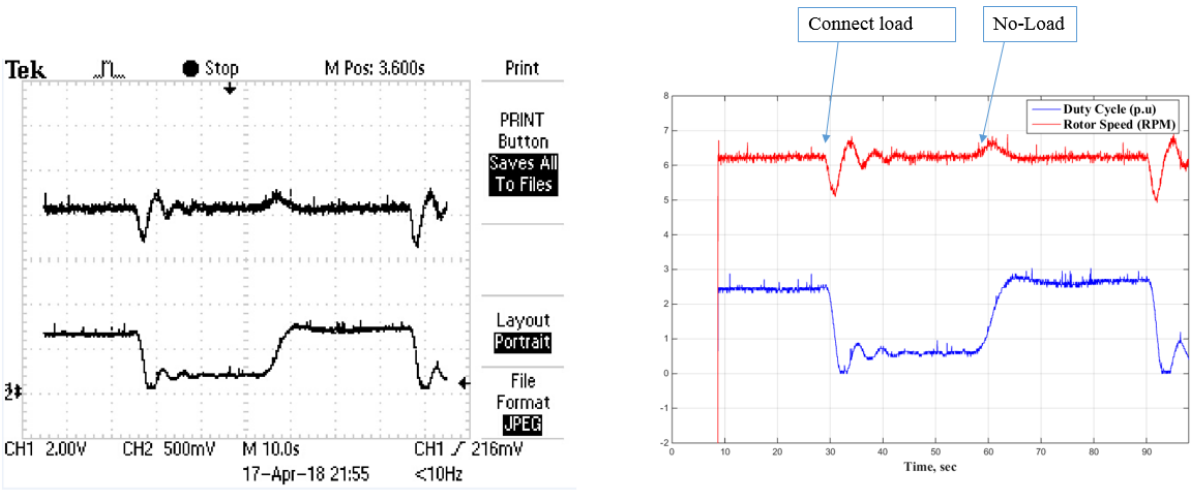

Figure 7.2. Time response of rotor speed 1000 RPM and duty cycle of PWM for connecting and disconnecting the resistive load at different times (experimental results)

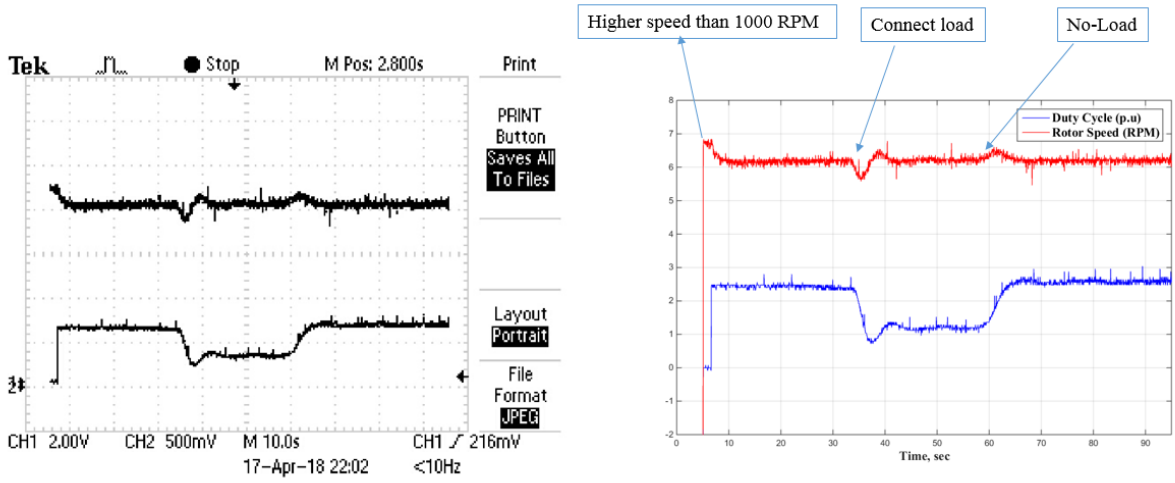

Figure 7.3. Time response of rotor speed 1000 RPM and duty cycle of PWM for connecting and disconnecting the inductive load at different times, where the rotor speed starts at 1100 PRM (experimental results).

The power system stabilizer is experimentally tested to control a three-phase, four-pole, 60 Hz synchronous generator speed that is effected by changing the load. The results are shown in Figures 7.2 -7.5.

In Figure 7.2, the rotor speed is 1000 RPM at 30 seconds the resistive load was connected to the synchronous generator stator winding, causing a decrease the rotor speed, and the controller reduces the excitation voltage by decreasing the duty cycle of the PWM. Decreasing the excitation voltage leads to lower damping torque on the rotor shaft, enabling the rotor speed to increase to 1000 RPM again. At 60 seconds, the load that leads to increasing speed is disconnected, so the controller will increase the excitation voltage in order to increase the damping torque until the speed goes back to 1000 RPM.

In Figure 7.3, we can see that the rotor speed starts at 1100 RPM, so the controller will increase the damping torque until the speed reverts to1000 RPM. At about 35seconds the inductive load is connected, which means that the speed will decrease and the controller will reduce the damping torque on the rotor shaft until the speed goes back to 1000 RPM.

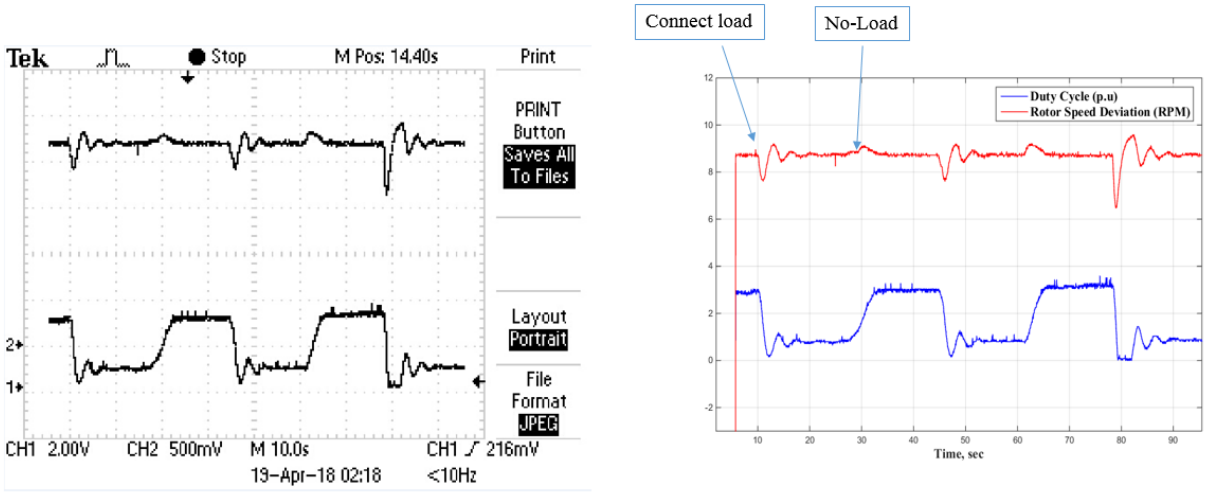

Figure 7.4. Time response of rotor rated speed of 1800 RPM and duty cycle of PWM for connecting and disconnecting the resistive load at different times (experimental results).

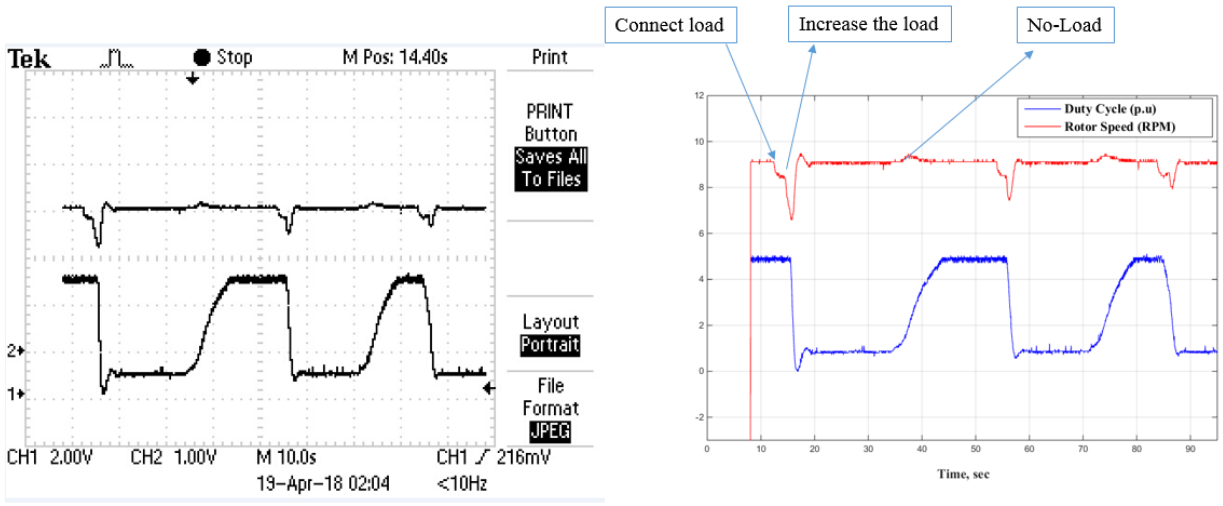

Figure 7.5. Time response of rotor rated speed of 1800 RPM and duty cycle of PWM for connecting and disconnecting the resistive load at different times (experimental results).

In Figure 7.4 and Figure 7.5, the rotor speed is 1800 RPM, which is the synchronous speed. At the synchronous speed, the rotor will have reduced vibration (noise) as well as reduced distortion, as indicated in Figures 7.4-7.5. The results show the effectiveness of the power system stabilizer, where it is reducing and increasing the damping torque in phase with the rotor speed change that is changed by connecting and disconnecting the resistive load at different times.

Conventional PID was used as the controller. For the results presented, only integral gain was positive. The proportional and derivative gains were both set to zero. This setup could be used to test the smart controllers developed in the thesis. It is to be noted that there were noises in the simulation results as well as in the experimental results.

7.3 Major Contributions of the Thesis

As a result of this research, one can conclude the following major contributions:

- A mathematical model of a single machine connected to the network has been introduced and linearized at a high voltage side of the generation unit instead of an infinite bus as in

the classical model. By using this modified model, one can design a power system stabilizer to improve power system stability for both single- and multi-machine power system. Several new equations have also been derived from this model. The mathematical model of the power system contains the parameters K_1-K_6 and K_{V1}-K_{V3}, which are functions of the generator's operating conditions.

- A reduction technique algorithm is discussed and checked for the power system model. The simulation tests of the original system and reduced-order model validate the reduced-order method. A comparison between the original power system model and the reduced-order model of the power system was carried out across a wide range of operating conditions and changes in parameters in order to test the effectiveness and reliability of the third-order model.
- The proposed artificial neural network power system stabilizer (ANN-PSS) was designed based on the reduced-order model of the power system, to improve the power system dynamic performance with changes in the loading conditions. In order to reduce the time needed to train the network in ANN-PSS, this research used a neural network with only three hidden neurons and three inputs to mimic the PID controller. The input signals to the ANN-PSS were the deviation speed $\Delta\omega$, the integral of speed change $\int \Delta\omega$, and the derivative of speed deviation $\Delta\dot{\omega}$. The digital simulation results show that the system with the proposed ANN-PSS yields proper damping characteristics at different operating conditions. The digital simulation results showed that the system with Lead-Lag PSS and ANN-PSS provide good damping characteristics with some operating conditions. However, the system with the ANN-PSS gives a better dynamic response compared to that of Lead-Lag PSS controller at the same operating conditions.

- The proposed novel fuzzy logic PSS (FLPSS) was designed based on the dynamic reduction of a power system model, aimed at improving the system dynamic performance according to changes in loading conditions. A proposed FLPSS was introduced, along with a new approach to determine the parameters of the fuzzy logic controller. The input signals to the FLPSS were the speed deviation $\Delta\omega$ and derivative of speed deviation $\Delta\dot{\omega}$. The number of rules was decreased from 49 (as in typical control rules) to just 9. As a result, the computational burden was greatly reduced. The numerical simulation results showed that the system with the proposed FLPSS produces good damping characteristics at different operating conditions. Also, the results showed that the FLPSS gives a better dynamic response compared with the ANN-PSS controller under the same operating conditions.
- A wavelet-based modified multi-resolution PID power system stabilizer (MMR-PID-PSS) was developed to improve power system stability under small disturbances. Wavelet transforms, multi-resolution analysis and optimum mother wavelet selection were briefly explained, after which an MMR-PID-PSS was designed based on a reduced-order power system. The proposed MMR-PID-PSS has three gains of k_{a^2}, k_{d^2} and k_{d^1} with the rotor speed deviation signal being chosen as the input of the proposed regulator. The rotor speed deviation is decomposed up to the second level of resolution using the discrete wavelet technique. The gain k_{a^2} is then used to adjust the low-frequency component of the rotor speed deviation signal at the second level of resolution $\Delta\omega_{a^2}$. The gain k_{d^1} is used to correct the derivative of the high-frequency component of the rotor speed deviation at the first level of resolution $\Delta\dot{\omega}_{d^1}$. The gain k_{d^2} is used to weight the integral of rotor speed deviation at the second level of resolution $\int \Delta\omega_{d^2}$. The proposed regulator was tested on a

single machine connected to the network and compared with FLPSS, designed in Chapter 5, under different operating conditions. Additionally, the proposed MMR-PID-PSS was tested with a four-machine ten-bus power system and with the well-known New England ten-machine 39-bus power system under various operating conditions. These conditions included the application of a self-clearing three phase-fault; a change in the voltage reference of one generator by a 10% step increase; and an increase in the output mechanical torque from the turbine mechanically coupled with a generator by a 0.7 p.u step increase. Under all types of disturbances, either for one machine or for a multi-machine power system, the power systems operating with the proposed MMR-PID-PSS gave a better dynamic response. As a result, the power system using the proposed controller has a greater stability margin, is able to deliver more power to the network, and has much reduced possibility to lose a generator, load, portion of the power system, or to have a blackout under different types of disturbances.

7.4 Suggestions for Future Work

In the course of this research, many aspects were investigated, and numerous conclusions were drawn with regards to a variety research issues. However, as with any ongoing research, there are several points which should be looked into in the future. These points are formed as suggestions, as follows:

Future research work should attempt to:

- Verify the effectiveness of the proposed power system stabilizers by experimental implementation in a power laboratory.
- Apply the proposed PSSs to a vast power system to study their efficacy using one of the commercial software packages used by power system companies.

- Extend this research to study wide area control (WAC), where controllers make use of remote measurements using phasor measurement units (PMUs) and control signals.
- The work in this thesis was limited to enhancing the overall power system stability through adding an auxiliary controller to the excitation system in the generation unit. For future improvement of power system stability, integrated smart stabilizers for both excitation and turbine speed governor system in the generation unit could prove invaluable.
- Extend this research to improve the power systems stability by controlling reactive power using smart controllers in electric power grids using compensators such as static synchronous compensators (STATCOMs), static synchronous series compensators (SSSCs), unified power flow controllers (UPFCs), etc.
- Implement the proposed control approach to control energy storage systems, such as superconducting magnetic energy stores (SMESs), flywheel energy storage (FES), etc. and to control superconducting fault current limiters (SFCLs), in the electric power grid in order to ensure reliable performance under a wide range of disturbances.
- Investigate the proposed smart controllers for renewable energy systems.

List of References

[1] H. A. Moussa and Yao-nan. Yu, "Dynamic of interaction of multi-machine system and excitation control," *IEEE Transaction on Power Apparatus and Systems*, Vols. PAS-93, no. 4, pp. 1150-1158, January 1974.

[2] V. A. Venikov and V. A. Stroev, "Power system stability as affected by automatic control of generators-some methods of analysis and aynthesis," *IEEE Transaction on Power Apparatus and Systems*, Vols. PAS-90, no. 6, pp. 2483-2487, February 1971.

[3] P. M. Anderson and A. A. Fouad, Power system control and stability, Ames, Iowa: Iowa state university press, 1977.

[4] F. P. Demello and C. Concordia, "Concept of synchronous machine stability as affected by excitation control," *IEEE Transaction on Power Apparatus and Systems*, Vols. PAS-88, no. 4, pp. 316-329, April 1969.

[5] J. L. Dineley and A. J. Morris, "The dynamic interaction of closely-coupled synchronous generators," *IEEE Transaction on Power Apparatus and Systems*, Vols. PAS-90, no. 5, pp. 2158-2165, February 1971.

[6] M. K. El-Sherbiny and D. M. Mehta, "Dynamic system stability, part-1 Investigation of the effect of different loading and excitation system," *IEEE Transaction on Power Apparatus and Systems*, Vols. PAS-92, no. 5, pp. 1538-1546, April 1973.

[7] P. Kundur, Power system stability and control, New York: McGraw-Hill, 1994.

[8] IEEE/CIGRE Joint Task Force, "Definition and classification of power system stability," *IEEE Transaction on Power Apparatus and Systems,* vol. 19, no. 2, pp. 1387-1701, August 2004.

[9] M. J. Basler and R. C. Schaefer, "Understanding power system stability," *IEEE Transaction on Industy Applications,* vol. 44, no. 2, pp. 463-474, April 2008.

[10] K. R. Padiyar, Power system dynamics stability and control, 2nd ed., Hyderabad, India 2008.

[11] D. Ruiz-Vega and M. Pavella, "A Comprehensive Approach to Transient Stability Control: Part I—Near Optimal Preventive Control," *IEEE Transactions on Power Systems,* vol. 18, no. 4, pp. 1446-1453, November 2003.

[12] E. V. Larsen and D. A. Swann, "Applying power system stabilizer: parts I-III," *IEEE Transactions on Power Apparatus and Systems* , Vols. PAS-100, no. 6, pp. 3017-3046, June 1981.

[13] D. Mondal, A. Chakrabarti and A. Sengupta, Power system samll signal stability analysis and control, 1st ed., London: UK, 2014.

[14] G. Roger, Power system oscillations, Norwell: MA:Kluwer, 2003.

[15] Y.-Y. Hsu and C.-Y. Hsu, "Design of a Proportional-Integral Power System Stabilizer," *IEEE Transactions on Power Systems,* vol. 1, no. 2, pp. 46-52, May 1986.

[16] M. Masrob, M. A. Rahman and G. George, "Enhancement of Power System Stability using a Power System Stabilizer," in *Newfoundland Electrical and Computer Engineering. Conference (NECEC),* St.John's, November 2013.

[17] D. M. Lam and H. Yee, "A study of frequency responses of generator electrical torques for power system stabilizer design," *IEEE Transactions on Power Systems*, vol. 13, no. 3, pp. 1136-1142, August 1998.

[18] M. J. Gibbard and D. J. Vowles, "Reconciliation of Methods of Compensation for PSSs in Multimachine Systems," *IEEE Transactions on Power Systems*, vol. 19, no. 1, pp. 463-472, February 2004.

[19] G. Gurrala and I. Sen, "Power system stabilizers design for interconnected power systems," *IEEE Transactions on power systems*, vol. 25, no. 2, pp. 1042-1051, May 2010.

[20] F. J. De Marco, N. Martins and J. C. Ferraz, "An Automatic Method for power system stabilizers phase compensation design," *IEEE Transactions on power systems*, vol. 28, no. 2, pp. 997-1007, May 2013.

[21] A. Kumar, "Power System Stabilizers Design for Multimachine Power Systems Using Local Measurements," *IEEE Transactions on Power Systems*, vol. 31, no. 3, pp. 2163-2171, May 2016.

[22] Z. Wang, C. Y. Chung, K. P. Wong and C. T. Tse, "Robust power system stabiliser design under multi-operating conditions using differential evolution," *IET Generation, transmission & distribution*, vol. 2, no. 5, pp. 690-700, March 2008.

[23] O. P. Malik and T. Abdelazim, "Power System Stabilizer Based on Model Reference Adaptive Fuzzy Control," in *Electric Power Components and Systems*, 2005.

[24] S. Zhang and F. L. Luo, "An Improved simple adaptive control applied to power system stabilizer," *IEEE Transaction on power electronics*, vol. 24, no. 2, pp. 369-375, February 2009.

[25] D. K. Chaturevida and O. P. Malik, "Generalized neuro-based adaptive PSS for multi-machine environment," *IEEE Transactions on power systems ,* vol. 20, no. 1, pp. 358-366, February 2005.

[26] T. T. Nguyen and R. Gianto, "Neural network for adaptive control coordination of PSSs and FACTs devices in multimachine power system," *IET Generation, transmission & distribution,* vol. 2, no. 3, pp. 355-372, 2008.

[27] M. Ramirez-Gonzalez and O. P. Malik, "Power System Stabilizer Design Using an Online Adaptive Neurofuzzy Controller With Adaptive Input Link Weights," *IEEE Transactions on Energy Conversion,* vol. 23, no. 3, pp. 914-922, September 2008.

[28] M. A. Masrob,, M. A. Rahman, G. H. George and B. Jeyasurya, "Development of Hybrid Procedure Controller Based on a Lead-Lag and Pole-Placement Power System Stabilizer Using a Different Linearization Approach," in *CIGRÉ Canada Conference*, Winnipeg, Manitoba, Canada, 2015.

[29] H. M. Soliman and . K. A. El Metwally, "Robust pole placement for power systems using two-dimensional membership fuzzy constrained controllers," *IET Generation, Transmission & Distribution,* vol. 11, no. 16, pp. 3966-3973, August, 2017.

[30] M. Nambu and Y. Ohsawa, "Development of an advanced power system stabilizer using a strict linearization approach," *IEEE Transactions on power systems,* vol. 11, no. 2, pp. 813-818, May 1996.

[31] A. K. Singh and B. C. Pal, "Decentralized Control of Oscillatory Dynamics in Power Systems Using an Extended LQR," *IEEE Transactions on Power Systems,* vol. 31, no. 3, pp. 1715-1728, May, 2016.

[32] K. Ogata, Modern control engineering, 5th ed., US: University of Minnesota, 2010.

[33] J. D'Azzo and C. H. Houpis, Linear control system analysis and design : conventional and modern, 4 ed., New York: McGraw-Hill, Inc., 1995.

[34] M. A. Furini, A. L. S.Pereira and P. B. Araujo, "Robust pole placement by coordinated tuning of power system stabilizer and FACTS-POD stabilizers," *Internationl journal of electrical power and energy systems*, vol. 33, pp. 615-622, 2011.

[35] C. Lu, Y. Zhao, K. Men, L. Tu and Y. Han, "Wide-area power system stabiliser based on model-free adaptive control," *IET Control Theory & Applications,* vol. 9, no. 13, pp. 1996-2007, April, 2015.

[36] R. S. Burns, Advanced control engineering, UK, 2001.

[37] S. Shanmuganathan and S. Samarasinghe, Artificial neural network modeling, Switzerland: Springer, 2016.

[38] Z. Zhang, O. P. Malik, G. S. Hope and G. P. Chen, "Application of an inverse input/output mapped ANN as a power system stabilizer," *EEE Transactions on Energy Conversion*, vol. 9, no. 3, pp. 433-441, September 1994.

[39] Y. Zhang, O. P. Malik and G. P. Chen, "Artificial Neural Network Power System Stabilizers in Multi-Machine Power System Environment," *IEEE Transactions on Energy Conversion*, vol. 10, no. 1, pp. 147-155, March 1995.

[40] P. Shamsollah and O. P. Malik, "Direct Neural Adaptive Control Applied to Synchronous Generator," *IEEE Transactions on Energy Conversion,* vol. 14, no. 4, pp. 1341-1346, December, 1999.

[41] B. Changaroon, S. C. Srivastava and D. Thukaram, "A Neural Network Based Power System Stabilizer Suitable for On-Line Training—A Practical Case Study for EGAT System," *IEEE Transactions on Energy Conversion,* vol. 15, no. 1, pp. 103-109, March 2000.

[42] R. Segal, M. L. Kothari and S. Madnani, "Radial Basis Function (RBF) Network Adaptive Power System Stabilizer," *IEEE Transactions on Power Systems,* vol. 15, no. 2, pp. 722-727, May 2000.

[43] D. K. Chaturvedi, O. P. Malik and P. K. Kalra, "Experimental Studies With a Generalized Neuron-Based Power System Stabilizer," *IEEE Transactions on Power Systems,* vol. 19, no. 13, pp. 1445-1453, August 2004.

[44] S.-M. Baek, J.-W. Park and G. K. Venayagamoorthy, "Power system control with an embedded neural network in hybrid system modeling," *IEEE Transactions on industry applications,* vol. 44, no. 5, pp. 1458-1465, September/October 2008.

[45] S. Kamalasadan and G. D. Swann, "A Novel System-Centric Intelligent Adaptive Control Architecture for Damping Interarea Mode Oscillations in Power System," *IEEE Transactions on Industry Applications,* vol. 47, no. 3, pp. 1487-1497, May/June 2011.

[46] S. Kamalasadan, G. D. Swann and R. Yousefian, "A Novel System-Centric Intelligent Adaptive Control Architecture for Power System Stabilizer Based on Adaptive Neural Networks," *IEEE Systems Journal,* vol. 8, no. 4, pp. 1074-1085, December 2014.

[47] M. Farahani, "A Multi-Objective Power System Stabilizer," *IEEE Transactions on Power Systems,* vol. 28, no. 3, pp. 2700-2707, August 2013.

[48] J. Harris, Fuzzy Logic Applications in Engineering Science, Netherlands: Springer, 2006.

[49] J. H. Lilly, Fuzzy control and identification, Hoboken, New Jersey: John Wiley & Sons, 2010.

[50] K. A. El-Metwally and O. P. Malik, "Fuzzy logic power system stabiliser," *IEE Proceedings - Generation, Transmission and Distribution,* vol. 142, no. 3, pp. 277-281, May 1995.

[51] H. A. Toliyat, J. Sadeh and R. Ghazi, "Design of Augmented Fuzzy Logic Power System Stabilizers to Enhance Power Systems Stability," *IEEE Transactions on Energy Conversion,* vol. 11, no. 1, pp. 97-103, March 1996.

[52] Y. Guo, D. J. Hill and Y. Wang, "Global Transient Stability and Voltage Regulation for Power Systems," *IEEE Transactions on Power Systems,* vol. 16, no. 4, pp. 678-688, November 2001.

[53] N. S. D.Arrifano, V. A. Oliveira and R. A. Ramos, "Fuzzy stabilization of power systems in a co-generation scheme subject to random abrupt variation of operating conditions," *IEEE Transactions on control system trchnology,* vol. 18, no. 1, pp. 384-393, March 2007.

[54] M. Ramirez-Gonzalez and O. P. Malik, "Simplified Fuzzy Logic Controller and its Application as a Power System Stabilizer," in *15th IEEE International Conference on Intelligent System Applications to Power Systems*, Curitiba, Brazil, November 2009.

[55] V. S. Vakula and K. R. Sudha, "Design of differential evolution algorithm-based robust fuzzy logic power system stabiliser using minimum rules base," *IET Generation Transmission & distribution ,* vol. 6, no. 2, pp. 121-132, 2012.

[56] M. Cloughley, K. M. Muttaqi and H. Du, "Damping of low-inertia machine oscillations using Takagi-Sugeno fuzzy stabilizer tuned by genetic algorithm optimaisation to improve

system stability," *IET Gneration, Transmission and Distribution,* vol. 8, no. 2, pp. 339-352, 2014.

[57] V. S. Vakula, A. Padmaja and K. R. Sodha, "Evolutionary Prisoner's Dilemma in updating fuzzy languistic model to damp power system osillations," *IET generation, transmission & distribution* , vol. 9, no. 5, pp. 445-456, 2015.

[58] W. A. Wikinson and M. D. Cox, "Discrete Wavelet Analysis of Power System Transients," *IEEE Transactions on Power Systems,* vol. 11, no. 4, pp. 2038-2044, November 1996.

[59] A. Bouzida, O. Touhami, R. Ibtiouen, A. Belouchrani, M. Fadel and A. Rezzoug, "Fault Diagnosis in Industrial Induction Machines Through Discrete Wavelet Transform," *IEEE Transactions on Industrial Electronics,* vol. 58, no. 9, pp. 4385-4395, September 2011.

[60] W. C. Santos, F. V. Lopes, N. S. D. Brito and B. A. Souza, "High-Impedance Fault Identification on Distribution Networks," *IEEE Transactions on Power Delivery,* vol. 32, no. 1, pp. 23-32, February 2017.

[61] M. A. S. K. Khan and A. A. Rahman, "A Novel Neuro-Wavelet-Based Self-Tuned Wavelet Controller for IPM Motor Drives," *IEEE Transactions on Industry Applications,* vol. 46, no. 3, pp. 1194-1203, May/June 2010.

[62] J. L. Rueda, C. A. Juárez and I. Erlich, "Wavelet-Based Analysis of Power System Low-Frequency Electromechanical Oscillations," *IEEE Transactions on Power Systems,* vol. 26, no. 3, pp. 1733-1743, August 2011.

[63] C. M. d. Sousa Neto, F. B. Costa, R. L. d. Araujo Ribeiro, R. L. Barreto and T. d. O. Alves Rocha, "Wavelet-Based Power System Stabilizer," *IEEE Transactions on Industrial Electronics,* vol. 62, no. 12, pp. 7360-7369, December 2015.

[64] W. G. Heffron and R. A. Phillips, "Effect of a Modern Amplidyne Voltage Regulator on Underexcited Operation of Large Turbine Generators," *Transactions of the American Institute of Electrical Engineers. Part III: Power Apparatus and Systems,* vol. 71, no. 1, pp. 692-697, August, 1952.

[65] A. E. Fitzgerald, C. Kingsley and U. Stephen, Electric Machinery, 7 ed., New York: McGraw-Hill, 2014.

[66] M. E. EI-Hawary, Electrical Power Systems Design and Analysis, 1 ed., New York: IEEE Press, 1995.

[67] Z. Zhu, G. Geng and Q. Jiang, "Power system dynamic model reduction based on extended Krylov subspace method," *IEEE Transaction on power systems,* vol. 31, no. 6, pp. 4483-4494, November 2016.

[68] S. Wang, S. Lu, N. Zhou, G. Lin, M. Elizondo and M. A. Pai, "Dynamic-Feature Extraction, Attribution, and Reconstruction (DEAR) method for power system model reduction," *IEEE Transaction on power systems,* vol. 29, no. 5, pp. 2049-2059, September 2014.

[69] G. Scarciotti, "Low computational complexity model reduction of power systems with preservation of physical characteristics," *IEEE Transaction on power system,* vol. 32, no. 1, pp. 743-752, January 2017.

[70] M. L. Ourari, L.-A. Dessaint and V.-Q. Do, "Dynamic equivalent modeling of large power systems using structure preservation technique," *IEEE Transaction on power systems,* vol. 21, no. 3, pp. 1284-1295, August 2006.

[71] S. Nabavi and A. Chakrabotty, "Structured Identification of Reduced-Order Models of Power Systems in a Differential-Algebraic Form," *IEEE Transactions on power systems,* vol. 32, no. 1, pp. 198-207, January 2017.

[72] E. J. Davison, "A Model for simplifying linear dynamic systems," *IEEE Transaction on automatic control,* vol. 11, no. 1, pp. 93-101, January 1966.

[73] M. Gibbard, P. Pourbeik and D. Vowles, Small-signal stability, control and dynamic performance of power systems, South Australia: Unversity of Adeliade, 2015.

[74] J. A. Momoh and M. E. El-Hawary, Electric Systems, Dynamics, and Stability with Artificial Intelligent Applications, New York: Marcel Dekker, Inc, 2000.

[75] M. A. Masrob, M. A. Rahman and G. H. George, "Design of a Neural Network Based Power System Stabilizer in Reduced Order Power System," in *IEEE 30th Canadian Conference on Electrical and Computer Engineering (CCECE),* Windsor, ON, Canada , April 30 to May 3, 2017.

[76] M. A. Masrob, M. A. Rahman, G. H. George and C. B. Butt, "Design of a Simple Neural Network Stabilizer for a Synchronous Machine of Power System via MATLAB/Simulink," in *IEEE International Electric Machines and Drives Conference (IEMDC),* Miami, FL, USA, May 21-24, 2017.

[77] Y.-Y. Hsu and K.-L. L. Liou, "Design of Self-Tuning PID Power System Stabilizers for Synchronous Generators," *IEEE Transactions on Energy Conversion,* Vols. EC-2, no. 3, pp. 343-348, September, 1987.

[78] J. Espinosa, J. Vandewalle and V. Wertz, Fuzzy logic, identification and predictive control, New York: Springer , 2004.

[79] S.-I. Ao, O. Castillo and X. Huang, Intelligent control and computer engineering, New York: Springer, 2011.

[80] k. Tomsovic and M. Y. Chow, "Tutorial on Fuzzy Logic Applications in Power Systems," IEEE-PES, Prepared for the IEEE-PES Winter Meeting in Singapore, January 2000.

[81] M. E. El-Hawary, Electric Power Application of Fuzzy Systems, New York: IEEE Press, 1998.

[82] S. K. Yee and J. V. Milanovic, "Fuzzy logic controller for decentralized stabilization of multi-machine power systems," *IEEE Transactions on fuzzy systems* , vol. 16, no. 4, pp. 971-981, August 2008 .

[83] M. A. Masrob, M. A. Rahman, C. B. Butt and G. H. George, "Design of a novel multi-input fuzzy logic power stabilizer for a reduced order power system," in *IEEE PES Asia-Pacific Power & Energy Engineering Conference (APPEEC)*, Xi'an, China, October, 2016.

[84] Y.-Y. H. Hsu and . C.-Y. Hsu, "Design of a Proportional-Integral Power System Stabilizer," *IEEE Transactions on Power Systems,* vol. 1, no. 5, pp. 46-52, May, 1986.

[85] A. Boggess and F. J. Narcowich, A First Course in Wavelets with Fourier Analysis, Hoboken, New Jersey: John Wiley & Sons, Inc, 2009.

[86] Mathworks, "Wavelet Toolbox™ User's Guide," version r2017., 2017.

[87] L. Debnath and F. A. Shah, Wavelet Transforms and Their Applications, 2nd ed., New York: Springer Science, 2015.

[88] G. Stang and T. Nguyen, Wavelets and filter banks, Wellesley, MA : Wellesley-Cambridge Press, 1996.

[89] M. V. Wickerhauser, Adapted Wavelet Analysis from Theory to Software, Piscataway, NJ, USA: IEEE Press, 1994.

[90] . D. B. Percival and A. T. Walden, Wavelet methods for time series analysis, New York, USA: Cambridge Univ. Press, 2000.

[91] D. K. Ruch and P. J. V. Fleet, Wavelet Theory, An Elementary Approach With Applications, A John Wiley & Sons, Inc., 2009.

[92] S. Mallat, A Wavelet Tour of Signal Processing, Burlington MA, USA: Elsevier, 2009.

[93] S. G. Mallat, "A Theoty for multiresolution signal decompensation: the wavelet representation," *IEEE Transactions in pattern analysis and machine intelligence,* vol. 11, no. 7, pp. 674-693, July 1989.

[94] R. S. PATHAK, The Wavelet Transform, India : ATLANTIS PRESS / WORLD SCIENTIFIC, 2009.

[95] S. Santoso and P. Hofmann, "Power quality assessment via wavelet transform analysis," *IEEE Transactions on Power Delivery,* vol. 11, no. 2, pp. 924 - 930, April 1996.

[96] G. G. Yen and K. Chung Lin, "Wavelet Packet Feature Extraction for Vibration Monitoring," *IEEE Transactions on Industrial Electronics,* vol. 47, no. 3, pp. 650-667, June 2000.

[97] E. Y. Hamid and Z.-I. Kawasaki, "Wavelet-Based Data Compression of Power System Disturbances Using the Minimum Description Length Criterion," *IEEE Transactions on Power Delivery,* vol. 17, no. 2, pp. 460-466, April 2002.

[98] M. A. S. K. Khan, "A Wavelet Based Speed Controller for Interior Permanent Magnet Motor Drives," Memorail University, PhD thesis, 2010.

[99] M. A. Khan, M. N. Uddin and M. A. Rahman, "A Novel Wavelet-Neural-Network-Based Robust Controller for IPM Motor Drives," *IEEE Transactions on Industry Applications*, vol. 49, no. 5, pp. 2341-2351, September/October 2013.

[100] S. A. Saleh, T. S. Radwan and M. A. Rahman, "Real-Time Testing of WPT-Based Protection of Three-Phase VS PWM Inverter-Fed Motors," *IEEE Transactions on Power Delivery*, vol. 22, no. 4, pp. 2108-2115, October 2007.

[101] C. K. Chui, Wavelets: A Mathematical Tool for Signal Analysis, Philadelphia: Society for Industrial and Applied Mathematics, 1997.

[102] L. A. Monzon, "Constructive Multiresolution Analysis and The Structure of Quadrature Mirror Filters," Yale University , PhD thesis, 1994.

[103] S. Parvez and Z. Gao, "A Wavelet-Based Multiresolution PID Controller," *IEEE Transactions on Industry Applications*, vol. 41, no. 2, pp. 537-543, March/April 2005.

[104] G. Ellis, Control System Design Guide, 3, Ed., USA: Academic Press, 2004.

[105] M. A. S. K. Khan and M. A. Rahman, "Implementation of a Wavelet-Based MRPID Controller for Benchmark Thermal System," *IEEE Transactions on Industrial Electronics*, vol. 57, no. 12, pp. 4160-4169, December 2010.

[106] S. K. M. A. Khan and A. M. Rahman, "Implementation of a New Wavelet Controller for Interior Permanent-Magnet Motor Drives," *IEEE Transactions on Industry Applications*, vol. 44, no. 6, pp. 1957-1965, November/December 2008.

[107] MATLAB version 8.4.0.150421 (R2014b), MathWorks Inc, September, 2014.

[108] R. A. Ramos et al, "Benchmark systems for small-signal stability analysis and control," IEEE PES Resource Center, IEEE PES Tech. Rep. TR-18, August, 2015.

[109] C. Canizares, T. Fernandes, E. Geraldi Jr., L. Gerin-Lajoie, M. Gibbard, I. Hiskens, J. Kersulis, R. Kuiava, L. Lima, F. DeMarco, N. Martins, B. C. Pal, C. Piardi, R. Ramos, J. d. Santos, D. Silva, A. K. Singh, B. Tamimi and D. Vowles, "Benchmark Models for the Analysis and Control of Small-Signal Oscillatory Dynamics in Power Systems," *IEEE Transactions on Power Systems,* vol. 32, no. 1, pp. 715-722, January, 2017.

[110] J. Chow and G. Rogers , "Power System Toolbox Version 3.0," Cherry Tree Scientific Software, Colbome, ON, Canada, 2008.

Appendix A

A.1 Single machine power system data

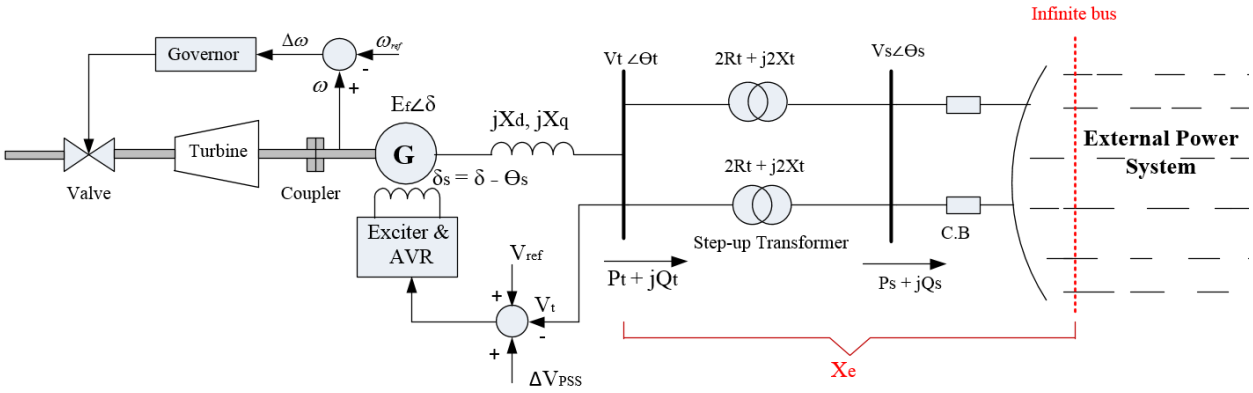

Figure A.1. Single line diagram of single machine power system

Table A.1. Synchronous generator rating and parameters

$S_{rated} = 920$ MVA	$V_{rated} = 18$ KV
$Speed_{rated} = 1800$ rpm	$P.F_{rated} = 0.9$
$x_{ls} = 0.215$ per unit	$r_s = 0.0048$ per unit
$x_d = 1.79$ per unit	$x_q = 1.66$ per unit
$x'_d = 0.355$ per unit	$x'_q = 0.357$ per unit
$x''_d = 0.275$ per unit	$x''_q = 0.275$ per unit
$T'_{dO} = 7.9$ sec	$T'_{qO} = 0.41$ sec
$T''_{dO} = 7.9$ sec	$T''_{qO} = 0.055$ sec
$H = 3.77$ sec	$D = 0$ per unit

Table A. 2. Parameters of excitation and governor turbine systems

$K_A = 80$ per unit	$T_A = 0.05$ sec
$K_E = -0.17$per unit	$T_E = 095$ sec
$K_F = 0.04$ per unit	$T_F = 1.0$ sec
$S_E = 0.92$ per unit	$T_R = 0.03$ sec
$T_T = 1.5$ sec	$T_G = 0.5$ sec
R = 0.05	

Appendix B

B.1 Four-machine ten-bus power system data

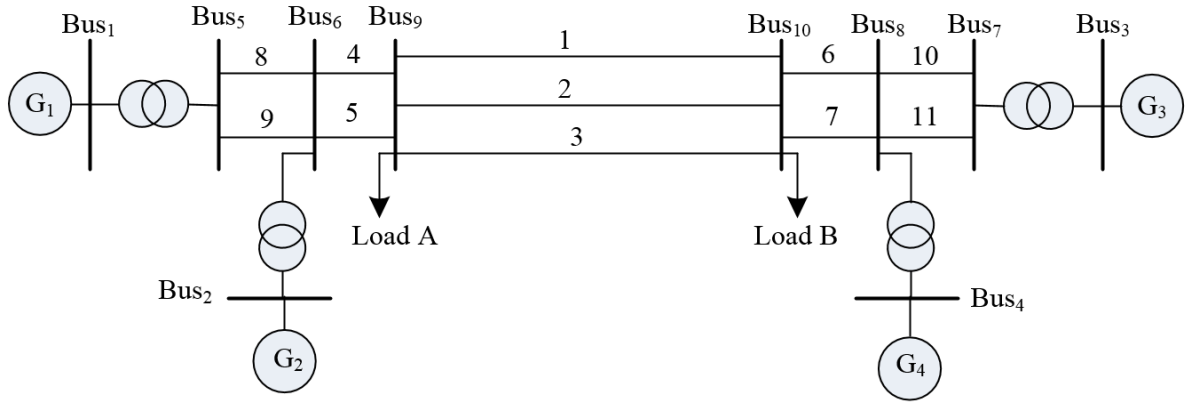

Figure B.1. Single line diagram of four-machine ten-bus power system

Table B. 1. Power flow data and results

Bus No.	Voltage. (p.u)	Angle (deg.)	P_G (p.u)	Q_G (p.u)	P_L (p.u)	Q_L (p.u)	B Shunt. (p.u)
1	1.03	8.2154	7.0	1.3386	0.0	0.0	0.0
2	1.01	-1.5040	7.0	1.5920	0.0	0.0	0.0
3	1.03	0.0	7.2172	1.4466	0.0	0.0	0.0
4	1.01	-10.2051	7.0	1.8083	0.0	0.0	0.0
5	1.0108	3.6615	0.0	0.0	0.0	0.0	0.0
6	0.9875	-6.2433	0.0	0.0	0.0	0.0	0.0
7	1.0095	-4.6977	0.0	0.0	0.0	0.0	0.0
8	0.9850	-14.9443	0.0	0.0	0.0	0.0	0.0
9	0.9761	-14.4194	0.0	0.0	11.59	2.12	3.0
10	0.9716	-23.2922	0.0	0.0	2.88	2.88	4.0

Table B. 2. Transmission line data on 100 MVA base

From bus number	To bus number	Series resistance R_s (p.u)	Series reactance X_s(p.u)	Shunt susceptance B(p.u)
1	5	0.001	0.012	0.00
2	6	0.001	0.012	0.00
9	10	0.022	0.22	0.33
9	10	0.022	0.22	0.33
9	10	0.022	0.22	0.33
9	6	0.002	0.02	0.03
9	6	0.002	0.02	0.03
3	7	0.001	0.012	0.00
4	8	0.001	0.012	0.00
10	8	0.002	0.02	0.03
10	8	0.002	0.02	0.03
5	6	0.005	0.05	0.075
5	6	0.005	0.05	0.075
7	8	0.005	0.05	0.075
7	8	0.005	0.05	0.075

Table B. 3. Synchronous machine data

Variable	Machine at Bus1	Machine at Bus2	Machine at Bus3	Machine at Bus4
X_l (p.u)	0.022	0.022	0.022	0.022
R_a (p.u)	0.00028	0.00028	0.00028	0.00028
X_d (p.u)	0.2	0.2	0.2	0.2
X'_d (p.u)	0.033	0.033	0.033	0.033
X''_d (p.u)	0.0264	0.0264	0.0264	0.0264
T'_{do} (sec)	8.0	8.0	8.0	8.0
T''_{do} (sec)	0.05	0.05	0.05	0.05
X_q (p.u)	0.19	0.19	0.19	0.19
X'_q (p.u)	0.061	0.061	0.061	0.061
X''_q (p.u)	0.03	0.03	0.03	0.03
T'_{qo} (sec)	0.4	0.4	0.4	0.4
T''_{qo} (sec)	0.04	0.04	0.04	0.04
H (sec)	54.0	54.0	54.0	54.0
D (p.u)	0	0	0	0

Table B. 4. Excitation system data

Gen #	K_A (p.u)	T_A (sec)	E_{FDmin} (p.u)	E_{FDmax} (p.u)
1,2,3,4	200	0.02	-6	6

Table B. 5. Hydro-Turbine governor system data

Gen #	T_W (sec)	T_G (sec)	Sigma (p.u)	T_2 (sec)	P_{max_fac} (p.u)	P_{min_fac} (p.u)
1,2,3,4	1	0.2	0.05	0	1.1	0.1

Appendix C

C.1 Ten-machine 39-bus (New England) power system data

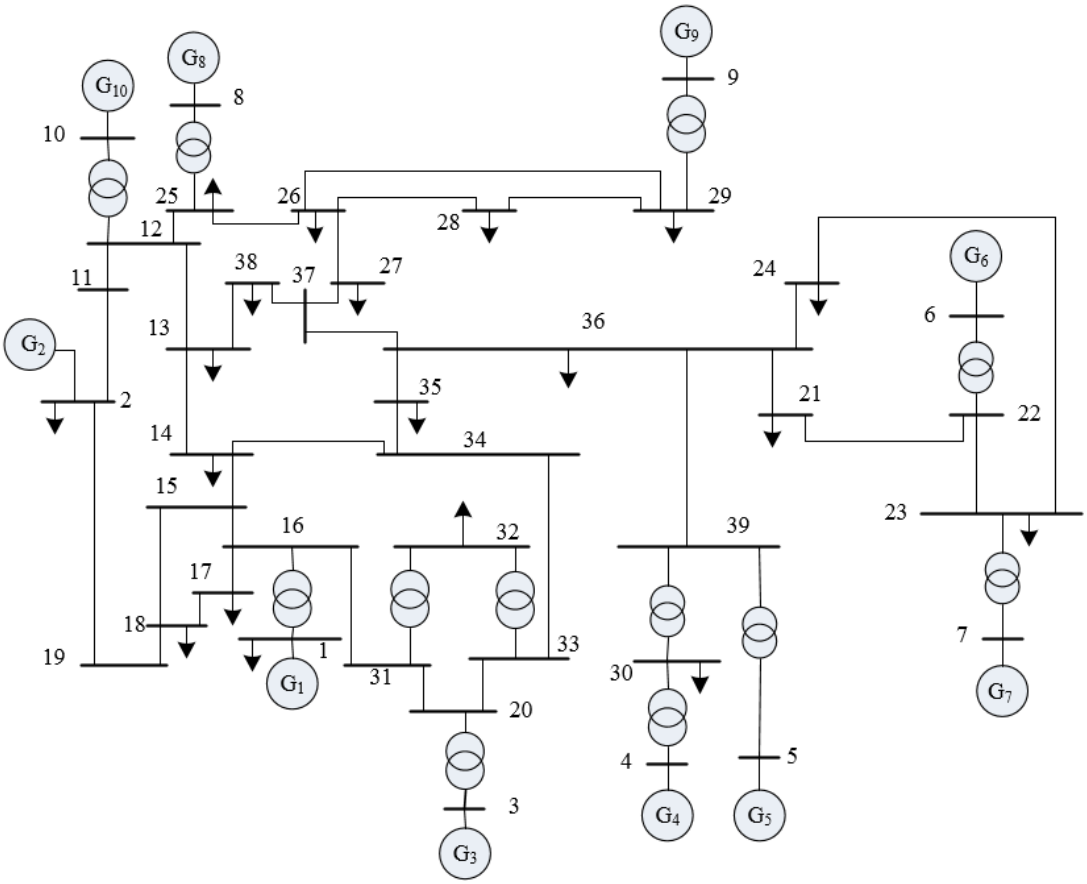

Figure C. 1. Single line diagram of 10-generator 39-bus power system

Table C.1. Synchronous Generator Data

Gen #	R_a	X_d	X'_d	X_q	X'_q	H	T'_{do}	T'_{qo}	T_c	D
1	0.0	0.2950	0.0647	0.2820	0.0647	30.3	6.56	1.5	0.01	0.0
2	0.0	0.0200	0.0060	0.0190	0.0060	500.0	6.0	1.7	0.01	0.0
3	0.0	0.2495	0.0531	0.2370	0.0531	35.8	5.7	1.5	0.01	0.0
4	0.0	0.3300	0.0660	0.3100	0.0660	26.0	5.4	0.44	0.01	0.0
5	0.0	0.2620	0.0436	0.2580	0.0436	28.6	5.69	1.5	0.01	0.0
6	0.0	0.2540	0.0500	0.2410	0.0500	34.8	7.3	0.4	0.01	0.0
7	0.0	0.2950	0.0490	0.2920	0.0490	26.4	5.66	1.5	0.01	0.0
8	0.0	0.2900	0.0570	0.2800	0.0570	24.3	6.7	0.41	0.01	0.0
9	0.0	0.2106	0.0570	0.2050	0.0570	34.5	4.79	1.96	0.01	0.0
10	0.0	0.2000	0.0040	0.1900	0.0040	42.0	5.7	0.50	0.01	0.0

T_C is the time constant of the dummy coil considered to represent transient saliency

Table C. 2. Transmission lines data

From bus #	To bus #	R_L	X_L	B_c
37	27	0.0013	0.0173	0.3216
37	38	0.0007	0.0082	0.1319
36	24	0.0003	0.0059	0.0680
36	21	0.0008	0.0135	0.2548
36	39	0.0016	0.0195	0.3040
36	37	0.0007	0.0089	0.1342
35	36	0.0009	0.0101	0.1723
34	35	0.0018	0.0217	0.3660
33	34	0.0009	0.0101	0.1723
28	29	0.0014	0.0151	0.2490

Continued from the previous page

26	29	0.0057	0.0625	1.0290
26	28	0.0043	0.0474	0.7802
26	27	0.0014	0.0147	0.2396
25	26	0.0032	0.0323	0.5130
23	24	0.0022	0.0350	0.3610
22	23	0.0006	0.0096	0.1846
21	22	0.0008	0.0135	0.2548
20	33	0.0004	0.0043	0.0729
20	31	0.0004	0.0043	0.0729
19	2	0.0010	0.0250	1.2000
18	19	0.0023	0.0363	0.3804
17	18	0.0004	0.0046	0.0780
16	31	0.0007	0.0082	0.1389
16	17	0.0006	0.0092	0.1130
15	18	0.0008	0.0112	0.1476
15	16	0.0002	0.0026	0.0434
14	34	0.0008	0.0129	0.1382
14	15	0.0008	0.0128	0.1342
13	38	0.0011	0.0133	0.2138
13	14	0.0013	0.0213	0.2214
12	25	0.0070	0.0086	0.1460
12	13	0.0013	0.0151	0.2572
11	12	0.0035	0.0411	0.6987
11	2	0.0010	0.0250	0.7500

Table C. 3. Load flow data

Bus #	V (p.u)	φ	P_G (p.u)	Q_G (p.u)	P_L (p.u)	Q_L (p.u)
1	0.98200	0.0	5.04509	1.36036	0.9200	0.4600
2	1.0300	-9.55016	10.000	1.95746	11.0400	2.5000
3	0.98310	3.20174	6.500	1.59104	0.00	0.00
4	1.01230	4.61664	5.0800	1.58151	0.00	0.00
5	0.99720	5.57217	6.3200	0.95582	0.00	0.00
6	1.04930	6.62654	6.500	2.76414	0.00	0.00
7	1.06350	9.46958	5.600	2.35485	0.00	0.00
8	1.02780	3.16537	5.400	0.63019	0.00	0.00
9	1.02650	9.04654	8.300	0.84790	0.00	0.00
10	1.04750	-2.47597	2.500	1.46483	0.00	0.00
11	1.03829	-7.79710	0.00	0.00	0.00	0.00
12	1.02310	-4.89487	0.00	0.00	0.00	0.00
13	0.99576	-8.07759	0.00	0.00	3.2200	0.0240
14	0.95894	-9.35310	0.00	0.00	5.00	1.840
15	0.95660	-8.29471	0.00	0.00	0.00	0.00
16	0.95688	-7.56925	0.00	0.00	0.00	0.00
17	0.95140	-9.9740	0.00	0.00	2.3380	0.8400
18	0.95276	-10.5017	0.00	0.00	5.220	1.7600
19	1.01028	-9.92054	0.00	0.00	0.00	0.00
20	0.95966	-4.71314	0.00	0.00	0.00	0.00
21	0.99046	-2.98024	0.00	0.00	2.7400	1.1500
22	1.01550	1.62430	0.00	0.00	0.00	0.00
23	1.01344	1.34841	0.00	0.00	2.7450	0.84660
24	0.98179	-5.45955	0.00	0.00	3.08600	0.92200
25	1.02088	-3.68919	0.00	0.00	2.2400	0.47200

Continued from the previous page

26	1.01822	-4.76321	0.00	0.00	1.3900	0.1700
27	1.00150	-6.92554	0.00	0.00	2.8100	0.7550
28	1.02204	-0.95906	0.00	0.00	2.0600	0.2760
29	1.02143	1.95588	0.00	0.00	2.8350	0.2690
30	0.98832	-0.62515	0.00	0.00	6.2800	1.0300
31	0.95760	-5.69316	0.00	0.00	0.00	0.00
32	0.93795	-5.68713	0.00	0.00	0.07500	0.8800
33	0.95912	-5.47342	0.00	0.00	0.00	0.00
34	0.96168	-7.20767	0.00	0.00	0.00	0.00
35	0.96683	-7.32475	0.00	0.00	3.200	1.5300
36	0.98196	-5.55956	0.00	0.00	3.2940	0.32300
37	0.99086	-6.73437	0.00	0.00	0.00	0.00
38	0.99197	-7.71437	0.00	0.00	1.5800	0.300
39	0.98770	0.34648	0.00	0.00	0.00	0.00

Table C. 4. Transformers data

From bus #	To bus #	R_T	X_T	Tap
39	30	0.0007	0.0138	1.0
39	5	0.0007	0.0142	1.0
32	33	0.0016	0.0434	1.0
32	31	0.0016	0.0434	1.0
30	4	0.0009	0.0272	1.0
29	9	0.0008	0.0156	1.0
25	8	0.0006	0.0232	1.0
23	7	0.0005	0.0272	1.0
22	6	0.00	0.0143	1.0
20	3	0.00	0.020	1.0
16	1	0.00	0.0250	1.0
12	10	0.00	0.0181	1.0

Appendix D

D.1 Industry standard of Lead-lag PSS (SIEMENS)

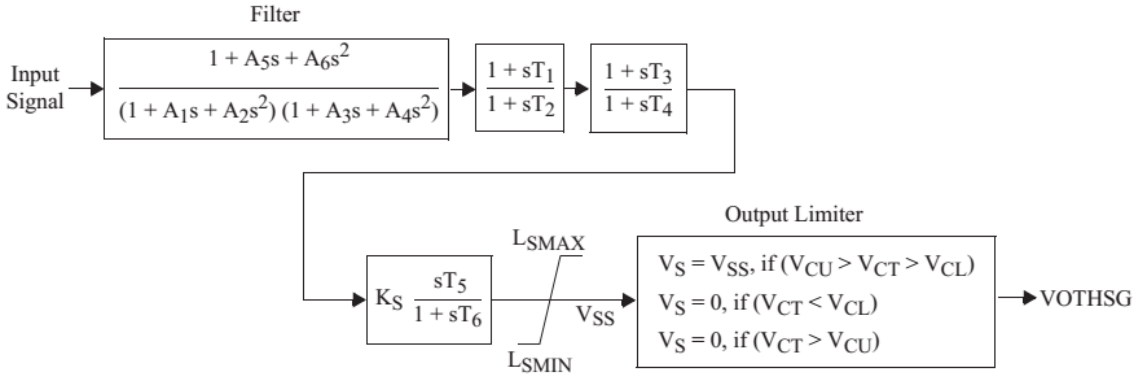

Appendix E

E.1 PIC control circuit that used in the experimental and its components

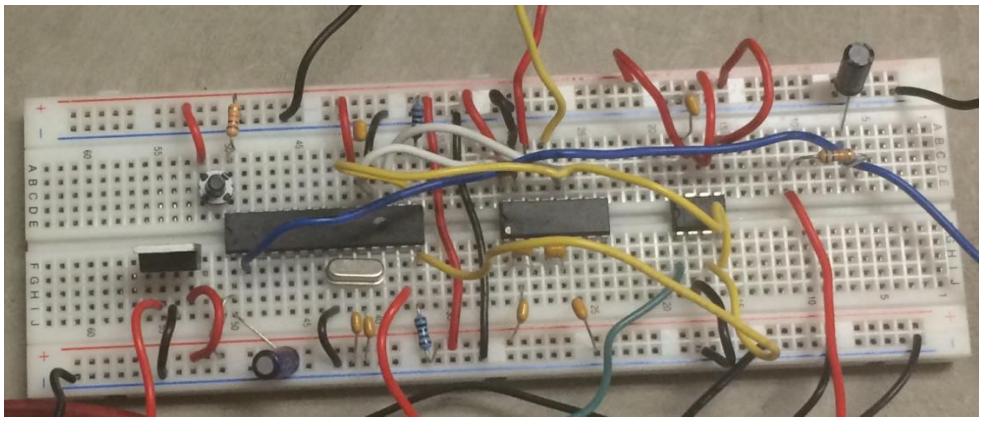

PIC control Circuit

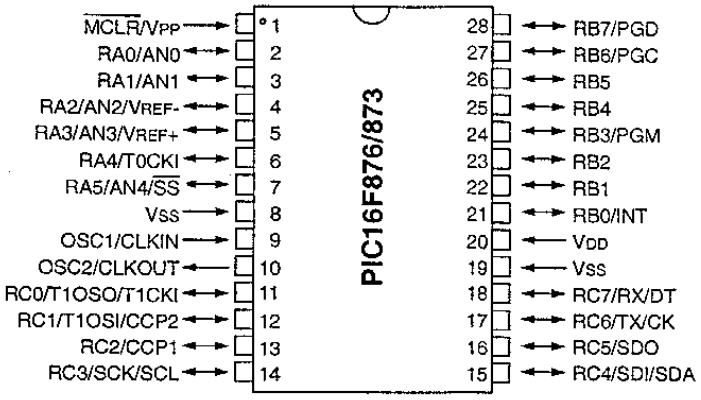

Peripheral Interface Controller (PIC) Chip

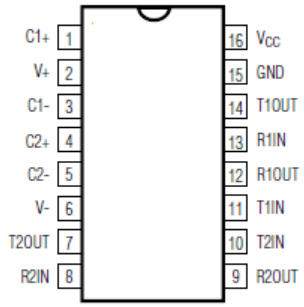

RS 232 Chip

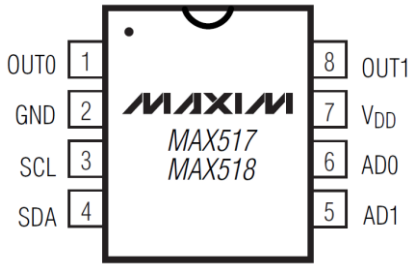
OUT0
1
GND
2
SCL
3
SDA
4
MAXIM
MAX517
MAX518
8
OUT1
7
VDD
6
AD0
5
AD1

DAC

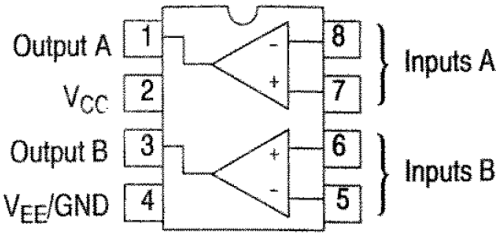
Output A
1
VCC
2
Output B
3
VEE/GND
4
8
7
6
5
Inputs A
Inputs B

OP AMP

Publications based on this research:

- M. Masrob, M. A. Rahman and G. George, "Enhancement of Power System Stability using a Power System Stabilizer," in *Proceedings of the 22nd Annual Newfoundland Electrical and Computer Engineering. Conference (NECEC)*, St. John's, November 2013.
- M. Masrob, M. A. Rahman and G. George and B. Jeyasurya, "Development of Pole Placement Power System Stabilizer Using a Different Linearization Approach", in *Proceedings of the 23rdAnnual Newfoundland Electrical and Computer Engineering Conference (NECEC)*, St. John's, NL, Canada, November 3, 2014.
- M. A. Masrob,, M. A. Rahman, G. H. George and B. Jeyasurya, "Development of Hybrid Procedure Controller Based on a Lead-Lag and Pole-Placement Power System Stabilizer Using a Different Linearization Approach," in *CIGRÉ Canada Conference*, Winnipeg, Manitoba, Canada, 2015.pp. 1-6.
- M.A, Masrob, M. A. Rahman, C. B. Butt and G. H. George, " A Novel Technique to Design a Hybrid Procedure Power System Stabilizer for a Reduced Order Power System", in *Proceedings of the 25thAnnual Newfoundland Electrical and Computer Engineering Conference (NECEC)*, November 10, 2016.
- M. A. Masrob, M. A. Rahman, C. B. Butt and G. H. George, "Design of a novel multi-input fuzzy logic power stabilizer for a reduced order power system," in *IEEE PES Asia-Pacific Power & Energy Engineering Conference (APPEEC)*, Xi'an, China, October, 2016. pp. 2611-2616.

- M. A. Masrob, M. A. Rahman and G. H. George, "Design of a Neural Network Based Power System Stabilizer in Reduced Order Power System," in *IEEE 30th Canadian Conference on Electrical and Computer Engineering (CCECE)*, Windsor, ON, Canada , April 30 to May 3, 2017. pp 1-6.
- M. A. Masrob, M. A. Rahman, G. H. George and C. B. Butt, "Design of a Simple Neural Network Stabilizer for a Synchronous Machine of Power System via MATLAB/Simulink," in *IEEE International Electric Machines and Drives Conference (IEMDC)*, Miami, FL, USA, May 21-24, 2017. pp 1-6.
- M. A. Masrob and M. A. Rahman, ” Design of a simplified fuzzy logic power system stabilizer for dynamic reduction of a power system mode”, in *IET International Conference on Resilience of Transmission and Distribution Networks (RTDN)*, Birmingham, UK, 26-28 Sept. 2017. Page 5 (6 .).
- A. Aktaibi, M.A. Masrob, G.H. George and M.A. Rahman, “Resilience of Power Transmission System Protection Using a New d-q Wavelet Hybrid Technique”, *in IET International Conference on Resilience of Transmission and Distribution Networks (RTDN)*, Birmingham, UK, 26-28 Sept. 2017. Page 3 (5 .).
- M. A. Masrob, M. A. Rahman and G. H. George, " Scheme of a Novel Wavelet-Based Multi-resolution Analysis Power System Stabilizer," Accepted in *IEEE 31th Canadian Conference on Electrical and Computer Engineering (CCECE)*, Quebec, Canada , May 13 to May 16, 2018.
- M. A. Masrob and M. A. Rahman “Wavelet PID Controller for Synchronous Machine Stabilizer” Accepted in *IEEE Power and Energy Society Motor Sub-Committee* at Portland, OR, USA, 5-10 August 2018.

- M. A. Masrob, M. A. Rahman and G. H. George, "Design of a Wavelet-based Stabilizer for Synchronous Machines" submitted to *IEEE Transactions on Energy Conversion-Emerging Electric Machines and Drives for Smart Energy Conversion* (The digest has been accepted, and completion of the first round of review has been done)